




EX LIBRIS
UNIVERSITATIS
ALBERTENSIS

The Bruce Peel
Special Collections
Library



Digitized by the Internet Archive
in 2025 with funding from
University of Alberta Library

<https://archive.org/details/0162010967121>

University of Alberta

Library Release Form

NAME OF AUTHOR: Jonathan Andrew Marc Brown

TITLE OF THESIS: A Study of the Interactions between
Electromagnetic Fields and Microtubules:
Ferroelectric Effects, Signal Transduction
and Electronic Conduction

DEGREE: Doctor of Philosophy

YEAR THIS DEGREE GRANTED: 1999

Permission is hereby granted to the University of Alberta Library to reproduce single copies of this thesis and to lend or sell such copies for private, scholarly or scientific research purposes only.

The author reserves all other publication and other rights in association with the copyright in the thesis, and except as hereinbefore provided neither the thesis nor any substantial portion thereof may be printed or otherwise reproduced in any material form whatever without the author's prior written permission.

Mon pays ce n'est pas un pays, c'est l'hiver.

– Gilles Vigneault

The moment of victory is much too short
to live for that and nothing else.

– Martina Navratilova

University of Alberta

**A Study of the Interactions between Electromagnetic
Fields and Microtubules: Ferroelectric Effects, Signal
Transduction and Electronic Conduction**

by

Jonathan Andrew Marc Brown



A thesis submitted to the Faculty of Graduate Studies and Research in partial
fulfillment of the requirements for the degree of Doctor of Philosophy

Department of Physics

Edmonton, Alberta

Fall 1999

University of Alberta

Faculty of Graduate Studies and Research

The undersigned certify that they have read, and recommend to the Faculty of Graduate Studies and Research for acceptance, a thesis entitled **A Study of the Interactions between Electromagnetic Fields and Microtubules: Ferroelectric Effects, Signal Transduction and Electronic Conduction** submitted by **Jonathan Andrew Marc Brown** in partial fulfillment of the requirements for the degree of Doctor of Philosophy.

Abstract

Microtubules have been the subject of intense research in the last ten years in particular as speculation has grown surrounding their involvement in a diverse range of biological and cognitive functions. In this context, this thesis focuses on microtubules with a view to develop simple models of electromagnetic effects in this important biological polymer. The goal of the work is to provide insight into fundamental questions of microtubule structure and function.

My modelling began with considering the ferroelectric properties of an individual microtubule. Each tubulin dimer of which the microtubule is comprised has an associated dipole which changes with conformational changes of the dimer. I have studied the conditions under which the interdimer dipole-dipole interactions are sufficient to result in a ferroelectrically ordered polymer. I find that the microtubule may adopt a conformation of ferroelectrically or antiferroelectrically ordered alternating protofilaments depending upon its lattice type. I have further studied whether defects introduced upon the lattice can propagate and constitute a form of intracellular signalling. The investigation demonstrates that such defects will indeed propagate in the presence of an action potential which is required to provide directionality.

I next studied the possibility of electrical conduction by microtubules and determined that their conductivity is strongly related to the relative and absolute hopping parameters in each of the three lattice directions. The microtubule can indeed have semi-conducting properties if the protofilament-protofilament interactions are sufficiently strong due to the triangular nature of its lattice.

Lastly, I have tried to unite the latest structural data on the atomic structure of tubulin with the microtubule structure, their assembly properties and their functions. The conclusion is that the electrostatics play a large role in the behaviour of microtubules.

Preface

The work presented in this dissertation was carried out at the Department of Physics at the University of Alberta, Edmonton and at the Institute for Microstructural Studies at the National Research Council, Ottawa between September 1994 and February 1999. The work was done under the supervision of Jack Tuszyński. Results from Chapters 4 and 5 have been published in the following articles:

- B. Trpišová and J.A. Brown, *Ordering of Dipoles in Different Types of Microtubule Lattice* International Journal of Modern Physics B **12** 543–578 (1998).
- J.A. Brown and J.A. Tuszyński, *Dipole Interactions in Axonal Microtubules as a Mechanism of Signal Propagation*, Physical Review E **56** 5834–5840 (1997).

In addition, some of the discussion of biological signalling in chapter 3 has been published in the conference proceedings from *Molecular Biophysics of the Cytoskeleton* which was held in Banff in August 1997:

- J.A. Brown and J.A. Tuszyński, *Reflections of Biological Signaling: Electronic conduction may be an important intracellular pathway*, Advances in Structural Biology **5** 115–125 (1998).

Some preliminary work from chapter 6 has been published in the following article:

- J.A. Tuszyński, J.A. Brown, and P. Hawrylak, *Dielectric Polarization, Electrical Conduction, Information Processing and Quantum Computation in Microtubules, are they Plausible?* Philosophical Transactions A - Proceedings of the Royal Society (London) **356** 1897–1926 (1998).

The bulk of the work from chapter 6 and the material of chapter 7 had not been submitted for publication at the time of this printing.

Acknowledgements

I would firstly like to thank Jack Tuszyński for his supervision. Over my stay at the University of Alberta, we have had many fruitful discussions together, within our group and with visiting academics. I would also like especially to thank Dave Sept who was also an active member of the biophysics group and someone with whom I often collaborated. I must also recognize the contributions of Pawel Hawrylak and Frank Marsiglio for their useful comments over the course of my investigations. My gratitude is extended also to Zbigniew Gortel for his support in the department and to Lynn Chandler who works tirelessly for the benefit of graduate students in our department. A brief note of thanks as well to the Natural Sciences and Engineering Research Council that has supported me during my studies.

I would also like to thank the following graduate students and post-docs for making my stay in Edmonton as enjoyable as it was: Warren Anderson, Adam Baig, Kristen Beaty, Nicolas Biais, Ian Blokland, Norm Buchanan, Kipp Cannon, Bryan Caron, Jim Cruickshank, Bahman Darian, Serge Droz, Anthony Faust, Jim Fuite, Jeremy Gallop, Shaun Hendy, Michael Jørgenson, Philip Kayal, Gene Kotik, Tomáš Kopf, Dave Lamb, Hans Jörg Limbach, Alick Macpherson, Connell McCluskey, Jo Molyneux, Jason Myatt, Mark Paetkau, Doug Ridgway, Yun Feng Shao, Dave Shaw, Patrick Sutton and Rob Thacker. Their encouragement, assistance and friendship was invaluable. I wish you all the best in your future endeavours.

I must finally acknowledge my best friends over the time that I've spent in Edmonton: Wai Lun Chan, Ilene Hermann, Bridget Kruisseelbrink, Rick H. Lee, John L. Plews, Tod Spence-Perkins, Dan Stern, Monique Tschofen and Karen Wiltse. The time we have spent together has enriched my life and made it so much easier being gay in Alberta. May the future bring you all that you wish.

Contents

1	Introduction	1
2	Cellular Biology Background	4
2.1	The Cytoplasm	5
2.2	The Cytoskeleton	7
2.2.1	Microfilaments	8
2.2.2	Intermediate Filaments	9
2.2.3	Microtubules	10
2.3	Structure of Microtubules	11
2.3.1	Microtubule Lattices and Defects	13
2.4	Microtubule Assembly	18
2.4.1	Individual Microtubule Assembly	18
2.4.2	Dynamic Instability, Ensemble Dynamics	20
2.5	Neuronal Microtubules	23
2.6	Chemistry of Tubulin	24
2.6.1	Variation of Isoforms	29
2.6.2	Post-translational Modification	30
2.6.3	Tubulin Conformations	31
2.7	Microtubule Associated Proteins	33
2.8	Drug Action on Microtubules	36
2.9	Elastic Properties of Microtubules	37
2.10	Force Generation by Motor Proteins	38
3	The Biology-Physics Interface	49
3.1	Energy Requirements	51
3.2	Biological Signalling	53
3.3	Biological Piezoelectricity	57
3.4	Biological Conduction	58
3.5	Protein Interaction with Environment	64
3.6	Symbiosis of Physics and Biology	67

CONTENTS

4	Dipole Ordering	74
4.1	Ising Model	74
4.2	A Biological Ising System	75
4.2.1	The Dipole Interaction Model	77
4.2.2	Boundary Conditions: Lattice Types	82
4.2.3	Monte Carlo Simulation	85
4.3	Results	86
4.3.1	MT 13A Lattice	87
4.3.2	MT 13B Lattice	87
4.3.3	Electric Fields	90
4.4	Lattice Defects	92
4.4.1	Alternate Protofilament Numbers	92
4.4.2	The Impact of MAPs	94
4.5	Summary of Dipole Ordering	96
4.6	Ordering of MT Bundles	97
5	Signalling by Microtubules	106
5.1	MT Lattice of Dipoles	109
5.2	New Model of Dimer Interactions	110
5.2.1	Model Features	112
5.3	Results	114
5.3.1	Propagation of Signals	116
5.4	Action Potentials	117
5.5	Discussion	118
6	Conduction by Microtubules	125
6.1	Modelling Conducting Polymers	125
6.2	Modelling the Protofilament chain	126
6.2.1	Quantum Double Well Picture	126
6.2.2	Second Quantization	130
6.2.3	Basis of States	132
6.2.4	Itinerant Electron Picture	133
6.2.5	Hubbard Model	136
6.3	Conduction in a Hubbard Model	139
6.3.1	Kubo Formula for Electrical Conductivity	140
6.3.2	Implementation of the Model	143
6.3.3	Proof: Conduction requires electronic state change	145
6.4	Results	147
6.4.1	1D Protofilament Chain	148
6.4.2	Triangular MT Lattice	157
6.5	Summary	168

CONTENTS

7	Unifying Concepts	173
7.1	Electrostatics	174
7.1.1	Electrostatic Potential around Tubulin	180
7.2	Variations by Tubulin Isotype	188
7.3	Proposed Investigations	196
7.4	Outstanding Issues	198
7.5	Conclusions	201

List of Tables

2.1	Major Components of Cytoplasm in a Typical Mammalian Cell	6
2.2	Accomodation of N protofilament MTs	15
2.3	Amino acid sequences of tubulin	27
2.4	The naturally occuring amino-acids	28
2.5	Localization and Homology of β -Tubulin	29
3.1	Biological Processes and Associated Energy Conversions	52
6.1	Conductivity comparison of tubulin polymers	169
7.1	Force-field parameter set comparison	178
7.2	Tubulin's Electrostatic Properties	180

List of Figures

2.1	Generalized animal cell	5
2.2	Filamentous actin	8
2.3	Major arrangements of actin filaments	9
2.4	Diagram of an intermediate filament	10
2.5	Diagram of a typical microtubule	12
2.6	The 13A and 13B microtubule lattices	14
2.7	Growth of an individual microtubule	19
2.8	Typical neuron with its microtubules	23
2.9	Diagram of the $\alpha\beta$ -tubulin dimer	25
2.10	“Ram’s horns” conformational change	32
2.11	Patterns of MAP attachment	34
2.12	Attachment of τ MAP	35
2.13	Motor protein ‘walking’ along MT protofilament	39
3.1	Valence and conduction band picture of two organic materials . .	60
3.2	Association of a metal ion or proton to a peptide	65
3.3	Proton ferries electron between donor and acceptor sites	66
4.1	Directions on the outer surface of a MT	77
4.2	Schematic diagram of energy variation with polarization	81
4.3	Nearest neighbour interactions in the A and B lattices	83
4.4	Ground states of MT 13A and 13B Lattices	88
4.5	Electric polarization and correlation functions of the MT 13A lattice	88
4.6	Electric polarization and correlation functions of the MT 13B lattice	89
4.7	Polarization of the MT 13A lattice subject to electric fields	91
4.8	Low energy configurations of MT 14A and 14B lattices	93
4.9	Long range correlation function of the MT 13A lattice with MAPs	95
4.10	MTs being drawn into the centrosome during mitosis	100
4.11	Electric fields induced by an action potential	101
5.1	Flip-flop problem solution	113
5.2	MT simulation figures	115
5.3	An action potential moving along an axon	118

LIST OF FIGURES

6.1	Potential energy profile along a protofilament	127
6.2	Bound state energy variation with quantum well depth	130
6.3	Form of the lowest energy bound state wave functions in 1D	131
6.4	Energy of the itinerant states as a function of U/t	136
6.5	Singlet states for two electrons on two sites	138
6.6	Optical conductivity of the two dimer, two electron system	149
6.7	Optical conductivity of the two dimer system with two, three and four electrons	150
6.8	Optical conductivity of the three-dimer system	152
6.9	Integrated conductivity of the three-dimer system	152
6.10	Optical conductivity spectrum variation with broadening parameter	154
6.11	Optical conductivity spectrum variation with temperature	154
6.12	Threshold to conduction as a function of protofilament length . .	155
6.13	Kinetic energy per electron as a function of system size	156
6.14	Lattice units for conductivity calculations	158
6.15	Optical conductivity of the tubulin sheet ($t_r = 0$)	160
6.16	Integrated conductivity of the tubulin sheet ($t_r = 0$)	160
6.17	Optical conductivity of the unwrapped 14-site lattice while $t_l = 0.4$	161
6.18	Integrated conductivity of the unwrapped 14-site lattice while $t_l =$ 0.4	161
6.19	Optical conductivity of the 14-site MT A lattice	163
6.20	Integrated conductivity of the 14-site MT A lattice	163
6.21	Optical conductivity of the 14-site MT B lattice	165
6.22	Integrated conductivity of the 14-site MT B	165
6.23	Comparison of the optical conductivity of the tubulin sheet with the MT A lattice and MT B lattice	167
6.24	Comparison of the integrated conductivity of the unwrapped MT lattice with the MT A lattice and MT B lattice	167
7.1	Polarizability illustration	176
7.2	Folding of the carboxy-terminus of the tubulin dimer	179
7.3	Lines parallel to the protofilament axis along which the electro- static potential was examined	181
7.4	Electrostatic profile along tubulin's exterior (1)	182
7.5	Electrostatic profile along tubulin's exterior (2)	182
7.6	Electrostatic profile along tubulin's exterior (3)	183
7.7	Electrostatic profile along tubulin's exterior (4)	183
7.8	Electrostatic profile along tubulin's exterior (5)	184
7.9	Electrostatic profile along tubulin's exterior (6)	184
7.10	Electrostatic profile along tubulin's exterior (7)	185
7.11	Electrostatic profile along tubulin's exterior (8)	185

LIST OF FIGURES

7.12 Protofilament-protofilament interaction	187
7.13 Comparing β_2 -tubulin with β_1 -tubulin	190
7.14 Methylation of α -Lys394	192
7.15 Substitution of alanine for β -Pro287	194
7.16 Catastrophe event reaction scheme	200

Chapter 1

Introduction

Microtubules are a component of most eukaryotic cells which have come under close scrutiny in the last two decades. Over this period of time, the focus has shifted from a basic understanding of their structure, which remains somewhat contentious, to the study of their assembly and disassembly processes and more recently to their secondary functions. The primary function of these biological polymers has long been known to provide support for the structure of the cell and to provide a railroad for motor proteins that crawl along the surface of microtubules and distribute organelles and vacuoles within the cell. They are also required for the separation of chromosomes during mitosis (cell division) when microtubules form the spindles that attach to pairs of replicated chromosomes and carry them to opposite ends of the cell. Microtubules are also the major structural constituent of axons, cilia and flagella which are responsible in specialized cells for signalling, cell motion and cellular locomotion.

The study of microtubules is an interesting problem to the physicist because of the physical properties of the microtubule. The microtubule is a dynamic polymer that undergoes growth and shrinkage nearly continually. In addition, in a process known as *dynamic instability*, individual microtubules of a cell may be in a growth phase coincident with other microtubules that are undergoing a period of shrinkage. The polar nature of the microtubule and its specialized

organization within various cell types also make it interesting. Despite properties such as the cylindrical geometry and the two-dimensional lattice of tubulin subunits that seem to simplify the microtubule riddle, the polymer is bathed in a sea of ions, lipids, peptides, sugars and water. This complex environment influences the physics in ways which can at best be either estimated or crudely approximated.

In the last ten years, there has been great speculation about the possible role of microtubules in processes as varied as information processing, electrical conduction, signal propagation and even consciousness. The work in this thesis looks at the physical logistics of these processes in an examination of whether they are feasible. It also makes predictions on the conductivity properties of microtubules and outlines the requirements on the tubulin protein for several physical processes to be possible. It does not propose that these processes actually occur within the cell. However as experimental investigations into these matters continue, it will be very interesting to see whether signal transduction and charge conduction are possible.

This thesis will introduce the reader, whose background is assumed to be in physics, to some elementary cell biology as necessary conceptual background. The structure of microtubules and their dynamics will then be reviewed before their electrical properties are examined. The interaction between the dipoles of neighbouring tubulin dimers will be considered to determine whether information processing or storage is possible in microtubules. I shall be particularly interested in axonal microtubules which are in parallel alignment with uniform polarity and which are able to interact with the transient electric field of nerve impulses. The response of these axonal microtubules to such fields will be quantified by considering the electric dipole of these molecules. The ability of microtubules to carry a current will then be studied using a Hubbard model of electron hop-

ping. The microtubule is amenable to such modelling since it is polymeric and we know that each dimer exists in at least two conformational states when a part of the microtubule. When the tubulin dimer changes its conformational state, the charge configuration is altered and the associated dipole also changes. The change in molecular geometry necessarily changes the local environment of charges and consequently its potential energy.

Very recently, an atomic picture of tubulin has been produced allowing for the first time a look at one conformation of this elusive protein. This thesis shall also examine this structure to predict physical properties which could be only heretofore estimated from the secondary structure. Finally, this thesis endeavours to show how principles of physics can be successfully applied to biological materials and somewhat the converse, that organic materials may lead to new experimental, theoretical and applied physics.

Chapter 2

Cellular Biology Background

Arguably, some of the most interesting biological work focuses on cellular and subcellular biology. Specifically, there is a strong desire to understand the mechanisms underlying life-giving and life-sustaining processes. Whether it be energy production from food sources, DNA replication, protein folding, intracellular signalling, cellular locomotion, cellular division or a host of other essential functions; the cell has the responsibility of performing these tasks and co-ordinating its efforts with those of other cells.

The fluid contents of a cell are known as the cytoplasm. Contained within the cytoplasm are certain smaller compartments known as organelles which are specialized to perform their respective functions. For the purpose of this thesis, only two of the cellular constituents are relevant: the cytoskeleton and the cytoplasm. Each of their respective properties shall be elaborated upon in this chapter. As mentioned above, the cytoplasm is the liquid medium bound within a cell, while the cytoskeleton is the lattice of filaments formed throughout the cytoplasm. Figure 2.1 illustrates a generalized animal cell in cross-section, complete with common organelles such as the nucleus that contains the genetic material, the mitochondria that produce readily accessible energy for the cell, the ribosomes that build protein molecules and the elements of the cytoskeleton. It should be noted that for clarity, this diagram has been substantially simplified and a

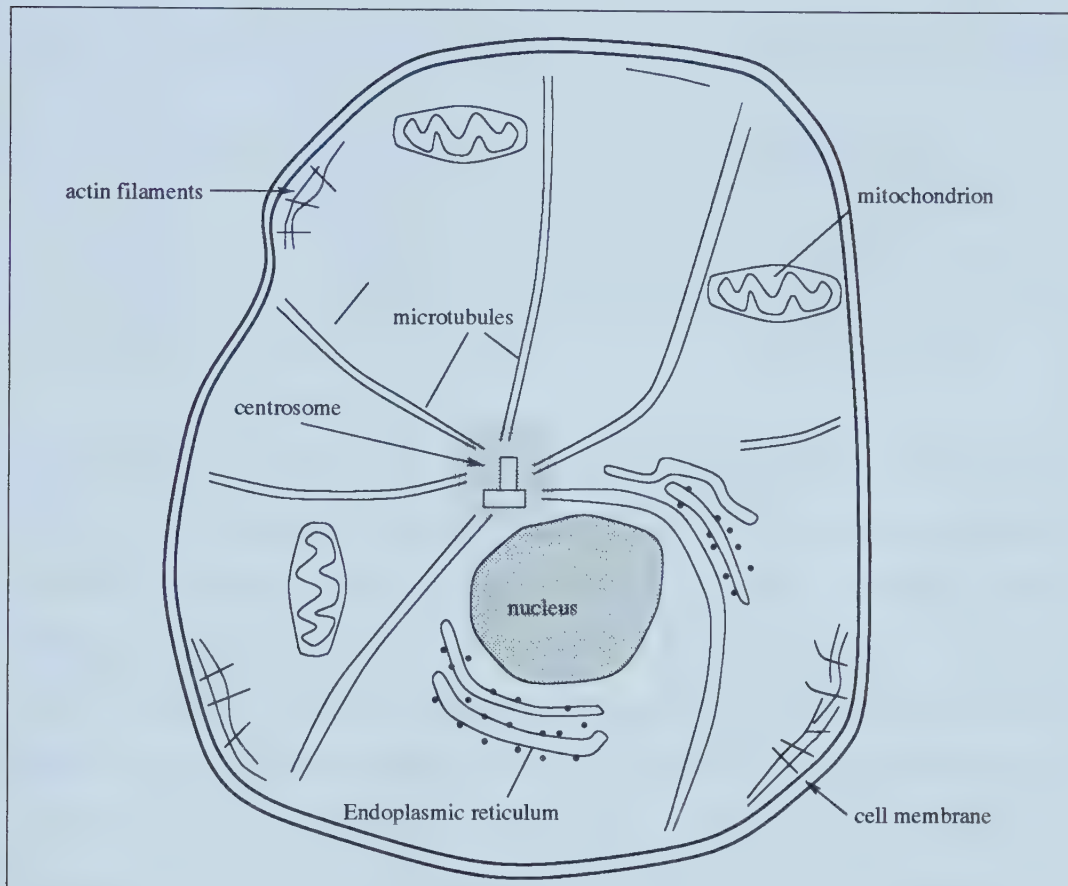


Figure 2.1: A generalized animal cell during interphase depicting the major cellular organelles including the nucleus, centrosome and radiating microtubules. The endoplasmic reticulum is dotted with ribosomes.

realistic depiction of the cytoskeleton would completely fill the cell.

2.1 The Cytoplasm

The cytoplasm is incredibly important because it provides the medium in which fundamental biophysical processes such as cellular respiration take place. Its properties are somewhat different than those of dilute aqueous solutions. The contents must be accurately known for *in vitro* study of enzymatic reactions, protein synthesis and other cellular activities. Typical constituents of the cytoplasm are listed in Table 2.1 [1]. Most cells maintain a neutral pH and their dry matter is

Table 2.1: Major Components of Cytoplasm in a Typical Mammalian Cell

Ions	Concentration	Non-ionic constituents	
K^+	140 mM	protein	200 – 300 mg/mL
Na^+	10 mM	actin	2 – 8 mg/mL
Cl^-	10 mM	tubulin	4 mg/mL
Ca^{2+}	0.1 μ M	pH	~ 7.2
Mg^{2+}	0.5 mM		

composed of at least 50% protein. The remaining dry material consists of nucleic acids, trace ions, lipids and carbohydrates. Most of the trace ions in the table are positively charged, however the cytoplasm cannot have any overall charge, the difference is made up of the other constituents such as proteins, bicarbonate (HCO_3^-), phosphate (PO_4^{3-}) and other ions which are for the most part negatively charged, a few of which are significantly electronegative. A few metallic ions are found which are required for incorporation into metallo-proteins but these ions such as iron(II) (Fe^{2+}) are typically found in nanomolar concentrations.

There is mounting evidence for the existence of two phases of the cytoplasm [2]. These are the so-called liquid and solid phases, sol and gel, respectively. In the solid phase, the major constituents of the cell are rendered immobile while in the liquid phase, the cytoplasm's viscosity does not differ significantly from water [2]. Diffusion within the cytoplasm is affected mainly by macromolecular crowding. In the solid phase, diffusion is slowed by a factor of three relative to diffusive movement in water. Such properties of the cytoplasm seem to be regulated in some sense by the cytoskeleton, but the manner by which this regulation is accomplished is unclear. It is believed that it involves the tangling and detangling of a mesh of various protein filaments [3, 4]. The important point is that once the cell has acted to organize itself, the transition to a solid phase can allow it to spend relatively minimal energy to maintain its organization.

2.2 The Cytoskeleton

The cytoskeleton is composed of three classes of filamentous protein: microfilaments, intermediate filaments and microtubules [1]. There has been some suggestion that another smaller class of cytoskeletal filaments exists but as yet there is no experimental evidence to support this claim [2]. Unlike the hardened skeleton that supports mammals such as humans, the cytoskeleton is a dynamic structure that undergoes continuous reorganization. The cytoskeletal network of filaments has the responsibility of defining the cell shape, protecting the cell from changes in osmotic pressure, organizing its contents, providing cellular motility and finally is responsible for separating chromosomes during mitosis.

Cell shape is regulated by a complex balance of both internal and external forces exerted by the extracellular matrix. This balance has been described by Ingber [5] and is known as tensegrity. Contractile actin bundles act as molecular cables. These cables exert a tensile force on the cell membrane and the internal constituents of the cell, pulling them all towards the nucleus. Microtubules act as struts that resist the compressive force of the cables. In many cases, it is important to maintain the cell's shape to preserve its functionality. Chen et al. [6] have shown by experiment how cells switch between genetic programs when forced to grow into specific shapes, while King and Wu [7] have shown on theoretical grounds how the cell geometry changes the susceptibility of the cell to electromagnetic fields.

The separation of chromosomes is accomplished by the cytoskeleton's largest constituents, the microtubules. During mitosis, microtubules connect to each of the chromosomes and align them along the cell's equatorial plate. A mysterious balance of forces prevents the microtubules from separating the chromosomes until all the chromosomes have become aligned and division may proceed in unison. We discuss these aspects of cytoskeletal behaviour by considering microtubule

sensitivity to electric fields and the role of microtubules in cellular signalling.

2.2.1 Microfilaments

Microfilaments have the smallest diameter of all the cytoskeletal threads and are the most common. They are composed of a protein known as actin and consequently are often referred to as actin filaments. Actin is not only found within all eukaryotic species, but in many cells it is the most abundant protein [1]. Filamentous actin, or F-actin, is a polymer of the protein known as globular actin or G-actin. These strands are capable of forming both stable and labile components within cells. The polymerization of F-actin from G-actin is a largely monotonic process that is dependent on ATP. The F-actin assembles according to a standard nucleation, elongation mechanism. Once assembled, microfilaments have a diameter of about 8 nm (Figure 2.2). Microfilaments are found linked

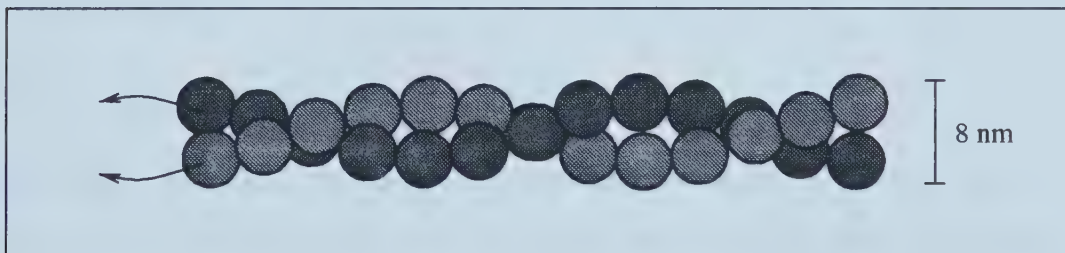


Figure 2.2: The 2-stranded helix of an actin-filament. Each of the F-actin strands has a polarity indicated by the arrows (each sphere represents a monomer of G-actin).

together by actin-associated proteins and congregate into one of three major forms (Figure 2.3). The polymerization dynamics and filament organization of actin has been modelled by Edelstein-Keshet et al. [8, 9]. In the configuration of parallel strands, microfilaments often form the core of microvilli, while in an anti-parallel arrangement, actin may act in conjunction with myosin to bring about muscle contraction in the presence of ATP. Microfilaments are often found with the lattice configuration near the leading edge of growing or motile cells where

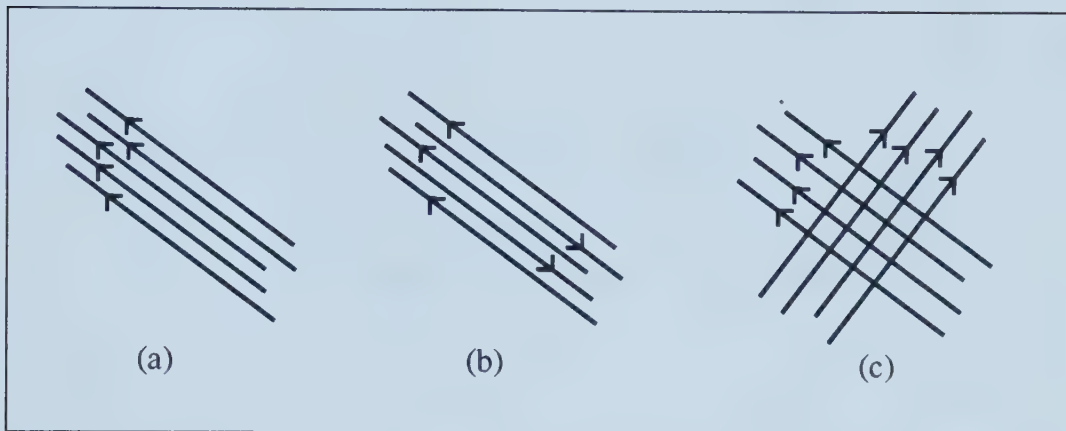


Figure 2.3: The three main arrangements of microfilament aggregation which form with the aid of actin-crosslinking proteins: (a) parallel bundles, (b) contractile bundles and (c) gel or lattice like arrangement.

they provide greater stability to the newly formed region. New actin filaments are nucleated at the leading edge of the cell's growth and trailing microfilaments are disassembled [1, 10].

2.2.2 Intermediate Filaments

Intermediate filaments have a diameter of about 10 nm and are formed by the polymerization of elongated fibrous protein molecules such as vimentin, keratins, desmins and the nuclear lamins. These molecules are quite unlike the globular molecules, tubulin and G-actin, that form microtubules and microfilaments, respectively. These protein molecules form dimers through an anti-parallel association of two molecules which has a coiled-coil configuration. Consequently, intermediate filaments are non-polar structures. Two dimers associate to form a symmetrical tetramer as depicted in Figure 2.4. The overlap between dimers allows for the filaments to stretch and, as a result, intermediate filaments are able to withstand large stresses without breaking [1]. The main role of intermediate filaments seems to be related to their structural strength. An extensive network of intermediate filaments surrounds the nucleus forming what is known as the

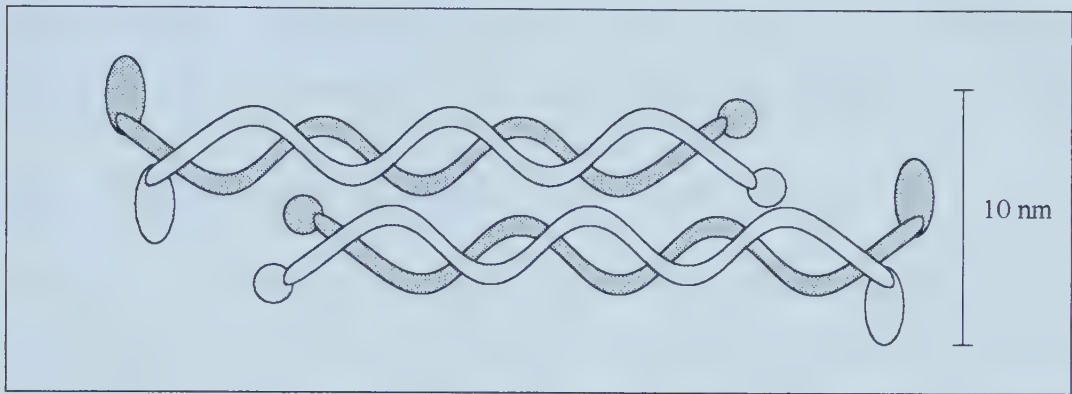


Figure 2.4: Schematic of an intermediate filament. The filamentous protein tetramer is non-polar and composed of two coiled-coil dimers.

nuclear envelope. The formation and disassembly of the nuclear lamina is regulated by phosphorylation. This allows for the elimination of the nuclear envelope prior to mitosis. The filaments also extend out into the cell periphery where they act to maintain cell integrity and may connect with the cell membrane [1]. Specific cells, such as neurons, have their own distinctive intermediate filaments, known as neurofilaments.

2.2.3 Microtubules

Microtubules (MTs) are the filaments of the cytoskeleton with the largest diameter, 25 nm. They are found in nearly all eukaryotic cells and are polymers of tubulin protein. MTs serve as tracks on which motor proteins may carry materials about the cell and serve as scaffolding to maintain the cell shape since they are among the most rigid structures within a typical cell. They also form the core of cilia and flagella which beat in a co-ordinated manner to either move objects along the cell membrane or to propel the cell through its environment. Within the cell body, the majority of the MTs emanate from a centriole. The negative ends of MTs are anchored at these microtubule organizing centres. The MTs *in situ* are interconnected and intraconnected by microtubule associated

proteins (MAPs). MAPs have a stabilizing effect on the dynamics of MTs. The versatility of MT function is examined in this thesis from a physical viewpoint.

2.3 Structure of Microtubules

Ledbetter and Porter [11] were the first to describe these tubules found within the cytoplasm and dubbed them both cytotubules and microtubules. The name microtubules has stuck and the general structure of the MT has since been well-established by light microscopy, immunofluorescence and cryoelectron microscopy [10, 12]. MTs are polymers formed from two largely homologous globular proteins, α -tubulin and β -tubulin. These two proteins are very closely structurally related and they bind together to form a heterodimer known as $\alpha\beta$ -tubulin. This dimer is the basic subunit which polymerizes to form the MT. The MT is a hollow tube with an outer diameter of 25 nm and an inner diameter of 15 nm (Figure 2.3). The tube is composed of strongly bound linear polymers, known as protofilaments, that are connected via weaker lateral bonds to form a sheet that is wrapped up to form a tube. We model the tubulin molecules as cylinders 5 nm in diameter and 8 nm in height. For simplicity, the dimer will be graphically represented by two equally sized spheres representing the α and β -monomers, respectively (Figure 2.6). The electron crystallography of Nogales et al. [13] has indeed shown that the α and β monomers are nearly identical. However, this small difference on the monomer level allows the possibility of several lattice types. In particular, the so called MT A and B lattices. Moving around the MT in a left-handed sense, protofilaments of the A lattice have a vertical shift of 4.92 nm upwards relative to their neighbours. In the B lattice, this offset is only 0.92 nm because the α and β monomers have switched roles in alternating protofilaments. This change results in the development of a structural discontinuity in the B lattice known as the seam. The lattice types and defects associated

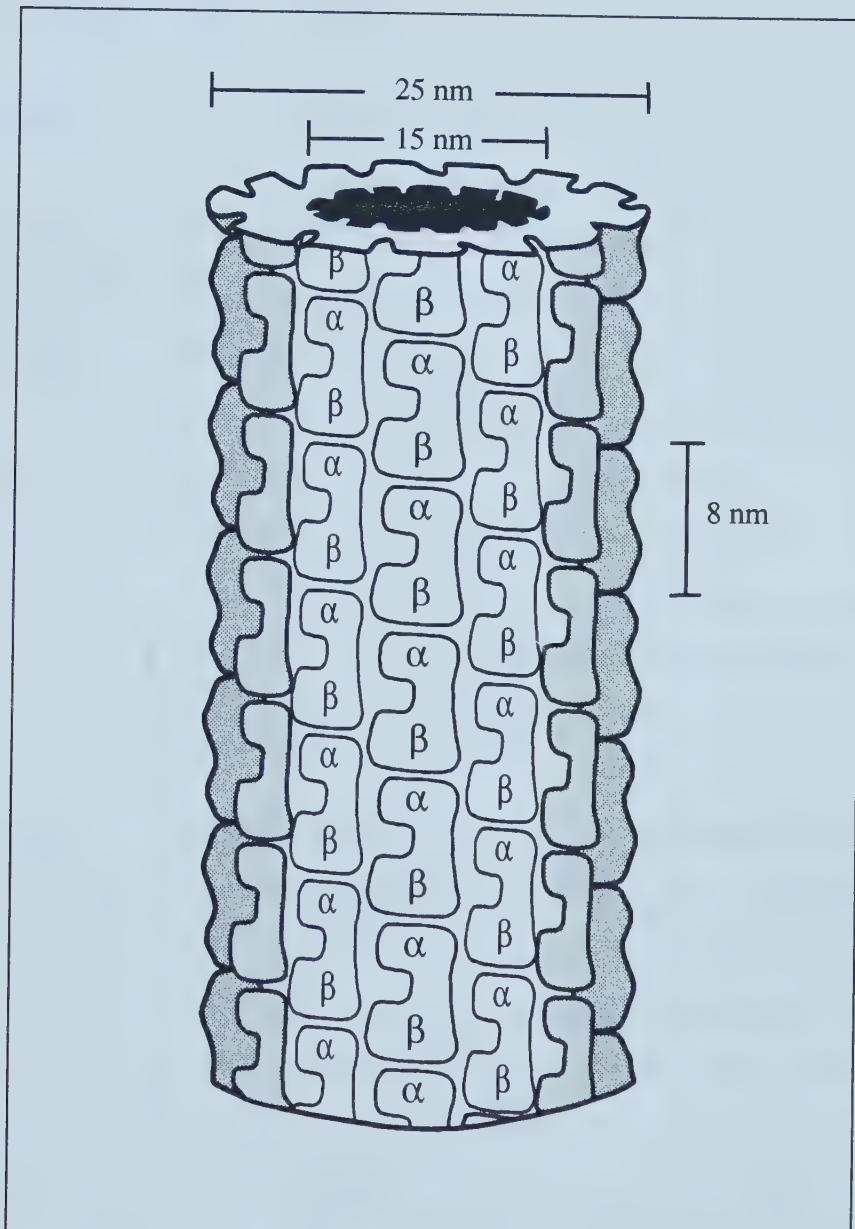


Figure 2.5: A section of a typical microtubule demonstrating the hollow interior which is filled with cytoplasm, the helical nature of its construction. Each vertical column is known as a protofilament and the typical MT has 13 protofilaments.

with the MT are discussed below.

2.3.1 Microtubule Lattices and Defects

The MT lattice has been vigorously studied over the past twenty years. In that time, two different lattices have been observed which have become known as the A lattice and the B lattice [12, 14]. The distinction between these lattices can be determined with reference to Figure 2.6. Focus on the gently rising helix which climbs the lattice in a left-handed fashion. In an A-lattice, one alternates between α and β subunits along this helix while in a B-lattice MT, the subunits are the same along this helix. In addition to lattice variation, it is also known from experimental observation that the number of protofilaments is variable from one MT to another. Although 13 protofilaments is by far the most common *in vivo*, Chrétien et al. [15] have observed that the protofilament number need not be conserved along the length of an individual MT. This leads to the emergence of a structural defect.

MTs with an A lattice and an odd number of protofilaments are distinguished from all other lattices because they are the only ones without a structural discontinuity known as a seam. In all other lattices, a seam exists where the interactions are mixed. That is to say that there are both A and B type lattice interactions in a single MT. The convention for describing MTs throughout will be of the number of protofilaments followed by the lattice type such as 13A or 14B. In Figure 2.6, the 13A and 13B lattices types are compared. On the left side of the figure, the MT lattice is shown unwrapped for clarity so that the difference between an A type and B type lattices may be understood. At the seam of the B lattice, which is indicated, the geometry is the same as that for the A lattice.

These lattice variations pose a modelling problem since MTs other than the 13A variety lack helical symmetry and possess a seam. If the screw angle of

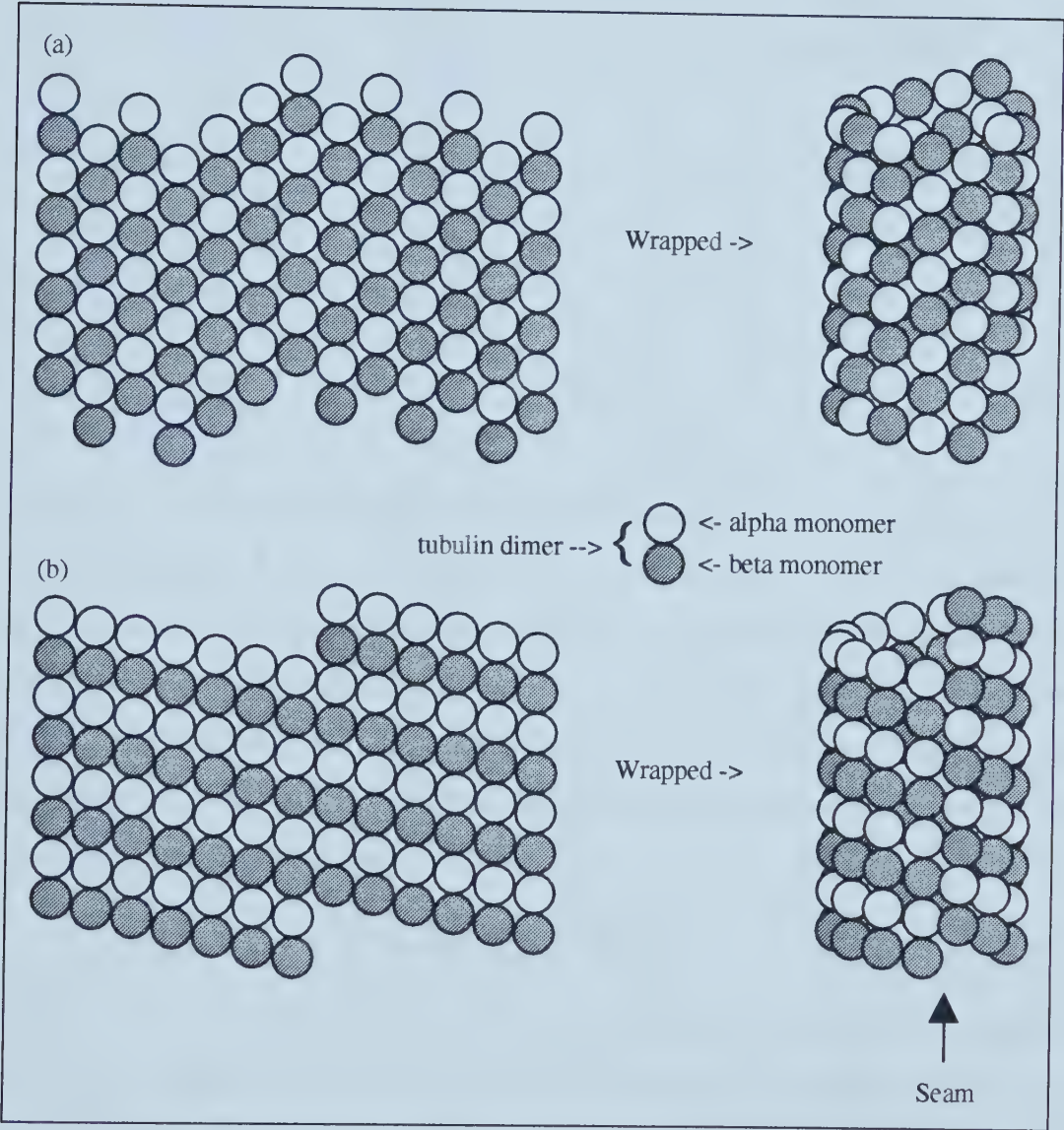


Figure 2.6: The 13A and 13B MT lattices: (a) in the A lattice, perfect helical spirals are formed. (b) in the B lattice, there is a structural discontinuity known as the seam.

Table 2.2: Accomodation of N protofilament MTs by the Wade and Chrétien [12, 16] model (skew angles) or by anomalous stretches between protofilaments

Protofilament Number	Skew Angle	Vertical Stretch (nm)	Single Stretch (nm)
9	0.38 °	-0.03	0.31
10	1.37 °	-0.12	1.23
11	-1.87 °	0.17	-1.85
12	-0.86 °	0.08	-0.92
13	0.00 °	0.00	0.00
14	0.73 °	-0.07	0.92
15	1.37 °	-0.12	1.85
16	-0.86 °	0.08	-1.23
17	-0.20 °	0.02	-0.31

the helix is maintained, the addition of a protofilament results in a mismatch at the seam where neither pure A nor B type interactions result. To preserve the symmetry of the lattice, the MT structure might adapt in two ways which have been examined by Wade and Chrétien [12, 16]. Their lattice accomodation theory allows for the protofilaments to become skewed relative to the MT axis. The degree of rotation, θ , away from parallel to the protofilament axis may be found by a simple geometrical analysis.

$$\tan \theta = \left(\frac{3}{13} - \frac{S}{N} \right) \left(\frac{a}{\delta x} \right) \quad (2.1)$$

where S is the start number of helices, N is the number of protofilaments, a is the monomer spacing (4.00 nm) and δx (5.15 nm) is the width of the tubulin molecule. The corresponding rotation is minimized for a MT of between 11 and 15 protofilaments when the start number, $S=3$. For a MT of 9 or 10 protofilaments, $S=2$ and for a MT of 16 or 17 protofilaments, $S=4$. The skew angles are easily computed and are listed in Table 2.2. These tiny skew angles allow the MT lattice to be strained minimally. The alternatives to allowing protofilaments to have small skew angles, relative to the vertical, is to deal with the mismatch of

0.92 nm (=3 helices x 4 nm / 13 protofilaments) for each unit deviation from 13 of the protofilament number, in another manner. Either the mismatch is spread evenly over all of the protofilaments, leading to an anomalous vertical stretch for such MTs; or else the entire mismatch is accomodated at the seam [17]. The values of these stretches are tabulated in Table 2.2 for MTs of between 9 and 17 protofilaments. The former possibility would presumably place a great deal of strain on the lattice. The lateral bonds between protofilaments would surely be weakened relative to the bond strength in the normal 13 protofilament MT. The latter possibility however, seems unattractive in our regard. If a seam with a longitudinal shift of several different sizes can be accomodated at one location of the MT, it would seem to be only consistent to allow a random sized longitudinal shift between all protofilaments. Such a possibility has been claimed by Sosa and Mulligan [18] whose back projection from X-ray crystallography of ncd-decorated microtubules showed evidence of more than one seam in many MTs. However, if the many differently sized shifts are possible, the bonding between protofilaments at the seam would presumably be very weak and one would have to believe that the contacts are neither covalent nor hydrogen bonds but simply hydrophobic bonds. The picture of binding between protofilaments is one in which they could almost slide past each other. Such behaviour, although predicted by Semënov [19], seems improbable and has never been observed. The idea that protofilaments have such flexible connections would explain how they can form with an anti-parallel alignment in the presence of zinc ion (Zn^{2+}). The zinc ion must simply pick out one orientation for hydrophobic bonding which is now favoured, anti-parallel versus parallel so long as the hydrophobic regions remain buried.

This model of MT assembly where the protofilament binding consists largely hydrophobic bonds is useful to explain MTs that appear to assemble as a sheet

before ‘zipping’ up along the seam and behind the assembly edge [20]. If the bonding were of a stronger and more specific type, it is difficult to imagine how this process could occur. However, the abundance of crystallographic results supports helical symmetry for the MT structure and stands against the possibility of completely arbitrary protofilament shifts. Still, the nearly identical α and β subunits make it difficult to reject structures such as the B lattice which maintains helical symmetry on the monomer level, but which fails to have true helical symmetry on the dimer level. Rather than having to propose complex changes to the MT structure, a small skew angle of less than 2.0° for microtubules with between 9 and 17 protofilaments or a consistent longitudinal offset between protofilaments is much more pleasing since very little strain is placed on the lattice. The evidence for a protofilament skew angle comes from the moiré patterns of Wade and Chrétien [12, 16]. These images gathered by cryo-electron microscopy are able to examine the periodic twist in MTs which do not have 13 protofilaments since the MT acts like a classical many-slit apparatus when imaged. As MTs with 13 protofilaments have protofilaments parallel to the axis of the MT, the pattern of light and dark bands remains constant along the length of the MT; but for those MTs with alternative numbers of protofilaments, the small skew angle gives rise to a periodicity in the light and shaded regions along the MT.

Our theoretical modelling considers MTs of various lattice types but does not allow for variation of the lattice type or protofilament number along the length of an individual MT. However, the models which are investigated do attempt to link dynamic instability to MT function. The idea of connecting the assembly process with the self-organization process of the dipole lattice is to explore how such a connection may explain the puzzling ensemble dynamics of microtubules grown *in vitro*. This is not so interesting for the information processing model

since we believe that only stable microtubules would be important in this regard.

2.4 Microtubule Assembly

As with virtually all aspects of microtubules, there is some controversy over their dynamics. Let us begin with the facts as determined by experiment. MTs are polar polymers formed by the association of tubulin dimers. When an individual MT is observed, it undergoes periods of almost steady growth interrupted by brief periods of very rapid shortening as illustrated in Figure 2.7. The transition from a growth period to a shortening period is known as a catastrophe event while the reverse is known as a rescue. The assembly dynamics at each end of the MT differ. The so-called plus end is between three and five times as dynamic as the negative end. That is to say that both the growth and shortening of the positive end of the MT occur at rates at least three times those of the negative end but both ends are dynamic in free MTs. Beyond the individual MT assembly dynamics are the ensemble dynamics and the property of their assembly known as *dynamic instability* [21, 22, 23]. What is intriguing is how the stochastic individual behaviour may result in smooth collective oscillations observed to take place at high tubulin concentrations [24, 25]. The answer is given simply by the application of statistical mechanics to ensemble averaging. A complete explanation of the above requires an application of the master equation formalism [26, 27] or alternatively, the use of chemical kinetics [28].

2.4.1 Individual Microtubule Assembly

As mentioned above, the assembly dynamics for an individual MT are stochastic. The rate of shortening is about ten times the rate of growth [29, 30] and a stochastic model may be developed to study individual MT growth. The probability of a single MT nucleating, growing, shortening and so on, depends on

the local concentration of tubulin with bound GTP, tubulin with bound GDP and other molecules relevant to the assembly process which are found within the cytoplasm. Many theoretical models have successfully reproduced the single MT growth behaviour such as that illustrated in Figure 2.7. The challenge is

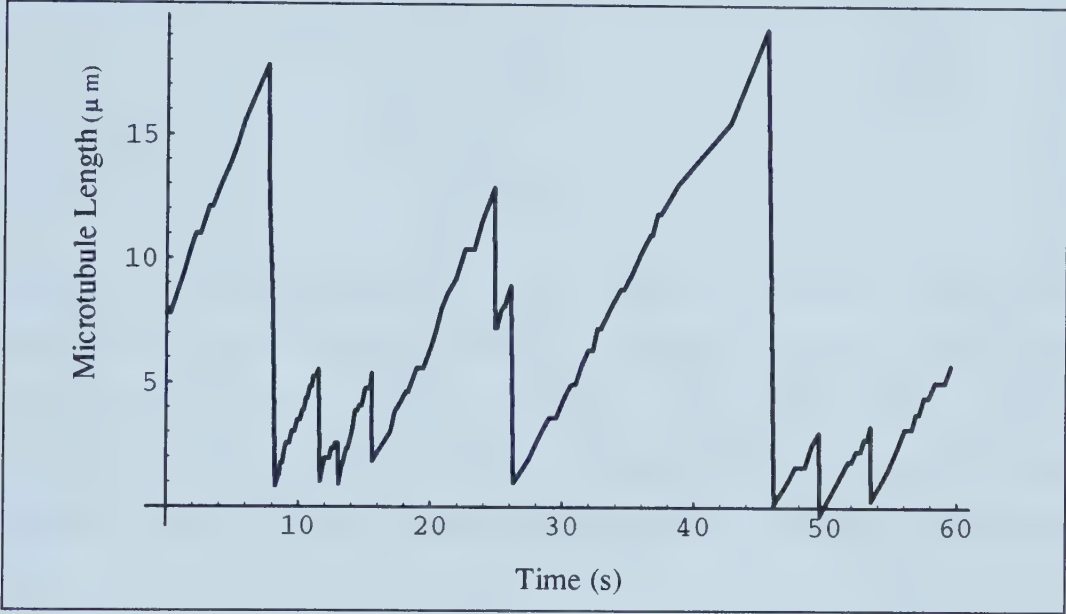


Figure 2.7: The growth of a single microtubule is erratic. Slow, steady growth is interrupted by large catastrophe events at about 8 s and 46 s while a rescue event occurs between two catastrophe events at about 26 s.

to use the same model to explain ensemble dynamics and dynamic instability; and in addition, to explain changes in the dynamics when reaction conditions are altered. Suppose the length of our MT is given by the value of the variable, x , at an instant of time, t . Now, if we discretize the time variable, we want to write a recursion formula for the length of the MT. In the simplest model, there are only two possibilities, the addition of a subunit or the complete collapse of the structure. Addition of a subunit may be modelled as follows:

$$x_{t+1} = x_t + a \quad (2.2)$$

where a is the subunit length. Complete collapse of the microtubule is simply modelled using:

$$x_{t+1} = 0. \quad (2.3)$$

Now suppose that the probability of the addition of a tubulin subunit is p , then

$$x_{t+1} = r(x_t + a) \quad (2.4)$$

where

$$r = \begin{cases} 0 & \text{if } s > p \\ 1 & \text{if } s \leq p \end{cases} \quad (2.5)$$

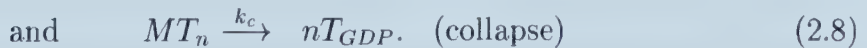
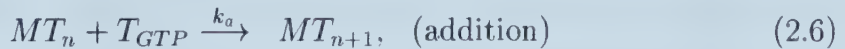
and s is a random number between 0 and 1. Even a crude model such as that just described may successfully capture the essential dynamics of MT growth when compared by Hurst analysis or a recursive map technique [31]. However, it lacks any predictive power given that individual collapse events are random. However, the ability to make predictions returns when collective dynamics are studied.

2.4.2 Dynamic Instability, Ensemble Dynamics

When an aggregation of MTs is studied, some collective properties develop. The most obvious behaviour is the phase transition behaviour of the system in that certain conditions lead to overall disassembly and largely a pool of tubulin dimers, while other conditions promote self-assembly of tubulin in MTs. Phases of MT polymerization are determined largely by the temperature and concentration of tubulin. For a given temperature, some critical concentration of tubulin is required in order to keep MTs from disassembling. Fygenson et al. [32] have discussed this phase transition and Sept [31] has further classified the non-disassembly phase into one where MTs assemble but are not nucleated and one where MTs are both nucleated and assembled. For a collection of MTs in an assembly phase, dynamic instability is the term given to the observation that

MTs are growing in the immediate vicinity of other MTs which are shortening. Dynamic instability has been observed *in vivo* and *in vitro* and highlights both the non-equilibrium nature of the problem and the stochastic nature of individual MT growth. Despite these observations, ensembles of MTs show collective oscillations given suitable conditions. Specifically, when the concentration of assembled tubulin is measured, it is observed to undergo smooth oscillations which are damped out as the energy source of GTP, is depleted. Sept et al. [28] have modelled the assembly dynamics from a chemical reaction-kinetics standpoint and has found good agreement with the experimental data.

The principal elements in the Sept et al. model can be summarized by the equations which follow. For simplicity, the MT is considered as a linear polymer rather than an object of 13 protofilaments. We shall denote a MT of length n subunits by MT_n . Note that in solution, the free tubulin subunits may be bound to either GTP or GDP at their exchangeable nucleotide site and shall be denoted T_{GTP} and T_{GDP} , respectively, only tubulin bound to GTP is able to polymerize. The simple reaction set consists of addition, nucleation and catastrophic collapse:



For simplicity, we have again assumed that all collapses are complete and to keep the model of MT assembly simple, one normally selects a specific number of dimers, n' , that will be required for nucleation. The exact value of this choice does not seem to have a large impact on the dynamics as long as it is relatively small. The first of the preceding equations is reversible and a rate constant for the back reaction is considered in general. This is not required for this discussion. These equations can also be supplemented by the reactivation of tubulin, to make

it assembly competent, which will occur when the concentration of GTP is high:



The free energy change associated with this reaction is less than the free energy change of GTP hydrolysis in solution and the difference is attributed to a structural change in the tubulin dimer. It is this conformational change which presumably makes assembly possible. The rate constants of these reactions, k_j , should also be in agreement with the probabilities assigned to corresponding reactions in the individual MT model. Furthermore, temperature dependence can be built into the rate constants using empirical data on the free energy of reactants and products. When at least one auto-catalytic reaction is added to the system, to provide a non-linear element, the dynamics change significantly. Consider an induced catastrophe event,



incorporated into the model, this reaction has been able to reproduce oscillations observed *in vitro* caused by either temperature jumps or the injection of GTP into the system. It also identifies domains where tubulin is incorporated into MTs steadily and regimes where disassembly is favoured. In addition, the model can reproduce the spatial pattern of MT assembly which are observed within cells simply by including a diffusive term in the equations of the assembly dynamics. This allows the model to be compared to the experiments performed independently by the Tabony [33] and Mandelkow [25] groups. Agreement has been found between this model and those empirical results. Generally, the statistical dynamics of MT assembly are now believed to be well understood except for the physical mechanism that triggers the catastrophes and the origin of the rescue events.

2.5 Neuronal Microtubules

The MTs of nerve cells (neurons) have a special arrangement. The arrangement is actually dependent on the location of the MT within the neuron. Nerve cells typically consist of an array of dendrites, a cell body which houses the nucleus and other organelles, and an axon which is a projection, often branched, that makes connections with other nerve cells or muscle cells. The dendrites are responsible

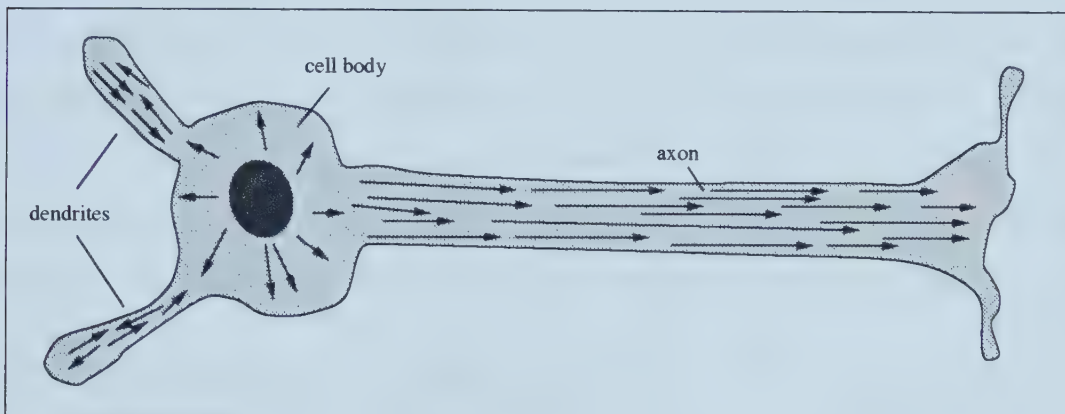


Figure 2.8: A neural cell is loaded with MTs. The orientation of the MTs is indicated by arrows in the figure. The actual cell body is much smaller relative to the cell extremities than depicted.

for receiving input from other neurons and the MTs found within them are not of uniform polarity. Their positive ends may lie directly away from or directly towards the cell body. Within the axon, that provides output to other neurons, the MTs are arranged in parallel bundles, uniformly directed with the plus ends pointing away from the cell body. The MTs within the axon are densely packed and have no mitotic function as nerve cells do not divide. Hence the abundance of these structures within an axon must be for structural support and possibly cell functions other than cell division such as signalling or material transport.

MTs run along the length of the axon right up to neural synaptic region. The synapse itself is the gap between a neuron and the second cell, either another

neuron or a muscle, that is signalled by the neuron in question. This signalling is accomplished through the release of a chemical, known as neurotransmitter, that diffuses across the narrow synaptic channel. What is interesting is the interplay between MTs and neurotransmitter release. While the action potential and the triggering of neurotransmitter release is largely a membrane event, calcium is known to be required to activate neurotransmitter release and similarly, the depolymerization of MTs has been shown to impair neurotransmission [34]. MTs were not originally believed to extend right up to the synapse but this was later shown to be an experimental artifact since some depolymerization of MTs normally occurred prior to imaging of an axon. The motor protein, dynein, has been shown to connect MTs directly to the synaptic membrane and provides an avenue for mechanical signalling [35] of neurotransmitter release by MTs.

2.6 Chemistry of Tubulin

Tubulin is quite an interesting protein. The tubulin that polymerizes to form MTs is actually a heterodimer of α -tubulin and β -tubulin. These two proteins are highly homologous and have 3D structures which are nearly identical. Although the similarity of α -tubulin and β -tubulin had long been suspected, the fact that tubulin has resisted crystallization for about 20 years prevented confirmation of this hypothesis until very recently. Nogales et al. [13] were able to perform cryoelectron crystallography on sheets of tubulin formed in the presence of zinc ion. A figure produced from the Nogales data, obtained from the protein data bank (PDB entry: 1tub), using MOLSCRIPT [36] makes clear the similarities between the two proteins. Each is composed of a peptide sequence more than 400 members long which is highly conserved between species. The amino acid sequences for these proteins may be compared given the data in Table 2.6 which lists the conventional one and three letter codes for the 20 naturally-occurring



Figure 2.9: A diagram of the tubulin molecule produced from the Nogales et al. electron crystallography data [13] shows the similarity between the α -subunit (upper half) and β -subunit (lower half). The stick outlines near the base of each subunit indicate the location of GTP when bound.

amino acids. Codes should be read from left to right and spaces are inserted each 10 residues for clarity. The sequences of a few representative samples of tubulin have been retrieved from the Swiss-Prot protein sequence database [37] and are shown in Table 2.3.

Based on the charge of the amino acid, the amino acids may be classified into 3 groups: those with a positive charge, those with a negative charge and the neutral residues. The size of the residue and its ability to react with other amino acids will affect protein folding and consequently function. The protein folding is known as tertiary structure. Public inspection of tubulin's tertiary structure has only been available since October of 1998, despite having sequences for several α - and β - tubulin isotypes from several species.

Mutations involve changes to the sequence of amino acid residues. This may occur by substitution, addition or deletion of one or more of the residues. If the change is for a residue with similar steric or electrostatic properties the mutated tubulin protein will likely fold properly and retain its function. However, a change that substitutes a residue whose properties differ substantially will likely result in a non-functional protein. Nevertheless, several different versions of the tubulin protein exist today and are known as isotypes when they exist within the same species. Both α -tubulin and β -tubulin appear in several isotypes. The isotypes are versions of these proteins which differ to a smaller degree than between the α and β variants. The different isotypes are expressed to varying degrees in specific cells types. For example, in humans, the β_2 isotype is found predominantly within neurons. Due to this localization of isotypes, there is suspicion that tubulin has adapted for specific functional reasons. There is also a third isoform family known as γ -tubulin. The γ species is found within the MT organizing centers and is important in the nucleation of new microtubules.

In addition to these differences in the structure of the tubulin monomers,

Human α_1 -tubulin amino-acid sequence (451 amino acids, 50157 Da)

```
MRECISIHVG QAGVQIGNAC WELYCLEHGI QPDGQMPSDK TIGGGDDSFN TFFSETGAGK
HVPRAVFDL EPTVIDEVRT GTYRQLFHPE QLITGKEDAA NNYARGHYTI GKEIIDLVLD
RIRKLADQCT RLQGFLVFHS FGGGTGSGFT SLLMERLSVD YGKKSLEFS IYPAPQVSTA
VVEPYSILT THTTLEHSDC AFMVDNEAIY DICRRNLDIE RPTYTNLNL IGQIVSSITA
SLRFDGALNV DLTEFQTNLV PYPRIHFPLA TYAPVISA EK AYHEQLSVAE ITNACFEPAN
QMVKCDPGHG KYMACCLLYR GDVVPKDVNA AIATIKTKRT IQFVDWCPTG FKVGINYQPP
TVVPGGDLAK VQRAVCMLSN TTAIAEAWAR LDHKFDL MYA KRAFVHWYVG EGMEEGEFSE
AREDMAALEK DYEEVGVHSV EGE GEEEGEE Y
```

Human β_1 -tubulin amino-acid sequence (444 amino acids, 49759 Da)

```
MREIVHIQAG QCGNQIGAKF WEVISDEHGI DPTGTYHGDS DLQLDRISVY YNEATGGKYV
PRAILVDLEP GTMDSVRSGP FGQIFRPDNF VFGQSGAGNN WAKGHYTEGA ELVDSVLDVV
RKEAESCDCL QGFQLTHSLG GGTGSGMGTL LISKIR EEP DRIMNTFSV PSPKVSDTVV
EPYNATLSVH QLVENTDETY CIDNEALYDI CFRTLRLTTP TYGDLNHLVS GTMECVTTCL
RFPGQLNADL RKLAVNMVPF PRLHFFMPGF APLTSRGSQQ YRALTVPDLT QQVFDAKNMM
AACDPRHGRY LTVA AVFRGR MSMKEVDEQM LNVQKNSSY FVEWIPNNVK TAVCDIPPRG
LKMAVTFIGN STAIQELFKR ISEQFTAMFR RKAFLHWYTG EGMD EMEFTE AESNMNDLVS
EYQQYQDATA EEEEDFGEEA EEEA
```

Human β_2 -tubulin amin-acid sequence (445 amino acids, 49831 Da)

```
MREIVHLQAG QCGNQIGAKF WEVISDEHGI DPTGTYHGDS DLQLERINVY YNEATGGKYV
PRAVLVDLEP GTMDSVRSGP FGQIFRPDNF VFGQSGAGNN WAKGHYTEGA ELVDSVLDVV
RKEAESCDCL QGFQLTHSLG GGTGSGMGTL LISKIR EEP DRIMNTFSV PSPKVSDTVV
EPYNATLSVH QLVENTDETY CIDNEALYDI CFRTLKL TTP TYGDLNHLVS ATMSGVTTCL
RFPGQLNADL RKLAVNMVPF PRLHFFMPGF APLTSRGSQQ YRALTVPELT QQMFDAKNMM
AACDPRHGRY LTVA AVFRGR MSMKEVDEQM LNVQKNSSY FVEWIPNNVK TAVCDIPPRG
LKMSATFIGN STAIQELFKR ISEQFTAMFR RKAFLHWYTG EGMD EMEFTE AESNMNDLVS
EYQQYQDATA EEEGEFEEEA EEVA
```

Table 2.3: The amino acid sequences of human α_1 -, β_1 - and β_2 -tubulin show a high degree of homology. The sequence is given along with the total number of amino acids and the molecular weight of the molecule.

1 Letter	3 Letter	Amino Acid	Polar	Charge
A	Ala	Alanine		
C	Cys	Cysteine	yes	
D	Asp	Aspartic Acid		$-e$
E	Glu	Glutamic Acid		$-e$
F	Phe	Phenylalanine		
G	Gly	Glycine		
H	His	Histidine		$+e^*$
I	Ile	Isoleucine		
K	Lys	Lysine		$+e$
L	Leu	Leucine		
M	Met	Methionine		
N	Asn	Asparagine	yes	
P	Pro	Proline		
Q	Gln	Glutamine	yes	
R	Arg	Arginine		$+e$
S	Ser	Serine	yes	
T	Thr	Threonine	yes	
V	Val	Valine		
W	Trp	Tryptophan		
Y	Tyr	Tyrosine	yes	

Table 2.4: The twenty naturally occurring amino-acids are listed along with their one and three letter codes as well as whether they have a polar character and whether they are charged. *Histidine has a pKa of 6.5 and consequently will be protonated and positively charged should the pH of the cytoplasm dip below this value.

they may undergo structural changes after being produced in the cell. These changes are known as post-translational modifications. These changes combined with various microtubule associated proteins (MAPs) that may bind to tubulin, change the functional properties of the assembled tubulin polymer.

2.6.1 Variation of Isootypes

In humans, six α isotypes and seven β isotypes of tubulin are found. Although the sequence of amino-acids is highly conserved overall, certain regions of α_1 -tubulin show divergence from α_2 -tubulin and so on. Recent studies have shown that the differences in α -tubulin are more subtle than those in β -tubulin [38]. Table 2.5 gives a comparison between the main β -tubulin isotypes in cows. The

Table 2.5: Localization and Homology of Bovine β -Tubulin

Isotype	Localization	Homology	Abundance in Brain (%)
β_1	everywhere, thymus	100.0	3
β_2	brain	95.0	58
β_3	brain, testis, tumours	91.4	25
β_4	brain, retina, trachea	97.0	11

location of cells expressing that particular variant of tubulin are given along with the homology in percent with β_1 which is derived from a comparison of primary sequences. Finally, the abundance of each tubulin isotype in the bovine brain is given.

There are some differences between MTs assembled from the various β -tubulins in terms of their assembly properties, cross-linking behaviour and drug interactions. Although MTs incorporate without difficulty more than one isotype of tubulin, we can consider MTs with primarily a single β isotype in order to distinguish their respective properties. MTs composed of β_2 and β_3 assemble more easily in the presence of the microtubule associated proteins, MAP τ and

MAP2; and these two MAPs have the same localization as the β_2 and β_3 isotypes *in vivo*. MTs polymerized from β_2 and β_4 tubulin may be connected by crosslinking proteins, but β_3 MTs may not. This may be a result of the conformations of the isotypes and the cross-linker length. MTs formed from β_3 tubulin are the primary MTs found in tumours but it is also the isotype which cannot be bound by colchicine, an anti-cancer drug. Therefore, one of the main differences between the β -tubulin isotypes is thought to be the available microtubule-associated protein binding sites on the outside of the protein's surface. Additional differences between the tubulin isotypes are found when 'tubulin decay' is studied. Specifically, sulf-hydryl groups become exposed over time and the β_2 isoform of tubulin seems to decay more quickly than β_3 . Finally, there is the issue of localization within the cell. The β_1 and β_4 isotypes are not found in cell nuclei but are present along with β_2 in the mitotic spindle.

Wilson and Borisy point out that the function of the β_4 isotype of tubulin in axonemes is suggestive that the interaction of tubulin with extrinsic proteins may direct the architecture and organization of MTs [39].

2.6.2 Post-translational Modification

Post-translational modifications are those changes to the tubulin molecule that occur after the protein has already been produced. These changes such as detyrosination, acetylation, γ -glutamylolation and phosphorylation are limited to the exposed portions of the protein molecule but may still affect some of the properties of the protein. Detyrosination of α -tubulin is an enzymatic process that removes the final amino-acid residue of the carboxy-terminal [40]. Behind this tyrosine residue lie several charged glutamic acid residues, thus the removal of the tyrosine makes the extended carboxy-terminal tail much more electronegative. Acetylation may occur at lysine-44 of α -tubulin and the addition of an

acetyl group to lysine neutralizes its positive charge. Similarly, γ -glutamylation can result in the addition of up to six glutamic acid residues to the already highly negatively charged carboxyl tail of tubulin [40]. Consequently, all of these post-translational modifications change the electrostatic properties of tubulin and hence its interaction with other molecules of tubulin. Phosphorylation is conversion of an alcohol group (OH^-) to a phosphate group (PO_4^{3-}). In this case, the addition is quite bulky and is often used to regulate enzymatic processes. The steric hindrance resulting from these modifications alters the binding affinities between the tubulin molecule and certain substrates such as GTP, MAPs and drugs such as colchicine. It is also believed that MT stability is affected by post-translational modification as well as membrane affinity of the MTs.

2.6.3 Tubulin Conformations

Much is to be made of tubulin's various conformational states in this thesis. There exists at present several different studies which confirm the existence of different conformational states of tubulin; however there is little quantitative information on the structural changes. The first indication that there was more than a single conformational state of tubulin came simply from observing the assembly of MTs as shown in Figure 2.10. Tubulin bound to GTP, or assembly-ready tubulin, binds together and forms straight protofilaments. However, polymerized GDP-bound tubulin forms curved protofilaments that sometimes close up on themselves to produce oligomer rings. Another manifestation of the different conformations came when Hyman et al. [41] measured the energy released from a slowly hydrolyzable analogue of GTP known as GMPCPP. The energy released when the analogue was bound to tubulin was reduced compared to the quantity of energy released by the free molecule. The speculation was that the difference must go into changing the conformation of the tubulin dimer. In ad-

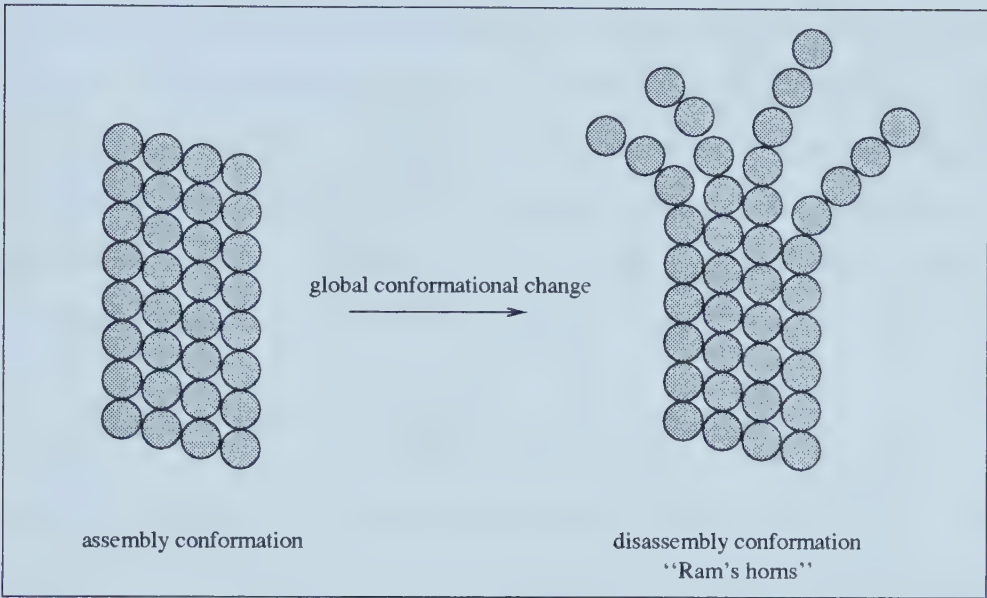


Figure 2.10: The global conformational change that occurs between assembly and disassembly phases is illustrated. The once straight protofilaments become curved after the individual tubulin subunits undergo a structural change.

dition, when GMPCPP was bound to tubulin in a MT, the energy release was further diminished. Again the assumption was simply that the energy difference is stored in the MT lattice and may be released upon disassembly or catastrophe events. More recently, Hyman et al. [42] reported on the observation of a structural change accompanying GTP hydrolysis. The change which was discovered was a length change in the monomer spacing from 4.05 nm to 4.20 nm. Thus energy may be stored locally as lattice deformation. This 4% change in tubulin’s length results in a new moiré pattern when the MTs are imaged by electron cryomicroscopy and different positions of equivalent peaks between the X-ray crystallographic diffraction patterns of GDP-MTs and GMPCPP-MTs. Finally in 1997, Tran et al. [30] commented on the dynamic instability of MTs with respect to severed MTs. The discovery was of three conformational states. There is some meta-stable intermediary state between growing and shrinking conformations. Tran et al. seems to believe that these may be tubulin with GTP bound,

with $\text{GDP}\cdot\text{P}_i$ bound and finally with GDP bound at the exchangeable site. This is similar to the hypothesis of Semenov in his review of MT research [19]. In any case, it seems that in addition to the multitude of α and β isotypes and the numerous post-translational modifications, that tubulin may also exist in several conformations. This thesis is an attempt to demonstrate some of the ramifications which could follow from this property of tubulin.

2.7 Microtubule Associated Proteins

Within the cells, MTs are not found on their own. Many other proteins are found which co-assemble with tubulin. As a group, they are known as microtubule associated proteins (MAPs). Like tubulin itself, these proteins come in a few different variants, hence MAP2A, MAP2C and so on. The most important of the MAPs are: MAP1, MAP2, MAP4 and MAP τ . MAPs have been observed to display numerous periodic patterns of attachment such as in Figure 2.11. Some MAPs such as τ bind to more than a single tubulin dimer and form a “clamp” on the MT. The reason for the various MAP attachments is unclear but the effects have been experimentally studied.

Each of the MAPs seems to serve a similar role but is localized in a different cell. MAP1 has two main forms known as MAP1A and MAP1B. MAP1B is predominantly an axonal protein and is found consistently in extending neurites, it is believed to promote the outgrowth of neurites by stimulating MT assembly. MAP1A on the other hand seems to stabilize the existing MTs of axons and dendrites. The expression of MAP1A is complementary to the expression of MAP1B such that once sufficient assembly has occurred, MAP1A may act to stabilize the MTs. Hirokawa's work [44] has shown that MAP1 forms cross-bridges between adjacent MTs, between MTs and membrane organelles and on rare occasions, between MTs and neurofilaments. A possible use of the cross-

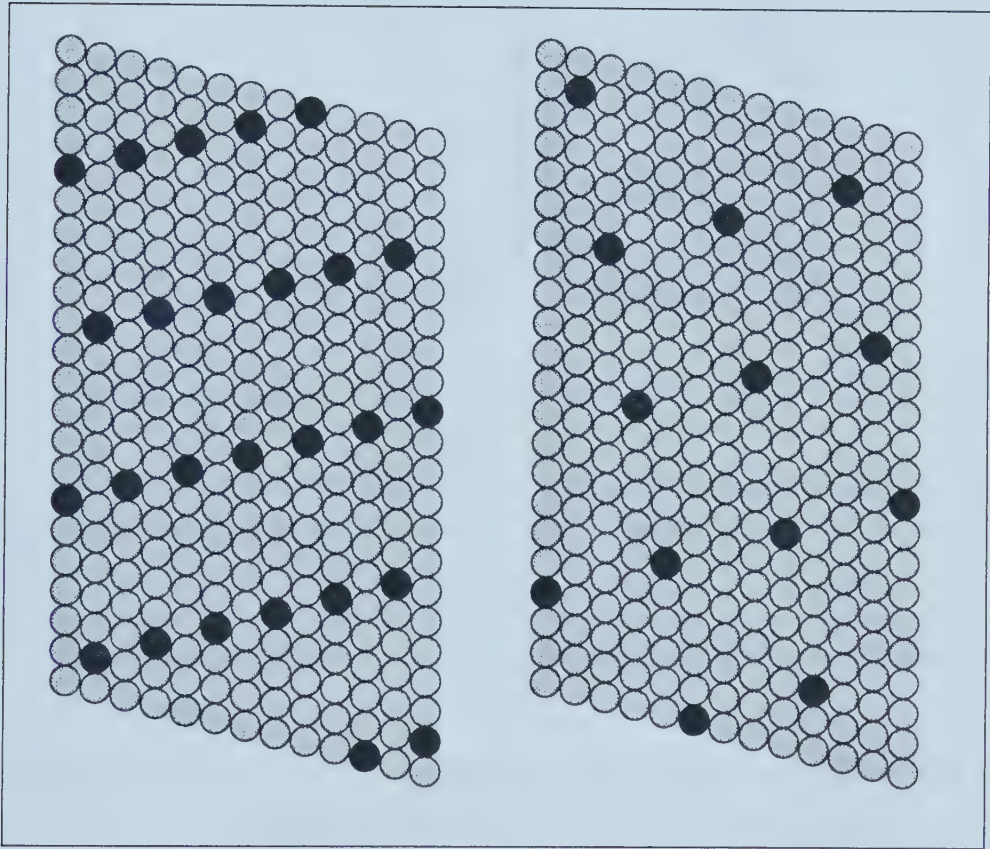


Figure 2.11: Patterns of MAP attachment are illustrated as described by Dustin [43]. On the left a 1:11 MAP:tubulin ratio pattern is displayed, a 1:22 ratio is shown on the right.

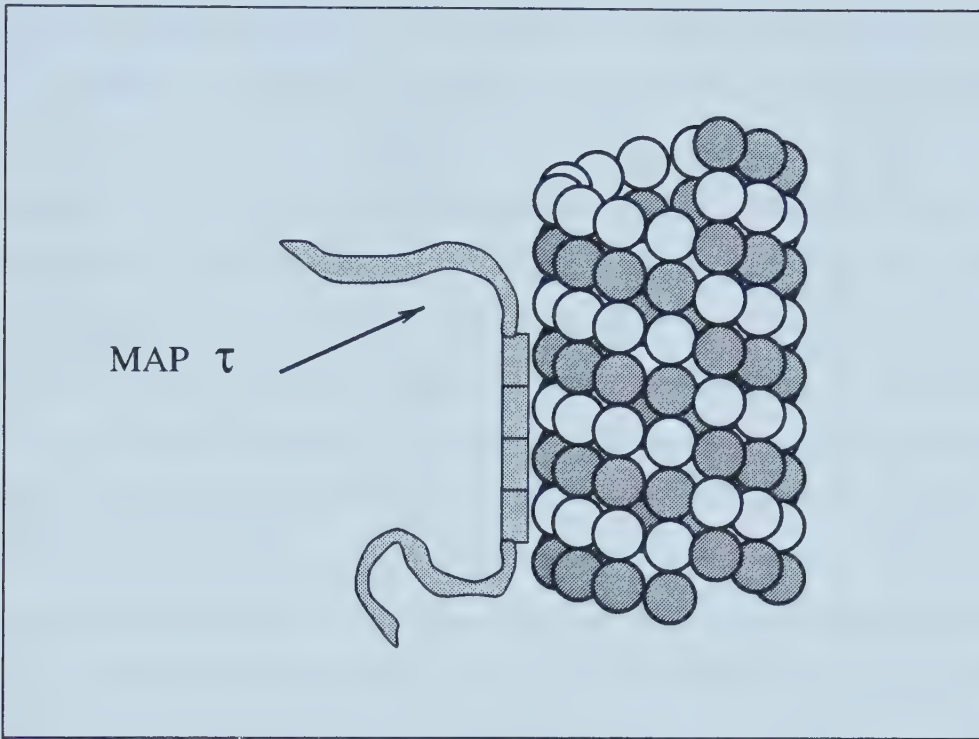


Figure 2.12: Attachment of τ MAP is to several tubulin subunits. The number of binding motifs is variable and is four in this image, where each is bound to a monomer of tubulin.

linking may be to regulate MT spacing within the cell, a feature noted since MTs were first identified [11].

The action of MAP2 is to stimulate MT polymerization and it acts by reducing the critical concentration of tubulin required. It is expressed exclusively in neuronal cells and its high molecular weight form is found only in dendrites. Tau is also localized to neurons, but is almost exclusively found within axons. Interest in this protein has been spurred by the discovery of its association with Alzheimer's disease. Tau protein like MAP1 forms arms extending from the MT when visualized using Hirokawa's technique. MAP2 and MAP τ are better promoters of MT assembly *in vitro* than MAP1. Both proteins are able to cause MT reorganization into bundles whereas MAP1 simply binds MTs together.

Finally, MAP2 seems to make MTs more rigid and promote assembly so the

effect is that MTs are longer. Tau on the other hand reduces *dynamic instability* by reducing the number of growth-to-shrinkage transitions, increasing the polymerization rate and reducing the depolymerization rate. MAP4 is found co-assembled with nearly all microtubules. It competes with MAP τ and promotes assembly. MAP4 also seems to be important in regulating the dynamics of MT assembly at the transition from interphase to mitosis. Since MTs are never found *in vivo* without at least some MAPs in their vicinity, the effects of MAPs on MT function must be considered. Although not usually considered in the same context, motor proteins such as kinesin and dynein are another sort of microtubule-associated protein. Their interaction with tubulin seems to be in a mechanical way only as they walk along the MT lattice transporting goods towards or away from the nucleus. They are also believed to play a role in force generation when chromosomes are separated by the MT spindles.

The thesis will consider MAPs and their association with MTs. The association between MAPs and tubulin may be instrumental in the ordering of dipoles and signal propagation. In the final chapter, we shall also consider the electrostatic potential about MTs in order to demonstrate how charge distributions on MAPs and motor proteins play a role in the binding between these molecules.

2.8 Drug Action on Microtubules

MTs are labile structures and this property is essential for their function in the process of mitosis. During the process of cell division, the mitotic spindle forms by the polymerization of MTs. During late anaphase the chromosomes separate as the spindle composed of MTs pulls them to each end, while the spindle itself shortens. As a result, the labile characteristic of MTs is essential since tubulin must first be free to bind onto a MT and later able to break free from a MT. Colchicine is an antimitotic drug used in the treatment of cancer, it works by

binding to the free tubulin [45]. Once bound, the tubulin is not able to add on to the end of MTs, and the spindle quickly shortens. The drug preferentially targets cancer cells since they are abnormally dividing. There are several antimitotic drugs which function in a similar manner to colchicine, such as vinblastine.

Another drug which affects MTs is known as taxol. This drug renders MTs less labile, promotes the assembly of free tubulin into MTs and also stops cell division but this time because the MTs are too stable. Tubulin subunits are bound strongly together and disassembly becomes improbable. Consequently, chromosomes cannot be separated by the force-generating MTs during anaphase of mitosis and cell division is prevented. Thus, taxol is used in cancer treatment. If MTs are shown to be important in some of the respects which are speculated over in this thesis, they are certain to become the target of many more drugs or therapies. Like the MAPs discussed in the previous section, we shall consider binding between the molecules and propose how electrostatics determine the drug function.

2.9 Elastic Properties of Microtubules

Physical properties of the cytoplasm were discussed earlier in this chapter and it only makes sense to discuss similar properties of the cytoskeleton and its components. This brief section has been postponed until close to the end of the chapter so that reference can be made to several processes which otherwise would have all been introduced at the same time. Gittes et al. [46] have measured MT flexural rigidity by thermal fluctuations in the MT shape and found interestingly that it is increased when MTs are treated with MAP τ , the MTs are most stabilized by preventing GTP hydrolysis. Thus in addition to the already discussed fact that hydrolysis of GTP can result in destabilizing the MT with respect to catastrophic disassembly, it also makes the polymer more flexible. It is interesting to

note that the application of taxol, that reduces MT assembly dynamics, actually reduces the mechanical rigidity of MTs [47].

The measured flexural rigidity for MTs corresponds to a Young's modulus of 1.4 GPa in normal MTs and can be raised by more than a factor of two to 3.4 GPa when hydrolysis is prevented [48]. In an independent study, a Young's modulus of 4.6 GPa was derived from the buckling of microtubules that required the application of a 10 pN force [49]. The Young's modulus of F-actin has also been measured and is of the same order of magnitude though conflicting measurements make actin both more and less rigid than MTs [50, 51]. This number is sufficiently large to imply that the cell must rely on depolymerization rather than deformation to effect a shape change.

This measured value of Young's modulus indicates that bending of a protofilament into an arc with radius of curvature of 20 nm, as observed by Mandelkow et al. [29], would require about 0.14 eV/dimer (3.2 kcal/mol) which is slightly less than the energy of GTP hydrolysis, 0.22 eV (5.1 kcal/mol). This is believed to explain the difference observed in the free energy release when free floating GTP is hydrolyzed compared to the hydrolysis of GTP bound to a MT.

2.10 Force Generation by Motor Proteins

One final open topic in the study of MTs and their associated proteins is the issue of force generation by motor proteins such as kinesin and dynein. There are two separate questions to be addressed: the first being how is the force generated for the movement of a motor protein and its cargo along the surface of the MT lattice; the second challenge is to explain how microtubules shorten and pull chromosomes to either end of the cell during mitosis.

Two of the principal motor proteins that attach to MTs are kinesin and dynein. While kinesin moves towards the plus end of a MT, dynein is negative

end directed. Each of these proteins consists of a globular head region and an extended coiled-coil tail section as shown in Figure 2.13. The study of motor

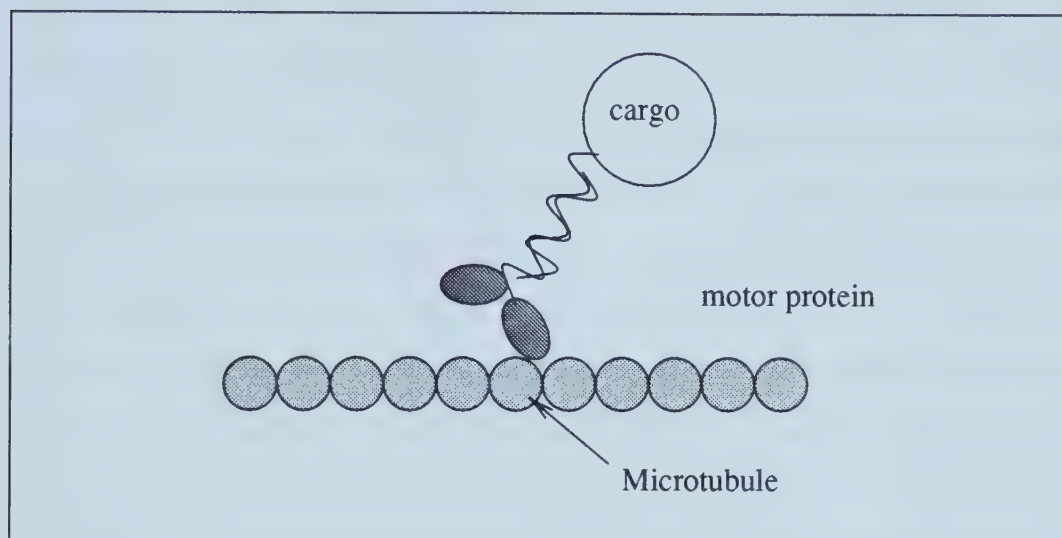


Figure 2.13: A motor protein is shown ‘walking’ along a MT protofilament.

proteins including myosin, which has a similar structure, has shown that while the long tail is able to increase the force generated by the molecular motor, the essential components for force generation are located within the globular head. Models of motor protein movement can essentially be divided into two different mechanisms, those with diffusion and those with a *power stroke* [52]. The efficient propagation of these proteins, often with pairs such as kinesin and dynein moving in opposite directions simultaneously and seemingly avoiding collisions led to the proposal that they may be directed by electrostatic interactions with the MT [53] and it is interesting to note that the binding of kinesin to MTs has since been shown to be primarily electrostatic [54].

The motion of the motor protein in either model is accomplished through the hydrolysis of ATP. The diffusion models require an oscillating potential that is presumably driven by a conformation change of the motor-MT bond. Activation of the complex by ATP leads to a potential that is relatively flat. Diffusion

occurs in this state and once the potential reverts to its asymmetric form, the geometry of the potential is such that forward propagation of the motor protein is favoured. A review of such schemes may be found thanks to Jülicher et al. [55]. In the power stroke models by contrast, it is the motor protein whose structure changes. Sometimes such models are envisioned as models of proteins walking since one imagines the protein to stretch and bind at a second location before relaxing to its original conformation when the ‘back leg’ releases its grip on the MT to start the process anew once additional ATP has arrived. Both models share similar features however this is often the preferred model for the description of the particular features of motor proteins. The motor protein has two or more distinct states where at least one conformational change occurs and is driven by ATP hydrolysis as has been experimentally demonstrated for myosin by Spudich et al. [56]. Phosphorylation of the motor protein such as in the case of myosin may lead to subsequent conformational changes. Thus the protein may be viewed as walking along the MT powered by ATP. It is interesting to note that the use of GTP to control MT dynamics and ATP to control motor protein motion along MTs, allows a cell to have control over both the cars (motor proteins) and the track (MTs) individually.

So, can this model of motor protein movement be successfully applied to the problem of chromosome separation? The prevailing model of how the MTs that form the mitotic spindle separate chromosomes is that motor proteins attach to the chromosomes and the distal ends of spindle MTs. The force generation is thereby developed locally by the motor proteins and cannot depend on the length of the MT. However, the force attracting the chromosome to the pole has been shown to increase as the spindle shortens [57]. Only a repulsive force from the pole or generated by the tubulin subunits of the microtubule would solve this difficulty. However, if it is the motor proteins are responsible for the

force generation, it must be explained how it is that the chromosome movement does not require ATP [58]. Therefore if the motor proteins are important for more than simply binding the chromosome, this has not been shown to date and the relationship between force and the length of the spindle MTs must still be explained.

Bibliography

- [1] B. Alberts, D. Bray, J. Lewis, M. Raff, K. Roberts, and J.D. Watson, *Molecular biology of the cell*, Garland Publishing, London, 1994.
- [2] K. Luby-Phelps, *Physical properties of cytoplasm*, Curr. Opin. Cell Biol. **6**, 3–9 (1994).
- [3] B. Hinner, M. Tempel, E. Sackmann, K. Kroy, and E. Frey, *Entanglement, elasticity and viscous relaxation of actin solutions*, Phys. Rev. Lett. **81**, 2614–2618 (1998).
- [4] E. Frey, K. Kroy, and J. Wilhelm, *Viscoelasticity of Biopolymer Networks*, Adv. Struct. Biol. **5**, 135–168 (1998).
- [5] D. E. Ingber, *Tensegrity: The architectural basis of cellular mechanotransduction*, Ann. Rev. Physiology **59**, 575–599 (1997).
- [6] C.S. Chen, M. Mrksich, S. Huang, G.M. Whitesides, and D.E. Ingber, *Geometric control of cell life and death.*, Science **276**, 1425–1428 (1997).
- [7] R.W.P. King and T.T. Wu, *Electric field induced in cells in the human body when this is exposed to low-frequency electric fields*, Phys. Rev. E **58**, 2363–2369 (1998).
- [8] L. Edelstein-Keshet, *A mathematical approach to cytoskeletal assembly*, Eur. Biophys. J. **27**, 521–531 (1998).

- [9] G. Civelecoglu and L. Edelstein-Keshet, *Modelling the dynamics of F-Actin in the cell*, Bull. Math. Biol. **56**, 587–616 (1998).
- [10] L.A. Amos and W.B. Amos, *Molecules of the cytoskeleton*, Macmillan Press, London, 1991.
- [11] M.C. Ledbetter and K.R. Porter, *A “Microtubule” in Plant Cell Fine Structure*, J. Cell Biol. **19**, 239–250 (1963).
- [12] D. Chrétien and R.H. Wade, *New data on the microtubule surface lattice*, Bio. Cell **71**, 161–174 (1991).
- [13] E. Nogales, S.G. Wolf, and K.H. Downing, *Structure of the alpha-beta tubulin dimer by electron crystallography*, Nature (London) **391**, 199–203 (1998).
- [14] L.A. Amos, *The microtubule lattice - 20 years on*, Trends Cell Biol. **5**, 48–51 (1995).
- [15] D. Chrétien, F. Metoz, F. Verde, E. Karsenti, and R.H. Wade, *Lattice-defects in microtubules: Protofilament numbers vary within individual microtubules*, J. Cell Biol. **117**, 1031–1040 (1992).
- [16] R.H. Wade, D. Chrétien, and D. Job, *Characterization of microtubule protofilament numbers. How does the surface lattice accommodate?*, J. Molec. Biol. **212**, 775–786 (1990).
- [17] I.M. Jánosi, D. Chrétien, and H. Flyvbjerg, *Modeling Elastic Properties of Microtubule Tips and Walls.*, Eur. Biophysics J. **27**, 501–513 (1998).
- [18] H. Sosa and R.A. Milligan, *Three-dimensional structure of ncd-decorated microtubules obtained by a back-projection method.*, J. Molec. Biol. **260**, 743–755 (1996).

- [19] M.V. Semënov, *New Concept of Microtubule Dynamics and Microtubule Motor Movement and New Model of Chromosome Movement in Mitosis*, J. theor. Biol. **179**, 91–117 (1996).
- [20] D. Chrétien, S.D. Fuller, and E. Karsenti, *Structure of Growing Microtubule Ends: Two Dimensional Sheets Close into Tubes at Variable Rates*, J. Cell Biol. **129**, 1311–1328 (1995).
- [21] T. Mitchison and M. Kirschner, *Dynamic instability of microtubule growth*, Nature (London) **312**, 237–242 (1984).
- [22] T. Horio and H. Hotani, *Visualization of the dynamic instability of individual microtubules by dark field microscopy*, Nature (London) **321**, 605–607 (1986).
- [23] L. Cassimeris, *Regulation of microtubule dynamic instability*, Cell. Motil. Cyto. **26**, 275–281 (1993).
- [24] M.F. Carlier, R. Melki, D. Pantaloni, T.L. Hill, and Y. Chen, *Synchronous oscillations in microtubule polymerization*, Proc. Natl. Acad. Sci. USA **84**, 5257–5261 (1987).
- [25] E.-M. Mandelkow and E. Mandelkow, *Microtubule oscillations*, Cell Motil. and Cytoskel. **22**, 235–244 (1992).
- [26] H. Flyvbjerg, T.E. Holy, and S. Leibler, *Microtubule dynamics: Caps, catastrophes, and coupled hydrolysis*, Phys. Rev. E **54**, 5538–5560 (1996).
- [27] B. Houchmandzadeh and M. Vallade, *Collective oscillations in microtubule growth*, Phys. Rev. E **6320**, 53 (1996).

- [28] D. Sept, H.-J. Limbach, H. Bolterauer, and J.A. Tuszyński, *A Chemical Kinetics Model for Microtubule Oscillations*, J. theor. Biol. **197**, 77–88 (1999).
- [29] E.M. Mandelkow, E. Mandelkow, and R. Milligan, *Microtubule dynamics and microtubule caps: A time resolved cryo-electron microscopy study*, J. Cell Biol. **114**, 977–991 (1991).
- [30] P.T. Tran, R.A. Walker, and E.D. Salmon, *A metastable intermediate state of microtubule dynamic instability that differs significantly between plus and minus ends*, J. Cell Biol. **138**, 105–117 (1997).
- [31] D. Sept, *Models of Assembly and Disassembly of Individual Microtubules and their Ensembles*, PhD thesis, University of Alberta, 1997.
- [32] D.K. Fygenson, E. Braun, and A. Libchaber, *Phase diagram of microtubules*, Phys. Rev. D **50**, 1579–1588 (1994).
- [33] J. Tabony and D. Job, *Spatial structures in microtubular solutions requiring a sustained energy source*, Nature (London) **346**, 448–451 (1990).
- [34] I.G. Iliev and A.G. Ivanov, *Effects of colchicine on the surface electrical properties and sodium channel current in neuroblastoma cells*, J. Bioelectricity **8**, 133–145 (1989).
- [35] M.L. Lacey and L.T. Haimo, *Cytoplasmic dynein binds to phospholipid vesicles.*, Cell Motil. Cytoskel. **28**, 205–212 (1994).
- [36] Per J. Kraulis, *MOLSCRIPT: A Program to Produce Both Detailed and Schematic Plots of Protein Structures*, Journal of Applied Crystallography **24**, 946–950 (1991).

- [37] A. Bairoch and R. Apweiler, *The SWISS-PROT protein sequence data bank and its supplement TrEMBL in 1998.*, Nucleic Acids Res. **26**, 38–42 (1998).
- [38] Q. Lu, G.D. Moore, C. Walss, and R.F. Ludueña, *Structural and functional properties of tubulin isotypes*, Adv. Struct. Biol. **5**, 203–227 (1998).
- [39] P.G. Wilson and G.G. Borisy, *Evolution of the multi-tubulin hypothesis*, Bioessays **19**, 451–454 (1997).
- [40] D.L. Sackett, *Structure and Function in the Tubulin Dimer and the role of the acidic Carboxyl Terminus*, Subcellular Biochemistry – Proteins: Structure, function and engineering **24**, 255–302 (1995).
- [41] A.A. Hyman, S. Salser, D.N. Drechsel, N. Unwin, and T.J. Mitchison, *Role of GTP hydrolysis in microtubule dynamics: information from a slowly hydrolyzable analogue, GMPCPP*, Molec. Biol. Cell **3**, 1155–1167 (1992).
- [42] A.A. Hyman, D. Chrétien, I. Arnal, and R.H. Wade, *Structural Changes Accompanying GTP Hydrolysis in Microtubules: Information from a Slowly Hydrolyzable Analogue Guanlyl-(α , β)-Methylene-Diphosphonate*, J. Cell. Biol. **128**, 117–125 (1995).
- [43] P. Dustin, *Microtubule*, Springer-Verlag, Berlin, 1984.
- [44] N. Hirokawa, *Molecular Architecture and Dynamics of the Neuronal Cytoskeleton*, pages 5–74, Wiley-Liss, New York, 1991.
- [45] A. Vandecandelaere, S.R. Martin, and Y. Engelborghs, *Response of microtubules to the addition of colchicine and tubulin-colchicine: evaluation of models for the interaction of drugs with microtubules.*, Biochemical J. **323**, 189–196 (1997).

- [46] F. Gittes, E. Mickey, and J. Nettleton, *Flexural rigidity of microtubules and actin filaments measured from thermal fluctuations in shape*, J. Cell Biol. **120**, 923–934 (1993).
- [47] H. Felgner, R. Frank, and M. Schliwa, *Flexural rigidity of microtubules measured with the use of optical tweezers*, J. Cell Sci. **109**, 509–516 (1996).
- [48] B. Mickey and J. Howard, *Rigidity of microtubules is increased by stabilizing agents*, J. Cell Biol. **130**, 909–917 (1995).
- [49] M. Elbaum, D.K. Fygenson, and A. Libchaber, *Buckling Microtubules in Vesicles*, Phys. Rev. Lett. **76**, 4078–4081 (1996).
- [50] R.D. Vale, C.M. Coppin, F. Malik, F.J. Kull, and R.A. Milligan, *Tubulin GTP hydrolysis influences the structure, mechanical properties, and kinesin-driven transport of microtubules*, J. Biol. Chem. **269**, 23769–23775 (1994).
- [51] P. Venier, A.C. Maggs, M.-F. Carlier, and D. Pantaloni, *Analysis of microtubule rigidity using hydrodynamic flow and thermal fluctuations*, J. Biol. Chem. **269**, 13353–13360 (1994).
- [52] S. Leibler and D.A. Huse, *Porters versus rowers: a unified stochastic model of motor proteins*, J. Cell Biol. **121**, 1357–1368 (1993).
- [53] J.A. Brown and J.A. Tuszyński, *Dipole Interactions in Axonal Microtubules as a Mechanism of Signal Propagation*, Phys. Rev. E **56**, 5834–5840 (1997).
- [54] G. Woehlke, A.K. Ruby, C.L. Hart, B. Ly, N. Hom-Booher, and R.D. Vale, *Microtubule Interaction Site of the Kinesin Motor*, Cell **90**, 207–216 (1997).
- [55] F. Jülicher, A. Adjari, and J. Prost, *Modeling molecular motors*, Rev. Mod. Phys. **69**, 1269–1281 (1997).

- [56] K.M. Ruppel, M. Lorenz, and J.A. Spudich, *Myosin structure/function: a combined mutagenesis-crystallography approach*, Curr. Opin. Struct. Bio. **5**, 181–186 (1995).
- [57] T.S. Hays and E.D. Salmon, *Poleward force at the kinetochore in metaphase depends on the number of kinetochore microtubules.*, J. Cell Biol. **110**, 391–404 (1990).
- [58] T.P. Spurck and H.J. Pickett, *On the mechanism of anaphase A: evidence that ATP is needed for microtubule disassembly and not generation of poleward force.*, J. Cell Biol. **105**, 1691–1705 (1987).

Chapter 3

The Biology-Physics Interface

The marriage of biology and physics may seem a strange one at first but in fact there has been a long-standing desire to understand physiological processes on a more fundamental level, even a molecular level. The development of the fields known as biochemistry and molecular biophysics has followed with the ambitious hopes of making progress in this regard. Unsatisfied with simply measuring the binding affinity of, for instance, an enzyme to its substrate, the investigation becomes one of explaining the binding affinity by determining the structure of the constituents and identifying the relevant binding site. In this example, one might then hope to synthesize a substrate which might be more strongly or weakly bound by the enzyme. Consider the following biologically important events which could be modelled: biochemical reactions, protein folding and assembly, immune response, transport phenomena, and biological signalling, to name a few. An improved understanding of any or all of these as they pertain to a specific biological quandary can have great pharmaceutical relevance if it leads to the development of a better drug.

In essence, the difference between living organisms and inanimate matter is the ability of living organisms to reproduce, to adapt and to control the aforementioned biological events with extremely fine precision. Any cells unable to co-ordinate these activities will not survive. Many of the molecules found in

living organisms are both large and complex. Proteins are the most varied and have the most diverse range of function. Their molecular masses range from the tens of thousands up to the millions. Conversely, the chemical subunits which make up biological molecules are not nearly so varied; essentially 20 amino acids are the building blocks of all proteins. Diversity is a simple result of the multitude of combinations. The functioning of biological systems must also be derived from this complexity; with specific organization of complex molecular systems providing specific functions while they continue to be governed by fundamental physical laws. The principle of complexity begetting function is a familiar one to physicists and has often been referred to as an emergent phenomenon. It is characteristic of atomic systems to display new properties as they become more complex [1]. Concepts such as temperature, entropy, sound waves and other collective excitations apply to a system of atoms but not to individual atoms.

While biochemistry studies mainly atoms in direct contact with each other, many biological phenomena arise from subtler, weaker, short- and long-range forces. The solvation and desolvation problem, for example, has yet to be treated theoretically due to computational limits although it is essential to the understanding of ligand binding in any physiological and hence wet environment. Biofunction is the result of specific chemical reactions and reaction cascades. Some molecules derive their function solely from quantum mechanical interactions while in other molecules, classical interactions with surrounding molecules and external fields, such as electromagnetic fields, are responsible for proper function. The main task facing theoretical biophysics today is the investigation of the physical characteristics of biological molecules and very simple biological systems such as enzymes, structural proteins and cellular membranes. In this study, one must remember to account for the openness of biological systems to the environment. They routinely exchange energy and matter with their environ-

ment and, in addition, many components of biological systems such as proteins are themselves undergoing continual renewal. Life is only possible because the timescale of protein stability is much longer than the timescale of their respective biological functions [1].

Biophysicists seek to understand biophysical processes by accounting for intramolecular and intermolecular interactions, and their resulting electronic and structural conformational changes; and by studying the transfer of electrons, protons, metallic ions and energy within biological systems. In condensed matter physics, such problems are solved by the methods of quantum mechanics, statistical physics and both equilibrium and non-equilibrium thermodynamics. However, since isolated biophysical systems are not found in nature, the description is complicated by the openness of living systems and their far-from-equilibrium nature. In this thesis, I am concerned with the properties of a particular protein, tubulin, and its polymerized form the MT. I am specifically concerned with its ferroelectric properties, its possible role in biological signalling and its conduction properties. An overview of the development of biophysics in these regards follows. The cell requires organization to operate effectively and I shall demonstrate how some of the cytoskeletal organization may be supported by physical interactions.

3.1 Energy Requirements

Energy production and energy transport are fundamental problems in biology since a majority of biophysical processes are endothermic and require energy input to be sustained. Energy must also be spent by the cell to maintain its composition and to combat the effects of entropy. It is of necessity that biological processes are coupled to exothermic processes such as ATP or GTP hydrolysis.





where P_i represents an inorganic phosphate group which is severed from the nucleotide triphosphate complex (NTP) leaving the nucleotide diphosphate (NDP)¹. The generation of ATP for cell use will not be examined in detail here but suffice it to say that: (i) mitochondria are organelles of the cell which break down sugars in the presence of oxygen to water and carbon dioxide with a net gain of ATP; and (ii) the process of ATP generation occurs through the use of several enzymes where notably cytochrome oxidase plays a crucial role in electron transport [2, 3, 4]. Of course, energy production and transport are not the whole story, but the conversion of energy from one form to another must be explained. With this view, energy production can also be viewed simply as conversion from the raw material, food sugars, into the refined product, ATP. A few biological processes and their corresponding energy conversions are summarized in Table 3.1. Several features are common among these energy conversion processes and should

Table 3.1: Biological Processes and Associated Energy Conversions

Biological Process	Energy Conversion
vision	light → electrical
nerve impulse	chemical → electrical
muscle contraction	chemical → mechanical
photosynthesis	light → chemical
cellular respiration	chemical (stored) → chemical
bioluminescence	chemical → light

be noted as they shall prove to be important when conduction in biomaterials is considered. They each occur along highly organized membrane-like structures, involve protein macromolecules in the form of enzymes and they all utilize the release of energy from the hydrolysis of the cell's refined product, ATP. The pur-

¹N represents the nucleotide which may be either adenosine (A) or guanosine (G).

pose of the organization seems at least in the case of photosynthesis and cellular respiration to effectively pass electrons between chemical species. This redox (reduction-oxidation) scheme demonstrates that biological systems indeed make use of electron transport and this adds some motivation to search for additional examples of electronic conduction within the cell.

All energy conversion processes make use of gradients. These may be chemical gradients such as the concentration of ions and other molecules, temperature gradients and even gravitational and electromagnetic potential gradients. Chemical gradients are the most important because they are the ones which can be manipulated by the cells. Since diffusion tends to erode these gradients rather quickly, it is essential that membranes are established to preserve concentration differences. Through the construction of ion channels and gates, the cell is able to extract useful work by coupling endothermic processes to the movement of an ion passively down a chemical gradient in much the same way a turbine may be powered by a waterfall behind a dam. The cell's ability to maintain a non-equilibrium system provides an attractive problem that is amenable to study by the physicist.

3.2 Biological Signalling

Signalling by varied means is required to regulate the complex behaviour of living systems from the simplest bacterium to yeast cells and larger eukaryotes such as humans. The difference between monocellular and multicellular organisms is that communication must necessarily be possible between its different cells. For any particular cell of the organism, this means that in addition to intracellular signalling, it must be prepared to both transmit and receive extracellular signals. The signalling mechanisms discovered so far exhibit the complexity of organic chemistry. In order to interpret signals from other cells, a cell requires special

membrane receptors which can detect the presence of a signalling molecules in the extracellular fluid. Albrecht-Bühler has proposed in his 'intelligent cell' model that cells are able to sense light through the use of centrioles [5]. Since the centrioles are always found with a perpendicular orientation, this would allow the cell to discern directional information about a signal through latitude and longitude measurements. That this would provide an invaluable signal receptor is clear, but the mechanism through which other cells might transmit such signals is unclear and will not be discussed further here other than to say that the proposal is that mitochondria may generate light signals at infrared frequencies. Excluding this hypothesis, the cell has several methods of communication through the use of its varied signalling molecules. The molecules are first packaged and then expelled from the cell. In the simplest type of messaging, the chemical signals are dumped outside the cell and carried diffusively. This method of communication is effective for only the signalling of nearby cells. Such local signalling is known as paracrine signalling. Synaptic signalling is a refined version of the paracrine model where the signal molecule, a neurotransmitter, is released at a specifically designed interface providing intimate contact between the source and target cells. This allows quick and direct signalling but still relies on diffusion to carry the signal molecules across the narrow junction. The last type of signalling, known as endocrine signalling, may be used when the target cells of the signal are either more distant or more widespread. These molecular signals known as hormones are secreted by the cell into the circulatory system. Thus although diffusion is used yet again, the stream of blood or sap may carry the signal a long distance. Due to the dilution effect of the circulatory fluid, hormones must be effective even at low concentrations such as $10^{-8} \text{ mol L}^{-1}$ [6].

The mechanism behind the workings of these extracellular messengers is of the familiar antigen-antibody type [7]. That is to say that there are specific

integral membrane proteins to which a signalling molecule may bind on the target cell's exterior. The general behaviour of these signalling systems is that binding of the signal molecule to the receptor induces a conformational change at the opposite end of the protein receptor which lies within the cell's interior. The conformational change may have a direct or indirect response. In the case of a direct response, the cytoplasmic domain of the protein becomes enzymatic and catalyzes a specific chemical reaction until the signal molecule at the extracellular end breaks down or becomes unbound. In the indirect case, the conformational change may release another signalling molecule on the cell's interior known as a G-protein. This G-protein may then bind to one or more other enzymes, either serving to activate or deactivate them. The indirect signal allows for the co-ordination of complementary reaction pathways and is one way in which the cell regulates its processes. Breaking the signalling scheme into many parts also allows for magnification of the signal at each step and makes it possible to ultimately have a large response to a small number of signal molecules. The final sort of response that is possible by ligand binding is the opening of ion channels. In this case, the conformational change of the receptor is such that a hydrophilic channel is opened through the cell membrane and allows passage of a specific charged species such as calcium ion (Ca^{2+}). The calcium ion is useful in particular because it exists outside of the cell in concentrations 10^4 times higher than the intracellular concentration. As a result, it diffuses into a cell easily and is used as a secondary signal. The mechanism for the operation of these signals has only been sketched briefly because they are well understood and are described in more detail in textbooks such as Alberts et al. [6].

The most interesting biophysics happens within the cell where the methods of signal transduction are yet to be fully elucidated. Intracellular signalling includes mechanisms such as the action potential which is electrical in nature and driven

by chemical potentials [8]. Sensitivity of individual cells to concentration and potential gradients is necessary if the cell is to respond to gravitational or electric fields. Intracellular signalling coordinates the orchestra of cellular processes to ensure that the entire cell works in harmony. In mitosis, chromosome segregation to each pole of the mother cell is mediated by MTs. However, the simultaneity of the separation must be explained and requires some kind of signal to be mediated by the MTs. Treadmilling by free MTs under conditions of dynamic instability should also be explained since the opposite ends of the MT have such coordinated behaviour. Recently, Maniotis et al. [9] demonstrated how pulling on actin filaments could induce changes within the nucleus. This illustrated that the cell was also sensitive to mechanical stimulation [10]. One hypothesis for the control which the cell has over these processes is an electromagnetic regulation. This form of signalling has the advantage that it is exceedingly rapid relative to extracellular signalling. The cytoskeleton seems to play a key role in each of these mysterious examples of cellular signalling.

Consider the action potential, this electrical signal passes along the neural membrane driven by a cascade of sodium ions flowing into the cell and is switched off by a delayed flow of potassium ions out of the cell. While the action potential moves, there is no attenuation of the signal. Only toxins, which can disable the function of voltage-gated ion channels, are able to stop the progress of the action potential. Thus the behaviour of the system appears soliton-like. The cytoskeleton adopts a configuration in neurons where the orientation of MTs is parallel with uniform direction within the axon, along which the cell transmits signals to other cells, but the MTs adopt an aligned configuration with a non-uniform direction in the dendrites where signals are received from other cells. Since there are molecular motors such as kinesin and dynein which move in opposite directions along MTs, one would suspect that there is another reason

for the specific structure that is seen rather than simply the ability to transport goods using the MTs. Otherwise, the MT should be free to have arbitrary orientation.

MTs are known to respond to both electric fields [11, 12, 13] and to magnetic fields [11, 14] and align themselves such that they are parallel to the field lines. The specific alignment in these two neuronal regions could be to make MTs insensitive to electric fields within dendrites but reinforce the susceptibility to electric fields within the axon. It has also been shown that in long cylindrical cells such as the geometry of an axon, electrical fields are able to penetrate most easily [15]. Within a cylindrical structure such as the MT, the electric field along the axis remains almost constant rather than decaying towards the center of the MT.

The key question of intracellular biological signalling is whether or not electron transport plays a role? The transfer of an electron between proteins results in a conformational change that has a physiological effect [16]. In the case of ion channels, the donation or acceptance of electrons changes their internal electrostatics and affects their function. This results in neuromodulation by changing in the response characteristics of the neuron and constitutes a reprogramming of neural networks.

3.3 Biological Piezoelectricity

Piezoelectricity is the electrical response of certain materials to strain and pyroelectricity is the electrical response of a material to a thermal gradient. Athenstädt has previously investigated piezoelectric and pyroelectric properties of several living systems and found that many structural tissues possess a permanent electrical polarization [17]. The subunits that comprise these tissues all have a permanent electric dipole. In particular, Athenstädt established that MTs are py-

roelectric and hence possess electric dipoles. This is consistent with the observed alignment of MTs assembled in the presence of electromagnetic fields [11, 12] and with calculations presented later in this thesis that estimate tubulin's dipole moment given its structure in zinc ion-induced sheets. In the 25 years which have passed since those studies, the piezoelectric property of many tissues has been confirmed [18, 19]. Tissues such as collagen and bone develop surface voltages of 10–150 mV in response to strain. The piezoelectric effect is exhibited because mechanical deformation or strain displaces some electrons towards the compressed surfaces. These surfaces become negatively charged [20]. There is supposition that these potential differences which develop may be interpreted within the cell and in the case of bone, it has been demonstrated that bone growth is stimulated in this manner.

In the case of MTs, the piezoelectric property could be important when mechanical stress is induced within the structure such as during chromosome separation. Indeed Salmon conducted experiments which demonstrated that changing the hydrostatic pressure within the cell could induce depolymerization of the spindle MTs [21, 22]. Conversely, when an external field such as that of an action potential acts, it would induce a stress on the MT. The resulting mechanical strain could be exactly the requirement for the release of neurotransmitter at the neural synapse. Such links between the mechanical properties of the cell and signalling are of special interest now that mechanical strain of the cytoskeleton has been shown to carry signals to the nucleus [9].

3.4 Biological Conduction

Although conductivity of organic materials was reported as early as the turn of the century in solid anthracene [23], Szent-Györgyi is generally given credit for giving birth to the belief that such electron transfer may be crucial to biological

processes [24, 25]. He suggested in 1941 that the mobile π -electrons of conjugated carbon double bonds may be transferred from molecule to molecule and that this may be fundamental to the workings of biological systems. Five years later, he reported the discovery of photoconductive effects for protein films [26]. The conduction within organic solids was then described by means of a band model as in traditional semiconductors. Conduction was viewed as an intrinsic property of the material where thermal excitation of electrons from a valence band to the conduction band leads to a dynamic equilibrium of electron-hole pairs and the result is the appearance of some number of available charge carriers. A typical organic material has a band gap too large for charge carriers to be present (Figure 3.1). Since the number of charge carriers is temperature dependent, the conductivity is also temperature dependent. The number density of charge carriers, n ,

$$n_i = n_i^0 \exp(-\epsilon/2kT) \quad (3.3)$$

is described by equation (3.3) where ϵ is the band gap, k is Boltzmann's constant, T the temperature and n_i^0 the density of carriers in the conduction band. The conductivity is then determined by summing the contributions to conduction by holes and by electrons where μ represents the carrier mobilities and e is the charge of an electron.

$$\sigma = |e|(n_e\mu_e + n_h\mu_h) \quad (3.4)$$

In the mid-1950's, the idea of semiconduction was ruled out by the masses due to the large activation energies in the range of several electron volts which were much higher than the energies observed in biological processes, typically less than 0.49 eV which is the free energy of ATP hydrolysis. However, several key points were overlooked at that time when organic semiconduction was dismissed. Firstly, measurements had been carried out only in dried systems whereas living systems function only when wet, typically 80% water. Rosenberg has since

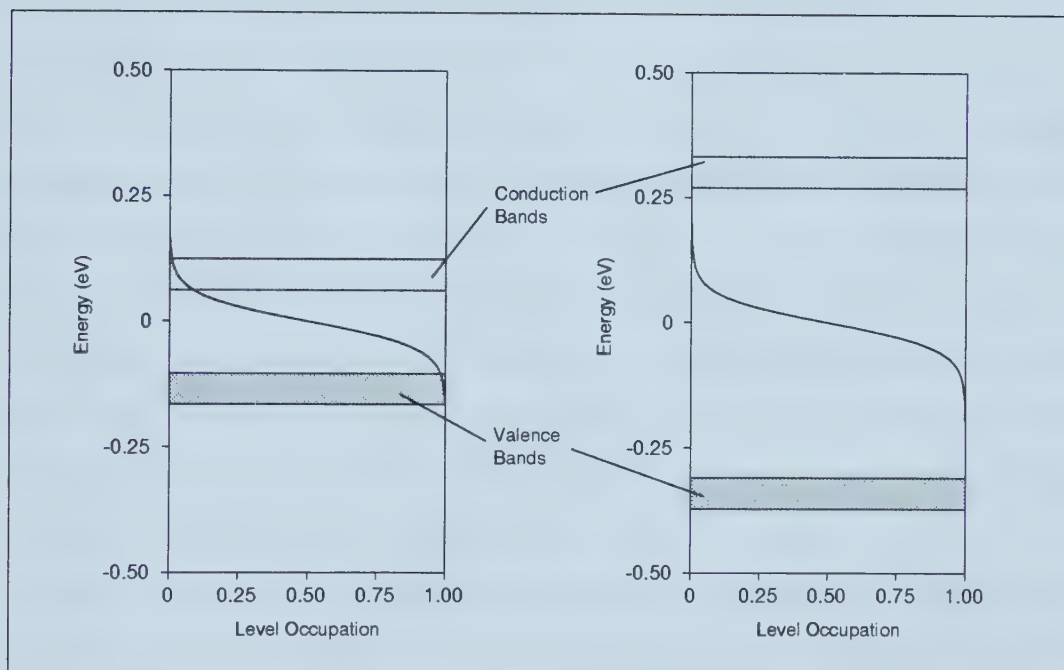


Figure 3.1: Valence and conduction band picture of two materials. On the left, the band gap is sufficiently small and the valence and conduction edges close to the Fermi level, so there will be some thermally excited electrons in the conduction band, and holes in the valence band. A more typical organic material band picture is shown on the right, often the band gap is greater than 3.0 eV. The curve superimposed on each band is simply a Fermi-Dirac distribution where the chemical potential is zero and the temperature is 300 K

shown that the presence of water causes significant changes in the activation energy [27, 28] and hence may improve the conductivity of proteins by a factor of up to 10^{10} ! The treatment of solvation remains a major difficulty in current studies of protein interaction and is crucial to analysis of the problem but requires sophisticated molecular and Brownian dynamics simulation to make much progress. Nevertheless, the wet environment cannot be ignored.

Secondly, certain proteins exist with unusual structures which seem to be specially designed for high electron conductivities and low activation energies. Essentially, these structures can be viewed akin to donor and acceptor impurities. Straub measured an activation energy of about 0.3 eV for cytochrome oxidase which is known to play a role in electron transport [29] and which is instrumental in the proton pump mechanism of energy production in mitochondria [30]. Most proteins have activation energies at least three times larger. Given the exponential dependence of the conductivity on the activation energy, this represents perhaps a factor of 10^6 improvement other things being equal.

Finally, conduction within individual structures may be quite different than conduction across the interfaces between these structures, this may be what is measured when an electrode is placed across a compressed mass of thousands of microscopic particles. Hence the conductivity may be higher within individual particles than previously deduced from the conductivity of a mass of particles and makes current work to measure properties of individual structures all the more relevant. Given these weaknesses described above in the case against organic conduction, and with a spirit of indifference toward the conventional thinking, work continued in the field to investigate conduction by organic materials. Eley et al. investigated conduction in proteins and found a weak semiconduction in dark conditions [31, 32, 33]. The conduction was also found to increase exponentially with hydration but it was not possible to conclude as to the cause. Pethig

and Szent-Györgyi carried out transport experiments [34] and found that DNA and RNA had reproducible conduction of the form of equation (3.3) with an activation energy of about 1.1 eV but the value of σ_0 in similar experiments has varied from 10^2 to $10^8 \Omega^{-1}\text{cm}^{-1}$. The fact that the familiar dependence of the conduction on temperature was measured meant that traditional explanations of conduction might be relevant, however the inability to reproduce experiments quantitatively underlined the difficulty of working with organic matter. This difficulty has been attributed to the high sensitivity of these systems to their environments and has significantly hindered progress in the study of their physical properties.

In the nearly 60 years following Szent-Györgyi's prediction, kinetic evidence has been gathered which supports semiconduction in living cells [35, 36]. More recently, the interest has been in understanding the mechanism of electron transfer in biological media. Until the last decade, the physics and chemistry of the liquid state has largely been applied to biology. This has not been sufficient to describe the complex physical processes observed and attention needs to be given to the structures and particles which are present. Two approaches may be adopted in the study of physical processes within organic extracts. The first is to test the solid-state physical properties of the extract such as its conductivity and piezoelectricity with the caveat that the discovery of novel properties does not imply that they play an important physiological role. The second option concerns the case where a biological process may be explained by the hypothesis of solid state processes in cells. The components of the biological system should then be isolated and their properties compared to the predictions of the corresponding condensed matter model. It is largely this latter approach that has been adopted in this investigation.

The phenomenon of electronic conduction is a well studied problem in con-

densed matter physics. It is the phenomenon by which a current may be passed through a material. The conductivity of a material is defined experimentally by the constant, σ , which relates the current density, \mathbf{J} , in the material to the electric field, \mathbf{E} , within the material by the following relationship:

$$\mathbf{J} = \sigma \mathbf{E}. \quad (3.5)$$

More generally, this parameter may actually be a tensor, $\sigma_{\alpha\beta}$, so

$$J_{\alpha} = \sigma_{\alpha\beta} E_{\beta} \quad (3.6)$$

relating the anisotropic response of the system to the external electric field. A material with an electrical conductivity in excess of $10^4 \text{ } \Omega^{-1}\text{cm}^{-1}$ is generally considered to be a conductor. Materials are classified as insulators when their electrical conductivity is less than $10^{-10} \text{ } \Omega^{-1}\text{cm}^{-1}$. Within the intermediate range from 10^{-9} – $10^3 \text{ } \Omega^{-1}\text{cm}^{-1}$, materials are classified as semiconductors. The term, organic semiconductor, has been used to describe organic compounds that exhibit properties inconsistent with electrical insulators. These organic materials may be grouped into three categories: molecular crystals (characterized by van der Waals bonds), charge transfer complexes (with covalent and coordinate bonding present) and polymers. Charge transfer complexes play an important role in biology as they are responsible for the generation of useable energy through the processes of respiration and photosynthesis. However, not all biological electronic conduction can be described by charge transfer complexes. In some cases, electron donors and acceptors are isolated from each other. Consequently, the carriers will reside in the vicinity of the same molecule for a long time before jumping to a neighbouring molecule. This view gives rise to a hopping model since electron mobility is low and governed by an activation energy. Such an interpretation is particularly useful whenever the material exhibits a periodic lattice; or has a sufficiently weak carrier concentration that interactions between

carriers are negligible [37]. The MT is an example of such a system with periodicity and we are optimistic that the hopping model we have selected shall give us an accurate picture of electrical conduction within this polymer.

3.5 Protein Interaction with Environment

It should be emphasized that a structured water medium surrounds all of the protein within a cell. This is the solvation problem mentioned earlier and is a result of the protein and its charged surface forming hydrogen bonds with the water. In addition, ions are found within the cytoplasm which may influence conduction properties by their interaction with the side chains of proteins or even their localization within charged pockets of the protein. Consequently, the study of dry proteins does not give an accurate portrayal of their properties. Some of these effects, of the environment surrounding the proteins, have been previously studied theoretically [38]. However, these studies do not predict the band gap to be sufficiently reduced to result in meaningful conduction.

The interaction of metal ions and protons with peptide groups is of great importance in the biophysical chemistry of proteins. Such interactions are involved in conformational changes of macromolecular structure and are the basis of one class of gated ion-channels. They may also affect physical properties and the chemical reactivity of biomolecules *in vivo*. These interactions between metal ions may also have an important role in genetic expression, metalloenzyme activity and metal-nucleic acid processes [39]. There are several possible modes of association which are depicted in Figure 3.2. The most likely as indicated by infrared spectroscopy and nuclear magnetic resonance studies is shaded in the figure. The most common of all such reactions is simply the association of a proton. This drastically changes the electrostatics of the problem so that at low pH when carbonyl groups are protonated, the structure of the protein differs

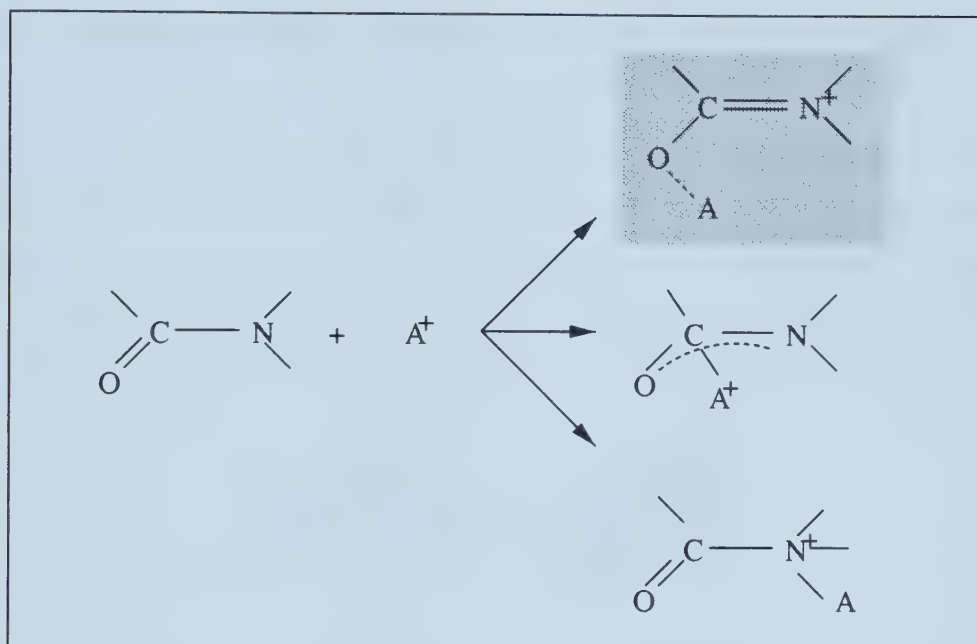


Figure 3.2: Association of a metal ion or proton to a peptide. The charged ion or proton (A^+) may form a bond with either the carbonyl oxygen, the carbonyl carbon or the nitrogen.

somewhat from its high pH form. Rather than changing the band gap, such interactions with metal ions may allow the protein to donate electrons to the metal ions thereby creating holes in the conduction band. Protons (H^+) seem to accept electrons much more readily than do lithium, sodium and larger metallic ions [39, 40]. This property led to some study of electronic conduction where protons act like a ferry but carry electrons in only one direction.

There are only three significant types of charge carriers: electrons, heavy ions and protons. The electrons have a high mobility and there are many familiar materials capable of supporting their conduction such as metals. Heavy ions can easily carry a charge but are immobile within solids. Protons fill the intermediate case, and while they present many experimental difficulties, they may exist within both liquid and solid media. Although three orders of magnitude heavier than an electron, the bare proton or H^+ ion is much smaller than any other ion

precisely because it does not carry any electrons. Within the cytoplasm, the proton will typically combine with water to form hydronium ion (H_3O^+) which is significantly larger but remains light compared to ions such as potassium. As a result, it has a higher mobility and the suspicion of hydronium's involvement in conduction is that it may hop along the outside of a protein becoming localized at negatively charged pockets of the protein. Protons might also act as carriers

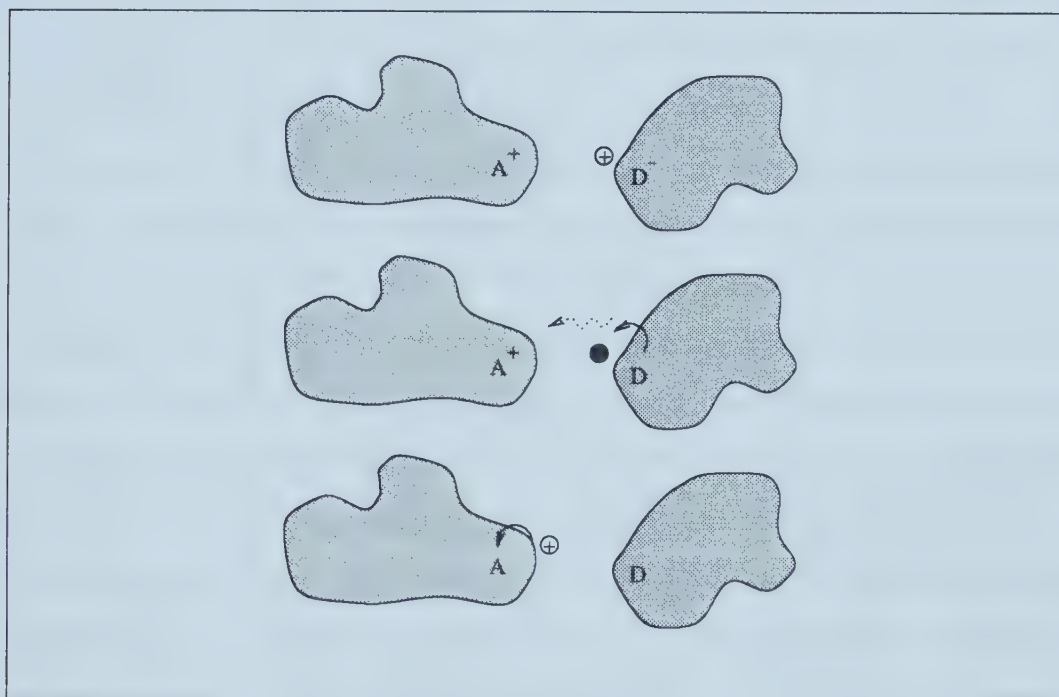


Figure 3.3: Proton ferries electron between donor and acceptor sites. The proton approaches the donor, accepts an electron and then may freely diffuse to the acceptor site where it then donates the electron. Once the donor and acceptor structures relax to their initial states, the process begins again.

of negatively charged ions or electrons [41]. Potential barriers are required at electron injection and ejection points to prevent short circuiting. The injected protons in this mechanism of conduction would come from chemical reactions, redox reactions, or a proton reservoir at high chemical potential such as the interior of a mitochondrion [42].

3.6 Symbiosis of Physics and Biology

Finally, before delving into the study of MTs, consider the benefits which the fields of physics and biology may reap from each other. Biology gains an unprecedented understanding of protein interactions and hence the ability, for example, to predict drug action. There could even exist the possibility of synthesizing proteins for specific enzymatic purposes or to provide faster turnover. Eventually, drugs could be tested by computer for side effects, by comparing the surface of the compound to naturally occurring agents circulating within the body.

The possible assets which physicists and engineers may gain from such study could be substantial if they are able to harness the special abilities of biological systems. Due to their microscopic size, biological systems are the target of experimental investigation for the purpose of reducing circuit dimensions further from the microscale to the nanoscale [43]. In particular, digital logic operations are desired and attempts are currently underway to build biological logic gates that can be controlled from outside of the system by an optical signal as proposed by Ashkenazi et al. [44]. They have designed a biochemical switch by connecting an electron donor group to an electron acceptor group. Enzymatic activity is switched on and off when the molecule switches between its two tautomeric states. The change of conformation occurs when an electron is transferred through conjugated carbon-carbon bonds over a 2 nm distance.

Producing nano-electronic systems using biomolecules could offer the possibility of mass production given that biological systems have the ability to self-assemble. Eventually, one might be able to construct a new nano-circuit and build it using the appropriately designed protein. In this respect, crude efforts are already underway and look promising. Kirsch et al. [45] are constructing wires with nanometer radii from MTs. They claim MTs are particularly well-suited for use as biomolecular templates for nanowires. The MTs are grown under

typical cellular conditions and then plated with nickel. The resulting wires have a 40–50 nm radius and show ohmic response when a current is passed along their length with a resistance of 1 k Ω . These wires are simpler to produce than carbon nanotubes and have a conductivity of about $5 \times 10^3 \Omega^{-1}\text{cm}^{-1}$ that is typical of a weak conductor. Such examples of logic gates and nanowires are simply selected as two of many efforts to gain a better understanding of organic structure which may have industrial significance.

Bibliography

- [1] A.S. Daydov, *Biology and Quantum Mechanics*, Pergammon Press, Toronto, 1982.
- [2] M. Wikstrom, *Identification of the electron transfers in cytochrome oxidase that are coupled to proton-pumping.*, *Nature (London)* **338**, 776–778 (1989).
- [3] M. Brunori and M.T. Wilson, *Electron transfer and proton pumping in cytochrome oxidase*, *Biochimie* **77**, 668–676 (1995).
- [4] O. Einarsdottir, K.E. Georgiadis, and A. Sucheta, *Intramolecular electron transfer and conformational changes in cytochrome c oxidase*, *Biochemistry* **34**, 496–508 (1995).
- [5] G. Albrecht-Buehler, *The Centrosome*, chapter Speculation about the function and formation of centrioles and basal bodies., pages 69–102, Academic Press, San Diego, 1992.
- [6] B. Alberts, D. Bray, J. Lewis, M. Raff, K. Roberts, and J.D. Watson, *Molecular biology of the cell*, Garland Publishing, London, 1994.
- [7] M.V. Volkenstein, *General Biophysics*, Academic Press, New York, 1983.
- [8] A.L. Hodgkin and A.F. Huxley, *Action Potentials Recorded from Inside a Nerve Fibre*, *Nature (London)* **144**, 710–711 (1939).

- [9] A.J. Maniotis, C.S. Chen, and D.E. Ingber, *Demonstration of mechanical connections between integrins, cytoskeletal filaments, and nucleoplasm that stabilize nuclear structure*, Proc. Natl. Acad. Sci. USA **94**, 849–854 (1997).
- [10] James Glanz, *Force-Carrying Web Pervades Living Cell*, Science **276**, 678–679 (1997).
- [11] P.M. Vassilev, R.T. Dronzine, M.P. Vassileva, and G.A. Georgiev, *Parallel arrays of microtubules formed in electric and magnetic fields*, Biosci. Rep. **2**, 1025–1029 (1982).
- [12] R.G. White, G.J. Hyde, and R.L. Overall, *Microtubule arrays in regenerating Mougeotia protoplasts may be oriented by electric fields*, Protoplasma **158**, 73–85 (1990).
- [13] W. Vater, R. Stracke, K.J. Böhm, C. Speicher, P. Weber, and E. Unger, *Behaviour of individual microtubules and microtubule bundles in electric fields*, preprint, 1998.
- [14] W. Bras, G.P. Diakun, J.F. Diaz, G. Maret, H. Kramer, J. Bordas, and F.J Medrano, *The Susceptibility of Pure Tubulin to High Magnetic Fields: A Magnetic Birefringence and X-Ray Fiber Diffraction Study*, Biophysical J. **74**, 1509–1521 (1998).
- [15] R.W.P. King and T.T. Wu, *Electric field induced in cells in the human body when this is exposed to low-frequency electric fields*, Phys. Rev. E **58**, 2363–2369 (1998).
- [16] G. Cavelier, *Short Note: Are Electron-Transport and Electron-Transfer involved in Intracellular Signalling?*, Medical Hypotheses **44**, 261–262 (1995).

- [17] H. Athenstaedt, *Pyroelectric and piezoelectric properties of Vertebrates*, Ann. N.Y. Acad. Sci. **238**, 68–94 (1974).
- [18] R.O. Becker and A.A. Marino, *Electromagnetism and life*, Suny Press, Albany, 1982.
- [19] J. Black, *Electrical Stimulation: Its role in growth, repair and remodelling of the musculoskeletal system*, Praeger, New York, 1991.
- [20] R.O. Becker and G. Selden, *The Body Electric Electromagnetism and the Foundation of Life*, W Morrow and Co., New York, 1985.
- [21] E.D. Salmon, *Pressure-induced depolymerization of spindle microtubules. I. Spindle birefringence and length changes.*, J. Cell Biol. **65**, 603–614 (1975).
- [22] E.D. Salmon, *Pressure-induced depolymerization of spindle microtubules. II. Thermodynamics of in vivo spindle assembly.*, J. Cell Biol. **66**, 114–127 (1975).
- [23] A. Pochettino, Atti Accad. Naz. Lincei. **15**, 355 (1906).
- [24] A. Szent-Györgyi, *Towards a new biochemistry?*, Science **93**, 609–611 (1941).
- [25] A. Szent-Györgyi, *Study of energy levels in biochemistry*, Nature (London) **148**, 157–159 (1941).
- [26] A. Szent-Györgyi, *Internal Photo-electric effect and band spectra in proteins*, Nature (London) **157**, 875 (1946).
- [27] B. Rosenberg, *Electrical Conductivity of Proteins*, Nature (London) **193**, 364 (1962).

- [28] B. Rosenberg, *Electrical Conductivity of Proteins. II. Semiconduction in Crystalline Bovine Hemoglobin*, J. Chem. Phys. **36**, 816–823 (1962).
- [29] K.D. Straub, *A Solid State Theory of Oxidative Phosphorylation*, J. Theor. Biol. **44**, 191–206 (1974).
- [30] D.A. Harris, *Bioenergetics at a Glance*, Blackwell Science, Oxford, 1995.
- [31] D.D. Eley, G.P. Parfitt, M.B. Perry, and D.H. Taysum, *The semiconductivity of organic substances, Part 1*, Trans. Faraday Soc. **49**, 79–86 (1953).
- [32] D.D. Eley and D.I. Spivey, *The semiconductivity of organic substances, Part 6 – A Range of Proteins*, Trans. Faraday Soc. **56**, 1432–1442 (1960).
- [33] D.D. Eley and D.I. Spivey, *The semiconductivity of organic substances, Part 9 – Nucleic Acid in the dry state*, Trans. Faraday Soc. **58**, 411–415 (1962).
- [34] R. Pethig and A. Szent-Györgyi, *Electronic Properties of Casein-Methylglyoxal Complex*, Proc. Natl. Acad. Sci. USA **74**, 226–228 (1977).
- [35] F.W. Cope, *A review of the applications of solid state physics concepts to biological systems*, J. Biol. Phys. **3**, 1–41 (1975).
- [36] E.C. Lin and H.F. Cantiello, *A Novel Method to Study the Electrodynamical Behavior of Actin Filaments. Evidence for Cable-like Properties of Actin*, Biophys. J. **65**, 1371–1378 (1993).
- [37] Y. Okamoto and Walter Brenner, *Organic Semiconductors*, Reinhold, New York, 1964.
- [38] C.-M. Liegener, P. Otto, R. Chen, and J. Ladik, *On the electronic band structure of periodic β -pleated sheet polypeptides in the presence of water and ions*, Theor. Chim. Acta **73**, 449–458 (1988).

- [39] A.K. Bakhshi, *Investigation of Electronic Conduction in Proteins and DNA*, Prog. Biophys. Molec. Biol. **61**, 187–253 (1994).
- [40] A.S. Davydov, *The Role of Proteins in Electron Transport at Large Distances*, Phys. St. Sol. **90**, 457–464 (1978).
- [41] R.N. Robertson and N.K. Boardman, *The link between charge separation and proton movement, and ATPase reactions*, FEBS Letters **60**, 1–6 (1975).
- [42] P. Mitchell, *Chemiosmotic Coupling in Oxidative and Photosynthetic Phosphorylation*, Glynn Research, UK, 1966.
- [43] D. Bray, *Protein molecules as computational elements in living cells*, Nature (London) **376**, 307–312 (1995).
- [44] G. Ashkenazi, D.R. Ripoll, N. Lotan, and H.A. Scheraga, *A molecular switch for biochemical logic gates: conformational studies*, Biosensors & Bioelectronics **12**, 85–95 (1997).
- [45] R. Kirsch, M. Mertig, W. Pompe, R. Wahl, G. Sadowski, K.J. Böhm, and E. Unger, *Three-dimensional metallization of microtubules*, Thin Solid Films **305**, 248–253 (1997).

Chapter 4

Dipole Ordering

4.1 Ising Model

The 1D Ising model consists of a lattice of spin variables, each of which may take on one of two values, +1 or -1. These spin variables interact with each other and with an external magnetic field. The Ising model is a useful starting point in our study of dipole ordering since we shall view the tubulin dimer as a two-state system. MT protofilaments have been observed to be either straight or curved and this is believed to be related to the conformation of the individual dimers. The change in the conformation of the dimer causes charge to be redistributed throughout the tubulin dimer and the two states are considered to be the result of charge localization at one of two binding sites on tubulin [1, 2].

The simplest Ising system consists of a string (one-dimensional lattice) of N sites in which only nearest neighbour interactions are considered. In such a system, the Ising Hamiltonian may be written as follows:

$$\mathcal{H} = -J \sum_{k=1}^N \sigma_k \sigma_{k+1} - h \sum_{k=1}^N \sigma_k, \quad (4.1)$$

where J represents the strength of the spin-spin interaction between nearest neighbours and h represents the strength of the interaction between the external magnetic field and the spin variables, σ_k [3]. A positive J represents a ferromagnetic interaction, that is an interaction which favours the pairing of neighbouring

spins. A negative J favours anti-parallel orientation for neighbouring spins. The model was first studied in 1925 by Ising [4] who solved the statistical mechanics of this 1D system analytically in the presence of a magnetic field.

While the 1D Ising model with nearest neighbour terms does not possess a phase transition at a finite temperature, the 2D Ising model does have a phase transition [5, 6] between a low-temperature ordered (ferromagnetic) phase and a high-temperature disordered (paramagnetic) phase. It exhibits many of the physical properties peculiar to magnetic systems. There are several different cases to consider in a 2D lattice. For example, in a finite rectangular lattice there will be two different interaction strengths to consider, J_h and J_v for the horizontal and vertical interactions, respectively. In addition, there is both the relative magnitude of the two interactions and their signs to consider. For a regular rectangular lattice, there is no frustration for free boundary conditions and consequently a well defined ground state exists. The lone degeneracy consists of a reversal of spin for all lattice sites. Obviously, this can be lifted by the application of a magnetic field. If the boundary conditions are cylindrical, toroidal or altogether specified in a more complicated manner, the ground state may include frustration. This simply means that the overall global lowest energy configuration includes some local interactions which are not minimized. Since the location of frustration can be anywhere on the lattice, these ground states are highly degenerate. This will be only one of the complications we shall deal with later. We will also consider several MT lattices, all of which are triangular and have three interactions to consider.

4.2 A Biological Ising System

In the early 1980s, the hypothesis was put forward that MTs may act as biological computers [7]. At that time, a model was proposed for the storage and processing

of information by these biological polymers. The idea was initially spawned by mounting indirect evidence that indicated that the cytoskeleton and MTs in particular may act as a cellular nervous system. Recently, this idea of a cellular nervous system has been given much credibility given the meticulous work of Albrecht-Bühler. While Hameroff envisaged the MTs as having information processing capability, Albrecht-Bühler postulates the centriole to be the cell's 'brain' with MTs performing signalling functions akin to the nerves and the actin filaments playing the role of a rudimentary musculature. In the Hameroff and Watt model of information storage and processing, each dimer of a MT represents a classical two state system [8]. The two states are directly related to the observed change in tubulin's conformation and behave as binary code for a biological computer. Since then, we have refined physically the above model [9]. Depending on whether the dimer is presently in the *up* or *down* state, the dimer's dipole adopts a corresponding orientation. Each dimer may then interact with its nearest neighbours and the MT lattice is thus the special lattice on which interactions are studied. The electroconformational energy of the MT is given by performing the sum over all dipole-dipole interactions. The analogous 2D Ising model has the following Hamiltonian:

$$\mathcal{H} = - \sum_{\substack{\langle nn \rangle \\ i,j,k,l}} J_{ijkl} \sigma_{ij} \sigma_{kl} + h \sum_{i,j} \sigma_{ij}, \quad (4.2)$$

where the σ_{ij} labels the spin variable at the site (i, j) which may be up $\sigma_{ij} = +1$ or down $\sigma_{ij} = -1$. h represents an external field conjugate to the spin variable σ and J_{ijkl} picks out the specific interaction for two nearest neighbour spin variables. The system under study differs slightly since the dipoles are not precisely opposite as are spins of an Ising system and the electric field and the dipoles are not exactly parallel. However, since there are only two possible dipole orientations, the system's behaviour is expected to show similarities to Ising systems.

4.2.1 The Dipole Interaction Model

This model of ferroelectric effects in MTs was inspired by the cellular automaton model of Hameroff et al. [2]. Within our model, there is no net charge on each dimer but there is instead a permanent and switchable dipole associated with each dimer, and consequently the overall structure may have an electric polarization. This change simplifies the study of the interaction of an electric field with the lattice. In comparison with the Ising model just mentioned, the spins, σ are replaced by electric dipoles, \mathbf{p} and the magnetic field, h , is replaced with the electric field, \mathbf{E} . One orientation of the dipole points along the protofilament axis, this is the up state (Figure 4.1). We have some freedom to choose the direction of the dipole in the down state since the electric dipole has not been measured in each of tubulin's conformational states.¹ We have chosen the down

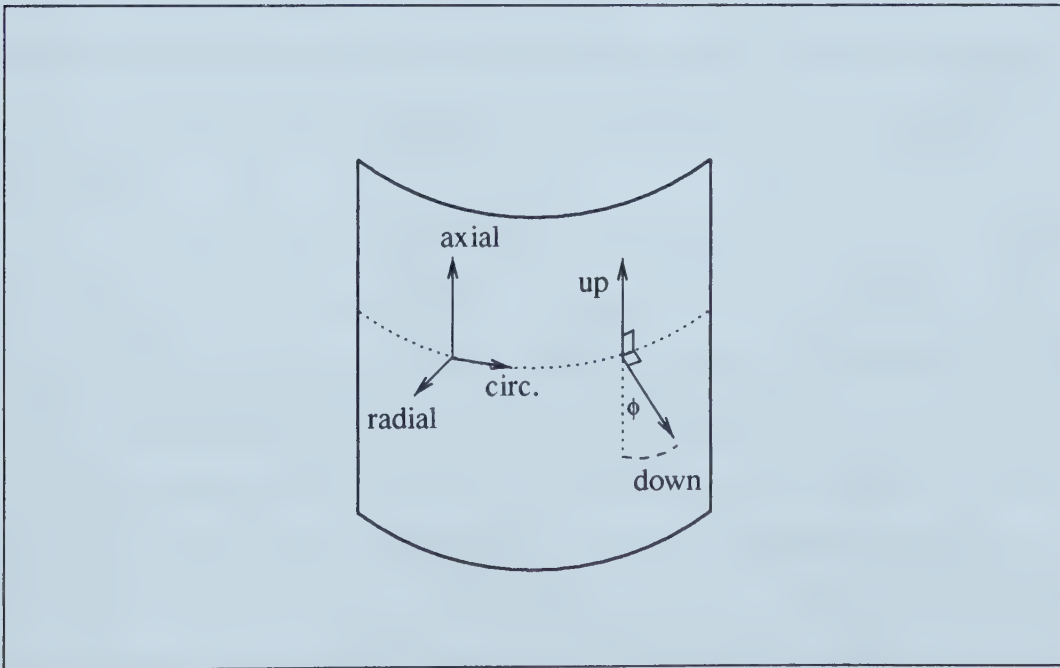


Figure 4.1: This view of the outer surface of a MT identifies the directions of fields we consider. The axial or vertical direction in this diagram points away from the cell body. At the right, the up and down directions which were selected for tubulin's dipole moment are shown ($\phi = 29^\circ$).

state's orientation in a direction which is roughly opposite to the direction of the up state but which is 29° from the vertical and points out radially away from the MT. This choice is based on the geometry of MT ends that are splaying apart during disassembly. Under these conditions, tubulin adopts a different conformation with curved protofilaments [10]. The results of simulations presented here have been carried out with $\phi = 29^\circ$ down states. Some degree of tilting is necessary if action potentials are to influence the dipole dynamics because the non-tilted dipole is entirely axial and the electric field of the action potential is largely radial [9]. Consequently, there would be no interaction unless one of the states has some radial component since the interaction energy between a dipole and an electric field, U_E , is simply

$$U_E = -\mathbf{p} \cdot \mathbf{E}, \quad (4.3)$$

where \mathbf{p} is the dipole moment and \mathbf{E} is the electric field. The interaction energy between two elementary dipoles, \mathbf{p}_1 and \mathbf{p}_2 , is given by the following well-known formula [11]:

$$U_{\text{int}} = \frac{1}{4\pi\epsilon\epsilon_0} \frac{\mathbf{p}_1 \cdot \mathbf{p}_2 - 3(\mathbf{p}_1 \cdot \mathbf{n})(\mathbf{p}_2 \cdot \mathbf{n})}{r^3}, \quad (4.4)$$

where ϵ is the relative permittivity of the medium, ϵ_0 is the permittivity of free space, \mathbf{n} is the normal vector pointing from the position of the first dipole to the second dipole and r is the distance separating the dipoles. Equations (4.3) and (4.4) are summed over all lattice sites and replace the Ising Hamiltonian of equation (4.2). The effect of the dipole interactions is that the lattice of dipoles will undergo a phase transition and self-organize below a critical temperature, into an energetically favoured configuration. At sufficiently high temperatures, the lattice has a random state – each individual dimer can be found in the up or down state in a rather arbitrary, uncorrelated fashion. At lower temperatures,

¹The dipole has since been determined in one conformational state of tubulin and this is discussed in Chapter 7.

the interaction energy dictates the dipole arrangement and the lattice becomes ordered. Our task is to investigate this transition in order to determine the likely state of a MT under physiological conditions.

There are two parameters in the model that are unknown and had to be estimated. One is the relative permittivity of tubulin in cytoplasm, ϵ , and the other is the magnitude of the dipole moment of tubulin, p . The dielectric constant of dry tubulin or of tubulin in solution has not been found in the literature although some experiments give permittivities in excess of 100 for some other proteins in solution [12]. Our choice of these parameters allows us to compare results with previous modelling attempts. Later on, we make use of new X-ray crystallography data on the structure of tubulin [13]. This allows us to perform a calculation of its dipole moment but only provides its value in the ‘straight’ conformation. The value which is required by the model is of the change in p between conformations, and this is simply estimated and compared for consistency. All of this dependence can be accounted for by a single parameter, Q , where

$$Q = p^2/\epsilon . \quad (4.5)$$

The dynamics of the model are unaffected by the choice of Q in the absence of a field, the value of Q simply scales the transition temperature. Larger values of Q increase interaction strengths and thereby increase the transition temperature. In the case of an electric field, the dipole-dipole term scales as Q while the electric field-dipole interaction scales only as \sqrt{Q} , and hence changing the value of Q influences not only the transition temperature but also scales the relative strength of the two interaction terms. We have chosen $Q = 12 \times 10^{-56} \text{ C}^2 \cdot \text{m}^2 \simeq 10800 \text{ (Debye)}^2$. For a dipole corresponding to an electronic charge, with a charge separation of one dimer unit, 8 nm, $\epsilon \simeq 13$ given this choice. This value for the tubulin dipole of $1.28 \times 10^{-27} \text{ C} \cdot \text{m}$ (384 Debye) has the same order of magnitude as some other globular proteins [12]. This may be a conservative estimate as

Athenstädt has reported the dipole moment of another fibrous molecule, collagen, to be about 15 000 Debye. The important number is not the total dipole but the change in the dipole, consequently the smaller figure that we report seems reasonable. It is important to note that the precise value of the dipole moment depends on the pH of the surrounding medium. The following results are derived from these estimates of the tubulin dimer's dipole moment. We shall comment on how any changes to these parameters affect the results of our simulations.

An investigation of the system's phase space determines the ground state of this classical system. Strictly speaking, this is the state of the system only at 0 K, as above absolute zero thermal fluctuations may allow the system to be in an excited state where some dimers have a conformation inconsistent with the ground state. The task is to quantify the *typical* conformation of the system at finite temperature. A simple method is to catalogue all states by their respective energies and to take a statistical average using a Boltzmann distribution for the probabilities as a function of the state's energy. The difficulty with this approach is simply the large number of states available in a MT. For a MT with 13 protofilaments and 1000 tubulin subunits in length, the number of states is $2^{13000} \approx 10^{4000}$. Obviously, such a problem is intractable and as a gross approximation, we reduce the problem to a much smaller lattice, for example, 13 protofilaments by 3 rows with the hope that most of the details are not destroyed by finite-size effects. A problem of 39 sites has 2^{39} or about 10^{12} different states. Thus one may attempt this problem but there are still some difficulties in adopting a statistical mechanical counting approach to attack the problem.

The difficulty of the statistical mechanical approach has to do with measuring the polarization of a lattice which has a degenerate ground state. The plot in Figure 4.2 shows the problem which is faced. At low temperatures, there are two ground states which are degenerate, one with polarization +1, the other

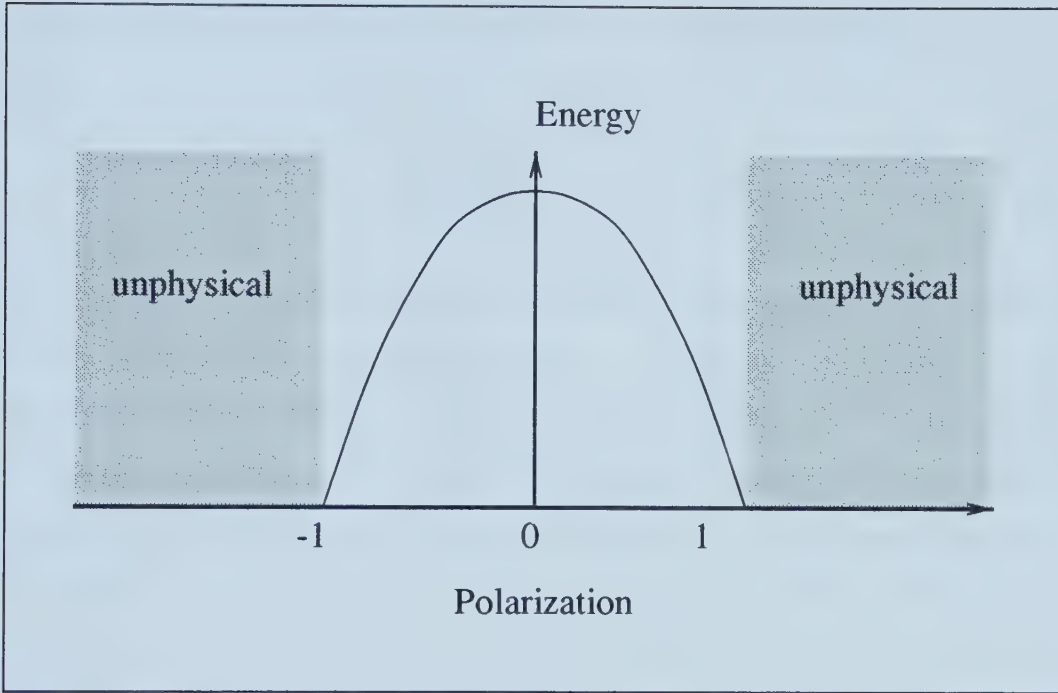


Figure 4.2: Schematic diagram of the average energy of system configurations with a given polarization.

with polarization -1. Since the states are equally likely, at zero temperature, the statistical mechanical average weights -1 with a probability of 0.5 and weights +1 with the same the probability. The statistical mechanical polarization, P_{sm} would therefore be zero, while the actual system would adopt either +1 or -1 but be far from the average.

$$\begin{aligned}
 P_{\text{sm}} &= \sum_i p_i P_i \\
 &\xrightarrow{\text{low } T} \frac{1}{2}(-1) + \frac{1}{2}(+1) = 0
 \end{aligned} \tag{4.6}$$

In this case, it is obvious that taking the absolute value of the polarization would be appropriate to pick up the actual polarization at low temperature. Unfortunately, this leads to difficulty for the high temperature behaviour. For

sufficiently high temperatures, all states have an equal probability.

$$|P_{\text{sm}}| = \sum_i p_i |P_i| \quad (4.7)$$

$$\xrightarrow{\text{high } T} \frac{1}{N} \sum_i |P_i| > 0.$$

where here, N represents the number of lattice configuration states. However, since the absolute value of the polarization is necessarily non-negative for each configuration, the statistical average of the absolute value, $|P_{\text{sm}}|$ gives a positive result rather than zero. The Monte Carlo simulation gives a typical value of the polarization rather than the average value of the polarization. Consequently, the Monte Carlo method lends itself to a determination of the phase transition because it is a numerical representation of the physical system and will therefore select some typical configuration for a given temperature. Below the transition temperature, its order parameter, polarization, will become non-zero. In the case of correlation functions, they become non-zero at temperatures above the transition temperature of the lattice because strong local interactions can dictate local clustering behaviour. Correlation functions of dipoles separated by larger distances however, will be sensitive to only ordering of the entire lattice. As an additional benefit, larger lattices can be sampled and all results presented for Monte Carlo lattices represent MTs of 13 protofilaments, each protofilament consisting of 1000 subunits.

4.2.2 Boundary Conditions: Lattice Types

Consider the interaction between dipoles of the MT lattice. From a purely structural point of view, the lattice type may seem insignificant, as one does not expect that it will change assembly dynamics or elastic properties much. However, from the point of view of dipole interaction, the lattice type is crucial. In the B lattice, dimers are aligned in nearly horizontal rows (Figure 4.3) and as a result,

there is a strong interaction between neighbouring protofilaments which favours antiparallel dipole orientations. In the A lattice, the neighbouring protofilaments are shifted vertically such that identical orientation of the dipoles is favoured. In either case, there is a strong interaction along individual protofilaments which favours similarly oriented dipoles. This observation shall be reflected when the

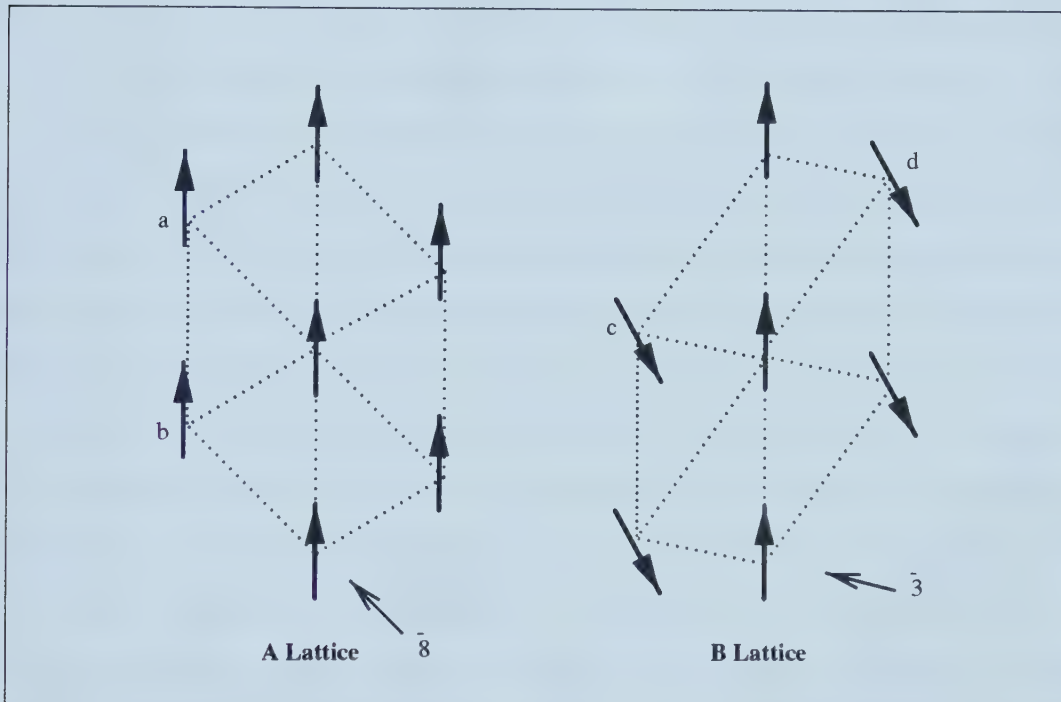


Figure 4.3: Nearest neighbour interactions: Along the protofilament, alignment is preferred so that the negative tails are close to the positive heads. Between protofilaments, the preferred orientation is determined by the vertical offset of the lattice. Left: Aligned protofilaments are preferred in the A lattice. Right: In the B lattice, anti-aligned protofilaments are preferred.

ground state behaviour of the A and B lattices are presented.

In addition to these changes which concern the bulk of the lattice, the lattice structure affects the closure of the MT and hence the boundary conditions when protofilament 1 joins with protofilament 13 (or protofilament N in a generalized MT). The monomer lattice of the MT is helical and arranged such that there is an upward offset between monomers of neighbouring protofilaments of

0.92 nm (12 nm/13) when moving around the MT in a left-handed sense. Since the monomer spacing along a protofilament is 4 nm, this represents a rise of 3 monomers for each loop of the helix, and hence the name $\bar{3}$ -start to the line of monomers which executes this path. However, there are two types of lattice which have been described in the literature, known as the A lattice and the B lattice [14, 15]. If one follows the $\bar{3}$ start helix, the monomers alternate (α - β - α - β -...) in the A lattice but remain the same in the B lattice (α - α - α - α -...) or (β - β - β - β -...), except at the seam, where there is an α - β link. Thus the A lattice has complete helical symmetry which the B lattice lacks. Since the dimer is the fundamental unit from which MTs are constructed, the dipole is associated with each dimer and the lattice change means that interactions are quite different between the two geometries. The MT lattice has a relatively small width, typically 13 subunits. Hence there are never more than 6 subunits of tubulin between any particular tubulin molecule and the seam, and as a result, the boundary conditions introduced at the seam play an important role in determining the equilibrium configuration of the system. In the MT 13A lattice which has alternating α and β subunits along the $\bar{3}$ start helix, there is no seam. In this perfectly helical system, the energy is minimized when protofilaments have uniform orientation. Hence there is a ferroelectric state with all spins pointed in the plus direction. In the MT 13B lattice, subunits do not alternate along the $\bar{3}$ start helix. There is also order at low temperatures, but the lowest energy state is not ferroelectric because while the interaction at the seam is of the A type, the interaction away from the boundary now favours anti-alignment of protofilament dipoles. Consequently, the ground state is a sequence of antiferroelectric protofilaments.

4.2.3 Monte Carlo Simulation

The lattice dynamics in our model are simulated using a standard Monte Carlo technique [16]. For each timestep, the energy of the present state and the opposite state are calculated. A change of state is a random event; the probability of its occurrence is determined by the temperature. The problems with the statistical mechanical approach were briefly outlined earlier, however the Monte Carlo approach has its own difficulties. In particular, it does a poor job of sampling in the ‘transition’ region from order to disorder. We have tried to overcome this difficulty by adopting several different approaches in concert that minimize the uncertainty near the transition temperature. We increased lattice size where possible to reduce finite-size effects and by a simple numbers argument, to reduce the noise in the sample. In addition, simulations have gradually reduced the temperature and used the last configuration of the previous temperature as a seed for the following simulation. This method of simulation is computational annealing. Finally, a correlation function has also been calculated between dimers separated by a large distance on the lattice. Long range order is the hallmark of a ferroelectric phase transition and this correlation function often seems to have a better defined transition temperature than an examination of a plot of the polarization.

A visual confirmation that the program is working properly is possible due to a visual display. With this display, it is observed that the MT will often condense into different ground states at either end and consequently, if the temperature is reduced sufficiently rapidly, an artifact of the cooling will persist once at low temperature the lattice is frozen. These domain walls are localized regions of stored energy since molecules located along the boundary find that the molecules of the two adjoining domains specify opposite conformations. Such frustration along the length of the MT will not be a particular focus since temperature

fluctuations in a living system are expected to be minimal and slow enough that flash-freezing will not be an issue as there is time for the ends of the MT to communicate, this in turn ensures that a global energy minimum shall be found. Since the global energy minimum is certain to be found, an advantage of the Monte Carlo simulation, is that it is also possible to begin from one of the true ground states at absolute zero and slowly increase the temperature. This has two benefits to working in the opposite direction. The first is that we do not have to worry about the problem of quick freezing which was explained above, and this allows the simulation to be conducted more quickly. Results are periodically compared to the case where the system is started at the warmest temperature and the thermal energy slowly reduced to check that there are no hysteresis effects.

4.3 Results

We are plotting an order parameter, P , representing scaled polarization, which is defined over the N lattice sites by

$$P = \frac{1}{N} \sum_{i,j} \sigma_{ij}, \quad (4.8)$$

where the σ_{ij} is +1 or -1 and describes the conformation of the dipole labelled (i, j) of the 2D cylindrical lattice. The other correlation functions which shall prove useful are χ_1 , defined by:

$$\chi_1 = \frac{1}{N} \sum_{i,j} \sigma_{ij} \sigma_{ij+1}, \quad (4.9)$$

and χ_L , defined by:

$$\chi_L = \frac{1}{N} \sum_{i,j} \sigma_{ij} \sigma_{ij+L}, \quad (4.10)$$

where L is half the length of the MT lattice under investigation. Along individual protofilaments, head-to-tail alignment of dipoles is preferred, so that the

positive end of one dipole is next to the negative end of the adjoining dipole. Consequently, dipoles will seek parallel alignment along a protofilament at low temperature when the MT lies in its ground state. This proves to be true of both the A and B lattices so these correlation functions just described are suitable for both lattice types.

4.3.1 MT 13A Lattice

Consider the two nearest neighbour dimers, labelled 'a' and 'b' that are located on the protofilament directly to the left of the central dimer in Figure 4.3. Relative to the interaction along the protofilament, J , there is an interaction of strength $0.35J$ along the direction 'a', and an interaction of strength $-0.22J$ along the direction 'b'. Both of these are smaller than the interaction along the protofilament, so indeed parallel alignment along the protofilament is expected. Of the off-protofilament interactions, the larger interaction 'a' is ferroelectric so neighbouring protofilaments adopt a configuration of parallel dipoles. Consequently, the ground state consists of all dipoles in parallel alignment as shown in Figure 4.4. Since the down state is tilted, with $\phi = 29^\circ$, the ground state is unique. Figure 4.5 shows the polarization of the MT 13A lattice which has a transition temperature of 240 K given our choice of lattice parameters. This value is about 20% lower than physiological temperature and we shall discuss how this transition temperature can be scaled in this chapter's summary. We will see that a small change in these estimated quantities can result in a prediction of a higher transition temperature which would imply an ordered MT 13A lattice at physiological temperature, 310 K.

4.3.2 MT 13B Lattice

In the B lattice, the situation is somewhat changed. The interaction strength along the protofilament remains J , however, there is an interaction of strength

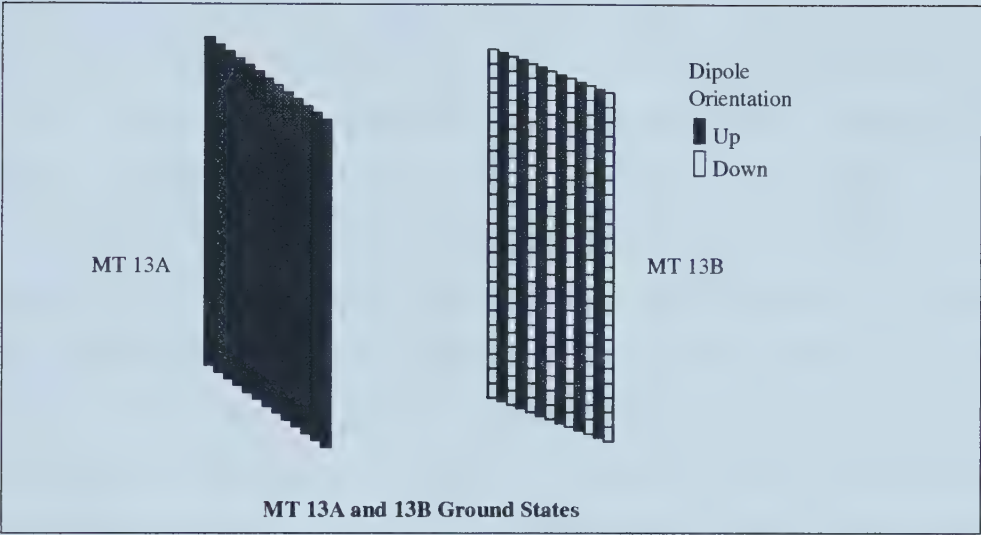


Figure 4.4: Left: Ground state of the MT 13A lattice, which is completely ferroelectric. Shading of dimers indicates their orientation. Right: Ground state of the MT 13B lattice, which demonstrates antiferroelectric order between neighbouring protofilaments.

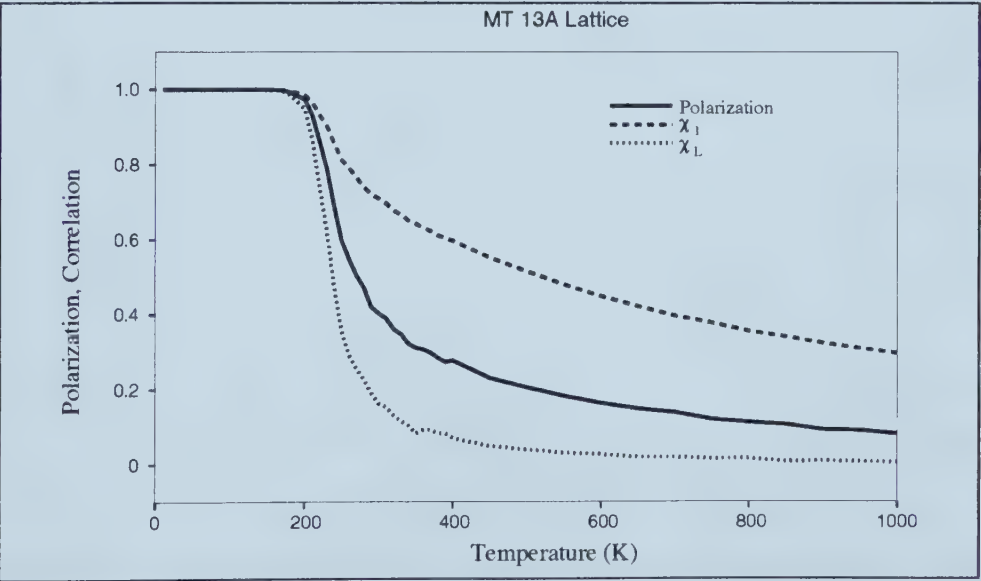


Figure 4.5: Electric polarization and correlation functions of the MT 13A lattice as a function of temperature, obtained from Monte Carlo modelling.

$-1.76J$ along the direction ‘c’, and an interaction of strength $0.39J$ along the direction ‘d’ as defined by Figure 4.3. The largest interaction dictates that there must be alternating dipole orientation along the corresponding direction ‘c’. Hence, given that dipoles must alternate along the helix defined by the ‘c’ direction, the other two interactions are conflicting but the interaction along the protofilament is larger. As a result, dipoles are still in parallel alignment along the protofilament. The entire lattice now consists of protofilaments with alternating dipole orientations as depicted in Figure 4.4. The transition temperature of 655 K for the MT 13B lattice is higher than that of the MT 13A lattice. This is not too surprising since the maximum interaction strength is larger in this lattice. The ordered 13B lattice has a polarization of $-\frac{1}{13}$ ($= \frac{6-7}{6+7}$) since six protofilaments have an up orientation and seven have a down orientation.

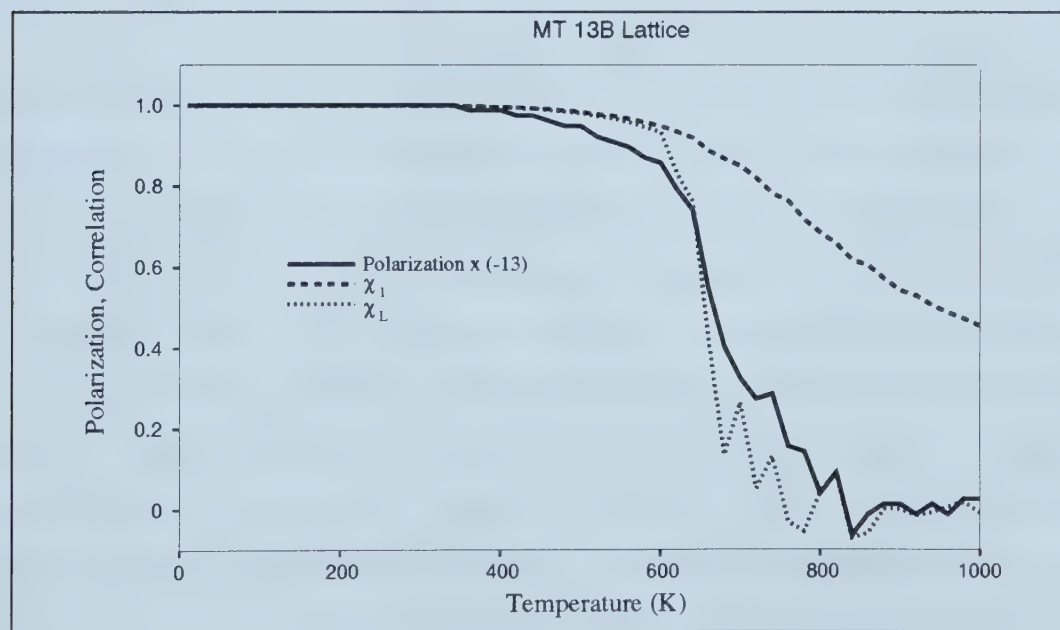


Figure 4.6: Electric polarization of the MT 13B lattice as a function of temperature. In the 13B lattice, one protofilament of 13 must be unpaired resulting in a finite polarization.

4.3.3 Electric Fields

An electric field can be applied to the dipoles and will change the lattice statistics by biasing a parallel dipole orientation. This is in direct analogy to the magnetic field in an Ising system. Here we are considering only the application of an electric field to the MT 13A lattice since it is the lattice with a large polarization in its ground state and consequently, the lattice which is most sensitive to electric fields. External electric fields need to be considered because in the axons and dendrites of nerve cells, electrical signals pass along the cell membrane subjecting the cell interior to strong transient electric fields. Particularly in the axon, where the orientation of the MT is fixed with respect to the field, the interaction is of great interest. Much more will be made of these fields in the following chapter when the dynamics of the interaction of action potentials and the MT lattice are studied. For now, we simply are interested in the static behaviour. The electric field introduces an anisotropy into the problem which will favour one conformation of tubulin compared to the other. That is, one conformation will have a dipole which is more aligned with the field than the other and hence will have a somewhat lower interaction energy. The result is that the lattice order is somewhat different than in the case where no external field has been applied. For fields of strength 10^5 V/m, 10^6 V/m and 10^7 V/m the results are plotted in Figure 4.7 and the effects of field strengths below 10^5 V/m appear to be negligible in the physiological temperature range. The field is applied in a direction along the axon in the direction of the up state, ie. along the protofilament axis. Our investigations show that the MT is sensitive to electric fields of the order 10^5 V/m; in physiological terms, this may be more usefully understood as 100 mV/ μ m and is smaller than the typical electric field of 10^7 V/m measured across cellular membranes. The important result is that the lattice remains ordered at a higher temperatures. Under the influence of electric fields of 10^5 V/m, 10^6 V/m and

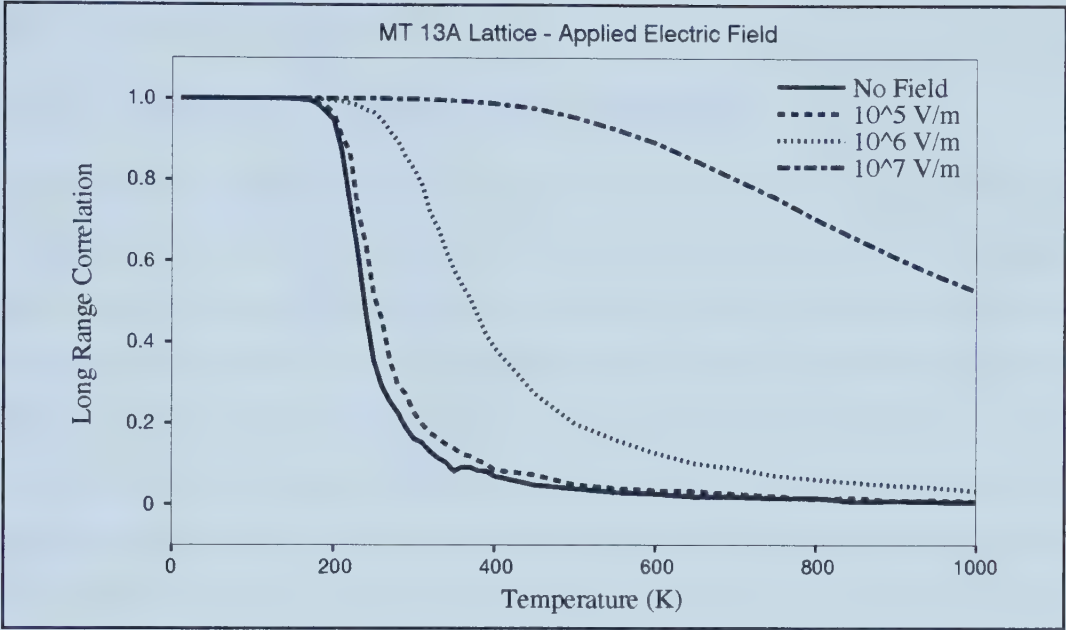


Figure 4.7: Polarization of the MT 13A lattice as a function of temperature as an electric field is applied in the direction of the up moment.

10^7 V/m, the ordering phase transition temperature is raised from 240 K to 250 K, 370 K and 1035 K, respectively.

The MT 13B lattice is also sensitive to electric fields, however, since its ground state includes protofilaments with opposite orientations, and a polarization of only $-\frac{1}{13}$, the impact of an electric field is reduced relative to the 13A lattice. A small electric field is sufficient to lift the degeneracy between ground states. For sufficiently large and unphysiological external fields, even the 13B lattice can be induced to be ferroelectric. These were among the tests carried out when the simulation program was tested. A more detailed account of the various simulations can be found in the doctoral thesis of Trpišova [17] or in the more recent article of Trpišova and Brown [18]. In this thesis, the simulation has been developed to study signal propagation so only the most relevant cases have been presented.

4.4 Lattice Defects

4.4.1 Alternate Protofilament Numbers

In addition to the effects of lattice type and applied fields upon the ordering of the lattice, there is also the question of how defects in the lattice have an impact upon dipole ordering. The two different types of lattice defect which we have considered are deviations in the protofilament number and the decoration of the lattice by MAPs. Firstly, consider lattice defects where the protofilament number is different than the usual 13. MTs with either 12 or 14 protofilaments are the next most common and *in vitro* there are often more 14 protofilament MTs than the biologically more relevant 13 protofilament polymers. In the case of these MTs, there is now a seam for both the A and B lattices. In the MT 14A lattice, the interaction at the seam is now B lattice-like, that is, those two neighbouring protofilaments favour anti-parallel orientation. These two protofilaments adopt anti-parallel ferroelectric ordering and the remaining protofilaments have some flexibility. That is, a ferroelectric seam must exist on the MT due to the dipole frustration. It should be distinguished from the seam we have discussed up until this point, which was structural. Since we have tilted dipoles, it turns out that this dipolar seam localizes at the structural seam as shown in Figure 4.8. This occurs because a lattice of dipoles all with the down state has a higher energy than the uniform all-up state. In the non-tilted case, its location is immaterial since it does not have an energetic consequence. So, one drawback to the MT 14A lattice is the relative lack of order as dipole interactions alone do not produce MTs with identical ferroelectric configurations; and this may be the reason that an odd number of protofilaments is preferred biologically. Even in this case where the seams are coincident, the column of down spins tracks back and forth between the two protofilaments bordering the physical seam, also seen in Figure 4.8. Similarly if we consider the MT 14B lattice, the bulk of the lattice imposes that

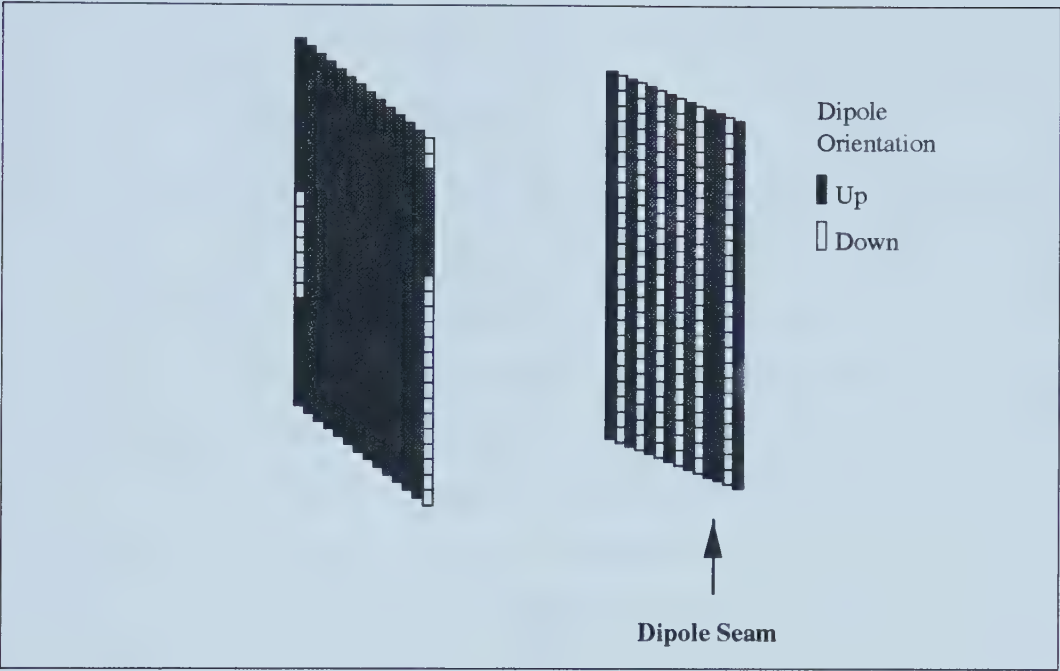


Figure 4.8: Left: Ground state of the MT 14A lattice where the dipole seam is coincident with the structural seam(at the edge in the diagram). Right: Low energy state of the MT 14B lattice where the dipole seam and structural seam do not coincide.

neighbouring protofilaments should have alternating dipole orientations; but at the structural seam which closes the MT cylinder, the preferred interaction is of parallel dipole orientations. The ground state occurs when the frustration is localized at the structural seam but there are several low energy states such as that pictured in Figure 4.8. This class of states has a dipole seam which can move without energetic costs around the lattice. The net polarization of the MT defined by equation (4.8) is zero in the ground state since the numbers of dimers in the up state and in the down state are equal and this is another reason why the correlation functions were defined to determine transition temperatures. Since the dipole of the up state and down state are not exactly opposite, the MT does retain a small electric polarization that, as speculated earlier, may be important for the directionality of motor protein motion and is certainly important for MT

spatial orientation.

4.4.2 The Impact of MAPs

We have also studied the impact which MT associated proteins, known as MAPs, have on dipole ordering in MTs. MAPs attach themselves to MTs in periodic patterns [19]. Their function is to stabilize the assembly properties of the MT. Our hypothesis is that this is accomplished by preventing the conformational change of the tubulin dimer to which it is attached. The net effect of such MAPs has been simulated given this assumption, and the result is qualitatively similar to the application of an electric field as can be seen in Figure 4.9. This may be understood by viewing the fixed conformation dipoles as seeds of order. In the limit where one could connect a MAP to each tubulin dimer in a MT, the lattice would be ordered at all temperatures and hence lower concentrations of MAPs are expected to help order the lattice. The MAPs do not actually change any of the interactions between sites which are not attached to MAPs. Their effect can be modelled in two different ways, firstly, the role of the MAP was considered as a structure which prevents the dimer to which it is attached from changing conformation. In the corresponding lattice of dipoles, certain spins were assigned the +1 state and not permitted to change. Secondly, we considered the possibility that MAP attachment neutralizes the existing dipole. In this latter case, the corresponding lattice of dipoles was assigned zeroes at the locations where MAPs were attached. The results were perhaps somewhat predictable and results for the MAPs with +1 states are shown in Figure 4.9. We found that the transition temperature was raised from 240 K in the absence of MAPs to 260 K, 280 K and 1000 K when MAPs were attached in the ratios of 1:48, 1:22 and 1:11, respectively. This is consistent with the interpretation of MAPs as local bias fields. When a MAP binds to the MT, it induces a specific conformation

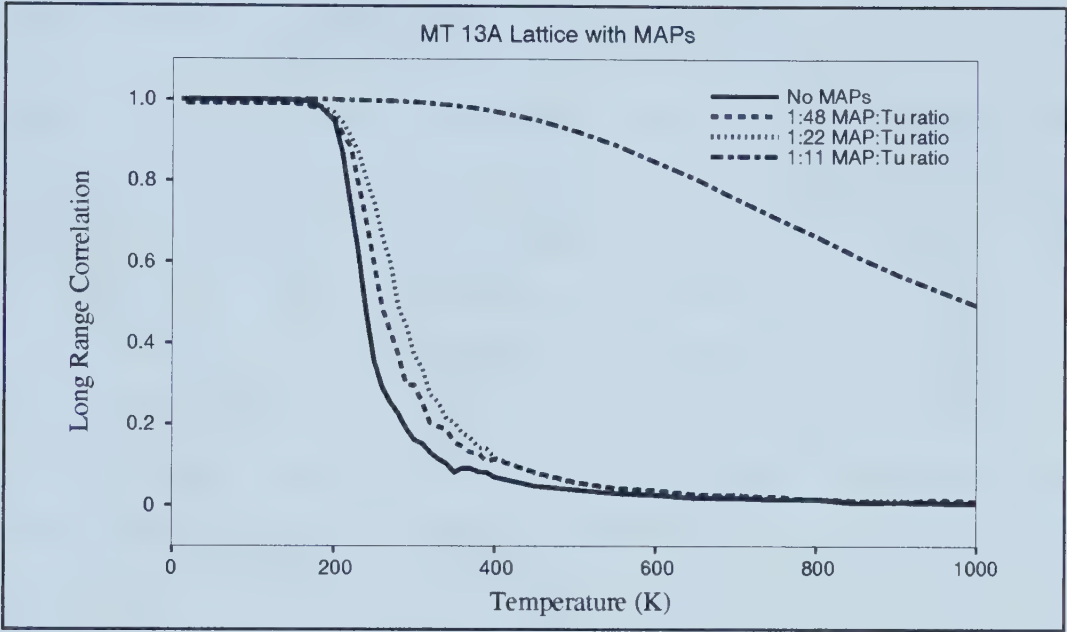


Figure 4.9: Long range correlation, χ_L , of the MT 13A lattice as a function of the ratio of MAPs to tubulin dimers. Ratios taken from Dustin and 1:22 means one in each 22 tubulin dimers is attached to a MAP and held in the up conformation.

of the associated tubulin dimers. When the 0 state for MAPs was employed, the transition to an ordered state required a lower temperature. This can be rationalized simply by considering that a gap has been left in the lattice and as a consequence, the average interaction strengths have been reduced throughout the lattice. Thus a lower thermal energy can overcome the dipolar order.

If the MAPs function as we have hypothesized, then weaker fields would suffice to order the lattice provided that the MAPs serve to hold sites in the conformation which they occupy in the ground state. This is the expected manner in which MAPs would bind because we know that MTs polymerized with MAPs are more stable than those polymerized in the absence of MAPs. The maintenance of an ordered resting state is crucial to the model of signal propagation along MTs because there is otherwise no way to identify a signal from thermal noise.

4.5 Summary of Dipole Ordering

Whether the MT is ordered at physiological temperature depends critically upon the magnitudes of the dipole moment, p , and the dielectric constant, ϵ , since these parameters determine the transition temperature from disorder to order. In the MT 13A lattice, we have found a transition temperature of about 240 K with $Q = 16 \times 10^{-56} \text{ C}^2 \cdot \text{m}^2$. In the case where the down state is directly opposite to the up state (the non-tilted case where $\phi = 0^\circ$), the corresponding transition temperature is slightly higher. This shows that the existence of a transition to order is quite robust but that the transition temperature is sensitive to the specific choice of the down dipole. Since all transition probabilities in the Monte Carlo simulation obey Boltzmann statistics, they are functions of $E/kT = p^2/\epsilon kT$. This parameter may be used to compare the transition temperature, T_c in two systems. Denote with primes the parameters, p and ϵ , in a second lattice system. Now the Boltzmann probability weights are equated between the two systems when,

$$\frac{p^2}{\epsilon kT} = \frac{p'^2}{\epsilon' kT'} \quad (4.11)$$

and finally the transition temperatures in the two systems can be compared:

$$T_c = T'_c \left(\frac{p}{p'} \right)^2 \left(\frac{\epsilon'}{\epsilon} \right). \quad (4.12)$$

This equation demonstrates the scaling of the transition temperature, T_c , in a MT which is not subject to electric fields. The values p' and ϵ' are the values which we have estimated while p and ϵ are the actual values of the dipole moment and permittivity of tubulin. The transition temperature scales directly with the square of p , and inversely with ϵ . The scaling is more complicated in the presence of electric fields since phase transition behaviour is governed by two parameters in this case, the second describing the strength of the external electric field-dipole interaction versus the dipole-dipole interactions. The main result is that the MT

13A lattice could easily exist in an ordered state at physiological temperatures without the application of external fields provided $p^2/\varepsilon > 20 \times 10^{-56} \text{ C}^2 \cdot \text{m}^2$.

Our original estimate of p^2/ε was about $16 \times 10^{-56} \text{ C}^2 \cdot \text{m}^2$ which comes within 25% of what the model requires for an ordered MT 13A lattice. This is already sufficient for the MT 13B lattice, that has recently emerged as the most biologically relevant lattice[20], to be ferroelectrically ordered. As we have shown, the application of an electric field along the length of the MT may serve to order the MT at higher temperatures than without an external field and the effect of MAPs may also organize the MT lattice. Consequently, we may be able to relax the requirements on p and ε which would be required for our cellular automaton model to predict an ordered lattice MT 13A under physiological conditions. We hasten to reiterate that at this point, the restrictions are not particularly stringent and it seems likely that the MT is ferroelectrically ordered at physiological temperature. In addition, thanks to the structure now available for tubulin [13], we are now certain that tubulin has a dipole moment in excess of our original estimate and that ordering of the dipoles seems likely at physiological temperature in both the 13A and 13B lattices.

4.6 Ordering of MT Bundles

While we have spoken in this chapter of dipole ordering as a result of local electromagnetic interactions, let's consider as well the effect which an electric field has on the entire structure. First, let's consider a uniform electric field such as that which exist between parallel plates. The interaction energy is the familiar $U_E = -\mathbf{p} \cdot \mathbf{E}$ which has been studied throughout the chapter. However, a MT in the cytoplasm is not anchored in the same way as a tubulin dimer is anchored within the lattice. Consequently, it may respond to the electric field by altering its orientation. Given the interaction above, there is a torque due to the electric

field,

$$\tau_E = \mathbf{p} \times \mathbf{E} \quad (4.13)$$

on the MT. This will tend to align the MT's dipole with the electric field and this is exactly what has been observed in experiments involving MTs completed now by several groups [21, 22, 23]. The frictional torque of the cytoplasm resists this reorientation. We can approximate this torque as the frictional force on a body moving through a viscous fluid multiplied by the length of the tubulin dimer, L . On dimensional grounds, this torque has the form

$$\tau_\eta \sim \sqrt{A} \eta v L \quad (4.14)$$

where A is the area of the dimer or MT perpendicular to its rotational motion, η is the viscosity of the cytoplasm and v is the velocity of the object. In this case $v = \omega L$ where ω is the rotational velocity of the object responding to the torque exerted by the electric field. Suppose we choose A from the dimensions of the tubulin dimer, 4 nm x 8 nm, L similarly is 4 nm and η is simply selected as the viscosity of water at physiological temperature, $\eta_{\text{water}} = 0.6915 \times 10^{-3}$ Pa.s. Equating these torques, we find that tubulin will respond to electric fields by rotating until aligned with the field at an angular speed of 5000 rad/s for a modest electric field, of 10 V/cm. However, for a single dimer, the electromagnetic torque is swamped by thermal effects and no such rapid reorientation is observed. However, once assembled into a MT, of perhaps 1000 subunits/protofilament, the electric torque becomes larger since τ_E increases linearly with the number of dimers N . The frictional torque, τ_η , also increases but as $N^{5/2}$. So we find that the characteristic re-orientation time, t , obeys the following proportionality:

$$t \propto p E \eta^{-1} L^{-3/2}. \quad (4.15)$$

The rotational speed for a MT of length 1000 subunits is on the order of 0.01 rad/s. Consequently, an electric field of 10 V/cm would be expected to cause MTs

to align themselves in roughly $\pi/\omega \simeq 3$ minutes which is in good agreement with the published results that report alignment over a period of about 10 minutes [21]. Given the ability of these fields to align dipoles, we must consider the various possible geometries of electric fields that exist within the cell. Most of these do not have homogeneous field distributions. Specifically, consider the electric fields around the centrosome and that of an action potential as pertinent examples.

There are always MTs emanating from the centrosome but during mitosis in particular, the orientation of the MTs relative to the centrosome is reminiscent of electric field lines surrounding a point charge. The mechanism which draws the MTs to either end of the cell and separates the chromosomes is still unclear, one possible explanation worth exploring is electromagnetic and is quite simple. Consisting of organized bundles of MTs, the centrosome is charged and surrounded by an electric field that is radially oriented with its magnitude given by:

$$E_r = \frac{1}{4\pi\epsilon\epsilon_0} \frac{q_c}{r^2}. \quad (4.16)$$

Furthermore, suppose this field is large enough to attract the MT towards the centrosome and during chromosome segregation, tear one subunit off the minus end of the MT, which would be consistent with the results of Vater and coworkers [23] who observed that MTs would break in sufficiently strong electric fields. We can calculate the electric field which would be required given the known geometric constraints and the tubulin-tubulin bond strength. Simply the difference between the electrostatic work performed on the first dimer and the second dimer should be equal to the bond energy. The interaction energy for an electric field with this geometry and an electric dipole is given as in equation (4.3). This expression is differentiated in the usual manner to arrive at an expression for the force. So,

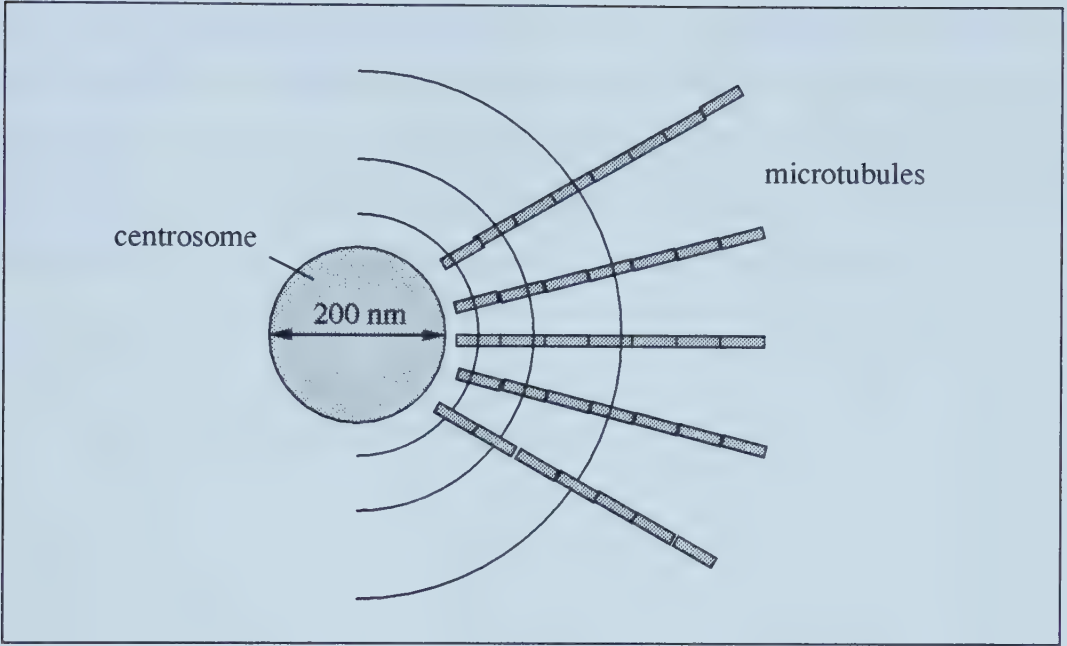


Figure 4.10: MTs are drawn into the centrosome during mitosis. One possibility is that this is electromagnetic and caused by a radial electric field emanating from the centrosome.

$$\begin{aligned} \text{bond energy} &= \Delta(\text{force}) \cdot \text{distance} \\ 4.0 \text{ kcal/mol} &\simeq \frac{p q_c}{2\pi\epsilon\epsilon_0} \left(\frac{1}{r^3} - \frac{1}{(r+a)^3} \right) \cdot a, \end{aligned} \quad (4.17)$$

where a is the dimer spacing of 8 nm, q_c is the charge on the centrosome and the other variables retain their meanings from earlier. This particular energy has been estimated from the difference in the free energy of GTP hydrolysis in solution (5.2 kcal/mol), compared to the free energy of hydrolysis when GTP is bound to a MT (0.9 kcal/mol). This energy can also be estimated from the Young's modulus of a MT and gives a value of 2.0 kcal/mol. Solving this equation for the charge on the centrosome, q_c , gives a value of only a few elementary charges, $q_c \sim \epsilon$, when r is selected a . This charge corresponds to an electric field of about 10^6 V/m. An individual tubulin dimer has a charge of negative

ten, so a MT of length $0.4\ \mu\text{m}$, has an excess of 1×10^4 electronic charges. The entire centrosome structure would therefore have a charge of roughly $5 \times 10^5\ e$. Unless screening effects due to counter-ions would lower the effective charge on the centrosome, this field seems large enough to explain the movement of MTs towards the centrosome and the tearing of subunits from the MTs.

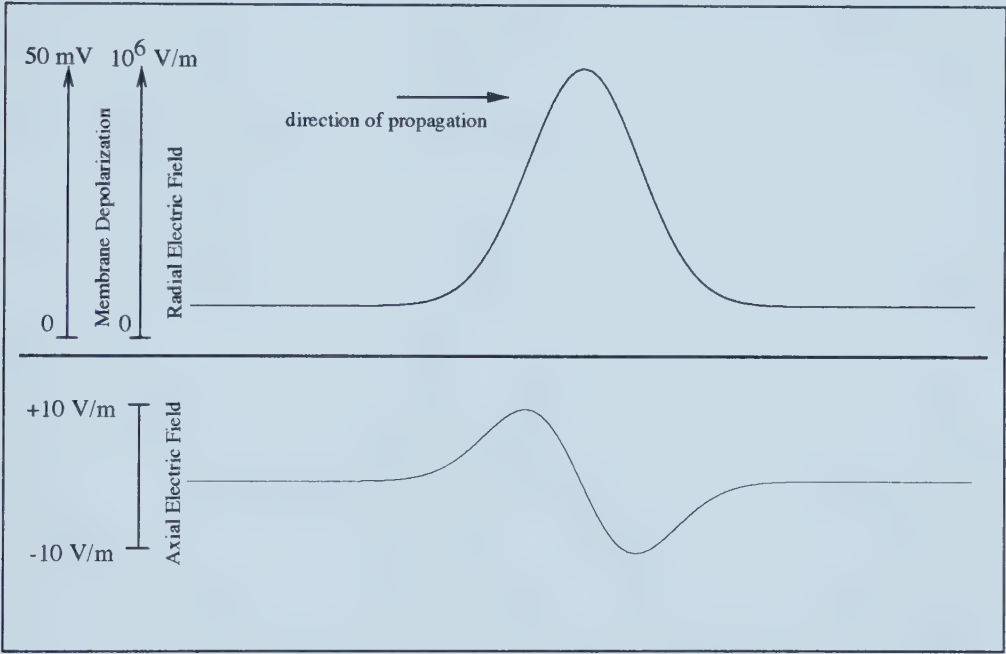


Figure 4.11: Electric fields induced by an action potential are both axial and radial however the radial field is much larger since the potential difference is separated by only the membrane thickness of about 5 nm rather than the width of the action potential itself which is about 5 mm. The radial field drops off quickly away from the membrane while the axial field remains approximately constant throughout the axon.

So, we see that electromagnetic effects may play a role in the ferroelectric state of the MT, that MTs may reorient in response to electric fields and finally, that an interaction with the static field surrounding a centrosome may be sufficient to describe the movement of MTs through the cytoplasm. The next logical question is how the MT may respond to dynamic electric fields. In the case of an action potential, transient electric fields are generated within the cell. We

will focus upon these fields which translate in synch with the action potential. From this reference frame, the electric fields are constant. The membrane depolarization gives rise to large radial field and a smaller axial field as shown in Figure 4.11. These effects shall be elucidated in the following chapter where the moving electric field of an action potential is considered.

Bibliography

- [1] S.R. Hameroff and R.C. Watt, *Do anesthetics act by altering electron mobility?*, *Anesth. Analg.* **62**, 936–940 (1983).
- [2] S.R. Hameroff, S. Rasmussen, and B. Mansson, *Artificial Life*, chapter Molecular automata in microtubules: Basic computational logic of the living state?, *SFI studies in the Sciences of Complexity*, Addison Wesley, New York, 1988.
- [3] Barry M. McCoy and Tai Tsun Wu, *The Two-Dimensional Ising Model*, Harvard University Press, Cambridge, MA, 1973.
- [4] E. Ising, *Beitrag zur Theorie des Ferromagnetismus*, *Z. Physik* **31**, 253 (1925).
- [5] L. Onsager, *Crystal Statistics. I. A Two-Dimensional Model with an Order-Disorder Transition*, *Phys. Rev.* **65**, 117 (1944).
- [6] C.N. Yang, *The Spontaneous Magnetization of the Two-Dimensional Ising Model*, *Phys. Rev.* **85**, 808 (1952).
- [7] S.R. Hameroff and R.C. Watt, *Information processing in microtubules*, *J. theor. Biol.* **98**, 549–562 (1982).
- [8] S. Hameroff, S.A. Smith, and R.C. Watt, *Automaton model of dynamic organization in microtubules*, *Ann. N.Y. Acad. Sci.* **466**, 949–952 (1986).

- [9] J.A. Brown and J.A. Tuszyński, *Dipole Interactions in Axonal Microtubules as a Mechanism of Signal Propagation*, Phys. Rev. E **56**, 5834–5840 (1997).
- [10] W.D. Howard and S.N. Timasheff, *GDP state of tubulin: Stabilization of double rings*, Biochem. **25**, 8292–8300 (1986).
- [11] J.D. Jackson, *Classical Electrodynamics*, John Wiley and Sons, Toronto, 1975.
- [12] J.B. Hasted, *Aqueous Dielectrics*, Chapman and Hall, London, 1973.
- [13] E. Nogales, S.G. Wolf, and K.H. Downing, *Structure of the alpha-beta tubulin dimer by electron crystallography*, Nature (London) **391**, 199–203 (1998).
- [14] L.A. Amos and A. Klug, *Arrangement of subunits in flagellar microtubules*, J. Cell Sci. **14**, 523–549 (1974).
- [15] L.A. Amos, *The microtubule lattice - 20 years on*, Trends Cell Biol. **5**, 48–51 (1995).
- [16] K. Binder, *Monte Carlo simulation in statistical physics : an introduction*, Springer-Verlag, New York, 1988.
- [17] B. Trpišova, *Dielectric Phases, Solitary Waves and Information Capacity in Microtubules*, PhD thesis, University of Alberta, 1996.
- [18] B. Trpišova and J.A. Brown, *Ordering of Dipoles in Different Types of Microtubule Lattice*, Intl. J. Mod. Phys. B **12**, 543–578 (1998).
- [19] P. Dustin, *Microtubule*, Springer-Verlag, Berlin, 1984.
- [20] A. Desai and T.J. Mitchison, *Microtubule polymerization dynamics*, Annu. Rev. Cell Dev. Biol. **13**, 83–117 (1997).

- [21] P.M. Vassilev, R.T. Dronzine, M.P. Vassileva, and G.A. Georgiev, *Parallel arrays of microtubules formed in electric and magnetic fields*, Biosci. Rep. **2**, 1025–1029 (1982).
- [22] R.G. White, G.J. Hyde, and R.L. Overall, *Microtubule arrays in regenerating Mougeotia protoplasts may be oriented by electric fields*, Protoplasma **158**, 73–85 (1990).
- [23] W. Vater, R. Stracke, K.J. Böhm, C. Speicher, P. Weber, and E. Unger, *Behaviour of individual microtubules and microtubule bundles in electric fields*, preprint, 1998.

Chapter 5

Signalling by Microtubules

The MTs of nerve cells are stable relative to their counterparts in the rest of the body. This stability allows them to participate in cellular signalling processes. Each of the MT's subunits, dimers of tubulin protein, has an electric dipole moment that contributes to the overall polarity of the structure. We propose that the orientation of the individual dipoles may be flipped due to a conformational change of the tubulin dimer if energy is supplied through GTP hydrolysis or via physical interactions. Thus, the MT lattice may be viewed as an electric dipole lattice with some overall polarization upon which signals, in the form of dipole patterns, may be propagated through dipole interactions that induce conformational changes. As a nerve impulse propagates along a neuron, the neuronal MTs are subjected to a large transient electric fields of 10^5 – 10^7 V/m that interact with the MT lattices. Based on the recent conjecture of information processing and/or energy transport by MTs [1], we have used a Monte Carlo technique to model the interactions between the MT's subunits and to investigate the response of the lattice to nerve impulses. This model of these interactions addresses the problem of thermal fluctuations in the dipole lattice and demonstrates how the nerve impulse may cause a signal to propagate along the MTs within the axon.

Nerve cells are responsible for much of the communication within the body. They may signal other nerve cells or muscle cells in order to produce muscle con-

traction using nerve impulses. These impulses are commonly referred to as action potentials. The structure of nerve cells consists of an array of dendrites, which gather input from other neurons; a cell body; and an axon, possibly branched, along which nerve impulses are transmitted to other cells. The axon may project for large distances from the cell body, greater than 1 m in the human spinal cord, and its content is distinct from the cell body. It is generally free of organelles, and filled by MTs and neurofilaments which are jointly known as the cytoskeleton. These filamentous proteins are arranged parallel to the axon. Each neuronal MT is typically about $100\text{ }\mu\text{m}$ long and spans more than 10^5 tubulin subunits. The MTs of the axon have uniform polarity and lie with their positive ends distal to the cell body [2, 3]. The network of cytoskeletal tubes is interconnected by high molecular weight proteins known as MT associated proteins (MAPs). Their precise function is not understood but tubulin dimers coassembled with MAPs *in vitro* are polymerized more easily and are more stable than MTs assembled from tubulin in the absence of MAPs [4]. Once the axonal MTs have been assembled, they are post-translationally modified and their properties are changed. These changes to the MTs cause them to become more stable [5, 6]. The post-translational, post-MT assembly change has also been frequently studied in the last decade. The transition from newly synthesized tubulin to detyrosinated tubulin within a MT can be used to estimate the age of an individual MT [3].

Additional structural stability allows the neuronal MTs to participate in a capacity greater than their primary cellular function. Their primary function is to act as a cellular backbone, and to serve as railway tracks for vesicle transport by motor proteins. Information processing [7, 8] and energy transport [9] have been proposed as secondary MT functions and several models of MT assembly [10, 11] have been described. Not only is the tubulin which makes up neuronal MTs specific to humans, but it is also specific to nerve cells and is known to be post-

translationally modified. The highly specialized nature of the functional protein suggests that it has been selected to perform a very specific function which we conjecture may be signal transduction. What is known with certainty is that they are assembled from GTP-rich tubulin dimers and that this GTP is hydrolyzed rapidly after the addition of the tubulin subunit. What is not yet known is what happens to this energy. We are proposing that some of the energy is stored in the lattice through a conformational change of the protein dimer. The hydrolysis of GTP releases about 4.6 kcal/mol of energy which the lattice could use to flip conformational states of individual tubulin dimers, each flip would require up to 2.0 kcal/mol of energy¹. The energy might then propagate along the MT through a sequence of dipole flips as the lattice reorients to accommodate the additional energy. These conformational changes or flips are believed to be the result of a mobile electron. It may be localized at one of two binding sites in the tubulin molecule. Movement of the electron from one binding site to the other causes the tubulin dimer and its electric dipole to re-orient. These two states that may be identified by the location of the free electron are the states which we shall hereafter discuss.

Hameroff et al. [1] devised a model of MT cellular automata in 1988 inspired by the belief that the cytoskeleton behaves as a cellular nervous system. After all, the cytoskeleton does regulate many complex cell activities such as vesicular transport, mitosis, cell growth, cell shape and locomotion [12]. Furthermore, Hameroff et al. cited numerous indirect indications supporting the hypothesis of information processing by neuronal microtubules. One of these was the link between MTs and Alzheimer's disease, the link has since been made specific to MAPs [13]. Hameroff et al. believed that automata behaviour within MTs

¹This value is a result of our simulations and based upon our estimated values of the tubulin dimer's dipole strength. The component of the dipole along the protofilament has now been calculated and is in line with our estimate.

could explain their capacity for intelligent organization. We feel our model is more physical than that of Hameroff et al. One reason is that dipole-dipole interactions are considered. As a result, no overall charge on individual tubulin molecules is required. The three-dimensional geometry of the MT lattice is also taken into account in our model; although this has a small effect on dipole-dipole interactions in comparison with the two-dimensional geometry of previous modelling, it is crucial when we consider the interaction with external fields like those transient fields of an action potential. Finally, our model incorporates thermal effects. The Hameroff-Rasmussen-Mansson scheme is a zero-temperature model in which signal propagation is an artifact of the model's design. The differences between our model and the Hameroff-Rasmussen-Mansson model will be discussed later.

5.1 MT Lattice of Dipoles

The MT lattice has been vigorously studied over the past twenty years. In that time, two different lattices have been observed which have become known as the A-lattice and the B-lattice[14, 15]. A-lattices with an odd number of protofilaments are distinguished from all other lattices because they are the only ones without a structural discontinuity known as a seam. In all other lattices, the interactions are mixed which means that there are both A and B type lattice interactions in a single MT. It is now known that the number of protofilaments is not only variable from one MT to another, though 13 protofilaments is by far the most frequent *in vivo*, but the protofilament number need not be conserved along the length of an individual MT [16]. The theoretical modelling we have completed considers MTs of various lattice types but does not allow for variation of the lattice type or protofilament number along the length of an individual MT. Dynamic instability [17, 18, 19] has not been accounted for in the model

since we believe that only stable microtubules are important from the point of view of cellular signalling. The idea of connecting the assembly process with the self-organization process of the dipole lattice is to explore how such a connection may explain the puzzling ensemble dynamics of microtubules grown *in vitro*.

As we have seen in the previous chapter, our model predicts that a MT 13B lattice would be ordered under physiological conditions and that MAPs would serve to order the MT 13A lattice as well within a neuron. We now consider the model of signal processing with the understanding that the underlying lattice is ordered. The organization of the B-lattice is of particular interest because while the MT retains a small overall polarization, neighbouring protofilaments have opposite polarization directions. We have also studied the self-organizing properties of the various MT lattices both in the presence and absence of static electric fields. The ordered MT lattice and its resultant polarization may be significant given that of the three types of cytoskeletal polymers: actin filaments, intermediate filaments and microtubules; it is the two polar structures which participate in material transport and cell motility through the use of their respective motor proteins. It is tantalizing to speculate that it might be this polarization which is responsible for guiding the motor proteins, kinesin and dynein, that travel along the MT in opposite directions [20, 21]. It would immediately explain why such transport is so efficient because collisions would not occur. The motor proteins would simply have to bind preferentially to a particular conformational state of tubulin.

5.2 New Model of Dimer Interactions

The primary reason for the development and subsequent extension of the Hameroff model has been to determine whether a MT lattice can process information. Consider the MT lattice of dimers in their α or β states as a binary

biological computer. The Hameroff model found that signals introduced onto the MT 13A lattice would propagate along protofilaments. The propagation was either bi-directional or uni-directional depending upon the choice of flipping force thresholds and whether they were symmetric or not. The model also admitted the possibility of signals which periodically flip back and forth between α and β states but did not move along the protofilaments. The moving patterns of defects were named gliders and the non-propagating defects were called blinkers.

The other feature of the Hameroff model was its ability to filter input signals. Some would propagate, others would be modified and would subsequently propagate and still others would be annihilated. Thus, the cellular automaton model accepted certain patterns and rejected others. We reproduced the results of the Hameroff model before proceeding with our own work. The first modification introduced was simply to replace the discrete charges with dipoles. Some arbitrary torque threshold was required akin to the force threshold of the original model. Most of the original features of signal transduction were still present in the modified model. The one difference was a shift in the direction of signal propagation from the N-S direction (along the protofilament) to the NW-SE direction (around the helix). Some shortcomings of the model were soon discovered; these have all been addressed in our new model. We will discuss the ramifications of the changes with respect to information processing in the description of the new model which follows and in the results.

The new model was inspired by a model introduced by Hameroff et al. [1] in 1988. In their cellular automaton model, a discrete charge was associated with each tubulin dimer. In our model, a dipole is associated with each dimer as described in the previous chapter. The MT is consequently an electrically polarized object. The interaction energy between two elementary dipoles is given

by the familiar formula of classical electricity and magnetism [22]:

$$E_{\text{int}} = \frac{1}{4\pi\epsilon\epsilon_0} \frac{\mathbf{p}_1 \cdot \mathbf{p}_2 - 3(\mathbf{p}_1 \cdot \mathbf{n})(\mathbf{p}_2 \cdot \mathbf{n})}{r^3}, \quad (5.1)$$

where ϵ is the relative permittivity of the medium, ϵ_0 is the permittivity of free space, \mathbf{p}_k is the k^{th} electric dipole moment, \mathbf{n} is the normal vector pointing from the position of the first dipole to the second dipole and r is the distance separating the dipoles.

5.2.1 Model Features

The MT lattice dynamics are simulated using a standard Monte Carlo technique [23]. For a given timestep, the energy of the present state and the opposite state are calculated. Whether a change of state occurs is a random event whose probability is determined by the availability of stored lattice energy, the temperature, and the threshold to reaction. Additional features of the model are: (i) the removal of artificial barriers to reaction which were introduced by Hameroff et al. [1] in their discrete charge model: and (ii) the removal of the unphysical flip-flop of states which plagued our early attempts at modelling this system.

In our model, the threshold to a dipole flip, in cases where one exists, is simply the maximum interaction energy encountered while turning one dipole in the presence of its nearest neighbours from its present state to the opposite state. The model removes the unphysical flip-flop of states by forbidding nearest neighbours from simultaneously changing states. Thus, when the dipole interaction favours paired dipoles and the current state of the neighbouring dipoles is up-down; in the next timestep, they may be up-down (unchanged), up-up or down-down but not down-up. When a dipole flips, the change in conformational energy is either removed from or added to the lattice at that location. After the evolution step, energy diffuses to neighbouring sites. Our simulations have been carried out with a diffusion constant which is isotropic and small enough that several timesteps

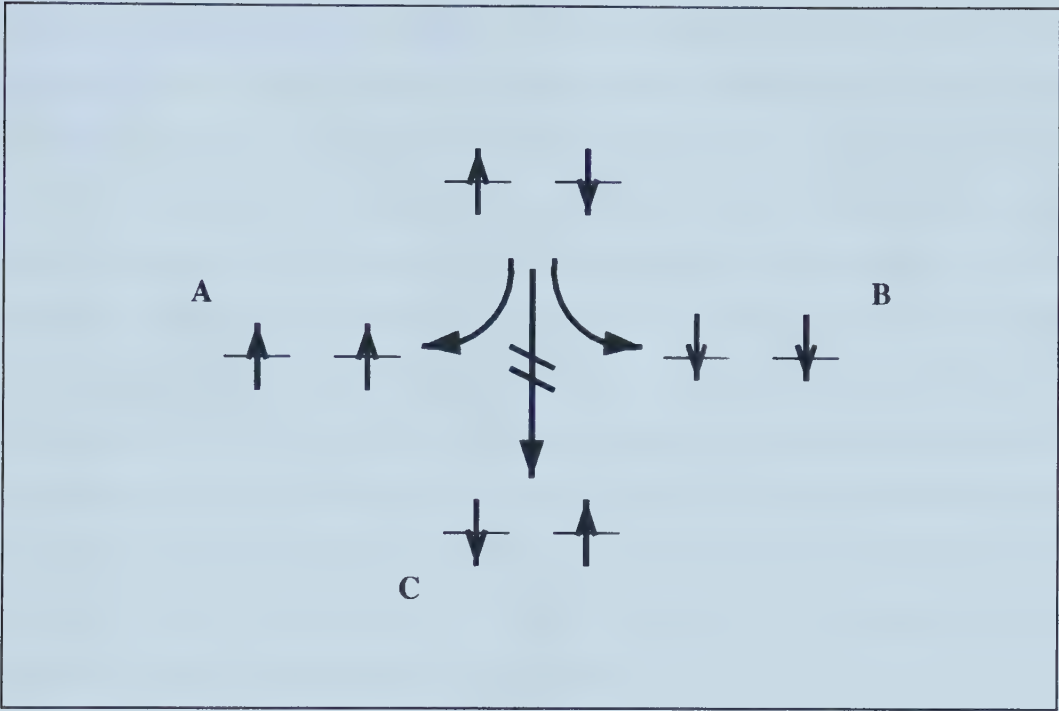


Figure 5.1: Flip-flop problem is solved by forbidding neighbouring dipoles from changing their orientation in any given timestep. Therefore the final states A and B are permitted but C is not, except by two separate state changes occurring in separate time steps.

are required for localized energy to dissipate. Energy is conserved by the lattice in our current model, and the boundary conditions are periodic. None of the energy is returned to the surrounding medium.

There are two free parameters in the model. One is the relative permittivity of tubulin, or more precisely that of tubulin in cytosol, ϵ . As an approximation, we are using the value $\epsilon = 10$. For comparison, the permittivity of water which is frequency dependent has a value of about 76 for the frequencies of physiological relevance. The dielectric constant of dry tubulin or of tubulin in solution has not been found in the literature. Hasted gives results from some experiments giving permittivities in excess of 100 for some other proteins in solution [24]. However, our choice allows us to compare results with previous modelling attempts. The

dynamics of the model are unaffected by the choice of ε but it simply scales the temperature. Larger values of ε reduce interaction strengths and thereby act like a temperature increase. The other number which is put in by hand is the dipole strength of the conformational states of tubulin. We have chosen the dipole magnitude, p , by considering the corresponding dipole charge to be an elementary charge in magnitude and the charge separation to be 8 nm which is the spacing between neighbouring tubulin molecule centers in an MT lattice. This gives a value of $p_o = 1.28 \times 10^{-27}$ C·m (384 Debye) which is comparable to the measured dipole moments of some other protein molecules [24]. The precise value depends on the pH of the surrounding medium. The following results are derived from these estimates. We shall comment on how changes to these parameters affect the results of our simulations ².

5.3 Results

The behaviour of the MT lattice has been simulated for temperatures between absolute zero and 1000 K. The polarization and nearest-neighbour correlation functions along the protofilament have been calculated as functions of temperature and discussed in the preceding chapter. The existence of an ordered phase is crucial if the MT is to be able to process information. When the lattice is not organized, this signifies that thermal fluctuations dominate over the dipole-dipole interactions and that entropy dominates the lattice. Upon such a background (Figure 5.2a), any signals introduced to the lattice would vanish. The simulations show that a highly ordered phase exists for both the MT 13A and MT 13B lattices at low temperatures.

²The component of tubulin's dipole along the protofilament which we have computed based upon new structural data is 337 Debye



Figure 5.2: Portions of three MTs are shown. Light boxes represent the 'up' state and dark boxes represent the 'down' state. (a) The B lattice above its critical temperature is disordered. (b) The B lattice below the critical temperature is ordered. (c) The A lattice just below the critical temperature but onto which a large defect has been introduced. Smaller thermal induced defects also dot the structure.

5.3.1 Propagation of Signals

A signal can be recognized as a particular sequence of anti-aligned dipoles on an otherwise well-ordered lattice. Associated with this signal or defect is some additional energy which is recovered when the anti-aligned dipole falls back to its original configuration. The energy may diffuse in all directions so with six nearest neighbours, a single defect is not likely to cause neighboring dipoles to flip since they receive only about a sixth of the required energy. However, a larger defect such as a group of three or more dimers might successfully maintain its integrity. This has been observed in our model, larger defects have larger lifetimes.

The interesting question is: how does the MT respond to the presence of defects on the ordered lattice? A defect could arise by GTP hydrolysis to GDP at the exchangeable site upon addition of an additional tubulin subunit or by the less frequent hydrolysis of GTP at the non-exchangeable site [25]. In either case, the energy released might go into changing the conformation of the molecule and its electric dipole.

It is important to note that the conformational state of tubulin is not coupled to GTP hydrolysis. These two events are separate but GTP hydrolysis can easily induce the conformational change. Some authors have directly linked these two events and on occasion have proposed the opposite causality, that the conformation change of tubulin induces GTP hydrolysis [26].

Unlike the Hameroff model, we do not observe the smooth propagation of signals along the MT unless some additional mechanism is added. As it stands, there is nothing to direct the propagation of the defect so it takes a random walk about the MT and its energy is slowly dissipated to the rest of the MT. The efficient propagation of signals could be restored by several mechanisms including: (i) the application of an external field which would bias signal propagation; (ii) an asymmetry in the dipole structure which simply makes it more favourable

to propagate in a particular direction; or (iii) mechanical stress if dipoles are coupled to a lattice distortion. The second mechanism could be the result of the bonding between tubulin dimers. If the energy deposited by a dipole flip is comparable with the vibrational energy of a particular bond, it is most likely that this energy would be propagated in that direction. The third mechanism would be the result of a piezo-electric effect [27]. There could also be some sort of refractory period which prevents the retrograde propagation of the signal. Since external fields are known to act upon MTs in neurons, the study of these fields and their interaction garners our attention.

5.4 Action Potentials

As expected, application of a large axial field of 10^6 V/m along the MT causes nearly all dipoles to orient themselves in the direction which most closely follows that of the field. Thus, a wave of dipole flips is induced along the MT as the field is translated along the MT. This is similar to what happens as an action potential moves along an axon, illustrated in Figure 5.3. The large radial field is felt by MTs in the vicinity of the cell membrane. Suppose the field is oriented in a direction which favours an alternate ordering for the lattice, such as is the case in MT, these dipoles will re-orient themselves. The field acts like a pump and stores energy in the lattice of dimers. Once the field has passed, these dimers may return to their original configuration and release their stored energy. A weaker field does not actually create defects by changing the orientation of dipoles in the ground state, but can act as a bias and direct the movement of any existing defects.

When the strength of the interacting action potential is large, such as for those MTs in close proximity to the cell membrane, a wave of structural deformation travels parallel to the action potential along the MT. As the wave reaches the MT

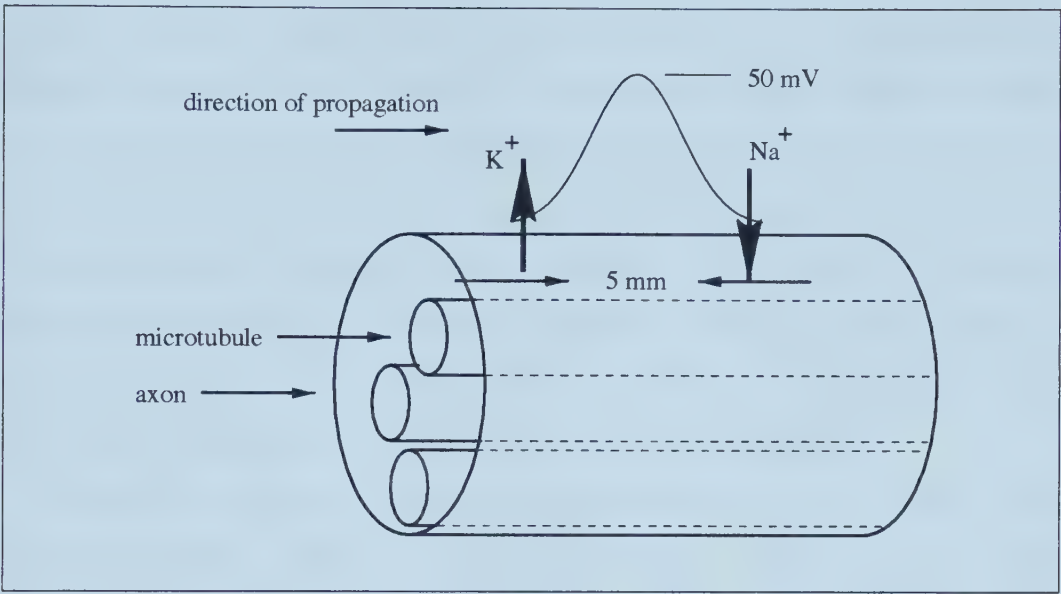


Figure 5.3: An action potential moving along an axon containing three MTs. There is an electric field caused by the potential difference once the ions are displaced and a magnetic field caused by the moving ions. The potential difference is typically 50 mV and its magnitude is represented by the curve above the axon. Given the membrane thickness, the transient electric field may be as high as 10^5 V/m within the membrane.

end, its effects are unclear. Once the MT relaxes to its ground state structure, energy should once again be available for cellular use if the structural change at the MT terminus is coupled to another cellular structure via a MAP. It might also simply serve as a cellular signal indicating when motor proteins should be activated, MT assembly instructions or any other host of functions associated with the MT terminal which could involve signalling another MT or some part of the axon terminal.

5.5 Discussion

The results of the Monte Carlo simulation are that the lattice of MT dipoles may be ordered at physiological temperatures. Consequently, we have begun to investigate the response of this system to perturbations which we are calling

signals. Once dipole defects have been induced upon the MT lattice, they may propagate along the length of the MT. While some non-linear effect or external guidance seems to be required, processing of these signals cannot be ruled out. Signal transduction from the distal end of the axon towards the cell body is at least theoretically possible – although unlikely in our opinion. Transduction along the length of the MT is simpler to explain from the proximal end to the distal end though because of the existence of action potentials and the need to explain how a signal may be passed from one MT to another.

Our simulations place a firm limit on the strength of the dipoles required for self-organization. The required dipole strength of about 1×10^{-27} C·m is comparable but slightly larger than the value which we estimated for tubulin. If the angle between the dipole directions of each of tubulin's conformational states is smaller than predicted, an even larger dipole strength would be required. Should the value for tubulin be smaller than this, information processing must be ruled out. Energy might still be passed along due to the passage of an action potential but it would be marked by the highly ordered configuration of the signal upon the random background. The quantity of energy associated with such an entropic change is much smaller than other values mentioned, only about 0.06 kcal/mol.

On the topic of information storage in MTs, the simple introduction of thermal energy seems to have removed the possibility of information storage in MT as was proposed by Hameroff et al. [28, 29]. The energy involved in flipping the conformation of the dimer would have to be significantly larger for such a form of storage to be possible. Not to mention the need for some kind of mechanism which would preserve the integrity of the information.

It is clear that electromagnetic properties are important in cell biology. The intrinsic polarity of MTs also seems to be very important, otherwise one would

expect the MTs within the axon to be randomly oriented. Whether the information processing hypothesis proves to be valid or not, the investigations into the interactions between cellular proteins and electromagnetic fields must continue. Our model includes both interactions between individual particles, protein molecules in this case, and an external field, the action potential. We hope it may serve as a starting point for future investigations.

Bibliography

- [1] S.R. Hameroff, S. Rasmussen, and B. Mansson, *Artificial Life*, chapter Molecular automata in microtubules: Basic computational logic of the living state?, SFI studies in the Sciences of Complexity, Addison Wesley, New York, 1988.
- [2] P.W. Baas, J.S. Deitch, M.M. Black, and G.A. Banker, *Polarity orientation of microtubules in hippocampal neurons: uniformity in the axon and non-uniformity in the dendrite*, Proc. Natl. Acad. Sci. USA. **85**, 8335–8339 (1988).
- [3] P.W. Baas and M.M. Black, *Individual Microtubules in the axon consist of domains that differ in both composition and stability*, J. Cell. Biol. **111**, 495–509 (1990).
- [4] E. Mandelkow and E.-M. Mandelkow, *Microtubules and microtubule-associated proteins*, Curr. Opin. Cell Biol. **7**, 72–81 (1995).
- [5] Y. Li and M.M. Black, *Microtubule Assembly and Turnover in Growing Axons*, J. Neuroscience **16**, 531–544 (1996).
- [6] N.K. Pryer, R.A. Walker, V.P. Skeen, B.D. Bourns, M.F. Soboeiro, and E.D. Salmon, *Brain Microtubule-Associated Proteins Modulate Microtubule Dynamic Instability in Vitro*, J. Cell Sci. **103**, 965–976 (1992).

- [7] S. Hameroff, J.E. Dayhoff, R. Lahoz-Beltra, A.V. Samsonovich, and S. Rasmussen, *Models for molecular computation: Conformational automata in the cytoskeleton*, Computer **Nov.**, 30 (1992).
- [8] J. A. Tuszyński, S. Hameroff, M.V. Satarić, B. Trpišová, and M.L.A. Nip, *Ferroelectric behavior in microtubule dipole lattices: Implications for information processing, signaling and assembly/disassembly*, J. Theor. Biol. **174**, 371–380 (1995).
- [9] M.V. Satarić, J.A. Tuszyński, and R.B. Žakula, *Kinklike excitations as energy-transfer mechanism in microtubules*, Phys. Rev. E **48**, 589 (1993).
- [10] P.M. Bayley, M.J. Schilstra, and S.R. Martin, *Microtubule dynamics instability: Numerical simulation of microtubules transition properites using a lateral cap model*, J. Cell Sci. **95**, 33–48 (1990).
- [11] H. Flyvbjerg, T.E. Holy, and S. Leibler, *Microtubule dynamics: Caps, catastrophes, and coupled hydrolysis*, Phys. Rev. E **54**, 5538–5560 (1996).
- [12] P. Dustin, *Microtubule*, Springer-Verlag, Berlin, 1984.
- [13] A. Alonso and I. Grundke-Iqbal, *Abnormal phosphorylation of tau and the mechanism of Alzheimer neurofibrillary degeneration: Sequestration of microtubule-associated proteins 1 and 2 and the disassembly of microtubules by the abnormal tau.*, Proc. Natl. Acad. Sci. USA **94**, 298 (1997).
- [14] D. Chrétien and R.H. Wade, *New data on the microtubule surface lattice*, Bio. Cell **71**, 161–174 (1991).
- [15] L.A. Amos, *The microtubule lattice - 20 years on*, Trends Cell Biol. **5**, 48–51 (1995).

- [16] D. Chrétien, F. Metoz, F. Verde, E. Karsenti, and R.H. Wade, *Lattice-defects in microtubules: Protofilament numbers vary within individual microtubules*, J. Cell Biol. **117**, 1031–1040 (1992).
- [17] T. Mitchison and M. Kirschner, *Dynamic instability of microtubule growth*, Nature (London) **312**, 237–242 (1984).
- [18] T. Horio and H. Hotani, *Visualization of the dynamic instability of individual microtubules by dark field microscopy*, Nature (London) **321**, 605–607 (1986).
- [19] L. Cassimeris, *Regulation of microtubule dynamic instability*, Cell. Motil. Cyto. **26**, 275–281 (1993).
- [20] A.A. Hyman and T.J. Mitchison, *Two different microtubule-based motor activities with opposite polarities in kinetochores*, Nature (London) **351**, 206–211 (1991).
- [21] N.R. Barton and L.S.B. Goldstein, *Going mobile: microtubule motors and chromosome segregation*, Proc. Natl. Acad. Sci. USA **93**, 1735–1742 (1996).
- [22] J.D. Jackson, *Classical Electrodynamics*, John Wiley and Sons, Toronto, 1975.
- [23] K. Binder, *Monte Carlo simulation in statistical physics : an introduction*, Springer-Verlag, New York, 1988.
- [24] J.B. Hasted, *Aqueous Dielectrics*, Chapman and Hall, London, 1973.
- [25] M.V. Semënov, *New Concept of Microtubule Dynamics and Microtubule Motor Movement and New Model of Chromosome Movement in Mitosis*, J. theor. Biol. **179**, 91–117 (1996).

- [26] D. Chrétien, S.D. Fuller, and E. Karsenti, *Structure of Growing Microtubule Ends: Two Dimensional Sheets Close into Tubes at Variable Rates*, J. Cell Biol. **129**, 1311–1328 (1995).
- [27] H. Athenstaedt, *Pyroelectric and piezoelectric properties of Vertebrates*, Ann. N.Y. Acad. Sci. **238**, 68–94 (1974).
- [28] S.R. Hameroff and R.C. Watt, *Information processing in microtubules*, J. theor. Biol. **98**, 549–562 (1982).
- [29] S. Hameroff, S.A. Smith, and R.C. Watt, *Automaton model of dynamic organization in microtubules*, Ann. N.Y. Acad. Sci. **466**, 949–952 (1986).

Chapter 6

Conduction by Microtubules

6.1 Modelling Conducting Polymers

In order to model conduction through a polymer such as the MT, an effective model of the mobile charges must be described. Electrons, as charged particles, interact with each other through the Coulomb interaction. The electron-electron interactions are particularly important in partly filled narrow bands such as those of transition metals [1]. For a collection of nuclei at positions \mathbf{R}_k with charge $Z_k e$ and of N electrons at positions \mathbf{r}_i , the fundamental microscopic Hamiltonian is given by

$$H = \sum_{i=1}^N \left(\frac{p_i^2}{2m} - \sum_k \frac{Z_k e^2}{|\mathbf{r}_i - \mathbf{R}_k|} \right) + \frac{1}{2} \sum_{i \neq j} \frac{e^2}{|\mathbf{r}_i - \mathbf{r}_j|}. \quad (6.1)$$

In this equation, the nuclei are taken to have negligible kinetic energy. The problem posed by equation (6.1) must be simplified for any real system to at least make the problem tractable. In particular, for the $\alpha\beta$ -tubulin dimer which is comprised of about 890 amino acids, this represents about 13000 nuclei. A gross simplification which we introduce is to treat each monomer as having an effective site energy. Fluctuations of the site energy on scales less than the monomer spacing are therefore washed out. The model which shall be used for calculation will be second quantized. Hence, conduction shall be modelled by

electron hopping. The Hamiltonian of the system is rewritten in the form

$$\hat{H} = \sum_{i,\sigma} \varepsilon_i \hat{c}_{i\sigma}^\dagger \hat{c}_{i\sigma} - \sum_{i \neq j, \sigma} t_{ij} \hat{c}_{i\sigma}^\dagger \hat{c}_{j\sigma} + \sum_i U_i \hat{c}_{i\uparrow}^\dagger \hat{c}_{i\uparrow} \hat{c}_{i\downarrow}^\dagger \hat{c}_{i\downarrow}. \quad (6.2)$$

This model, known as a Hubbard model [2], will be developed step by step and the choices of t , U and ε which represent respectively the hopping or resonance integral, the Coulomb interaction and the site energies, will be motivated. Of these parameters, the ratio of the electron repulsion to the kinetic energy parameter, U/t , may be the most important. Conjugated polymers are often modelled with $U/t \simeq 4$.

6.2 Modelling the Protofilament chain

When conduction along a complex polymer such as a MT is to be studied, it is convenient to first model the protofilament chain which is one dimensional. The individual tubulin dimer is first modelled and one may then consider these dimers joined together. The dimer shall be modelled as two quantum wells. These wells represent binding sites for electrons which may hop between each of the sites. We can estimate the relevant parameters of the well depth and the well width from kinetic studies and with a knowledge of the molecule's overall geometry. Once the bound states and their energies are known for this system, this knowledge may be applied to a second quantization scheme. This procedure permits us to make progress without specifically requiring us to solve for the wavefunction of the system.

6.2.1 Quantum Double Well Picture

In Figure 6.1, a one-dimensional (1D) chain of quantum double wells is pictured. The potential energy alternates on α and β sites. This variation in the energy is attributed to the difference in tubulin's local geometry resulting from GTP

hydrolysis. The tubulin dimer has a non-exchangeable GTP binding site on its α -monomer and an exchangeable GTP binding site on its β -monomer. The difference between α and β binding sites is in this model attributed to the conformational change which follows GTP hydrolysis. This event is associated with an energy change of about 0.1 eV. While this energy difference between the well depths is known, the actual depth is not. The depth of the deeper well, f_1 , has been selected as 0.4 eV initially. Given this value, there is a 25% difference in well depths. If f_1 is much larger, the dimer nature of the protofilament is lost because the wells are effectively the same depth.

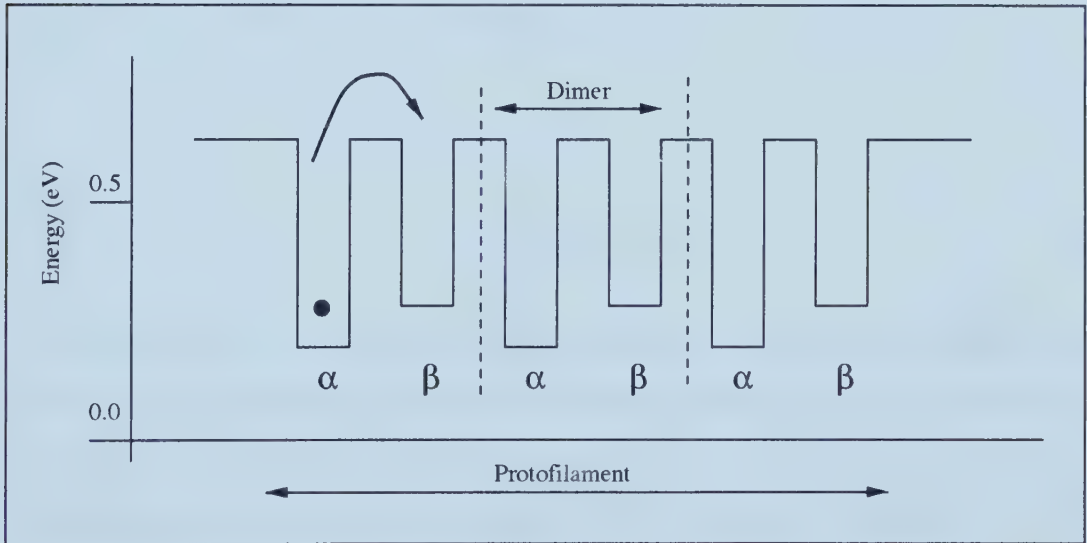


Figure 6.1: One-dimensional chain of quantum wells representing the energy profile along a MT protofilament where the α and β monomers have alternating site energies.

The results for the single electron eigenstates of a double quantum well may be found in a rather straight-forward manner using a transfer matrix method. We begin by solving the time-independent 1D Schrödinger equation in each interval

in which the piece-wise constant potential is defined. This equation

$$\hat{H}\psi = \frac{\hat{p}^2}{2m}\psi + \hat{V}\psi = E\psi, \quad (6.3)$$

has the following solution if $E > V$,

$$\psi(x) = A \cos(kx) + B \sin(kx) \quad (6.4)$$

where

$$k = \frac{a\sqrt{2m(E - V)}}{\hbar} \quad (6.5)$$

and a is included in the definition so that x is dimensionless. In the case where $E < V$, the solutions are non-propagating and may be expressed as

$$\psi(x) = Ae^{\kappa x} + Be^{-\kappa x} \quad (6.6)$$

where

$$\kappa = \frac{a\sqrt{2m(V - E)}}{\hbar}. \quad (6.7)$$

Thus, the solution to the Schrödinger equation is easily found in each region defined by the changes in the potential energy. Now, matching conditions are applied at each interface. The values of the wave function and its derivative are matched at each change of the potential. This gives a 2×2 matrix relating the coefficients in the wave function expansion.

$$\begin{pmatrix} A_2 \\ B_2 \end{pmatrix} = \begin{pmatrix} {}^{2,1}M_{11} & {}^{2,1}M_{12} \\ {}^{2,1}M_{21} & {}^{2,1}M_{22} \end{pmatrix} \begin{pmatrix} A_1 \\ B_1 \end{pmatrix} \quad (6.8)$$

In the above equation, the superscript to the left of the M denotes which coefficients are being linked. The subscripts indicate the matrix element. In an iterated fashion,

$$\begin{pmatrix} A_n \\ B_n \end{pmatrix} = \left({}^{n,n-1}\hat{M} \right) \left({}^{n-1,n-2}\hat{M} \right) \dots \left({}^{3,2}\hat{M} \right) \left({}^{2,1}\hat{M} \right) \begin{pmatrix} A_1 \\ B_1 \end{pmatrix}, \quad (6.9)$$

and one eventually arrives at the following:

$$\begin{pmatrix} A_n \\ B_n \end{pmatrix} = \begin{pmatrix} {}^{n,1}M_{11} & {}^{n,1}M_{12} \\ {}^{n,1}M_{21} & {}^{n,1}M_{22} \end{pmatrix} \begin{pmatrix} A_1 \\ B_1 \end{pmatrix}. \quad (6.10)$$

Now, for bound states $A_1 = B_n = 0$ so that the wave function decays outside the region of the quantum wells. Therefore,

$$B_n = 0 \quad \Rightarrow \quad {}^{n,1}M_{22} = 0. \quad (6.11)$$

This matrix element is computed numerically since it is the product of $(n - 1)$ matrix multiplications. Using this method, the energy is varied and whenever this matrix element becomes zero, a bound state has been found corresponding to that energy value. Consider the following parameters for our quantum double well, $a = 2$ nm and $f_1 = f_2 = 0.4$ eV which are the approximate values for the protofilament chain. For a single dimer consisting of two wells, one may solve for the bound state without difficulty. One finds that there are two bound states for this problem. As the number of dimers is increased, this may no longer be performed analytically and is better suited to numerical analysis. The energy of the lowest bound states is plotted as the depth of the wells, $f_1 = f_2 = f$, is varied in Figure 6.2. Each line actually represents two states which are found with nearly the same energy. The lowest energy states are the symmetric wavefunctions which are centered on each of the wells. The next two bound states represent the antisymmetric wavefunctions which again may be centered on one of the wells. At significantly higher energies, another excited state develops which is more distributed and has a higher fraction of its wavefunction within the barriers. Consequently, the height of the barrier has a larger effect upon the energy of that state. These bound state solutions to the 1D Schrödinger equation are displayed in Figure 6.3. We then interpret the energy level structure of the protofilament as its length is extended. As the number of dimers, n , is increased, energy bands develop as hybrid orbitals form across the polymer. Essentially, one

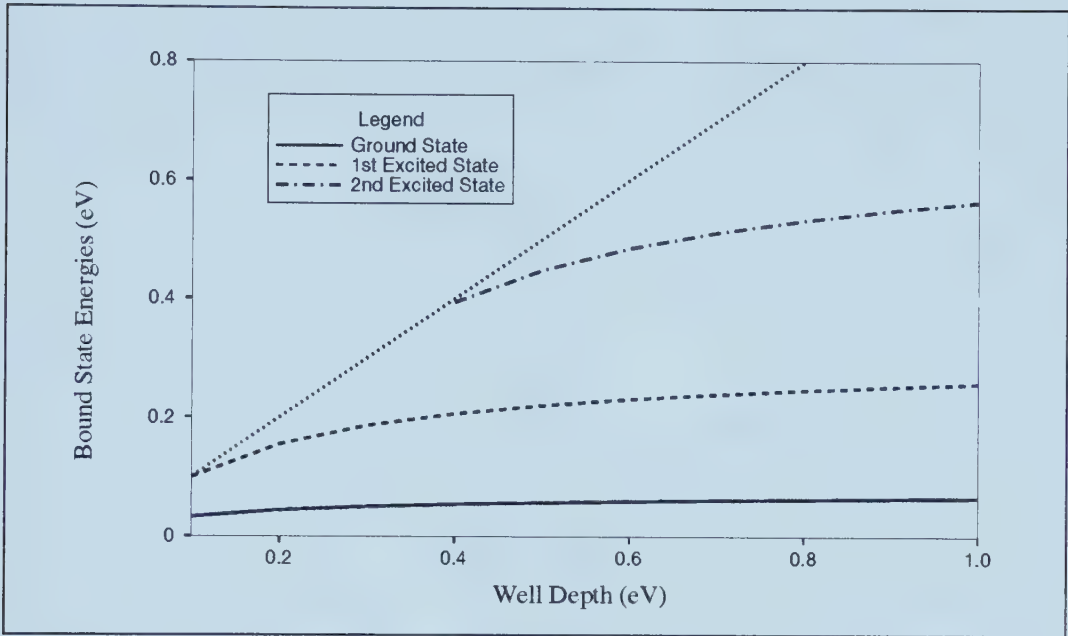


Figure 6.2: Variation of the bound state energies with the depth of the double quantum wells, $f_1 = f_2$. The straight line indicates where the bound state energy is equal to the well depth.

band is of hybridized symmetric orbitals and the higher lying band of hybridized anti-symmetric orbitals. These bands correspond nearly exactly to the bound states and that the width of these energy bands is small, only about 0.01 eV. The separation between the lower band and the upper band which consists of distributed orbitals is important because it relates to the energy required to excite the system to states where electron movement becomes possible.

6.2.2 Second Quantization

Even with only a single electron, we may second quantize our system. The Hamiltonian becomes

$$\hat{H} = \sum_{i,\sigma} \epsilon_i \hat{c}_{i\sigma}^\dagger \hat{c}_{i\sigma} - \sum_{i \neq j, \sigma} t_{ij} \hat{c}_{i\sigma}^\dagger \hat{c}_{j\sigma} \quad (6.12)$$

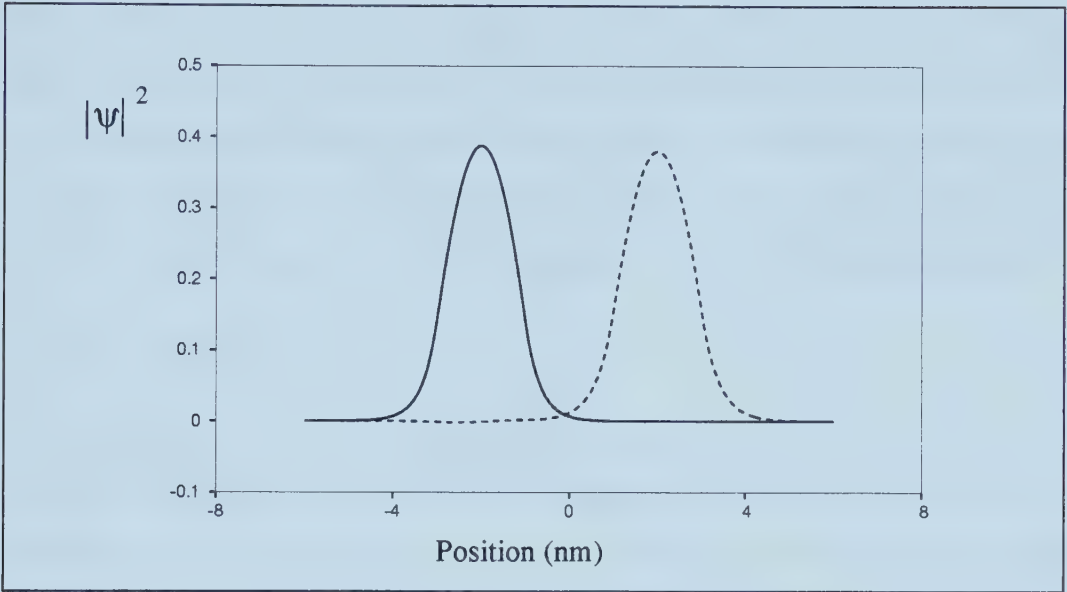


Figure 6.3: Form of the lowest energy bound state wave functions in 1D.

where the operators $\hat{c}_{i\sigma}^\dagger$ and $\hat{c}_{i\sigma}$ are the usual fermion creation and annihilation operators, and where i runs from 1 to $2n$ representing the two sites on each of the n dimers. The ϵ_i represent the potential energy at each site and the kinetic terms t_{ij} account for hopping from one site to another. In general, these terms will vary between sites but we will simplify the matter and choose a constant value, t . Since there are no interactions between the states with spin $+\frac{1}{2}$ and those with spin $-\frac{1}{2}$, the state space may be divided into two identical subspaces labelled by the electron spin. In each of these subspaces, the matrix corresponding to this chain of dimers is tridiagonal and may be diagonalized to determine the itinerant eigenstates of the system. The effect of the kinetic term can be analyzed in this new model.

The benefit of this model is that we are able to proceed without computing electron eigenstate wavefunctions. In many electron problems, the wavefunctions become very complicated, ($\Psi = \Psi(\phi_1, \phi_2, \dots, \phi_n)$), generally given by a Slater-

like determinant where the individual electron wavefunctions have their own complicated spatial dependence. This difficulty is avoided in this formalism. In addition, once Coulomb interactions appear in the Hubbard model, we shall not have the difficulty of dealing with integrals of the form $\int \frac{e^2}{r} d^3\bar{x}$ and the introduction of cutoffs to handle divergences which arise from these terms.

6.2.3 Basis of States

The Hubbard model is the simplest second-quantized model to capture all of the essential features of a real system of interacting particles [3]. In this model, the particles, electrons, are the fundamental excitations. All states may be built up from the vacuum using the usual fermion creation operators. For example,

$$|4 \uparrow\rangle = c_{4\uparrow}^\dagger |\Omega\rangle \quad (6.13)$$

and represents the state with an electron of up spin localized in an orbital on site 4. As the number of electrons increases, we must impose a normal ordering on these states. Consider the following two-electron states:

$$|2 \uparrow 5 \downarrow\rangle = c_{2\uparrow}^\dagger c_{5\downarrow}^\dagger |\Omega\rangle \quad \text{and} \quad |5 \downarrow 2 \uparrow\rangle = c_{5\downarrow}^\dagger c_{2\uparrow}^\dagger |\Omega\rangle. \quad (6.14)$$

Since the electrons are indistinguishable, the states must be the same. However,

$$|5 \downarrow 2 \uparrow\rangle = -|2 \uparrow 5 \downarrow\rangle$$

as written simply by using the fermion anti-commutation relations. As a result, we choose to label states uniquely beginning with the lowest site number and proceeding to the highest from left to right. When the same site occurs with both up and down spin electrons, the up spin shall come first. Hence, the following states are properly labelled in a normal ordered fashion:

$$|3 \downarrow 4 \downarrow\rangle, \quad |1 \uparrow 2 \uparrow 2 \downarrow\rangle, \quad |1 \uparrow 1 \downarrow 3 \downarrow 4 \uparrow\rangle;$$

and represent two-, three- and four-electron states, respectively. The Pauli exclusion principle must also be respected so no two electrons may occupy the same site with the same spin. With these rules, the basis in which all work shall be carried out is now defined. Once the number of sites is selected, n , and the number of electrons is determined, n_e , the number of distinct electronic states is given by

$$\binom{2n}{n_e} = \frac{2n!}{n_e!(2n - n_e)!}. \quad (6.15)$$

These states are built up by applying in normal order each of the combinations of n_e -electron states.

6.2.4 Itinerant Electron Picture

An individual dimer may be studied using a Hubbard model. We begin with the following Hubbard Hamiltonian:

$$\hat{H} = \sum_{i,\sigma} \epsilon_i c_{i\sigma}^\dagger c_{i\sigma} - \sum_{i \neq j, \sigma} t_{ij} c_{i\sigma}^\dagger c_{j\sigma} + \sum_i U_i c_{i\uparrow}^\dagger c_{i\uparrow} c_{i\downarrow}^\dagger c_{i\downarrow}. \quad (6.16)$$

In this case, there are two sites so i and j run from 1 to 2, and σ represents the spin on the electron. The first term represents the energy of an electron localized at each site, the second term is a kinetic energy term for electron hopping and the last term is the electron-electron interaction term. Note that in general, the Coulomb repulsion may take on different values at each site. We try to solve the problem by considering the electron-electron term as a perturbation to study how it affects the electronic states of the dimer. The Hamiltonian in the absence of the final term may be diagonalized by the following unitary transformation:

$$\alpha_{1'\sigma}^\dagger = \frac{1}{\sqrt{2}}(c_{1\sigma}^\dagger + c_{2\sigma}^\dagger) \quad (6.17)$$

$$\alpha_{2'\sigma}^\dagger = \frac{1}{\sqrt{2}}(c_{1\sigma}^\dagger - c_{2\sigma}^\dagger). \quad (6.18)$$

The linear combination of operators is simple because we have made the site energies ϵ_1 and ϵ_2 equal. These new operators are easily shown to obey the usual

anti-commutation relations for fermions and are said to be in the itinerant or distributed electron basis. The Hamiltonian may now be rewritten in terms of these new operators,

$$\hat{H} = \sum_{\sigma} (\epsilon + t) \alpha_{1\sigma}^{\dagger} \alpha_{1\sigma} + \sum_{\sigma} (\epsilon - t) \alpha_{2\sigma}^{\dagger} \alpha_{2\sigma} + \frac{1}{2} \sum_{\substack{i,j,l,m \\ \sigma \neq \sigma'}} V_{ijlm} \alpha_{i\sigma}^{\dagger} \alpha_{j\sigma'}^{\dagger} \alpha_{l\sigma'} \alpha_{m\sigma}. \quad (6.19)$$

It appears that there are two sites with different site energies. Call these new sites 1' and 2' to differentiate them from the physical sites 1 and 2. For the remainder of this section, the primes on the indices will be dropped for notational convenience. However, the subscripts of U still refer to the physical sites. For our choice of the potential in (6.16), the form of V_{ijlm} may be solved. It turns out that all terms with $\sigma = \sigma'$ are zero, this expresses the fact that the Coulomb interaction preserves the electron spin and that, since the repulsion is simply on-site, the two electrons must have the opposite spins. We are therefore concerned only with the cases where $\sigma \neq \sigma'$. The result is

$$V_{ijlm} = \frac{1}{4}(U_1 + U_2) \quad (6.20)$$

when an even number of indices are equal to 1 (eg. V_{1111}, V_{2112}) and

$$V_{ijlm} = \frac{1}{4}(U_1 - U_2) \quad (6.21)$$

when an odd number of indices are equal to 1 (eg. V_{1112}, V_{1222}). In order to study the effect of the introduction of this interaction, a basis of states is selected. Consider the two electron states, there are six distinct possibilities which have been labelled as follows:

$$\begin{aligned} |1\rangle &= \alpha_{1\uparrow}^{\dagger} \alpha_{1\downarrow}^{\dagger} |\Omega\rangle & |4\rangle &= \alpha_{1\downarrow}^{\dagger} \alpha_{2\uparrow}^{\dagger} |\Omega\rangle \\ |2\rangle &= \alpha_{1\uparrow}^{\dagger} \alpha_{2\uparrow}^{\dagger} |\Omega\rangle & |5\rangle &= \alpha_{1\downarrow}^{\dagger} \alpha_{2\downarrow}^{\dagger} |\Omega\rangle \\ |3\rangle &= \alpha_{1\uparrow}^{\dagger} \alpha_{2\downarrow}^{\dagger} |\Omega\rangle & |6\rangle &= \alpha_{2\uparrow}^{\dagger} \alpha_{2\downarrow}^{\dagger} |\Omega\rangle, \end{aligned} \quad (6.22)$$

where the vacuum state is represented by $|\Omega\rangle$. Acting with our Hamiltonian on this basis gives us the matrix form of the Hamiltonian,

$$\hat{H} = \begin{pmatrix} 2(\epsilon+t) + \frac{\langle U_1+U_2 \rangle}{4} & 0 & \frac{\langle U_1-U_2 \rangle}{4} & \frac{\langle U_2-U_1 \rangle}{4} & 0 & \frac{\langle U_1+U_2 \rangle}{4} \\ 0 & 2\epsilon & 0 & 0 & 0 & 0 \\ \frac{\langle U_1-U_2 \rangle}{4} & 0 & 2\epsilon + \frac{\langle U_1+U_2 \rangle}{4} & -\frac{\langle U_1+U_2 \rangle}{4} & 0 & \frac{\langle U_1-U_2 \rangle}{4} \\ \frac{\langle U_2-U_1 \rangle}{4} & 0 & -\frac{\langle U_1+U_2 \rangle}{4} & 2\epsilon + \frac{\langle U_1+U_2 \rangle}{4} & 0 & \frac{\langle U_2-U_1 \rangle}{4} \\ 0 & 0 & 0 & 0 & 2\epsilon & 0 \\ \frac{\langle U_1+U_2 \rangle}{4} & 0 & \frac{\langle U_1-U_2 \rangle}{4} & \frac{\langle U_2-U_1 \rangle}{4} & 0 & 2(\epsilon-t) + \frac{\langle U_1+U_2 \rangle}{4} \end{pmatrix}. \quad (6.23)$$

The Hamiltonian is then diagonalized in order to determine its eigenstates. In the absence of the Coulomb repulsion ($U = 0$), the electrons are localized on the $2'$ site with energy $2(\epsilon - t)$, the gap to the first excited state being $2t$. However, as U is increased, the effect of the Coulomb interaction raises the energy of the ground state relative to the excited singlet states which do not feel the Coulomb repulsion. Consequently, the gap between the ground state and the first excited state is actually reduced through the introduction of U as shown in Figure 6.4. Thus, when conductivity is being considered, it is important to bear in mind that the gap is reduced by the presence of the electron-electron interactions. In a MT when electron-electron interaction must be accounted for and in which the large number of dimers implies a high density of states, there is hope that the energy required to excite electrons may be small and that semiconductor behaviour could result.

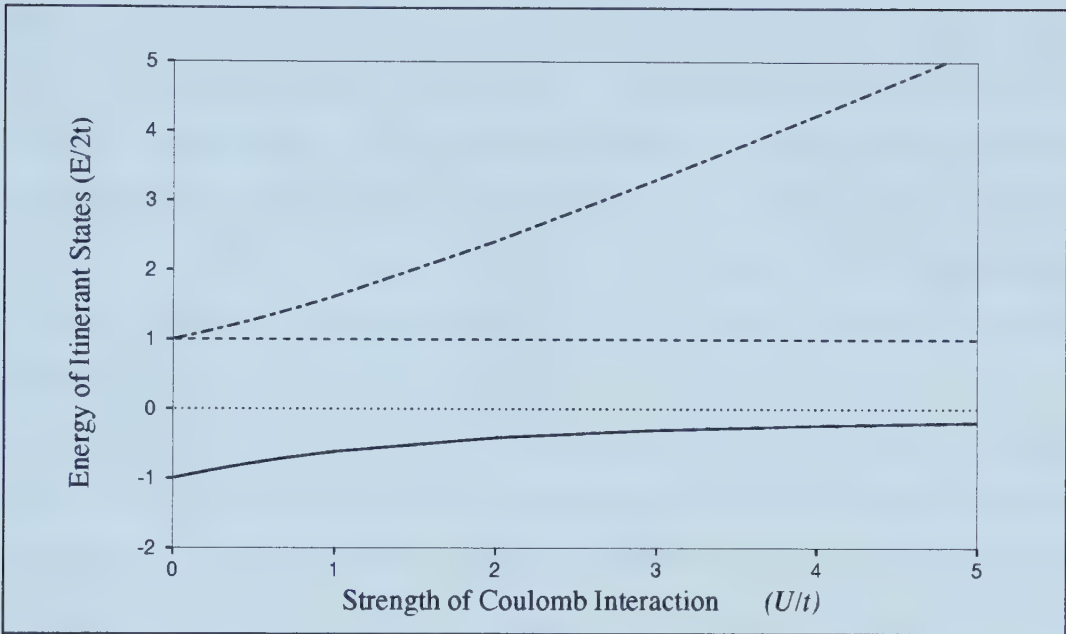


Figure 6.4: Energy of the itinerant states as a function of U/t with the energy plotted in units of $2t$.

6.2.5 Hubbard Model

We have already mentioned the Hubbard model and played with it for a toy system that consisted only of a single electron. The Hubbard Hamiltonian is:

$$\hat{H} = \sum_{i,\sigma} \epsilon_i \hat{c}_{i\sigma}^\dagger \hat{c}_{i\sigma} - \sum_{i \neq j, \sigma} t_{ij} \hat{c}_{i\sigma}^\dagger \hat{c}_{j\sigma} + \sum_i U_i \hat{c}_{i\uparrow}^\dagger \hat{c}_{i\uparrow} \hat{c}_{i\downarrow}^\dagger \hat{c}_{i\downarrow} \quad (6.24)$$

where the first term represents the local potential or the site energy. The second term is our kinetic term and represents the hopping of particles between sites. In our model, hopping shall be restricted to nearest neighbours. The final term accounts for electron-electron repulsion now that we have gone to a many-electron system. In our simple model, this is limited to an onsite interaction. To this point, we have made each of the site energies equivalent, ($\epsilon_i = \epsilon$), since the Hamiltonian conserves the particle number, this term may be ignored as a trivial constant. We have also made the electron repulsion the same at all sites ($U_i = U$).

In the pictures which follow, $U = 2.0$ eV which is the energy associated with two bare electrons lying about 0.7 nm apart. This choice seems reasonable within a well of width 2.0 nm. The lone complication lies within the kinetic term, where the hopping parameter will depend on the two sites between which the electron hops. However since we will first be considering the MT protofilament, it shall initially be a constant as well $t = 0.4$ eV where the choice comes from the separation of the energy bands in the 1D Schrödinger picture.

Since the Hamiltonian conserves both particle number and the overall spin of each state, we are free to work in subspaces enumerated by the spin of the states it contains. This reduces the problems slightly since it is possible to consider individually the spin +1, spin 0 and spin -1 systems separately in a two-electron system. In addition, the symmetry implies that the spin +1 and spin -1 systems have the same conductive properties. We also find that the ground state is always a state consisting of the lowest possible total spin.

Later on we will consider systems where the site energy is varied. This differentiation between the monomers is expected to result in different behaviour for systems below and above half filling compared to the current situation where a symmetry exists. Systems of one, two and three dimers were initially studied and we did consider the possibility of different hopping parameters for inter-dimer and intra-dimer jumps. Although this situation was eliminated in the final model, it is still instructive since when we add additional protofilaments to model the MT, there will be a different value of the hopping parameter for jumps along the protofilament and those between protofilaments. The systems that were studied at half-filling where there is one electron available for each binding site and we are able to compare the systems with the same filling fraction. In addition, the half-filled situation is the most complicated one since there are more possible electronic configurations than for any other degree of filling.

When the inter-dimer hopping term is small relative to the intra-dimer hopping term $t_{\text{inter}} < t_{\text{intra}}$, the form of the ground state is independent of the number of dimers. In each case, the ground state is a linear combination of singlet states on each dimer. The singlet states are those where two electrons are paired on an

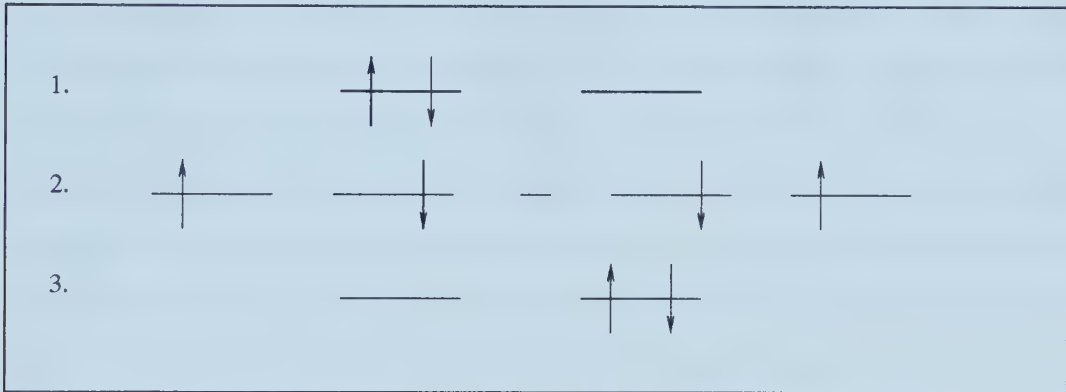


Figure 6.5: The three singlet states for two electrons on the two sites of the tubulin dimer consist of paired electrons spins on the α site, paired electrons on the β site or the anti-symmetric combination of paired electrons on separate sites.

individual binding site, or where the state consists of the anti-symmetric combination of an up electron and a down electron on neighbouring binding sites of the dimer (Figure 6.5). When the kinetic term is absent, the ground state is a combination of anti-symmetric orbitals on each dimer. As the kinetic term is turned on, it competes with the Coulomb repulsion and the other singlets are allowed.

When the inter-dimer hopping parameter is increased, the density of states becomes more uniform between the ground state and the highest energy eigenstate. This is important because the gap between the ground state and the first excited state of the system is diminished. Since the hopping term within a dimer is largest, the system prefers to have two electrons with the same spin within the

same dimer in the ground state. The kinetic term acts like an attractive force but between neighbouring sites rather than the Coulomb repulsion which is onsite. The most interesting observations from the point of view of conduction are the formation of bands in the new model. The band formation is dependent upon the hopping parameter between dimers. When this parameter is small relative to the intra-dimer hopping, $t_{\text{inter}}/t_{\text{intra}} \sim 0.1$, there remains a rather large gap between the ground state and the first excited state of about $2t_{\text{intra}}$ which is reduced as the repulsion term increases. However, when the hopping between dimers is equal to the hopping within dimers, $t_{\text{inter}} \sim t_{\text{intra}}$, the gap is minimized. In the event that $t_{\text{inter}} > t_{\text{intra}}$, we would effectively have to relabel the dimers and we would then return to the picture where $t_{\text{inter}} < t_{\text{intra}}$.

One might also be interested in the properties of the system when an additional charge carrier is added and the system is no longer in the special, half-filled state. When an additional electron is added to the system, the ground state becomes degenerate. Once again, the ground state has the smallest possible absolute value of spin. This does not immediately imply conduction because one eigenstate consists entirely of basis states with a total spin $+\frac{1}{2}$, the other of basis states with a total spin $-\frac{1}{2}$. As a result, the usual analysis has to be completed in order to comment further. This will be completed in the results section which follows.

6.3 Conduction in a Hubbard Model

The relative simplicity of the Hubbard model has now been described. How then do we find the physical quantities that we are so interested in? We simply appeal to our conventional ideas of response functions such as conductivity. We ask what sort of current could we measure through our sample if we exposed it to an external electric field with the assumption that the response shall be linear

provided the perturbing field is small. Kubo was the first to derive formulae for the electrical conductivity in solids and his derivation is repeated in the following section [4]. We shall work in the Coulomb gauge so that we may write the vector potential for a uniform electric field along the direction of the chain, $A(t)$, as simply

$$A(t) = \frac{cE(t)}{-i\omega} e^{-i\omega t}. \quad (6.25)$$

Now, we must add a coupling term to the Hubbard Hamiltonian (6.24) to account for the interaction with the electric field. A canonical transformation exists for a tight-binding system [5]. One lets

$$\hat{c}'_i = \hat{c}_i e^{-ieA(t)x_i/c}. \quad (6.26)$$

The kinetic term of (6.24) shall be denoted by H_0 and by applying the transform given above, it becomes:

$$\hat{H}'_0 = -t \sum_{i\sigma} \left[\hat{c}_{i\sigma}^\dagger \hat{c}_{i+1\sigma} e^{-ieA(t)/c} + \hat{c}_{i\sigma}^\dagger \hat{c}_{i-1\sigma} e^{ieA(t)/c} \right] \quad (6.27)$$

where a is the lattice spacing and c is the speed of light. Expanding to second order in the vector potential,

$$\hat{H}_A = \frac{A}{c} \hat{j} - e \frac{A^2}{c^2} a^2 \hat{H}_0, \quad (6.28)$$

where

$$\hat{j} = ieat \sum_{i\sigma} (\hat{c}_{i\sigma}^\dagger \hat{c}_{i+1\sigma} - \hat{c}_{i\sigma}^\dagger \hat{c}_{i-1\sigma}). \quad (6.29)$$

So, the energy of the original system is corrected to this order and the interaction term is proportional to the current.

6.3.1 Kubo Formula for Electrical Conductivity

Suppose a time-dependent external electric field is applied to a solid,

$$E_\alpha^{\text{ext}}(r, t) = \Xi_\alpha^{\text{ext}} e^{iq \cdot r - i\omega t}, \quad (6.30)$$

where α represents the Cartesian coordinate directions. In a linear response theory, the induced current is proportional to the applied electric field:

$$J_\alpha(r, t) = \sum_\beta \sigma'_{\alpha\beta}(q, \omega) \Xi_\beta^{ext} e^{iq \cdot r - i\omega t}, \quad (6.31)$$

where $\sigma'_{\alpha\beta}$ is a parameter relating the observed current density to the applied field's direction, its periodicity and frequency. However, the symbol appearing in equation (6.31) is not the conductivity we seek. Rather, we want the conductivity which represents the response to the total electric field in the solid, a quantity that can be measured. This conductivity takes into account all of the currents, induced by the external fields, that create their own electric fields. Thus we seek $\sigma_{\alpha\beta}$ that relates the macroscopic electric field to the currents of the system.

$$J_\alpha(r, t) = \sum_\beta \sigma_{\alpha\beta}(q, \omega) E_\beta e^{iq \cdot r - i\omega t} \quad (6.32)$$

$$E_\alpha(r, t) = \Xi_\alpha e^{iq \cdot r - i\omega t} \quad (6.33)$$

$$\sigma_{\alpha\beta} = \text{Re}(\sigma_{\alpha\beta}) + i \text{Im}(\sigma_{\alpha\beta}) \quad (6.34)$$

We write the Hamiltonian of the system as $\hat{H} + \hat{H}'$ where the latter term contains the electric field which we shall introduce as a time-dependent perturbation. The evolution of the operators is given as follows [6]:

$$\hat{j}(x, t) = e^{i\hat{H}t} \hat{j}(x) e^{-i\hat{H}t}. \quad (6.35)$$

where \hat{H} represents the unperturbed Hamiltonian. Thus the interaction picture is adopted. The Kubo formula for electrical conductivity gives the result in terms of a current-current correlation function:

$$\sigma_{\alpha\beta}(q, \omega) = \frac{1}{\omega} \int_0^\infty dt e^{i\omega t} \langle \Omega | \hat{j}_\alpha^\dagger(q, t) \hat{j}_\beta(q, 0) - \hat{j}_\beta(q, 0) \hat{j}_\alpha^\dagger(q, t) | \Omega \rangle + i \frac{n_o e^2}{m\omega} \delta_{\alpha\beta} \quad (6.36)$$

where $|\Omega\rangle$ represents the ground state of the system which has not been perturbed by the electric field. The first term in (6.36) is known as the incoherent

contribution to the conductivity and this is the term we shall focus upon. Now, we use (6.35) in the above equation and use the fact that the basis we are using is that of the eigenstates of H . We insert unity in the following manner

$$\sum_n |n\rangle\langle n| = 1, \quad (6.37)$$

where the states $|n\rangle$ are the eigenstates of H . Hence, when H acts upon these states, it simply returns the eigenenergy E_n . Consider the first term in the equation, it becomes

$$\sum_n \int_0^\infty dt e^{i\omega t} \langle \Omega | e^{i\hat{H}t} \hat{j}_\alpha^\dagger(q, 0) e^{-i\hat{H}t} | n \rangle \langle n | \hat{j}_\beta(q, 0) | \Omega \rangle \quad (6.38)$$

$$= \sum_n \int_0^\infty dt e^{i\omega t} e^{iE_\Omega t} e^{-iE_n t} \langle \Omega | \hat{j}_\alpha^\dagger(q, 0) | n \rangle \langle n | \hat{j}_\beta(q, 0) | \Omega \rangle \quad (6.39)$$

and setting $\alpha = \beta$ since we are interested at this stage only in conduction in the same direction as the field,

$$\sum_n \int_0^\infty dt e^{i\omega t} e^{i(E_\Omega - E_n)t} |\langle n | \hat{j}_\alpha(q, 0) | \Omega \rangle|^2 \quad (6.40)$$

At finite temperatures, we may replace the ground state with a sum over each of the eigenstates. We must be careful to properly normalize the conductivity under this replacement. Consequently, the new expression is a little more complicated:

$$\left[\sum_n \int_0^\infty dt e^{i\omega t} \sum_m \left(e^{-\beta E_m} e^{i(E_m - E_n)t} |\langle n | \hat{j}_\alpha(q, 0) | m \rangle|^2 \right) \right] / Z, \quad (6.41)$$

and

$$Z = \sum_m e^{-\beta E_m}. \quad (6.42)$$

The temperature now appears as $\beta = 1/(kT)$ and Z is the canonical partition function. Substituting into (6.36), we now have the following expression for the electrical conductivity parallel to the field.

$$\sigma_{\alpha\alpha} = \sum_{m,n} \frac{1}{\omega} \int_0^\infty dt e^{i\omega t} e^{-\beta E_m} \left[e^{i(E_m - E_n)t} |\langle n | \hat{j}_\alpha | m \rangle|^2 - e^{i(E_n - E_m)t} |\langle m | \hat{j}_\alpha | n \rangle|^2 \right] / Z \quad (6.43)$$

To simplify the expression, we swap the summation indices in the second term. This allows us to collect some of the terms together

$$\sigma_{\alpha\alpha} = \sum_{m,n} \frac{1}{\omega} \int_0^\infty dt e^{i\omega t} (e^{-\beta E_m} - e^{-\beta E_n}) \left[e^{i(E_m - E_n)t} |\langle n | \hat{j}_\alpha | m \rangle|^2 \right] / Z \quad (6.44)$$

Now, if we perform the integration and let $\omega \rightarrow \omega + i\omega'$ with a small imaginary component, so that the time integral converges, we find $\sigma_{\alpha\alpha}$ (subscript dropped hereafter) is now

$$\sigma(\omega) = \frac{i}{\omega} \sum_{m,n} (e^{-\beta E_m} - e^{-\beta E_n}) \left[\frac{|\langle n | \hat{j}_\alpha | m \rangle|^2}{\omega - (E_n - E_m) + i\omega'} \right] / Z \quad (6.45)$$

We now apply the well known identity, $1/(u + i\epsilon) \rightarrow \text{P}(1/u) - i\pi\delta(u)$ to arrive at the following result where only the real part of the conductivity has been kept:

$$\begin{aligned} \sigma(\omega) &= \frac{\pi}{Z} \cdot \frac{1}{\omega} \sum_{m,n} (e^{-\beta E_m} - e^{-\beta E_n}) |\langle n | \hat{j}_\alpha | m \rangle|^2 \delta(\omega - (E_n - E_m)) \\ &= \frac{\pi}{Z} \frac{(1 - e^{-\beta\omega})}{\omega} \sum_{n,m} e^{-\beta E_m} |\langle n | \hat{j}_\alpha | m \rangle|^2 \delta(\omega - (E_n - E_m)) . \end{aligned} \quad (6.46)$$

This is formula for the conductivity which may be found in Mahan's book [7].

6.3.2 Implementation of the Model

The DC conductivity is calculated by a procedure through which a sum rule is used. This procedure has been described by Maldague and others [7, 5]. The sum rule states that

$$\int_0^\infty \sigma'(\omega) d\omega = -\frac{\pi e^2}{2} a^2 \langle K \rangle \quad (6.47)$$

where

$$\sigma'(\omega) = D \delta(\omega) + \sigma_{\text{kubo}}(\omega) \quad (6.48)$$

and $\langle K \rangle$ is the expectation value of the kinetic energy term of the Hamiltonian. The strategy of computing $\sigma(\omega)$ and subsequently the Drude contribution at either zero or finite temperature is reasonably straight-forward. The first step is

to construct the matrix corresponding to the Hamiltonian, equation (6.2), in a subspace which is defined by the geometry of the lattice, the number of electrons, and the total electron spin. The difficulty in computing the physical properties from such a model is apparent immediately. Given a moderately sized lattice of say ten dimers and eight electrons of arbitrary spin, the corresponding space is about 77 million states. A matrix of dimension 77 million square has about 5.9×10^{15} elements. Thus the simple storage of the matrix would require at least 5.9×10^6 gigabytes of memory. Obviously, working on a moderately sized lattice, we are restricted to a low concentration of electrons. Due to electron-hole symmetry, we are also able to study the nearly filled situation [8]. However, in order to study properties near half-filling, we are restricted to small lattices. Special approximations for the half-filled case are most useful when the ratio U/t is either very large or very small, in practical terms, differing by perhaps an order of magnitude. Since our interest lies in the region where U and t are comparable, these approximations are not particularly useful.

When this model is implemented for the calculation of $\sigma_{\text{kubo}}(\omega)$, one term is singled out by Fye et al. [9] as being potentially dangerous in the calculation. This is a term which would give rise in the Kubo calculation to a contribution at $\omega = 0$. Specifically, Fye restricts the following sum to $m \neq 0$:

$$\sum_m \frac{\langle m | \hat{j} | n \rangle}{E_m - E_0}. \quad (6.49)$$

However, it is proven below in the single- and two-electron cases that in fact, the contribution of this term to the conductivity is zero. The result is easily generalized at finite temperature and the meaning is both clear and obvious. Conduction is the result of electron movement, consequently if the final state is the same as the initial state, no electron movement has occurred and no conduction results.

6.3.3 Proof: Conduction requires electronic state change

Consider first single electron states only residing on N sites and I suppress for simplicity here the spin index. This does not take away anything from the proof since the spin of the initial and final states is the same and when conduction is considered, the up spin electrons and down spin electrons are treated independently by the conduction operator, \hat{j} . The conduction operator may be represented as follows:

$$\hat{j} = \sum_m^{N-1} (\hat{c}_{m+1}^\dagger \hat{c}_m - \hat{c}_m^\dagger \hat{c}_{m+1}). \quad (6.50)$$

and an arbitrary electronic state, $|n\rangle$ as follows:

$$|n\rangle = \sum_i^N a_i \hat{c}_i^\dagger |\Omega\rangle. \quad (6.51)$$

Therefore, we want to show that the following inner product, $\langle n|\hat{j}|n\rangle$ is indeed zero. We will use the fact that in this representation, all of the coefficients, a_i , in the expansion above (eq. 6.51) are real since the Hamiltonian we are working with is Hermitian. The fermion anticommutation relation shall also be used repeatedly.

$$\begin{aligned} \langle n|\hat{j}|n\rangle &= \sum_i^N \sum_j^N \sum_m^{N-1} a_i a_j^* \langle \Omega | \hat{c}_j (\hat{c}_{m+1}^\dagger \hat{c}_m - \hat{c}_m^\dagger \hat{c}_{m+1}) \hat{c}_i^\dagger | \Omega \rangle \\ &= \sum_i^N \sum_j^N \sum_m^{N-1} a_i a_j^* \left(\langle \Omega | \hat{c}_j \hat{c}_{m+1}^\dagger \hat{c}_m \hat{c}_i^\dagger | \Omega \rangle - \langle \Omega | \hat{c}_j \hat{c}_m^\dagger \hat{c}_{m+1} \hat{c}_i^\dagger | \Omega \rangle \right) \\ &= \sum_i^N \sum_j^N \sum_{m=1}^{N-1} a_i a_j^* (\delta_{j,m+1} \delta_{m,i} - \delta_{j,m} \delta_{m+1,i}) \\ &= \sum_j^N \sum_i^{N-1} a_i a_j^* \delta_{j,i+1} - \sum_i^N \sum_j^{N-1} a_i a_j^* \delta_{j+1,i} \\ &= \sum_i^{N-1} a_i a_{i+1}^* - \sum_j^{N-1} a_{j+1} a_j^* \\ &= \sum_i^{N-1} (a_i a_{i+1} - a_{i+1} a_i) \\ &= 0 \end{aligned} \quad (6.52)$$

The two electron case is similar and will be shown in brevity. A similar proof can be completed for the n electron case, but becomes cumbersome. The same properties shall be used in this proof as before with the additional property that $a_{ik} = -a_{ki}$ which stems from the fermionic anticommutation relation, and that $a_{ik} = 0$ if $i = k$ which is a result of the Pauli exclusion principle. The conduction operator remains the same as above, and the state $|n\rangle$ under consideration has the following expansion:

$$|n\rangle = \sum_i^N \sum_j^N a_{i,j} \hat{c}_i^\dagger \hat{c}_j^\dagger |\Omega\rangle. \quad (6.53)$$

Calculation of the inner product $\langle n|\hat{j}|n\rangle$ is as follows:

$$\begin{aligned} \langle n|\hat{j}|n\rangle &= \sum_{i,j,r,s}^N \sum_m^{N-1} a_{ij} a_{rs}^* \langle \Omega | \hat{c}_s \hat{c}_r \left(\hat{c}_{m+1}^\dagger \hat{c}_m - \hat{c}_m^\dagger \hat{c}_{m+1} \right) \hat{c}_i^\dagger \hat{c}_j^\dagger | \Omega \rangle \\ &= \sum_{i,j,r,s}^N \sum_m^{N-1} a_{ij} a_{rs}^* \langle \Omega | \left(\hat{c}_s (\delta_{r,m+1} - \hat{c}_{m+1}^\dagger \hat{c}_r) \hat{c}_m \hat{c}_i^\dagger \hat{c}_j^\dagger \right) | \Omega \rangle \\ &\quad - \text{same terms}(m \leftrightarrow m+1) \\ &= \sum_{i,j,r,s}^N \sum_m^{N-1} a_{ij} a_{rs}^* \left(\delta_{r,m+1} \langle \Omega | \hat{c}_s \hat{c}_m \hat{c}_i^\dagger \hat{c}_j^\dagger | \Omega \rangle \right. \\ &\quad \left. - \langle \Omega | \hat{c}_s \hat{c}_{m+1}^\dagger \hat{c}_r \hat{c}_m \hat{c}_i^\dagger \hat{c}_j^\dagger | \Omega \rangle \right) - \text{s.t.}(m \leftrightarrow m+1) \\ &= \sum_{i,j,r,s}^N \sum_m^{N-1} a_{ij} a_{rs}^* \left(\delta_{r,m+1} \langle \Omega | \hat{c}_s \hat{c}_m \hat{c}_i^\dagger \hat{c}_j^\dagger | \Omega \rangle \right. \\ &\quad \left. - \delta_{m+1,s} \langle \Omega | \hat{c}_r \hat{c}_m \hat{c}_i^\dagger \hat{c}_j^\dagger | \Omega \rangle \right) - \text{s.t.}(m \leftrightarrow m+1) \\ &= \sum_{i,j,r,s}^N \sum_m^{N-1} a_{ij} a_{rs}^* \{ \delta_{r,m+1} (\delta_{i,m} \delta_{j,s} - \delta_{i,s} \delta_{j,m}) \\ &\quad - \delta_{m+1,s} (\delta_{i,m} \delta_{r,j} + \delta_{r,i} \delta_{m,j}) - \text{s.t.}(m \leftrightarrow m+1) \} \\ &= \sum_{i,j,r,s}^N \sum_m^{N-1} (\delta_{m+1,r} \delta_{j,s} \delta_{i,m} - \delta_{m+1,r} \delta_{i,s} \delta_{j,m} \end{aligned}$$

$$\begin{aligned}
& -\delta_{i,m}\delta_{m+1,s}\delta_{j,r} + \delta_{m+1,s}\delta_{i,r}\delta_{j,m} - \delta_{m,r}\delta_{j,s}\delta_{i,m+1} \\
& + \delta_{m,r}\delta_{i,s}\delta_{j,m+1} + \delta_{i,m+1}\delta_{m,s}\delta_{j,r} - \delta_{m,s}\delta_{i,r}\delta_{j,m+1}) \\
= & \sum_{j,r,s}^N \sum_i^{N-1} a_{ij}a_{rs}^* (\delta_{i+1,r}\delta_{j,s} - \delta_{i+1,s}\delta_{j,r}) \\
& + \sum_{i,r,s}^N \sum_j^{N-1} a_{ij}a_{rs}^* (\delta_{j+1,s}\delta_{i,r} - \delta_{j+1,r}\delta_{i,s}) \\
& + \sum_{i,j,s}^N \sum_r^{N-1} a_{ij}a_{rs}^* (\delta_{j,r+1}\delta_{i,s} - \delta_{i,r+1}\delta_{j,s}) \\
& + \sum_{i,j,r}^N \sum_s^{N-1} a_{ij}a_{rs}^* (\delta_{i,s+1}\delta_{j,r} - \delta_{i,r}\delta_{j,s+1}) \\
= & \sum_j^N \sum_i^{N-1} (a_{i,j}a_{i+1,j}^* - a_{i,j}a_{j,i+1}^*) + \sum_i^N \sum_j^{N-1} (a_{i,j}a_{j+1,i}^* - a_{i,j}a_{i,j+1}^*) \\
& + \sum_s^N \sum_r^{N-1} (a_{s,r+1}a_{r,s}^* - a_{r+1,s}a_{r,s}^*) + \sum_r^N \sum_s^{N-1} (a_{s+1,r}a_{r,s}^* - a_{r,s+1}a_{r,s}^*) \\
= & 2 \sum_j^N \sum_i^{N-1} (a_{i,j}a_{i+1,j}^* + a_{j,i}a_{i+1,j}^* + a_{j,i+1}a_{i,j}^* - a_{i+1,j}a_{j,i}) \\
= & 2 \sum_j^N \sum_i^{N-1} (a_{i,j}a_{i+1,j} - a_{i,j}a_{i+1,j} - a_{i,j}a_{i+1,j} + a_{i,j}a_{i+1,j}) \\
= & 0
\end{aligned}$$

This result simply provides another check for the numerical computation since $\langle n|\hat{j}|n\rangle$ should be identically zero.

6.4 Results

When the results are interpreted, it is useful to be able to convert easily from the energy scale on the abscissa to the corresponding wavelength of a photon, λ . The relation which exists can be summarized as follows:

$$\lambda = \frac{1240 \text{ nm} \cdot \text{eV}}{\text{Energy}}. \quad (6.55)$$

So that in the plots which are displayed, the visible light range is between 1.75 eV and 3.10 eV. Energies larger than this range correspond to ultraviolet wavelengths

and lower energies correspond to infrared wavelengths. Since cells respond to light in the near-infrared [10], and centrioles which are composed of MTs are proposed to be the site of light detection [11], absorption in this energy range is of great interest. These energies should also be compared to the energy available from ATP and GTP hydrolysis which are 0.49 eV and 0.22 eV, respectively. These values provide limits for the interaction of chemical energy in the conduction process.

6.4.1 1D Protofilament Chain

All calculations were carried out with open boundary conditions along the protofilament. When more complicated geometries are considered, the lateral boundary conditions will be specified. To summarize the results for the 1D chain, we must differentiate between zero temperature and finite temperature calculations. At zero temperature, the linear polymer results are summarized concisely by saying that there is no DC conductivity. This has been the result of my calculations and agrees with the previous modelling of Hubbard systems [5]. The finite temperature results will be presented following a discussion of the AC conductivity. There are peaks in $\sigma(\omega)$, also known as the optical conductivity, which correspond to excitations between electronic states of the polymer. Electronic excitation results in electron redistribution and hence the development of a current. There is much to learn from these results which shall prove to be useful in the analysis of the results from the full MT. Calculations include a broadening of all δ -functions. This finite width, ϵ , helps to account for scattering through processes not included in the model, such as phonons and disorder. When this parameter is larger than the mean energy level spacing, the model approximates a continuum of states. We have selected $\epsilon = 0.02$ eV to present our results which is roughly kT . This value is smaller than the three energy scales important to the Hubbard model,

t , U and $4t^2/U$ [12] so we expect to be able to pick out features corresponding to specific transitions in the predicted optical spectra. We shall present a few results with different values of the broadening, ϵ to illustrate its effect. It does not have an effect on the predictions of the MT's conduction properties.

We shall begin with a very simple system consisting of only two dimers. In addition, we shall begin with $t = 0.4$ eV, $U = 2.0$ eV and equal site energy on the α and β monomer sites. This system can support up to eight electrons. Figure 6.6

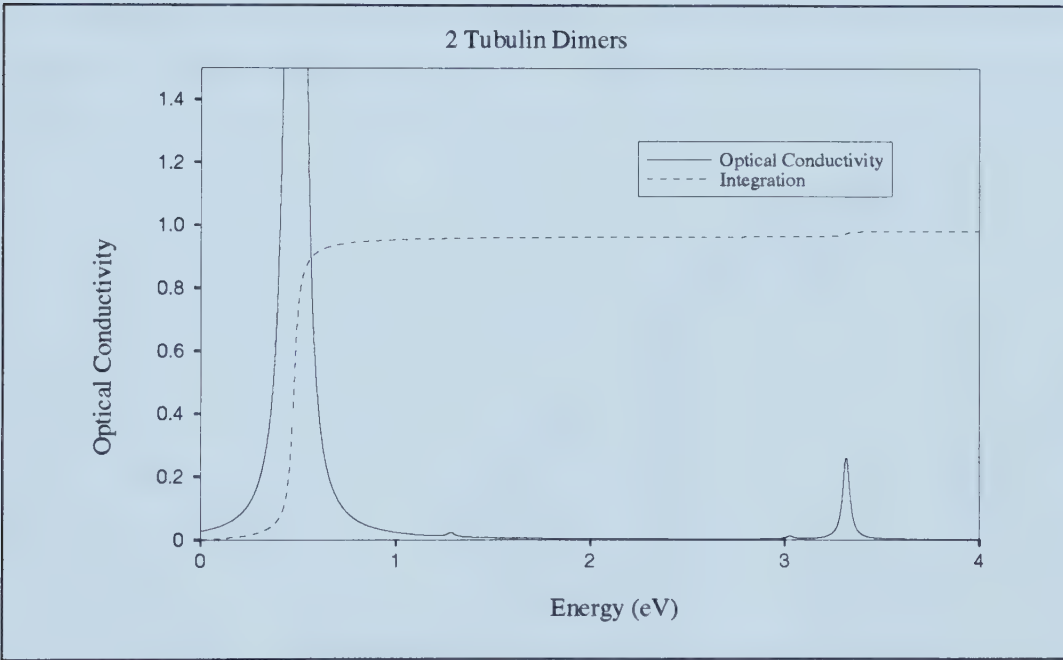


Figure 6.6: Optical conductivity and the scaled integrated conductivity is plotted for the two dimer, two electron system. The fact that the material is an insulator may be recognized as the integral approaches unity as the energy increases.

shows the optical conductivity of the two dimer system of two electrons. This spectrum consists of a large peak centered about 0.48 eV and a much smaller peak at 3.32 eV. The positioning of the large peak is such that it represents about 20 times the thermal energy at physiological temperatures. We shall present a few results at other temperatures to show how the results vary with temperature.

Now, the first change which we can consider to the system above is to leave its size alone but to increase the number of electrons present. The single electron case has been omitted since the absence of an electron-electron term makes the problem uninteresting. Since the system has symmetry with respect to holes and electrons and its capacity is 8 electrons, the optical conductivity results are identical for two electrons and six holes to the system with six electrons and two holes. Consequently, we need only to consider the cases from two electrons up to half-filling, four electrons in this case. The results for these systems are presented in Figure 6.7. The predicted spectra for the two and three electron

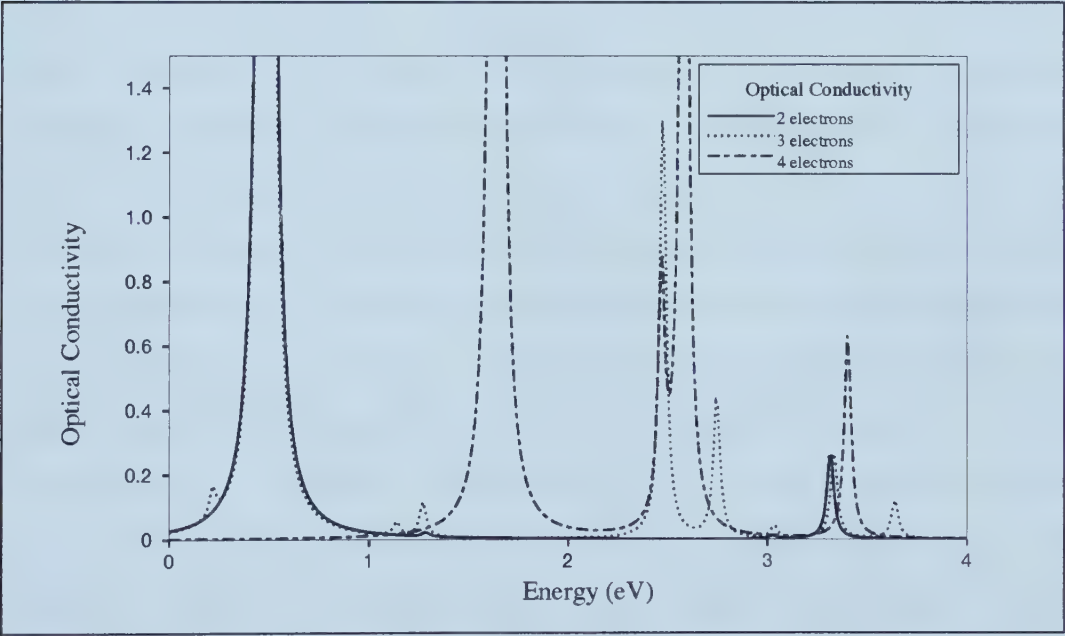


Figure 6.7: Optical conductivity of the two dimer system with two, three and four electrons

cases are quite similar. The differences include a new but small peak in the three electron spectrum at an energy just below the major peak and variations in the detail of the absorption band centered about 2.6 eV. However, the qualitative similarity of the two spectra is remarkable in terms of band locations. Contrast

these two cases with the four-electron system which corresponds to half-filling. The difference is that the peak in the optical conductivity spectrum increases dramatically from about 0.48 eV to 1.64 eV. This change indicates how the half-filled case is special. The ground state in this system largely consists of electrons spread out to minimize the Coulombic energy. Exciting this system by moving any particular electron will come at the cost of greatly increasing the electron-electron repulsion and consequently, the location of the required excitation energy corresponds roughly to U , the value of the Coulomb interaction.

As the length of the polymer is increased, results remain qualitatively similar. In the three-dimer structure, results are shown for the conductivity in Figure 6.8 and for the integrated conductivity in Figure 6.9. Once again, the spectra are quite similar for all fillings aside from the half-filled case which consists of six electrons. By consulting the figure of the integrated conductivity, the shift of the conductivity to higher energies can be clearly seen as the filling fraction increases towards half filling. We now present results where the broadening parameter, ϵ , and the temperature have been varied to see the effect which they have on the results. Figure 6.10 demonstrates that as the width is decreased, the spectrum becomes sharper. Note how the two peaks in this simple spectrum which occur near 2.5 eV are successively blended into a band as the ϵ is increased. Peaks represent transitions from one specific electron configuration to another and are weighted with the associated conductivity. However, as the sampling width is broadened, we are better able to account for a spectrum that might be experimentally measured and which will have a finite resolution. The value which has been selected for presenting figures is 0.02 eV unless otherwise stated. The effect of changing the temperature is to excite electron configurations other than the ground state. Consequently, transitions from one excited state to another can now contribute to the conductivity. Figure 6.11 shows how this often re-

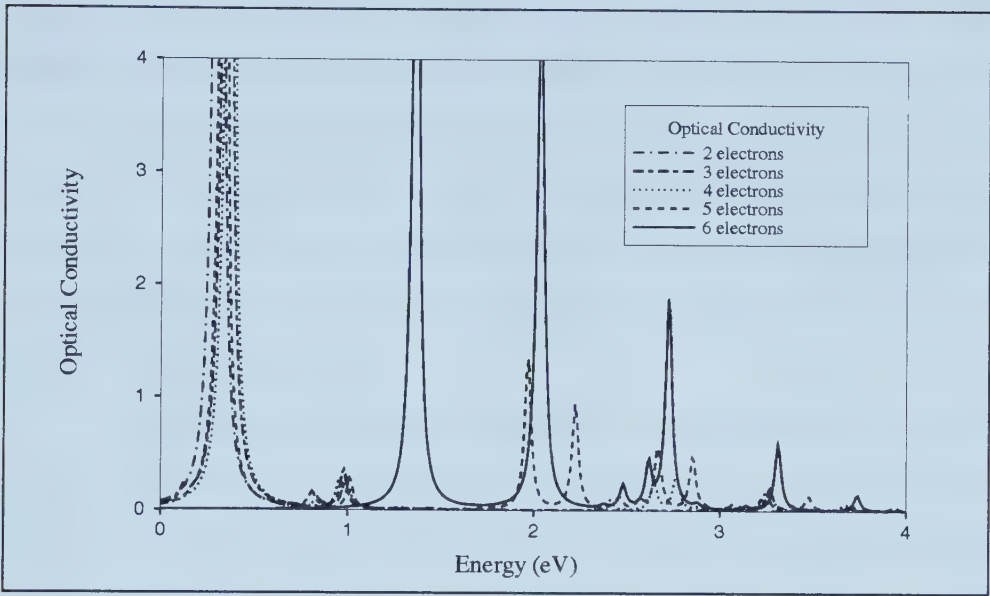


Figure 6.8: Optical conductivity of the three-dimer system from two electrons through half filling.

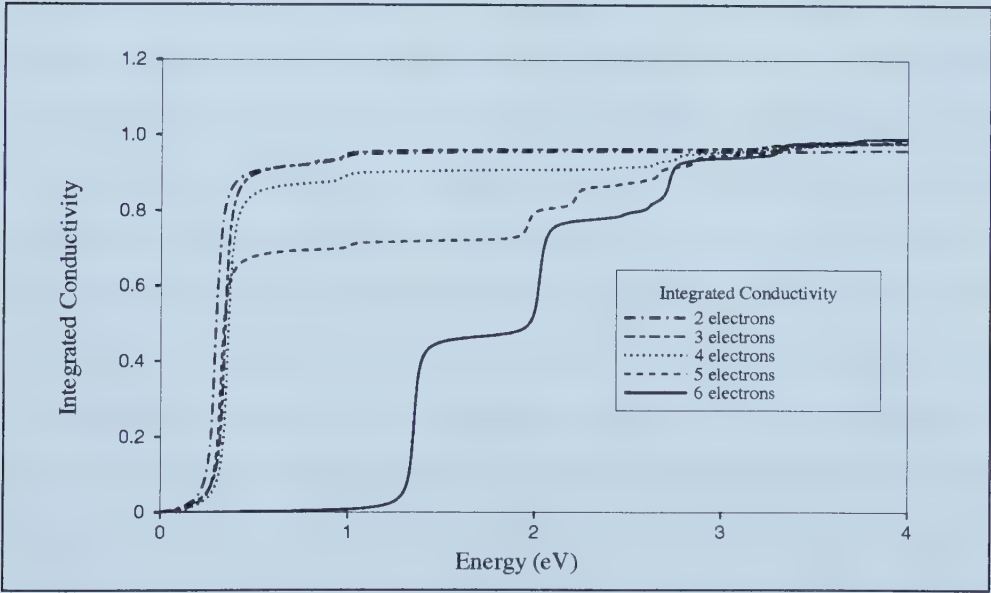


Figure 6.9: Integrated optical conductivity of the three-dimer system shows that indeed the protofilament is an insulator. The gap for excitation of the half filled polymer is seen easily here.

duces the gap to conduction, all the major peaks in the 300 K spectrum shift slightly towards lower energies in the 3000 K spectrum but many more features develop as well as states which previously did not contribute to conductivity may make transitions to excited states. Physiological temperature of 300 K ($kT = 0.026$ eV) is small relative to the system's energy scales, consequently lowering the temperature further causes very little change to the spectrum and thus these results have not been shown.

The next thing to consider with MTs is the variation of the site energy. If the α -tubulin and β -tubulin sites have different energies, then the MT A and B lattices can be distinguished. The effect of this change on the optical spectrum however seems to be small when individual protofilaments are considered. The spectra corresponding to the dimers where the site energies oscillate back and forth along the chain contain additional absorption peaks however, this simply amounts to fine structure when compared to the corresponding spectra for the monomer systems. In addition, the sum rule shows that protofilaments remain insulators. We shall return to investigate the effect of alternating α and β sites when the entire MT lattice is considered. In this case, the presence of α and β sublattices changes the overall geometry of the system and may lift the helical symmetry of the lattice that exists when only monomers are considered.

Another concern is the size of the system. Can we extrapolate to a system the length of a typical MT by considering the results from these small systems? There are a few parameters which we can consider individually and which can be compared as the size of the system changes and which can also be compared to the values in the MT lattice which is triangular. These parameters are the threshold to conductivity, and the expectation value of the kinetic energy operator. The threshold to conductivity is simply the location of the first absorption peak in the optical spectrum. It is a decreasing function of the polymer length. Starting

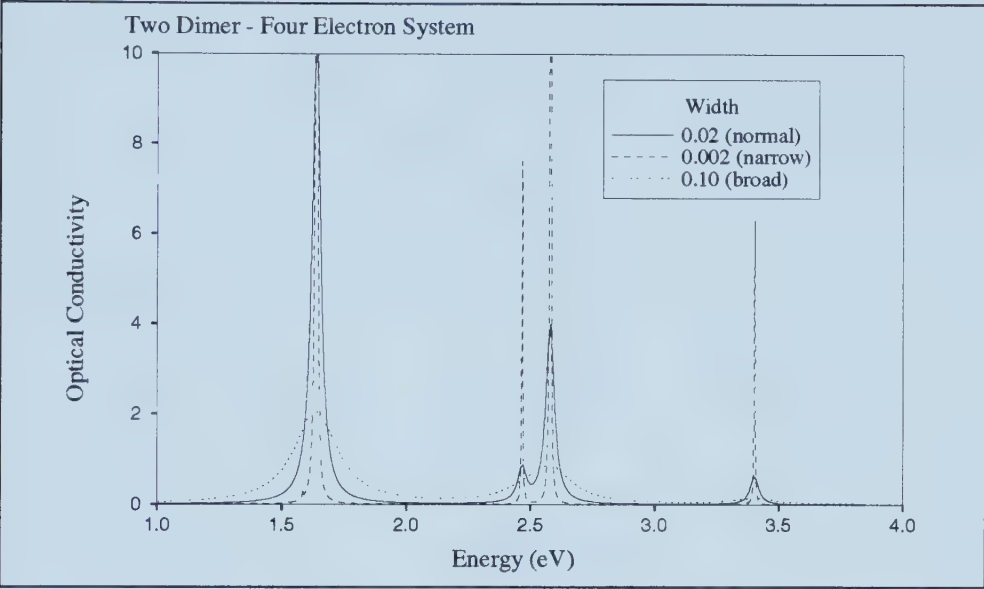


Figure 6.10: Optical conductivity spectrum variation with the broadening parameter.

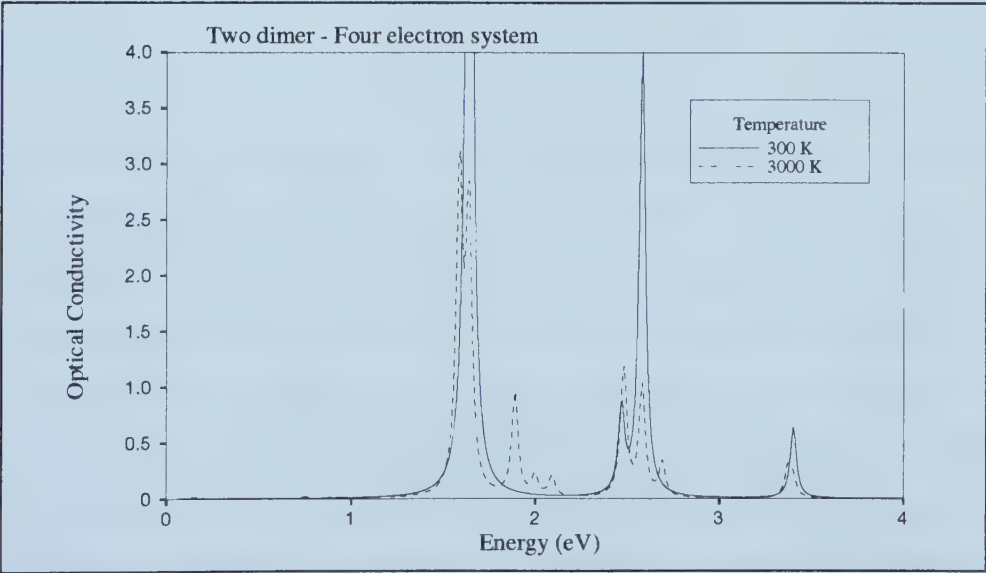


Figure 6.11: The variation of the optical conductivity spectrum with temperature is shown.

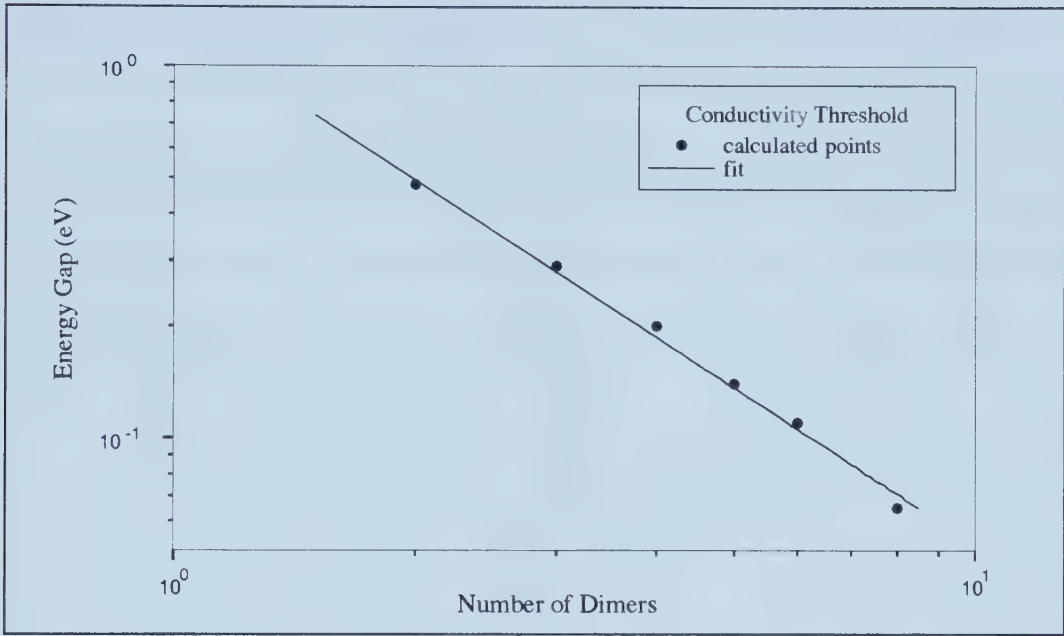


Figure 6.12: Threshold to conduction as a function of protofilament length.

at 0.48 eV for the two-dimer system, it seems to drop a little faster than $1/n$ for systems consisting of n dimers and containing two electrons. The fitted value in Figure 6.12 varies $\propto 1/n^{1.4}$. Extrapolating to larger values of n , this gap appears certain to fall into the range where these excited states could be thermally excited. The protofilament then develops a finite DC conductivity at finite temperature where thermal excitation can result in population of the low-lying excited states. However, even for systems of 20 dimers, this is a daunting task to perform the matrix diagonalization. It is interesting that although the first peak does move towards zero, the fraction of the conductivity it contains is gradually diminished. This may be partially explained by the fact that these longer polymers have a smaller electron density when they contain two electrons than the shorter polymers. Some of the conduction continues to reside in a peak located close to t in the energy spectrum. In the 2D lattice, there is a

phase transition in the dimensionality. DC conduction becomes possible even at zero temperature. However, we shall still be concerned about the boundary conditions since calculations are being performed on a small lattice. Consider the kinetic energy/electron which has been calculated in a Hubbard model with our parameters for t and U and with either one, two or three protofilaments. Figure 6.13 demonstrates how the kinetic energy of each electron approaches the

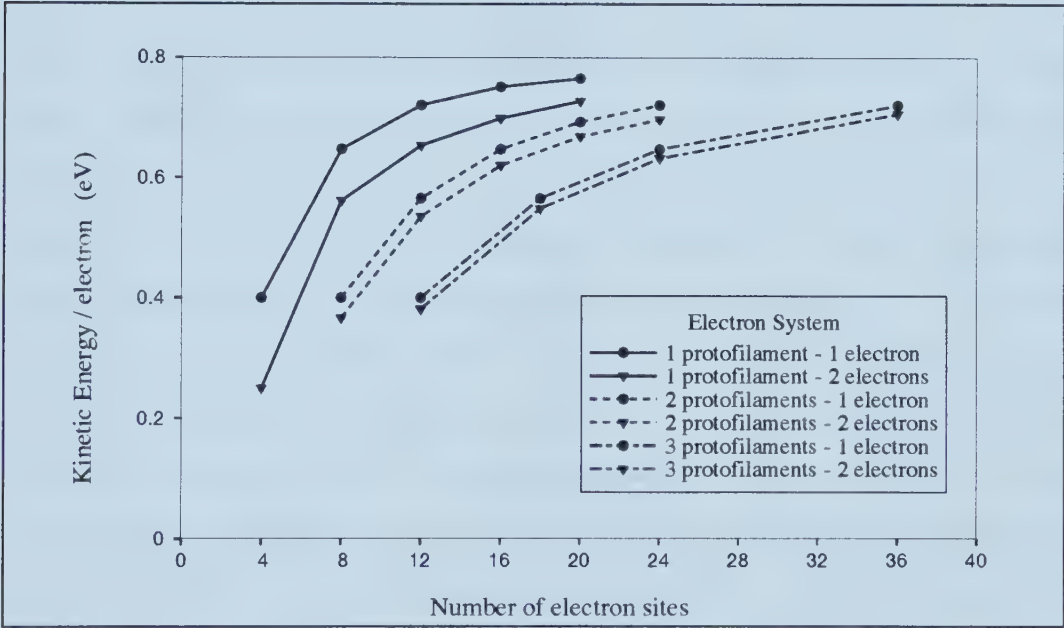


Figure 6.13: Kinetic energy per electron as a function of system size.

limit of $2t$ or 0.80 eV as the size of the system increases. We can easily see that for more than about 20 electron sites, the average kinetic energy of each electron starts to approach the infinite limit and we expect that the results obtained from our model should converge to the long protofilament limit in a similar manner. In particular, we are considering 28 electron sites in our MT model which span 3 protofilaments. While this is not the ideal situation, the boundary conditions are not expected to create huge effects in our results. We are also using open

boundary conditions as they minimize the boundary effects when compared with a variety of periodic boundary conditions.

6.4.2 Triangular MT Lattice

Now, as we come to consider the entire MT lattice rather than single protofilaments, the immediate problem is the size of the system. This problem that was mentioned earlier on in the thesis within the context of ferroelectric configurations, rears its head again. The solution to the problem has been to consider a much smaller unit cell but also to incorporate boundary conditions which are consistent with the larger system which we are not able to study exactly. Consequently, the unit cells depicted in Figure 6.14 are the basis for the calculations. In the A lattice used for the calculations, the α -dimers connect to β -dimers along the $\bar{3}$ -start helix both within the lattice and at the seam when the MT is wrapped up. In the B lattice, the connections are α - α or β - β along the $\bar{3}$ -start helix and never α - β . For comparison, calculations have also been carried out with a flat tubulin sheet, specifically an A lattice MT lacking periodic boundary conditions in the lateral direction. This simulates the MT when it has unwrapped. The main thing to recall is that the MT lattice is triangular and has three distinct hopping directions. As well, since protofilaments are strongly bound together along their length but relatively weakly bound to other protofilaments, one expects the hopping parameter to be much smaller when an electron moves between protofilaments.

The calculations have been carried out with the same parameters as in the one-dimensional case, $U = 2.00$ eV, $t = 0.40$ eV along the protofilaments and the site energies have been set equal to zero for all sites. The value of the hopping parameter along the $\bar{3}$ -start helix is called t_l (left) and that along the 8-start helix that connects diagonally from a monomer in a direction up and to the right

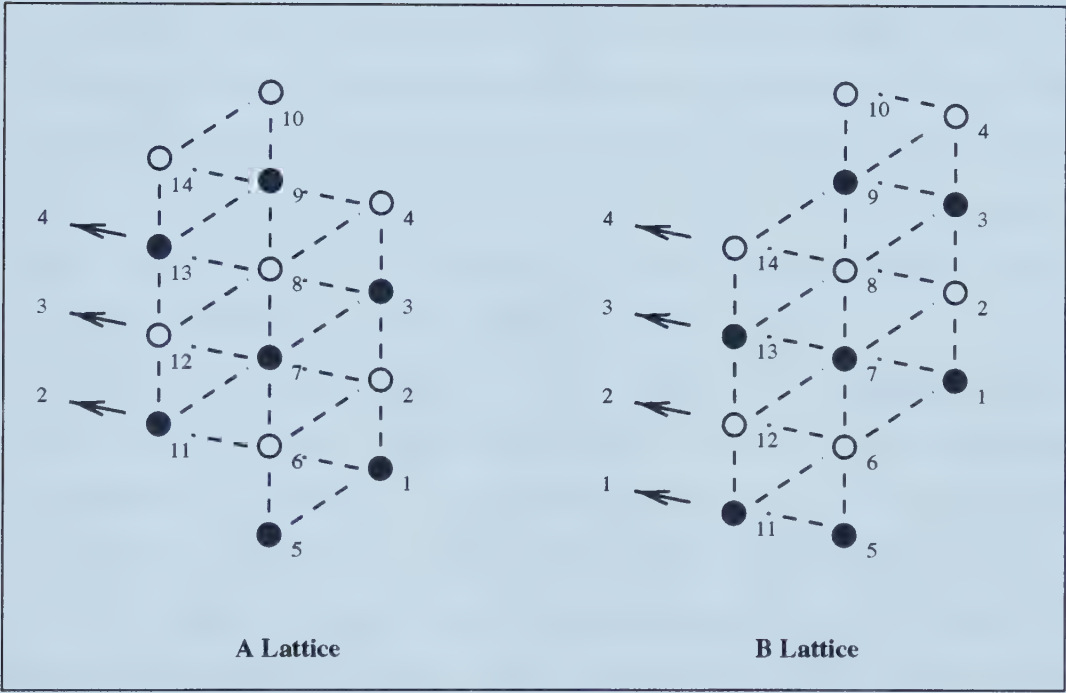


Figure 6.14: Lattice unit cells for conductivity calculations. The unit cell on the left corresponds to the MT A lattice while that on the right corresponds to the MT B lattice.

is called t_r (right).

We consider first the results of the MT lattice which has not rolled up to form a tube. Furthermore, the first case considered is that of a tubulin sheet where $t_r = 0$ and only the value of t_l is varied. The results are shown in Figures 6.15 and 6.16. Since $t_r = 0$, the nature of the lattice remains rectangular to this point. The optical conductivity spectrum is once again presented along with its integral, normalized by the expectation value of the system's kinetic energy. When $t_l = 0$, this particular system is equivalent to individual protofilaments. The two peaks in the optical spectrum arise from the fact that the protofilaments have different lengths. The absorption peaks of 0.22 eV and 0.40 eV correspond roughly to those of the two-dimer and three-dimer two electron cases discussed earlier in the chapter. The difference here is that the two electrons are spread over three protofilaments and consequently the effect of the electron repulsion is reduced. However, as t_l is increased from zero, the entire lattice becomes accessible and the protofilament character of the optical spectrum is lost. The two peaks of the t_l spectrum coalesce into a single peak with a larger activation energy. A second but smaller absorption peak forms just above 0.50 eV. In the plot of the integrated conductivity, we can see that there is also a smaller peak at 0.16 eV when $t_l = 0.10$ eV. The source of this peak is an absorption for conduction along the direction of t_l . When t_l is increased to 0.40 eV, this peak occurs at 0.61 eV. Thus this peak seems to occur at roughly $1.5t_l$. The activation energy for conduction along the protofilament axis also increases but is not as sensitive to t_l . Finally, examination of the integrated conductivity demonstrates that the total absorption combines such that the Drude weight remains zero.

Next, consider the analysis of Figures 6.17 and 6.18 where t_l is fixed at 0.4 eV and t_r is allowed to vary. Thus, the triangular nature of the system is captured in this model. The results immediately show a difference from the cases of an

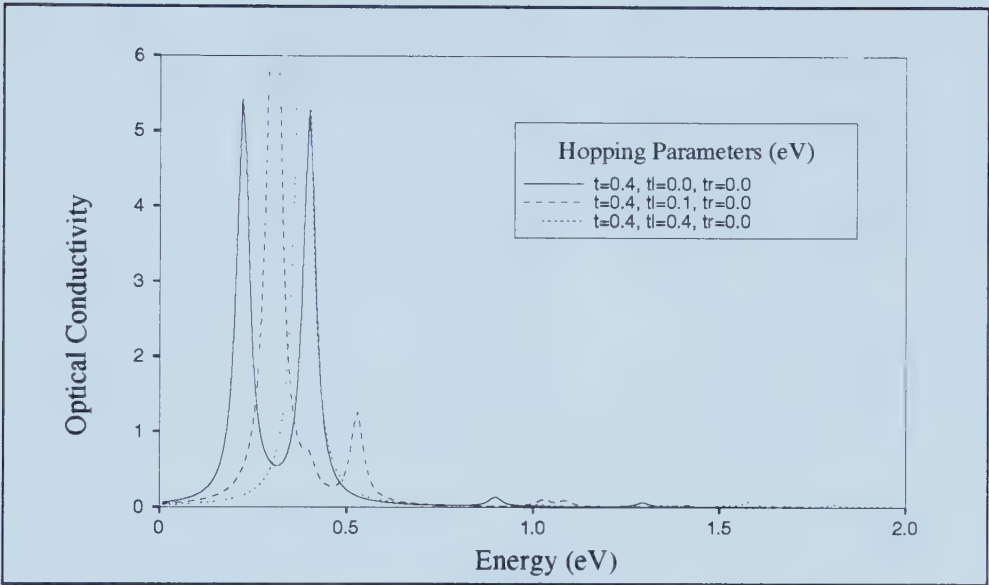


Figure 6.15: Optical conductivity along the protofilament axis of the tubulin sheet consisting of a 14-site lattice with two electrons while $t_r = 0$ and t_l is varied.

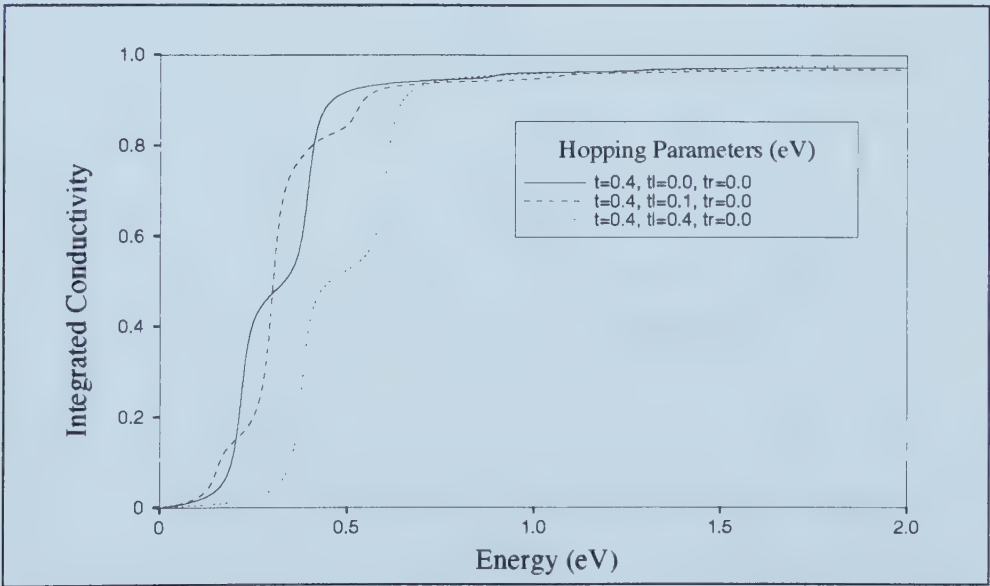


Figure 6.16: Integrated conductivity of the tubulin sheet with two electrons while $t_r = 0$ and t_l is varied.

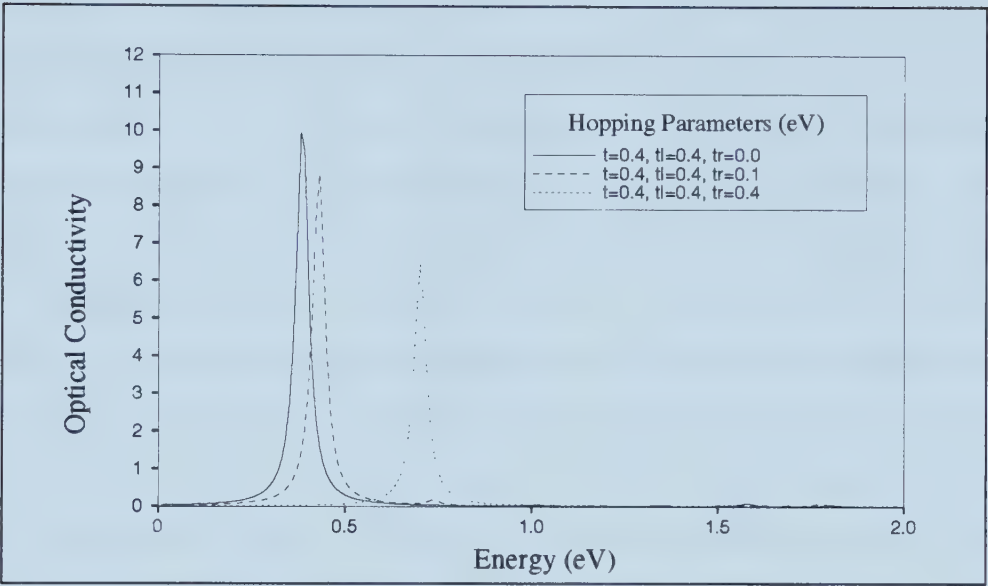


Figure 6.17: Optical conductivity along the protofilament axis of the unwrapped 14-site lattice with two electrons while $t_l = 0.4$ and t_r is varied.

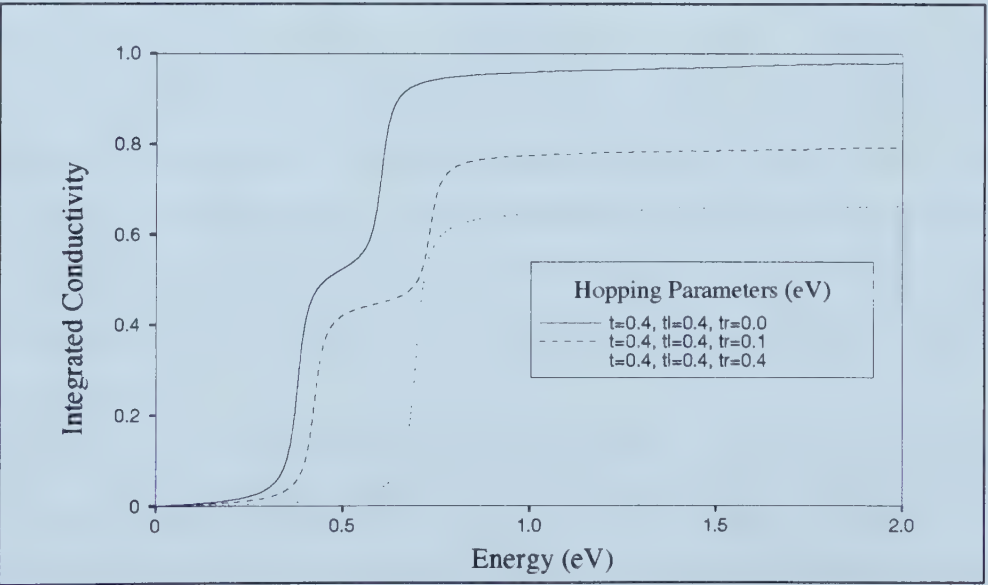


Figure 6.18: Integrated conductivity of the unwrapped 14-site lattice with two electrons while $t_l = 0.4$ and t_r is varied.

individual protofilament and of a tubulin sheet. One notes that the behaviour is inconsistent with that of an insulator, that is, the Drude weight is non-zero. Again, this can be read immediately by noting that the integrated conductivity does not approach unity as the energy is increased in Figure 6.18. If the optical conductivity is analyzed for all three directions, we find that the largest peak or peaks occur for at the same location for all directions but with different weightings. The first line traces the results for $t_r = 0.00$ eV and has peaks at 0.38 eV and 0.61 eV. Once the third hopping direction is allowed, the peak absorption is raised slightly to 0.43 eV for $t_r = 0.10$ eV and a smaller peak forms at 0.74 eV. The lower peak consists mainly of hopping along the protofilament while the second peak consists largely of hopping along the t_l direction, which also corresponds to a large hopping parameter. Once t_r is raised to 0.40 eV so that it has the same magnitude as the other hopping parameters, there is only a single peak at 0.70 eV. While it corresponds mainly to hopping along the protofilament, the difference between the directions is simply that the number of lines of lattice points in each direction varies as does the number of lattice points that each line contains. Since the direction along the protofilament corresponds to the largest number of lines, the conduction is largest in that direction. Given the results we have calculated so far, we have seen that all parameters t , t_l and t_r being non-zero leads to there being a non-zero Drude weight in the unrolled MT lattice or tubulin sheet.

We consider now the effect of applying the MT A lattice boundary conditions to our system. In Figures 6.19 and 6.20, we see that in comparison with the $t_l = t_r = 0$ case, changing only t_l to a finite quantity while still maintaining t_r as zero is sufficient to result in a non-zero Drude weight. Thus the periodic boundary conditions in the lateral direction seem to act in a manner similar to the additional hopping directions of the unwrapped lattice. When the kinetic

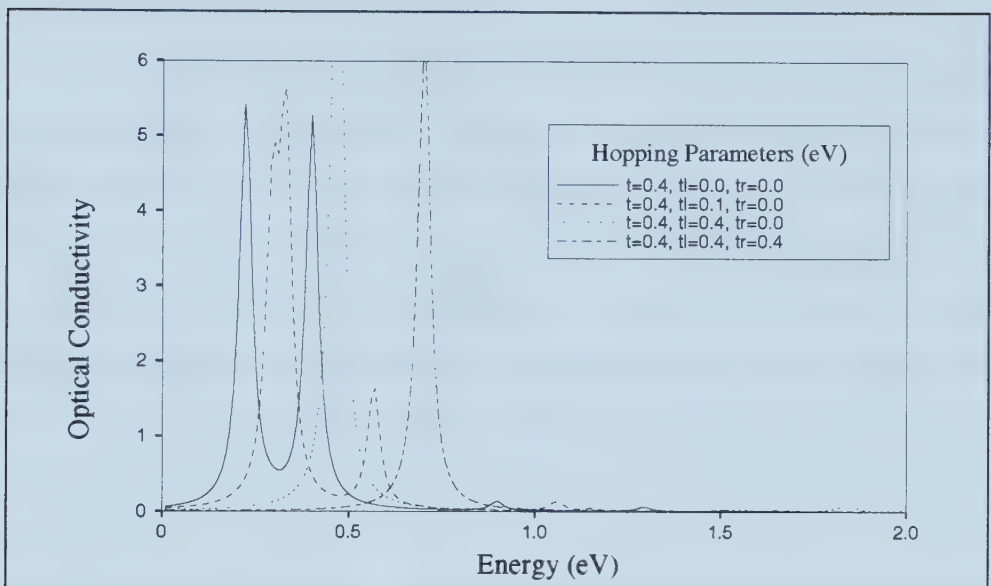


Figure 6.19: Optical conductivity along the protofilament direction of the 14-site MT A lattice with two electrons.

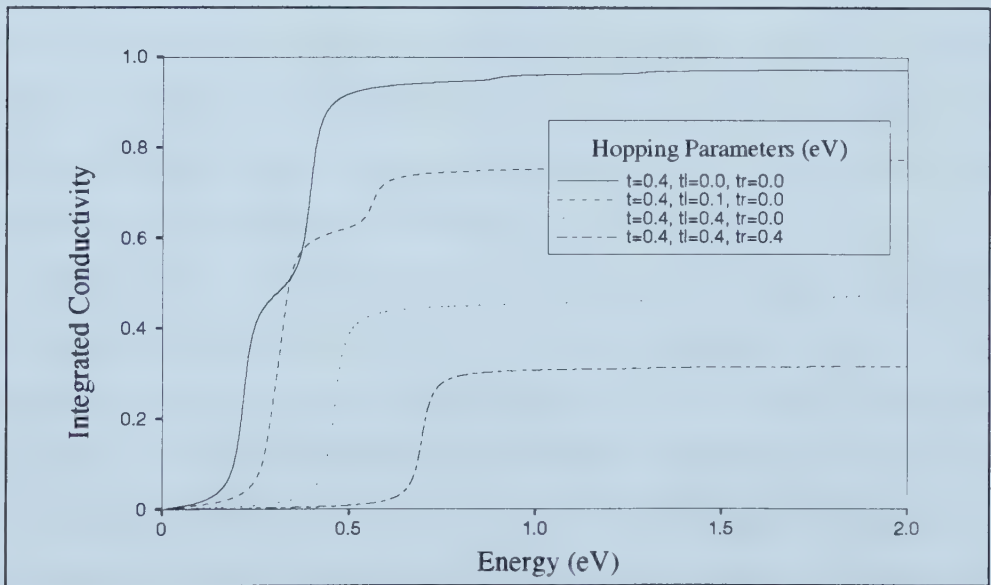


Figure 6.20: Integrated conductivity of the 14-site MT A lattice with two electrons shows a non-zero Drude weight for finite t_l .

parameters between protofilaments are set to zero, the optical conductivity spectrum shows that there are two large absorption peaks at about 0.23 eV and 0.40 eV. As t_l is increased, these peaks move higher in energy and the second peak becomes smaller in integrated weight. Eventually, once $t_l = t$, there is a single large peak near 0.47 eV. Introduction of the third hopping direction serves only to raise further the absorption peak, up to 0.70 eV in the case where the hopping parameter is 0.40 eV in all directions. However, raising the value of the lateral hopping parameters does increase the Drude weight as normalized by the expectation value of the kinetic energy. At this point, it should be mentioned that similar behaviour results when t_l is kept as zero and t_r made finite for the A lattice.

When the MT B lattice boundary conditions are applied for comparison with the MT A lattice, results are very similar qualitatively though specific spectral differences remain. From Figures 6.21 and 6.22, one can see that more conduction results in the B lattice for a small t_l , such as 0.1 eV, than in the MT A lattice by comparing with Figure 6.20. However, even the positioning of absorption peaks is similar in the two lattices. Again, it is sufficient for only one of t_l or t_r to be non-zero for the Drude weight to be finite.

Finally, we come to comparing the MT A and B lattices with the unwrapped tubulin sheet and in addition with individual protofilaments of tubulin dimers. There is an interesting geometrical interpretation to the results. Results show that the MT A and MT B lattices have identical conduction properties when $t_l = t_r$. This results because our calculations have considered all monomers to have the same site energy rather than alternating the site energy. Consequently, the B lattice can be viewed as an A lattice with the opposite helicity but the same structure. The sign of the system's helicity does not affect the conduction properties along the major axis. The unwrapped MT lattice is not as good a

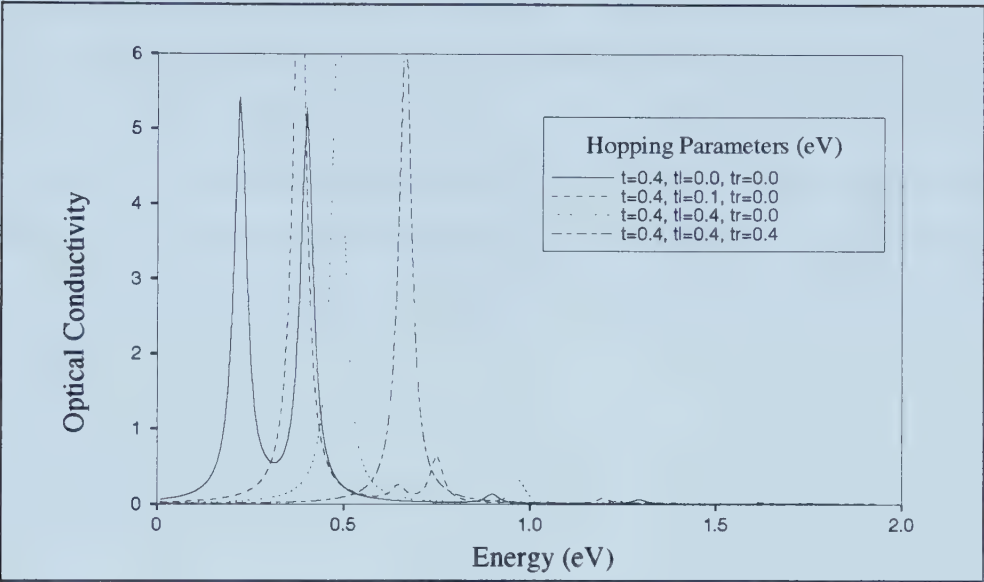


Figure 6.21: Optical conductivity along the protofilament direction of the 14-site MT B lattice with two electrons.

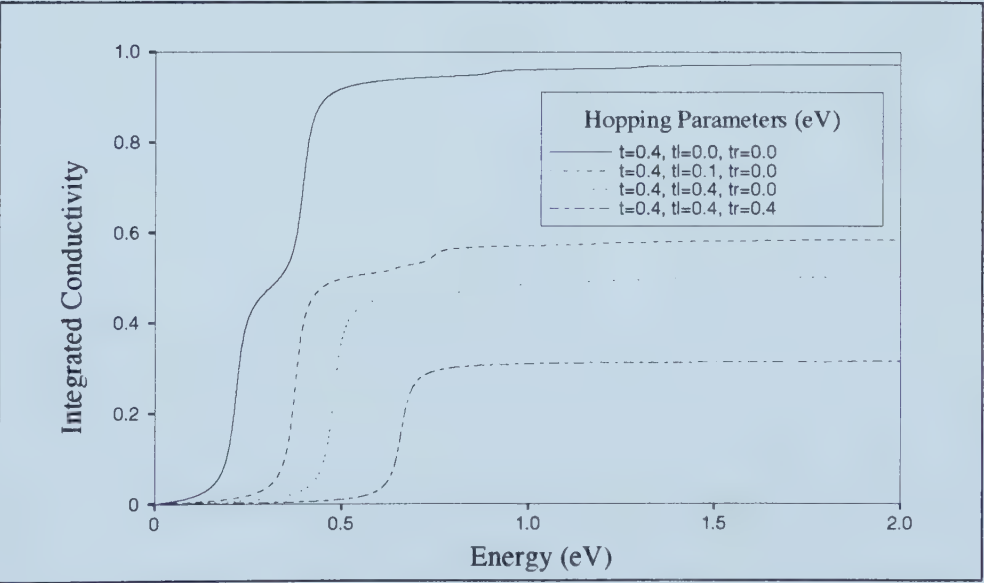


Figure 6.22: Integrated conductivity of the 14-site MT B with two electrons shows a non-zero weight for finite t_l .

conductor as some of the hopping freedom has been removed from the lattice but does remain conducting provided that both t_l and t_r are non-zero.

If we consider the case where one of t_l or t_r is quite small, however the wrapping of the lattice is much more important. As discussed earlier, the unwrapped tubulin sheet is an insulator while the MT A and B lattices may carry electrons. This observation is especially interesting given that MTs have been observed to zip up and essentially change their structure from that of a tube to that of a sheet *in vivo*.

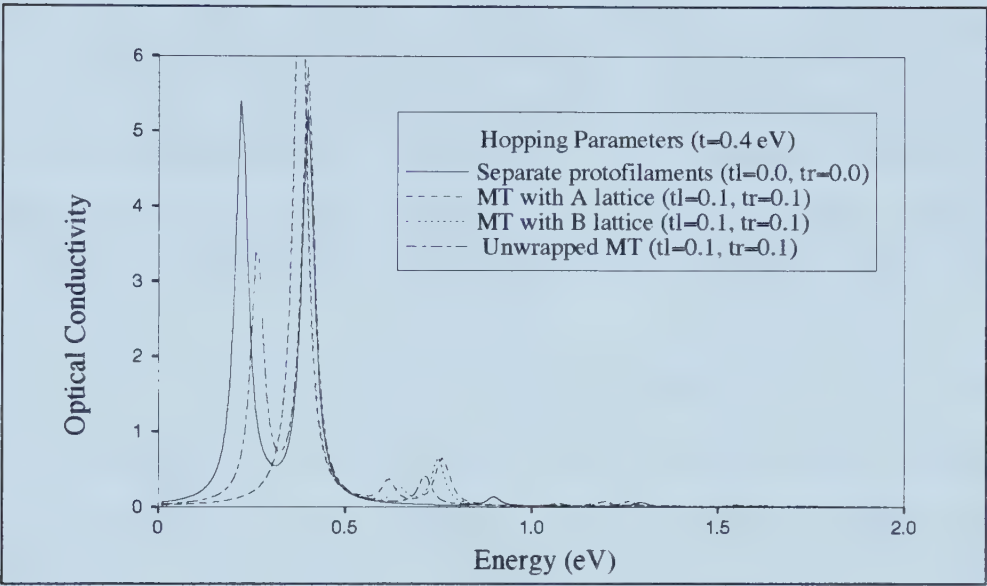


Figure 6.23: Comparison of the optical conductivity of the tubulin sheet with the MT A lattice and MT B lattice.

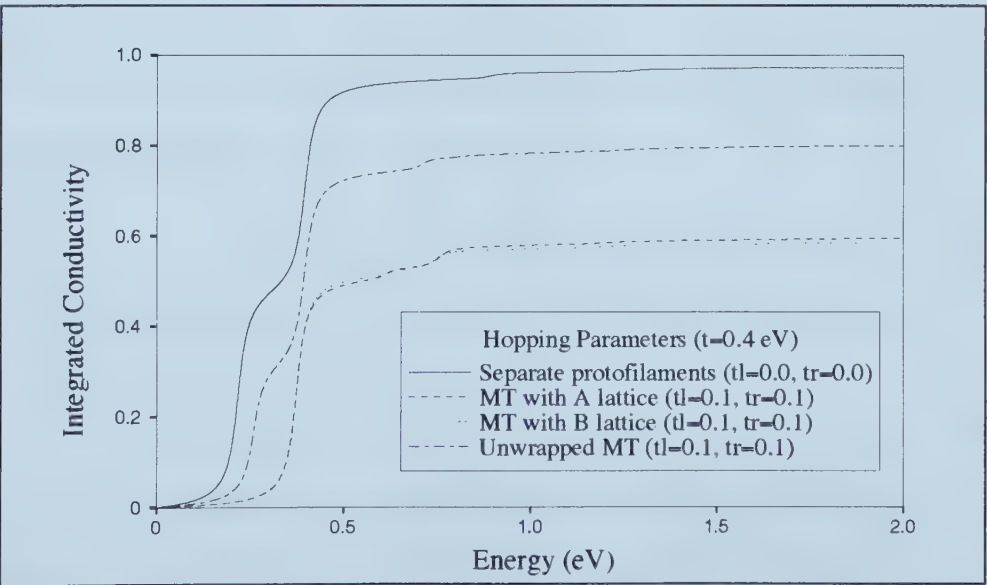


Figure 6.24: Comparison of the integrated conductivity of the unwrapped MT lattice with the MT A lattice and MT B lattice.

6.5 Summary

The calculations based on the Hubbard model of electron hopping show that the MT is not an insulator but that its conductivity depends on the lattice geometry and whether the MT is wrapped up or not. How well or poorly does one expect the MT to conduct relative to known semi-conductors? Referring back to equations (6.47) and (6.48), the Drude peak of the MT is simply given by D as

$$\frac{D}{2} = -\frac{\pi e^2}{2} a^2 \langle K \rangle - \int_0^\infty \sigma_{\text{kubo}}(\omega) d\omega. \quad (6.56)$$

Since this corresponds to a delta function in the absorption spectrum centered at $\omega = 0$, it indicates a perfect conductor and D represents the weight of this delta function. In order to determine the conductivity, the relaxation processes of the polymer must be elucidated. However, we shall compare the Drude weight between the various lattices as a measure of their conductivity. In this equation, the constants can be factored and what remains is the fraction that can be read from the graphs presented earlier. The Kubo fraction (KF) is the limit of the integral as the frequency tends to infinity.

$$\frac{D}{2} = -\frac{\pi e^2}{2} a^2 \langle K \rangle (1 - \text{KF}), \quad (6.57)$$

and by returning constants of the system so that the dimensionality of D is correct,

$$D = -\frac{\pi n e^2 a^2}{\hbar} \frac{\langle K \rangle}{t} (1 - \text{KF}). \quad (6.58)$$

Finally, we are in a position to predict the conductivity of individual MTs of varying lattice types. For the following calculations, the electron density has been taken to be of two electrons within the lattice of 14 dimers and corresponds to a density of $1.8 \times 10^{18}/\text{cm}^3$. Thus the results must assume that the conductivity remains constant as the length of the polymer is extended, provided the degree of filling remains the same.

Table 6.1: Calculated conductivity derived from the Drude weight for tubulin polymers of varied structure.

Tubulin Structure	Hopping parameters (eV)	Conductivity ($\times 10^4 \Omega^{-1} \text{ m}^{-1}$)
Individual protofilament	$t_l = t_r = 0.0$	non-conducting
Tubulin sheet	$t_l = t_r = 0.04$	0.94
	$t_l = t_r = 0.10$	2.0
	$t_l = t_r = 0.40$	6.3
MT A lattice	$t_l = t_r = 0.04$	1.8
	$t_l = t_r = 0.10$	4.5
	$t_l = t_r = 0.40$	16.0
MT B lattice	$t_l = t_r = 0.04$	1.9
	$t_l = t_r = 0.10$	4.7
	$t_l = t_r = 0.40$	16.0

The values in Table 6.5 should be compared with the conductivity of metals, such as copper ($6 \times 10^7 \Omega \text{ m}^{-1}$) and iron ($1 \times 10^7 \Omega \text{ m}^{-1}$). Indeed the values can also be compared to the intrinsic semiconductors germanium ($2.5 \Omega \text{ m}^{-1}$) and silicon ($4 \times 10^{-4} \Omega \text{ m}^{-1}$). Given these comparisons, the MT may indeed be quite a good semi-conductor given our assumptions. What is particularly interesting is the way that the conduction properties depend on the lattice and the particular boundary conditions. The situation can be compared to carbon nanotubes which have a similar size and structure to MTs. In addition, theoretical consideration of nanotube structure predicts that the conduction properties depend on the boundary conditions. In the case of nanotubes, this means the way in which the graphene sheet is wrapped up to form the nanotube. It is quite interesting that particular sets of boundary conditions produce a semi-conducting nanotube while the appropriate choice of wrapping the nanotube gives rise to metallic conduction [13].

One possible cellular use for a conducting MT would be a signalling mech-

anism that would explain the synchronized segregation of chromosomes. When MTs pull chromosomes to opposite ends of a dividing cell, the moment of separation is highly co-ordinated. One mechanism to explain the simultaneity of chromosome division is to consider a signal emanating from the centrosomes. In this scenario, electrons would be transported along the MTs, and then accumulate at the kinetochores that connect the MTs to the chromosomes. Coulombic repulsion would then cause the chromosomes to separate or at least activate the enzyme that binds each pair of chromosomes together. Thus the synchrony of separation may be explained.

The ability to change from an insulator to a conductor by a simple geometrical change could be biologically relevant even without observing a single electron to be conducted along the MT since it is the conductivity property that affects the way the cell views and responds to external electromagnetic fields. Specifically, the reflectivity of MTs to electromagnetic fields is high when they are conducting and consequently, they could act to direct infrared signals to the interior of the centrosome. Since the centrioles are maintained at right angles to each other, the cell would be able to determine the location in latitude and longitude of a light source if the MTs are conducting. Peaks in the AC conductivity are all at energies significantly above the thermal activation threshold so no conductivity is expected along a darkened MT, but photoconduction in the infrared-visible range is possible. Therefore it is possible that this photo-activated conduction has functional repercussions.

Bibliography

- [1] D. Baeriswyl, *The role of electron-electron interactions in conducting polymers*, Synthetic Metals **57**, 4213–4224 (1993).
- [2] J. Hubbard, *Electron correlations in narrow energy bands*, Proc. Roy. Soc. **A276**, 238–257 (1963).
- [3] Elliott H. Lieb, *The Hubbard Model*, chapter The Hubbard Model: some rigorous results and open problems, Plenum Press, New York, 1995.
- [4] R. Kubo, *Statistical-Mechanical theory of irreversible processes I. General theory and simple applications to magnetic and conduction problems*, J. Phys. Soc. Japan **12**, 570–586 (1957).
- [5] P. F. Maldague, *Optical spectrum of a Hubbard chain*, Phys. Rev. B **16**, 2437–2446 (1977).
- [6] S. Doniach and E.H. Sondheimer, *Green's Functions for Solid State Physicists*, W.A. Benjamin Inc., Don Mills, 1974.
- [7] Gerald D. Mahan, *Many-Particle Physics*, Plenum Press, New York, 1981.
- [8] F. Marsiglio, *Evaluation of the BCS approximation for the attractive Hubbard model in one dimension*, Phys. Rev. B **55**, 575–581 (1997).

- [9] R.M. Fye, M.J. Martins, D.J. Scalapino, J. Wagner, and W. Hanke, *Optical-conductivity properties of one-dimensional Hubbard rings: Repulsive- U and attractive- U cases*, Phys. Rev. B **45**, 7311–7314 (1992).
- [10] G. Albrecht-Buehler, *Changes of cell behavior by near-infrared signals.*, Cell Motil. Cytoskel. **32**, 299–304 (1995).
- [11] G. Albrecht-Buehler, *Altered drug resistance of microtubules in cells exposed to infrared light pulses: Are Microtubules the “Nerves” of Cells?*, Cell Motil. Cytoskel. **40**, 183–192 (1998).
- [12] W. Stephan and P. Horsch, *Optical properties of one- and two-dimensional Hubbard and t - J models*, Phys. Rev. B **42**, 8736–8739 (1990).
- [13] M.S. Dresselhaus, G. Dresselhaus, and P.C. Eklund, *Science of fullerenes and carbon nanotubes*, San Diego : Academic Press, 1996.

Chapter 7

Unifying Concepts

The challenge is to link concepts of MT structural dynamics and function which are macroscopic properties, with the microscopic properties of tubulin's structure, its electrostatic properties, individual MT dynamics, flexural rigidity, post-translational modifications and so forth. The picture which emerges is one in which the MT is perhaps the most multi-functional cellular component.

In particular, the functioning of neuronal MTs is a subject that this thesis attempts to demystify. The central nervous system is responsible for brain function and muscle signalling to produce movement through muscle contraction. It is composed of millions of neurons, the longest of which may span about 1 m in humans. Signalling in neurons is a largely digital process. That is to say that the action potential is an all or nothing phenomenon that proceeds without attenuation along the neural membrane. However, there is evidence that a type of analog processing is responsible for determining the resting state of a neural membrane [1]. It is also analog signalling which occurs at synapses between neurons and at the neuromuscular junction. The analog 'signalling' is more correctly termed a biasing as it changes the likelihood of the phase transition which occurs when the membrane is depolarized. This is precisely how mood-altering drugs function by changing the background such that action potential propagation is either highly favoured or suppressed.

The lossless propagation of the action potential is essential to trigger release of neurotransmitter at the synapse. However, there is strong evidence that calcium ion is also required within the neuron to allow the signal to be transmitted. Since the neuron is a structure rather densely packed by MTs, the key question facing a biophysicist studying MTs is, “Are the MTs required for neurotransmitter release?” It seems that MTs indeed play a role in membrane excitability [2]. Studies have shown that colchicine, a drug that induces MT depolymerization, effectively reduces a neuron’s capacity to signal other nerve cells. The drug ultimately stops the activity of some potassium, calcium and sodium channels but the mechanism that underlies how the MT coordinates ion channel function is not understood. Colchicine may even be applied to the exterior of the cell and have an effect which supports the idea that the MTs extend into the cell membrane. Therefore MTs would seem to play a supporting role in the transmission of nerve impulses across the synapse. In this light, we have studied these polymers in an effort to understand the physical mechanisms that underlie this function.

7.1 Electrostatics

The electromagnetic properties of any structure can in principle be calculated if the structure is known with atomic detail. Strictly speaking, this is a quantum mechanical problem because the bonding between atoms must be described so that the electron distribution is best characterized. A classical view is adopted to render computation possible. This electrostatic limit is generally applicable as long as we do not consider bonding between the test charge and the molecule, specifically the protein, under consideration. In practice, the process of describing electric fields about molecules is one of assigning partial charges to atomic positions based on the electronegativity of the atoms. It also involves the association of dipoles to molecular bonds. The resultant fields are then compared to

empirical measurements. After years of theoretical and experimental work, this practice has been refined and parameters adjusted to best reflect reality. This has meant the inclusion of effects due to atoms which are separated by more than a single bond and ultimately to functional groups such as entire amino-acid groups when molecules such as proteins are studied. Simply placing a partial charge on each atomic site does not describe the electromagnetic field well compared to *ab initio* calculations on small molecular systems with up to perhaps 100 electrons. One may instead attempt to represent the electrostatic potential and field of a molecule by placing a sequence of multipoles at its center of mass. However, the use of distributed multipole analysis (DMA) provides a much more accurate representation of the electrostatic field about a molecule. Due to the size of small groups, diatomics, triatomics and tetraatomics may each be described to high precision using only monopoles, dipoles and quadrupoles. Indeed even for large systems, the DMA does a reasonable job of representating the electrostatic potential. This is a result of the fact that dipoles and quadrupoles are the most important terms for description of molecular bonding.

Consider two polar molecules such as water and ammonia. Placing these two molecules in proximity to each other results in the water molecule feeling the electric field of the ammonia molecule and vice-versa (Figure 7.1). Beyond simply producing a torque on the water molecule, the electric field of the ammonia molecule may induce a change in the dipole of water by causing a change in the equilibrium configuration of the water molecule. Such a change is known as polarization and in calculating the molecular field about a collection of atoms, electronegativities, multipole polarizabilities and hyperpolarizabilities must all be known due to the mutual polarization between polar species.

In addition, one must be careful when the geometry of the protein is not in its equilibrium configuration since equilibrium electrostatic parameters may

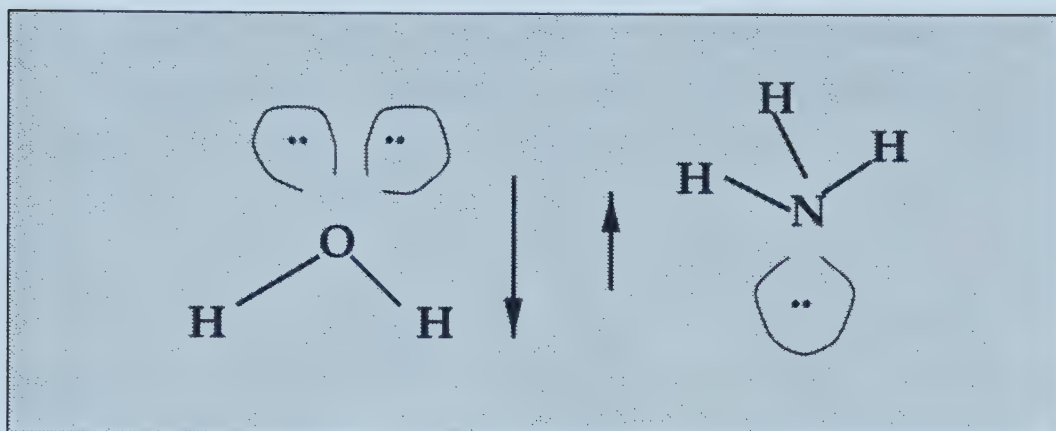


Figure 7.1: A water molecule is depicted on the left and a molecule of ammonia on the right. Their native dipoles are illustrated beside each molecule. However, their polarizabilities will determine to what extent the magnitudes will change in the presence of the other molecule.

not strictly be applicable. Dykstra has estimated that bond lengths should be between 0.9 and 2.0 times their equilibrium separation to remain within the range of applicability [3]. This shall not be a concern for the modelling of the local electric field about tubulin since we shall consider only the equilibrium configuration. In the case of the MT, its subunits α - and β -tubulin must be studied. Each monomer is comprised of approximately 450 amino acids and in the neighbourhood of 7000 atoms. The good news from the point of view of modelling the electrostatic field about the protein is that beyond a certain distance, the so-called Debye length, we can ignore electrostatic effects due to screening. This is the important length scale as the Bjerrum length that compares electrostatic effects with thermal effects is larger. In our case, we shall say that beyond 2.0 nm, interactions will be neglected; be they of charge-charge, charge-dipole or van der Waals nature. The potential is gradually switched off in the calculation so there are no discontinuities in the electrostatic potential, ϕ . This is in fact close to the true situation since ions in the surrounding solution will screen any surface charges. The results presented for the electrostatic potential in this chapter rep-

resent ‘vacuum’ results given that the solvent is not explicitly taken into account. If the surrounding mixture of ions is considered, then the potential due to a point charge does not fall off simply as $1/r$, but instead as

$$\phi \propto \frac{1}{r} e^{-Kr} \quad (7.1)$$

where K^{-1} is the Debye length, typically 0.6 nm under physiological conditions. Since we consider locations within 1.0 nm of the MT surface, they are not screened by the ions of the solution as there is not sufficient room for even water to be located in the intervening space.

Tubulin has only been imaged to atomic resolution within the last two years following 20 years of difficult work with this protein. Nogales et al. published the structure of α - and β -tubulin which were co-crystallized in the heterodimeric form [4]. Imaging was completed in the form of so-called zinc sheets. The presence of zinc(II) ion, causes the tubulin heterodimers to form anti-parallel protofilaments. These sheets do not curl up to form the familiar MT but rather remain flat and are therefore suitable for electron crystallography. The work establishes that the structures of α - and β -tubulin are nearly identical and confirms the consensus speculation. A detailed examination shows that each monomer is formed by a core of two β -sheets that are surrounded by α -helices. The monomer structure is very compact, but can be divided into three functional domains: the amino-terminal domain containing the nucleotide-binding region, an intermediate domain containing the taxol-binding site, and the carboxy-terminal domain, which probably constitutes the binding surface for motor proteins [4]. However, studies of motor protein motion along MTs with the carboxy-terminus clipped and our own theoretical model of motor protein movement suggest that motor protein interaction is important with the outer MT surface but not specifically the carboxy-tail.

Calculations of the potential energy were calculated with the aid of molecular

dynamics package known as TINKER [5]. This computer program serves as a platform for molecular dynamics simulations and includes a facility to use protein specific force-fields. The most common of these parameter sets for proteins are AMBER and CHARMM with an additional TINKER parameter set that remains under development. Since the dipole moment was the most important value that we wanted to calculate, these various parameter sets were compared for a few proteins¹.

Table 7.1: Comparison of the AMBER, CHARMM and TINKER parameter sets

Protein Code	Calculated Dipole (Debye)			Barlow & Thornton (Debye)
	AMBER	CHARMM	TINKER	
1fdx	234.7	234.3	210.4	238
1fd1	550.4	556.2	597.3	535
5fd1	290.1	293.5	343.0	
7rsa	420.2	423.3	427.4	481
7tln	568.8	578.7	703.3	711

Table 7.1 compares the results of the AMBER [6], CHARMM [7], and TINKER [5] parameter sets with the calculated dipole moment of Barlow and Thornton [8] derived from experimental measurements of the dielectric increment of the protein in solution. Comparison of each of the molecular parameter sets with the experimentally derived value shows that they each have the good predictive features. The variation arises due to the fact that these parameter sets have been optimized on specific sets of proteins. Since the AMBER and CHARMM data sets are more established, each gave similar results for the test proteins and were

¹The PDB (protein database) code consists of a number and three other characters. The leading number indicates whether the atomic data for the protein has been superceded by new data, in that 2tub would be the name of tubulin's updated PDB file and would replace 1tub. The full names of the four proteins listed are respectively *peptococcus aerogenes* ferredoxin (fdx), *azotobacter vinelandii* ferredoxin (fd1), ribonuclease A (rsa) and phage T4 lysozyme (lzm).

reasonably close to the result derived from experiment, they were selected as the molecular parameter sets of choice. AMBER was selected over CHARMM on the basis of that it is a more up to date parameter set. The overall performance of the program gave us confidence that the results it provided for tubulin were meaningful.

The first thing studied using TINKER was the overall charge, and dipole on the tubulin molecule. It turns out that tubulin is quite highly negatively charged at physiological pH but that much of the charge is concentrated on the C-terminus. This is the one portion of the tubulin dimer which was not imaged due to its freedom to move following formation of the tubulin sheet. This tail of the molecule extends outward away from the MT and into the cytoplasm and has been described by Sackett [9]. At neutral pH, the negative charge on the

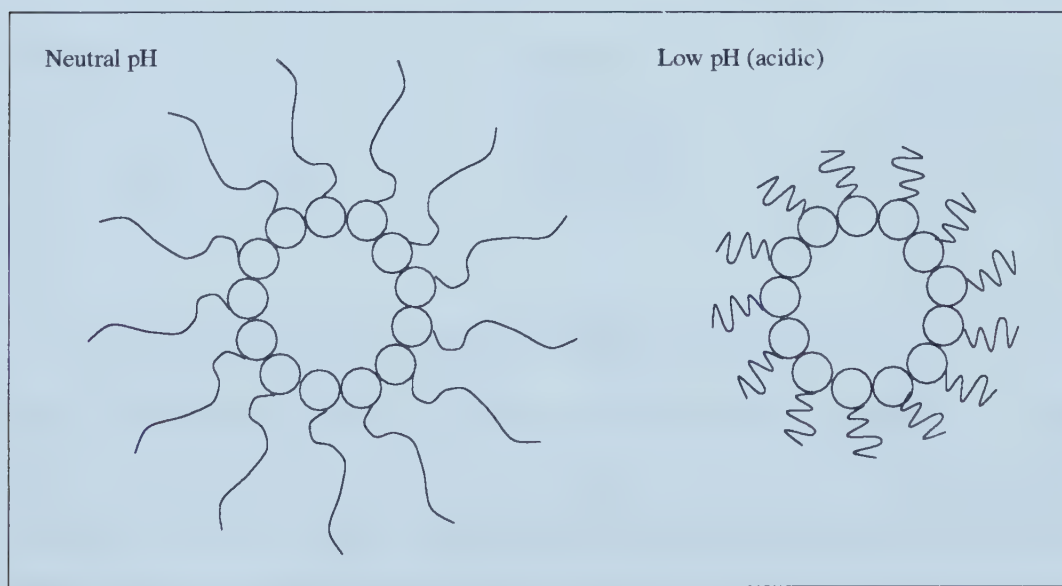


Figure 7.2: Cross-section of a MT including the carboxy-terminus of the tubulin subunits. Folding of the carboxy-terminus of the tubulin dimer demonstrates the change in the geometry of the molecule with pH. Neutral pH is shown on the left, the tail folds at lower pH as the negative charges are screened.

carboxy-terminus causes it to remain extended due to the electrostatic repul-

sion within the tail. Under more acidic conditions, the negative charge of the carboxy-terminal region is reduced by associated hydrogen ions. The effect is to allow the tail to acquire a more compact form by folding. Although, this is probably the largest structural change which occurs due to changes in the cell's pH, we shall see that other structural changes, the result of post-translational modification, can similarly affect the electrostatics of the tubulin dimer.

Table 7.2: Tubulin's Electrostatic Properties (tail region excluded)

Tubulin Properties	Calculated Value
charge (electronic charges)	-10
dipole (Debye)	1714
components: $\begin{Bmatrix} p_x \\ p_y \\ p_z \end{Bmatrix}$	$\begin{Bmatrix} 337 \\ -1669 \\ 198 \end{Bmatrix}$

The x -direction coincides with the protofilament axis. The α monomer is in the direction of increasing x values relative to the β monomer. This is opposite to the usual identification of the β monomer as the 'plus' end of the MT, but all this identifies is whether the MT is pointed towards or away from the cell body.

7.1.1 Electrostatic Potential around Tubulin

The electrostatic potential along the protofilament first sparked our interest. The profile of the electrostatic potential provides several very interesting results. These can be traced to an examination of the electrostatic potential on the inside of the MT, on its external surface and at the protofilament-protofilament interface. Studying the electrostatics within the MT cylinder in concert with molecular dynamics simulations should provide a wealth of information on the bound water problem. However, we have confined our examination largely to the surfaces of tubulin that form the exterior surface and the protofilament-protofilament contacts when assembled into a MT. The first result that may

be derived from the electrostatic potential are those regions of the MT's outer surface that are negatively charged and which may attract hydrogen ions. If electronic conduction occurs by proton ferrying as discussed in Chapter 3, then the locations where protons would bind are clarified. Finally, it also identifies locations on the MT where motor proteins may bind as in the case of at least one motor protein, kinesin, its attachment has been shown to be primarily electrostatic [10]. In calculating the electrostatic potential, 2.0 nm was selected as the

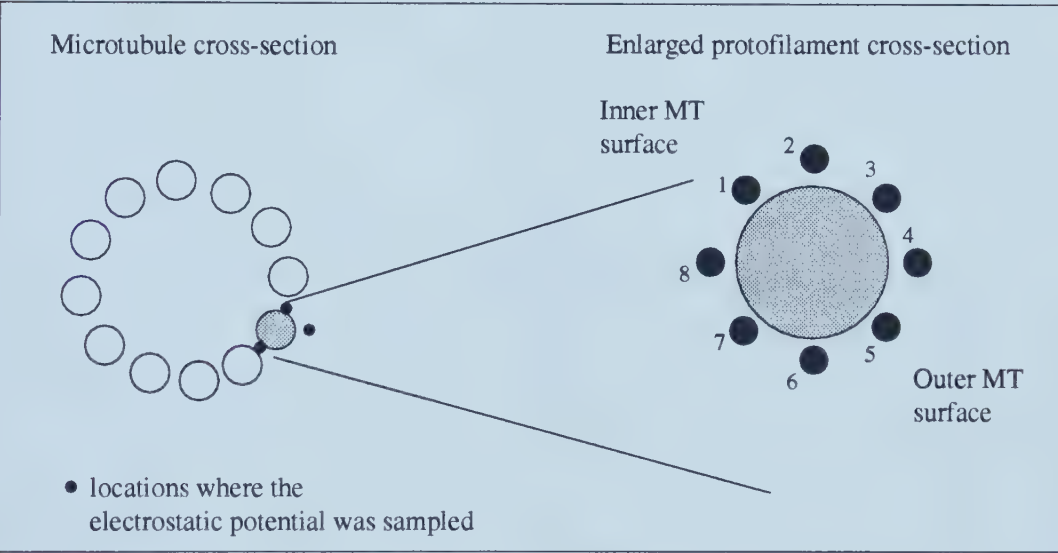


Figure 7.3: A MT cross-section illustrates where the electrostatic potential was examined along lines parallel to the protofilament axis (a line perpendicular to the plane of the page).

cutoff distance for charge, dipole and van der Waal interactions. The electrostatic potential was calculated for a 12.0 nm segment of the line, thereby including an additional 2.0 nm above and below each tubulin molecule. Periodic boundary conditions were then applied in the direction of the protofilament because this is the configuration of the tubulin dimers within a MT. The resulting profiles of the electrostatic potential are shown in Figures 7.4 through 7.11 and are located about the tubulin dimer as shown in Figure 7.3. The lateral boundary conditions were not considered in the calculation of the potential. The interactions

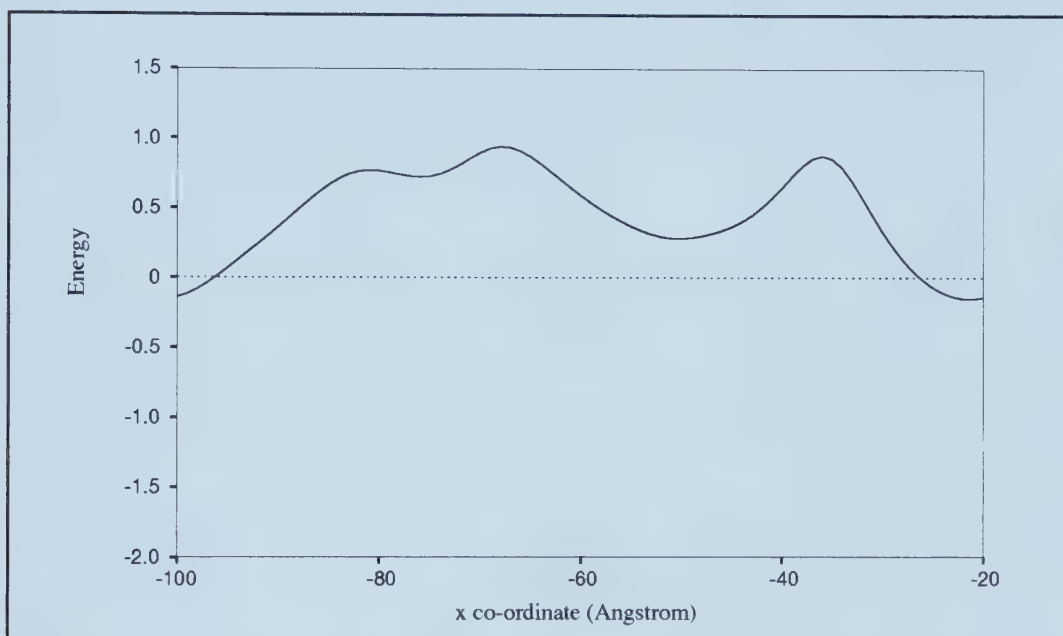


Figure 7.4: Electrostatic profile along line 1 of tubulin's exterior that is on the inside of the MT.

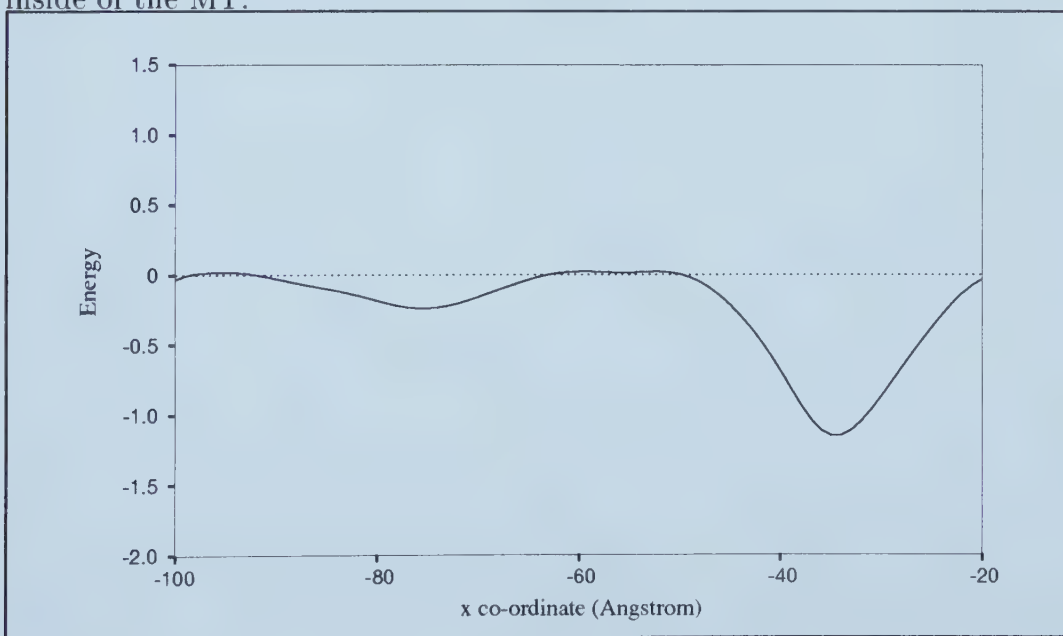


Figure 7.5: Electrostatic profile along line 2 of tubulin's exterior that is on the inside of the MT.

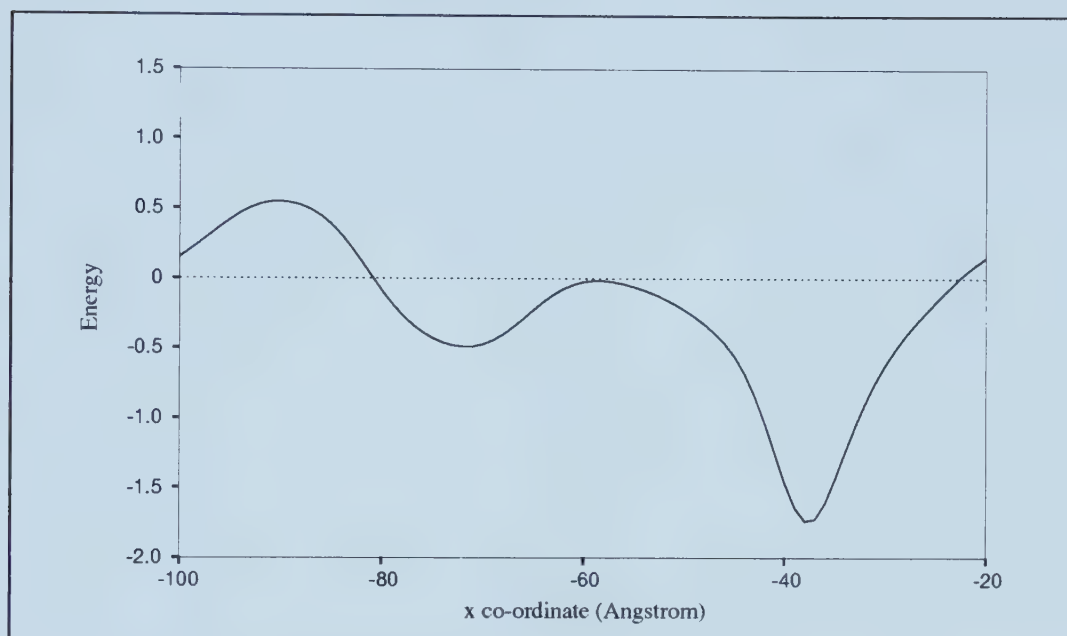


Figure 7.6: Electrostatic profile along line 3 of tubulin's exterior that is on the A side of the protofilament-protofilament interface.

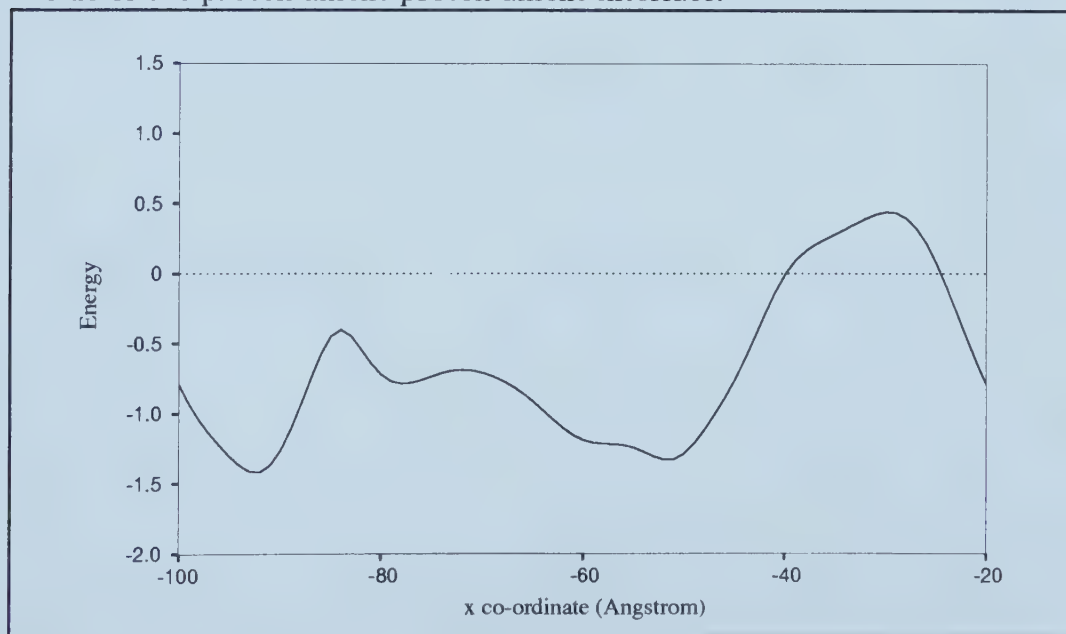


Figure 7.7: Electrostatic profile along line 4 of tubulin's exterior that is on the A side of the protofilament-protofilament interface. The profile is largely negative indicating that the surface is negatively charged.

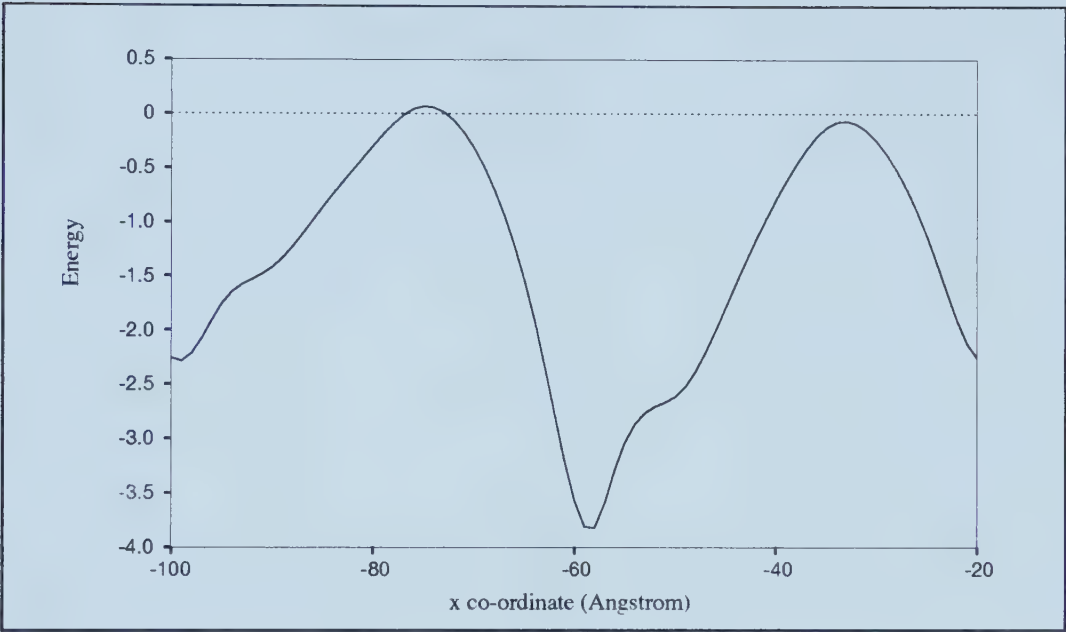


Figure 7.8: Electrostatic profile along line 5 of tubulin's exterior that is on the outside of the MT.

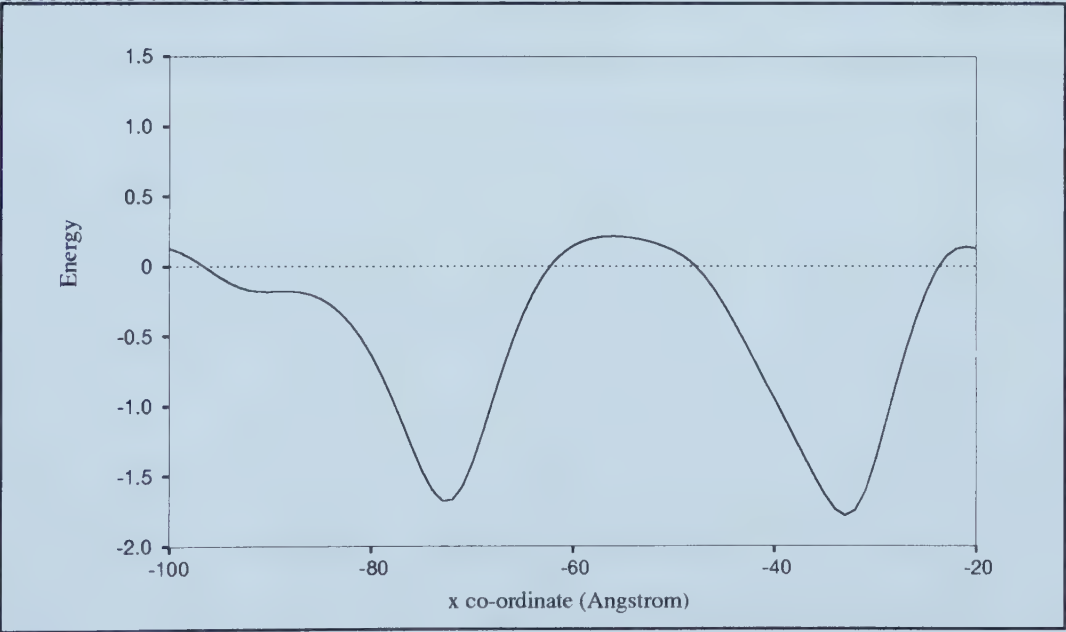


Figure 7.9: Electrostatic profile along line 6 of tubulin's exterior that is on the outside of the MT. The large negative surface charges help to keep the carboxy-tail away from the MT surface.

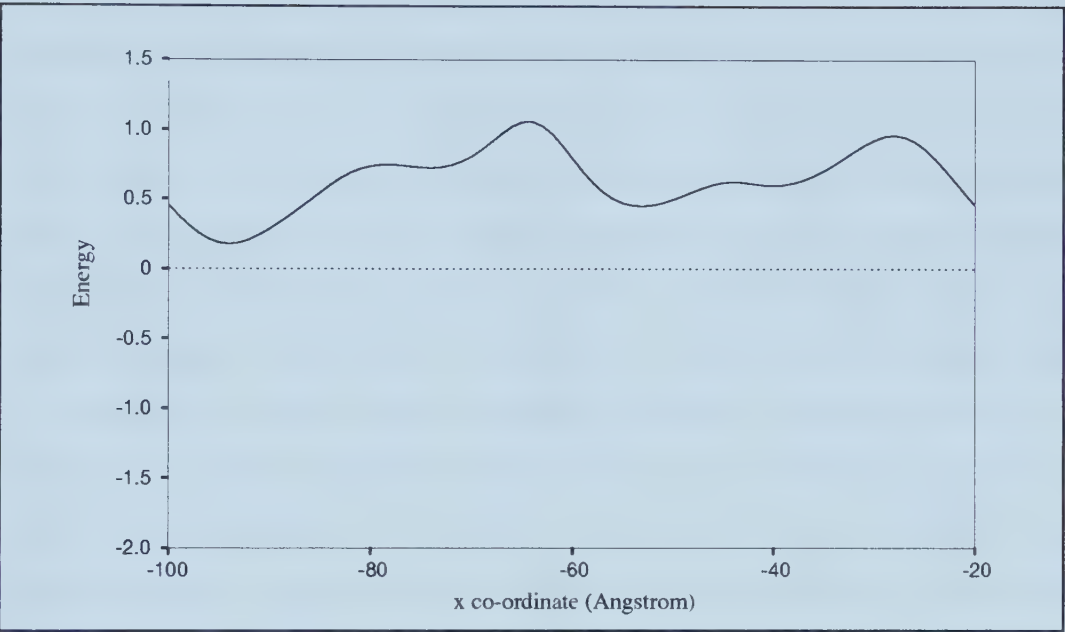


Figure 7.10: Electrostatic profile along line 7 of tubulin's exterior that is on the B side of the protofilament-protofilament interface. The largely positive surface charge is complementary to the opposite side of the dimer and contributes to protofilament-protofilament binding.

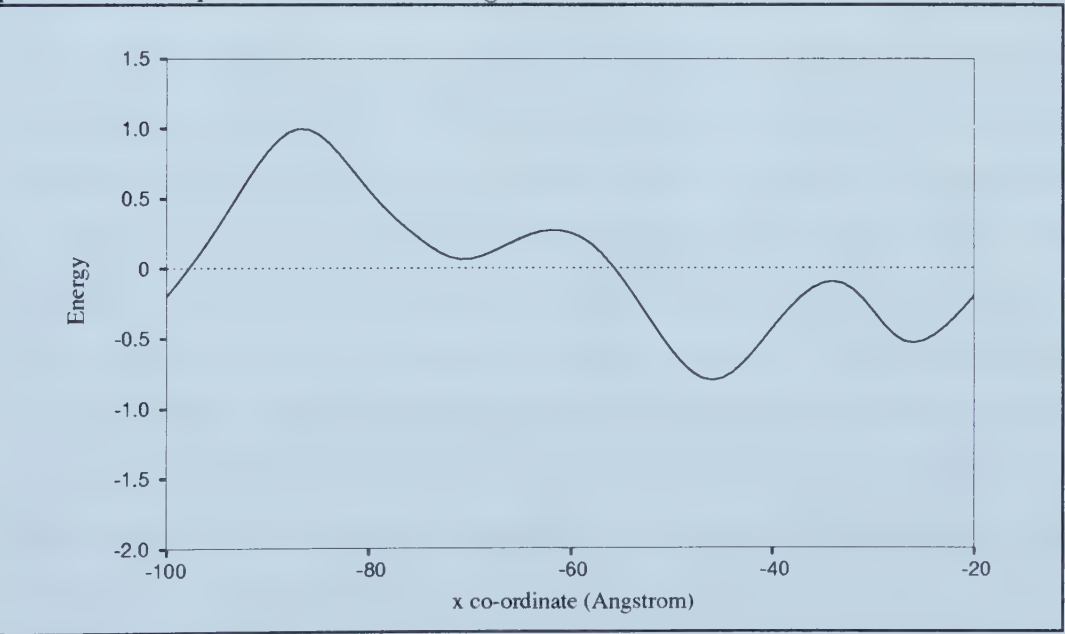


Figure 7.11: Electrostatic profile along line 8 of tubulin's exterior that is on the B side of the protofilament-protofilament interface.

at the protofilament-protofilament interface will be discussed momentarily by considering the potential as one approaches from either side of the interface and due to the 2.0 nm cut-off length, the electrostatic profiles along the inner and outer surfaces of the tubulin dimer shall not be greatly affected. Along the 'sides' of the tubulin dimer where the surface is effectively buried through binding to neighbouring protofilaments, there are certain features of these bound regions that are suggestive of how the MT subunits interact to form the tubulin sheet.

Consider the profile of the electrostatic potential in Figures 7.6 and 7.7 and compare them with the profiles in Figures 7.10 and 7.11. These are the left and right sides respectively, of the tubulin molecule, which interact laterally to hold one protofilament together with neighbouring protofilaments. In these figures, each unit of energy represents 14.4 kcal/mol or 0.62 eV. This is roughly the energy available from the hydrolysis of two to three molecules of GTP or just a little more than the hydrolysis of one molecule of ATP. What is interesting is that the electrostatic potential is largely negative on the left side and positive on the right side. Thus there is a net electrostatic attraction between tubulin dimers with parallel alignment when their opposite sides face each other. In fact if the minima in the left side's profile are aligned with the maxima in the electrostatic potential of the right side, we find that the neighbouring tubulin dimer will be shifted by 1.4 nm or 5.4 nm which compares reasonably well to the observed 0.9 nm or 4.9 nm offsets that depend on the lattice type. The simple change of a residue on the surface offers the possibility of specifying one shift and locking the resulting MT into either the A or B type lattice. Hence post-translational modification or more likely the expression of a particular isotype over another could select a specific lattice.

In the event that we wish to consider tubulin aggregations such as the zinc(II) ion-induced sheets that were prepared in the tubulin structure determination ex-

periments, there is a difficulty that the protofilaments have an anti-parallel configuration. As a result, proceeding on the premise that electrostatic interactions

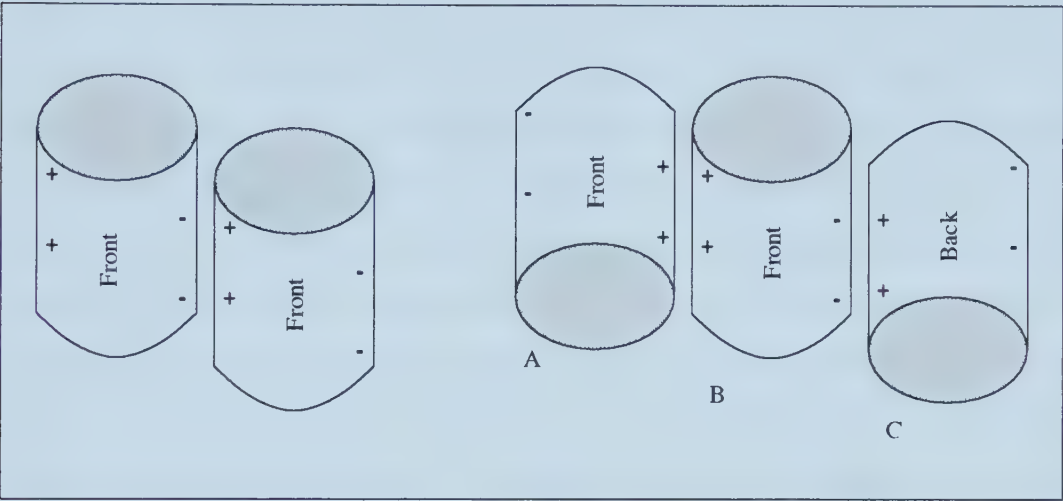


Figure 7.12: Protofilament-protofilament interaction. At left, tubulin dimers associate such that there is a vertical offset between protofilaments. At right, when the dimer's up-down orientation is reversed, it must also be rotated from front to back since the interaction between A and B is destabilizing but the interaction between B and C is stabilizing.

determine the protofilament-protofilament binding, the zinc(II) ion must work to alter this interaction. Since the pattern of the electric potential consisting of two electrostatic wells on one side and two electrostatic peaks on the opposite side must be maintained, to explain the efficient binding of the dimers into the lattice of the tubulin sheet or MT, the potential is presumably not tremendously distorted. Since each tubulin dimer will be affected in the same manner, forming anti-parallel protofilaments does require that either the energy profile changes such that each side has a well and a peak in the potential or conversely that there is a small change in the potential which now favours binding where the 'front' of the tubulin dimer is presented to an observer along protofilaments with the first orientation while the 'back' of the tubulin dimer faces the observer for the

protofilaments with the opposite orientation.²

Along the outer surface of the MT, the profiles in Figures 7.8 and 7.9 of the electrostatic potential must be considered. Overall, the surface is either neutral or negatively charged. It is particularly interesting that here again, there are two deep wells which are locations favourable for positively charged protein surfaces such as the head domain of motor proteins. In fact, these wells with a depth of 10–20 kcal/mol and a width of about 1 nm represent a localized electric field of between 10^4 and 10^5 V/m which is not uncommon on atomic scales. In fact, it is this knowledge of the structure of the electrostatic potential that is the basis for an improved model of motor protein motion along MT surfaces but which goes beyond the scope of this thesis. The important features are simply its periodicity in that the α -monomer looks very similar to the β -monomer electrostatically and the presence of binding regions for positively charged substrates.

7.2 Variations by Tubulin Isotype

An interesting avenue of study which has also become possible involves the comparison of the various tubulin isotypes by considering their electrostatic properties. Since the tubulin structure is now available, it is possible to consider making changes to the structure on a computer and then to calculate the resulting changes in the electrostatic potential surrounding the tubulin dimer. As discussed in the cell biology chapter, substitution of one amino-acid for another may be conservative or non-conservative. The former occurs when the substituted amino-acid has similar charge and steric characteristics. However, the interesting changes are those which are non-conservative. It is in this light that I have examined three different substitutions to the β_1 -tubulin structure. In one case, I have simply exchanged one known tubulin isotype for another, and sec-

²This prediction was recently confirmed in conversation with Ken Downing who was part of the group that solved the tubulin structure.

ondly I have made two targeted substitutions based on the discussion of Burns and Surridge [11] who explain that the methylation of α -Lys394 prevents MT assembly and that the substitution of alanine for β -Pro287 specifies 13 protofilaments.

I have used the tubulin structure from the β_2 isotype and made the appropriate substitutions to arrive at the β_1 isotype. I have then looked in the regions where structural differences exist and examined the changes in the electrostatic potential. The changes which are examined here concern the region of β -tubulin from residues 231–235. This region was selected because in a sequence of five amino acid residues, three of them change. The location of these residues is near the inner surface of the MT. The residues **ATMSG** of the Nogales data are changed for **GTMEC** from β_2 to β_1 tubulin. The change at position 234 is particularly significant because the serine residue, **S**, is exchanged for glutamic acid, **E**, which carries a negative charge. One therefore expects some region to become attractive to protons. In order to interpret the following set of figures, all distances are quoted in Angstroms and energies in kcal/mol. The more darkly coloured regions represent locations where the potential is negative and that attract protons or positively charged molecules. The lightly coloured regions are those regions which exclude protons. Figure 7.13 depicts a contour plot of the electrostatic potential in this region and what is interesting in this case is the channel in the lower lefthand corner of each picture. In the upper figure that represents the β_2 -tubulin isotype, a channel appears to exist that is open for proton movement, while in the lower figure which represents the β_1 -tubulin isotype, a barrier seems to prevent proton movement through this part of the protein. Upon closer inspection, we see how the glutamic acid has reduced the potential barrier of the region. In fact, a local minimum exists at the mouth of this channel that will facilitate proton movement through the narrow channel since it may be able to

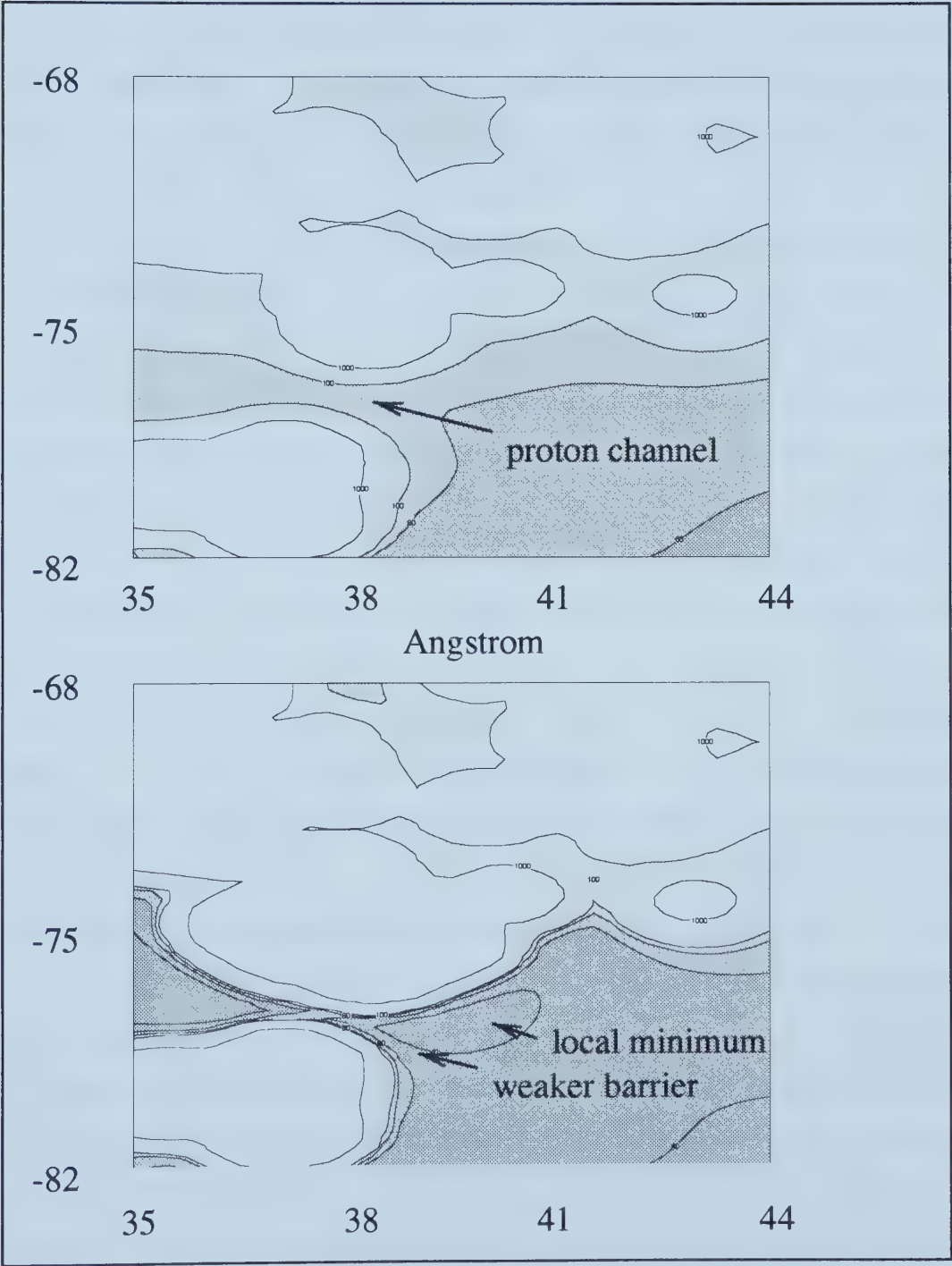


Figure 7.13: The energy landscape of β_2 -tubulin (above) is compared with that of β_1 -tubulin (below) in the neighbourhood of residues 231–235.

trap them briefly. Thus this one example shows how the nervous system's β_2 -tubulin isotype may trap protons that are to be used to ferry electrons about. The β_1 -tubulin would be more likely to allow the proton to escape. Should a proton become associated with an electron, the narrowness of the channel in the case of β_2 -tubulin would also aid in trapping the proton.

The methylation of α -Lys394 involves the addition of a methyl group to the existing amino group at the end of the lysine residue. The location of the α -Lys394 is on the surface of the α -monomer but facing the MT exterior. This change serves to screen this charge from the surroundings since the methyl group has somewhat more bulk than a single hydrogen atom. Consequently, the local electrostatic properties are changed. In each of the figures, it is clear that locally the electrostatic potential is such that protons feel a slight repulsion from the MT surface which agrees with the charge on the lysine residue. However, once the residue has been methylated, a well for positively charged objects develops further up along the MT's outer surface. Given the location of this change which is a long way from the dimer-dimer interaction site which is responsible for the polymerization of protofilaments and also the fact that this is not near the protofilament-protofilament interface, it is difficult to understand how this prevents MT polymerization. The solution to this problem must be by one of two mechanisms. The first would hypothesize the interaction of the tail with this negatively charged region of the MT surface and that this interaction impairs MT assembly. Since the tail is negatively charged itself, it would be driven to extend into the cytoplasm away from the MT surface and seems unlikely to interfere with MT polymerization. Consequently, the more likely mechanism in my view is that the tubulin adopts a different configuration that is not conducive to polymerization. In particular, this lysine residue is in the region of the GTP binding region of the α -tubulin monomer. While this molecule of GTP is not

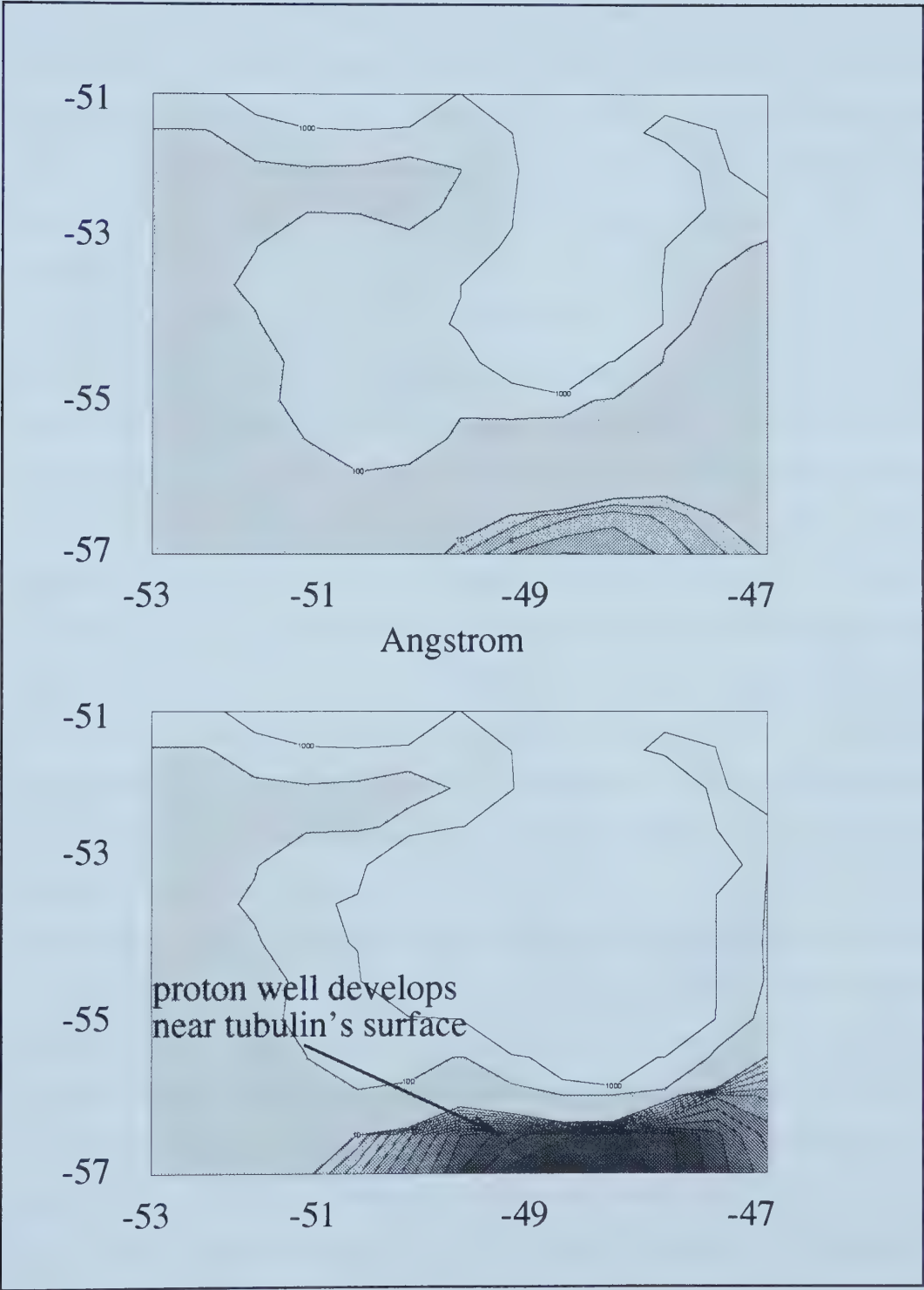
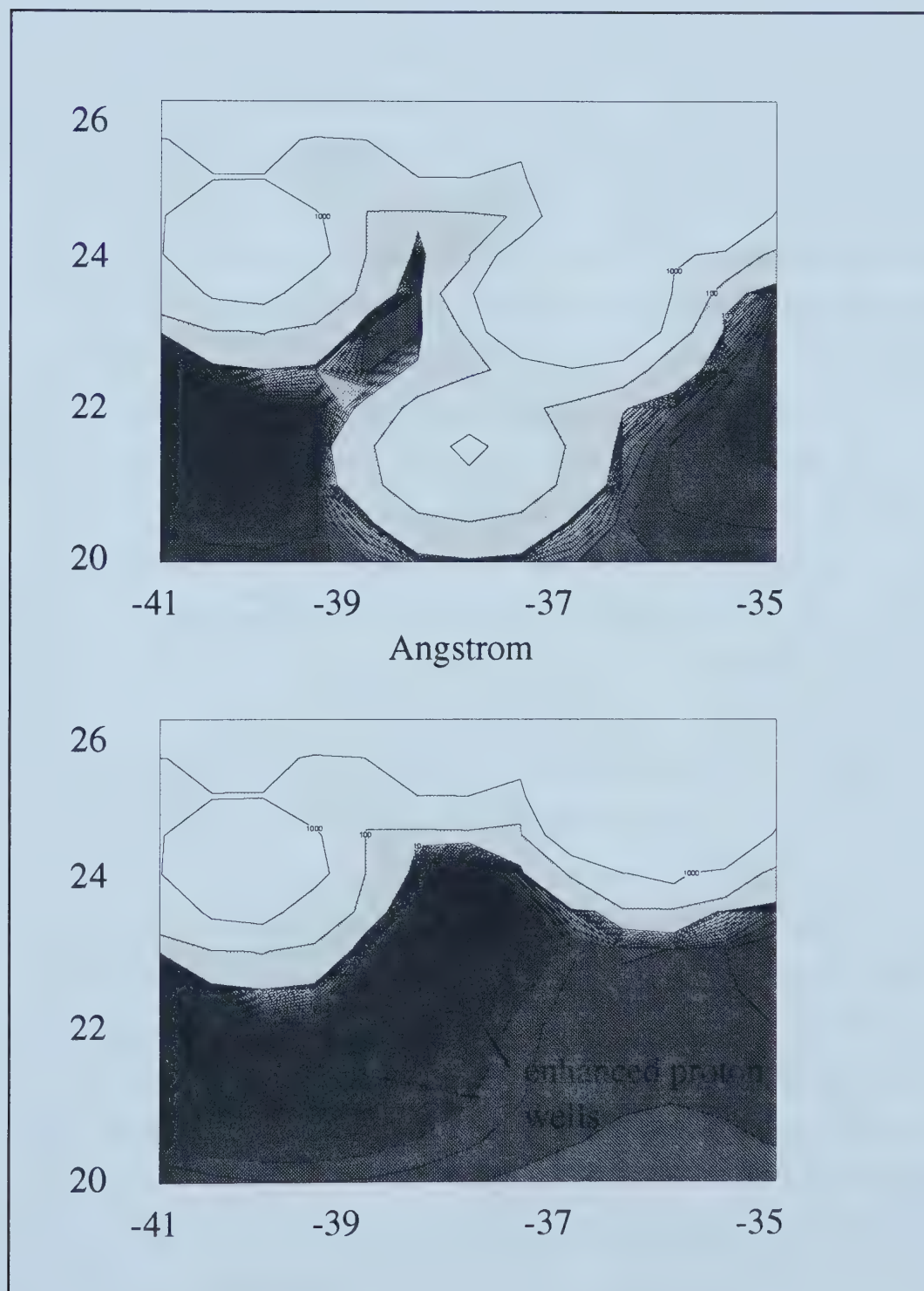


Figure 7.14: Methylation of α -Lys394 demonstrates the large proton well that develops once the lysine residue is shielded.

hydrolyzed upon MT polymerization, it remains essential for this process. Thus it seems likely that this change prevents GTP association with the α -monomer of the tubulin dimer and thereby prevents MT assembly. This can be rationalized when one considers that the phosphate group carries a negative charge and that consequently, it will be repelled as the GTP molecule attempts to bind the α -monomer.

The substitution of alanine for β -Pro287 was a simple change to make as the β and δ carbon atoms are exchanged for hydrogen atoms and the γ carbon atom deleted. The β -Pro287 residue is compact and its location is on the surface of the β -monomer. It is close to the α -monomer in the axial direction and at the protofilament-protofilament interface in the circumferential direction around the tubulin molecule. The result of the alanine for proline substitution is apparent in Figure 7.15. Not only does the smaller alanine residue allow protons to come closer to the surface of the tubulin molecule, but in fact, a large binding pocket for a positively charged molecule is developed near $(y, z) = (23.5, -38.5)$. Since this pocket becomes so much more prominent after the proline has been substituted by alanine, the binding to a neighbouring protofilament at this location becomes much stronger relative to the unsubstituted tubulin dimer. Provided this location has a corresponding surface with an angular position favouring 13 protofilaments, strengthening this contact will tend to fix the number of protofilaments. By controlling the location of corresponding contacts, the protofilament number could theoretically be adjusted to be most any number. The fact that the contact areas are almost exactly opposite each other on the tubulin dimer gives a MT flexibility to choose a protofilament number that is close to the ideal 13. If these regions are much closer, in angular terms, about the circumference of the tubulin dimer than a lower number of protofilaments would be expected.

Even this rather cursory look at the electrostatic potential about tubulin has

Figure 7.15: Substitution of alanine for β -Pro287.

revealed glimpses of some fundamental questions. A periodic potential with a depth comparable to the free energy of ATP hydrolysis has been observed on the outer surface of the MT. This seems to explain the tight binding of motor proteins to MTs and to explain the ATP activation of these molecules. We have also seen how changing between tubulin isotypes changes the electrostatic potential, in our specific case, to modulate proton mobility. Targeted substitution and post-translational modifications with known physical consequences demonstrate that indeed electrostatics govern tubulin's assembly properties. It is apparent how one side of a tubulin dimer attracts the opposite side of another dimer, how the vertical offset between protofilaments arises and even how the number of protofilaments is specified in the structure of tubulin. Beyond this, the gross structure of tubulin sheets was predicted and then verified. All that remains is to explain dimer-dimer interactions along the protofilament. This will likely have to wait until additional structural information is available on the α - and β -tubulin monomers, and on the free $\alpha\beta$ -dimer. This additional information is required to understand the dimerization process, that presumably includes the formation of a covalent bond, and to distinguish it from the dimer-dimer association which is much weaker. Since GTP is present near the interface for the formation of both of these bonds and the fact that GTP hydrolysis is concomitant with dimer-dimer association, an understanding of the interaction may be indeed gleaned from electrostatics but one must also consider the GTP molecule and associated water molecules. In the case where a covalent bond forms, the purely electrostatic picture may not be complete since a quantum mechanical interpretation is required. The conclusion is that the structure's polymerization characteristics will be better understood once the molecule is successfully imaged in additional conformations.

7.3 Proposed Investigations

There remain several questions to be answered in the study of MTs and their functions. Over the course of this research, I have devised several experiments, many of them simple, which should be carried out to either support or rule out the various uses for which MTs have been proposed. I have equally suggested theoretical avenues to explore.

Tubulin dimers should be polymerized from a specific α -tubulin isotype, say α_1 -tubulin and with two or more β -tubulin isotypes. The experiment would simply be to determine whether any of these mixtures could be separated by an electronic technique. Successful separation of the MTs by the application of an electric field would demonstrate the importance of the MT interaction with electric fields and the specialization of tubulin isotypes for this function. This has already been shown, but such a result would lend much weight to the idea that the tissue-specific expression of isotypes occurs to take advantage of the individual isotypes' electrical properties. An experiment with a similar feel would include the simple polymerization of MTs from tubulin under the conditions of a non-uniform electric field. In particular, concentric conductors would provide an interesting geometry as they would simulate the electric field that may surround the centrosome. While the MTs are expected to form such that they emanate radially from the center of such a construction, another interest would be to see how the MT responded to large electric fields. Such an experimental geometry naturally has the largest field closest to the central conductor. It would be possible to see whether sufficiently large electric fields applied in this manner could tear individual tubulin subunits away from a MT. This should be contrasted with a large uniform electric field that one expects to either reorient the MT or to translate the entire structure. If this tearing away of subunits were observed, it would be highly suggestive of the mechanism important to explain chromosome

segregation by MTs. Current suggestions seem inadequate to explain how the MTs efficiently disassemble as their ends approach the centrosome during mitosis. An electrostatic basis would justify early scientists who long ago were struck by the similarity in appearance between certain electromagnetic phenomena and biological processes.

Another experiment which could be carried out would simply be to measure the tryptophan fluorescence of MTs with GDP bound at the exchangeable site of β -tubulin as has been carried out and discussed by Sackett and Bhattacharyya [12]. In their experiments, the shift in tryptophan fluorescence demonstrated the conformation change of the tubulin as it was progressively denatured. This initial experiment should be followed by a measurement of the tryptophan fluorescence of MTs with GMPCPP bound at the exchangeable site. A shift would be indicative of a structural change accompanying the hydrolysis process as GDP-bound MTs have already undergone hydrolysis while the GMPCPP-bound MTs only experience slow hydrolysis. This would not be the first experiment to show that conformational change follows assembly into MTs, but would demonstrate a change in the emission characteristics of the molecule.

The lifetime of neural MTs should be measured in the presence and in the absence of action potentials. This would determine whether the passage of nerve impulses actually stabilizes the existing MTs and whether there exists a sort of biological 'use it or lose it' principle. In addition, this experiment would elucidate whether the increased stability of neural MTs is the result of a specific neuronal isotype (β_2 -tubulin), an artifact of post-translational modifications or else a sort of positive feedback mechanism mediated by the action potential. This line of investigation is of great interest for a disease such as Alzheimer's where neural MTs become disorganized. The answer would provide information on whether MT damage impairs nerve impulse propagation or if in fact the causality is

reversed.

The removal of the centrosome from a cell would provide another clue to the mystery of mitosis. While it is known that cell division does not begin until the centrosome has duplicated itself, it would be interesting to see how removal of the centrosome after duplication affects mitosis. The question here is two-fold since the centrosome may be required for either or both of the following needs of the cell. Firstly, MT spindles must be anchored in a central location and secondly, the spindles must be drawn together. Since the MTs forming the spindles do not seem to be in direct physical contact with the centrosome, we are interested in the hypothesized function of the centrosome that is to tear tubulin subunits off the end of the spindles.

7.4 Outstanding Issues

The alignment of MTs to magnetic fields has been observed but has not been explained by this thesis. Assuming the usual form for the interaction of an object's dipole with an external magnetic field,

$$U_B = -\mathbf{m} \cdot \mathbf{B}, \quad (7.2)$$

where \mathbf{m} is the magnetic dipole moment and \mathbf{B} is the magnetic field, the MT must have a permanent magnetic dipole or one must be induced by the application of the magnetic field. A permanent magnetic dipole seems an unreasonable hypothesis due to the absence of magnetic ions in tubulin since it would require a current to be flowing continually through the MT. In addition, since the alignment of the MTs is along the field lines, the magnetic dipole would be along the protofilament axis and hence the current generating this dipole moment would be the result of charge movement around the MT rather than along its length as discussed in the preceding chapter. While current movement around the MT is

possible, it is not the preferred direction of current flow in our model presented in the last chapter. In addition, a constant current flow would require some sort of biological superconductivity. Instead, let us simply assume that a magnetic field is able to induce a moment to which the field then couples. Since biology is abound with transient current flows such as the sodium and potassium currents of action potentials and the calcium currents that preceed neurotransmitter release, it is natural to assume that their associated magnetic fields are responsible for inducing charge movement within biological structures.

Another problem which we have not addressed in this thesis is a description of MAP and drug function. The collection of MAPs and drugs that interact with MTs is diverse. While the electrostatic picture of tubulin renders it possible to design new antigens that could bind the protein, exploring the specifics of MAP 2, MAP τ or taxol function requires structural data of tubulin in both the 'naked' and 'dressed' states where the reference is to whether or not tubulin is covered by the antigen. Normal MT function requires a balance in the assembly properties of tubulin. Disturbing this delicate balance with colchicine causes MTs to depolymerize as bonds become too weak; while disturbing it with taxol makes MTs too rigid and again unable to perform normal functions. Thus one is led to believe that the antigen function is to lock tubulin molecules into unusual conformations which have new bonding and hence elastic properties as a result of the change. The location of the antigen-tubulin binding will determine whether it affects assembly dynamics or other MT functions.

Finally, one puzzle that we have not directly addressed but which I comment on for the sake of completeness is the catastrophe event that may occur during assembly. Since it occurs in MTs that contain only GDP at their exchangeable nucleotide site, let us assume that the change is exothermic. Let us further assume that the event is purely stochastic and thus the collapse must be

thermally activated but with only a moderate barrier of a few kT . This approximation seems reasonable given that studies of catastrophe frequency variation with assembly conditions give mixed results [13, 14]. It is only neuronal MAPs which significantly reduce the catastrophe events. This leads to the following reaction scheme. We may view the entire polymer as unstable in that the con-

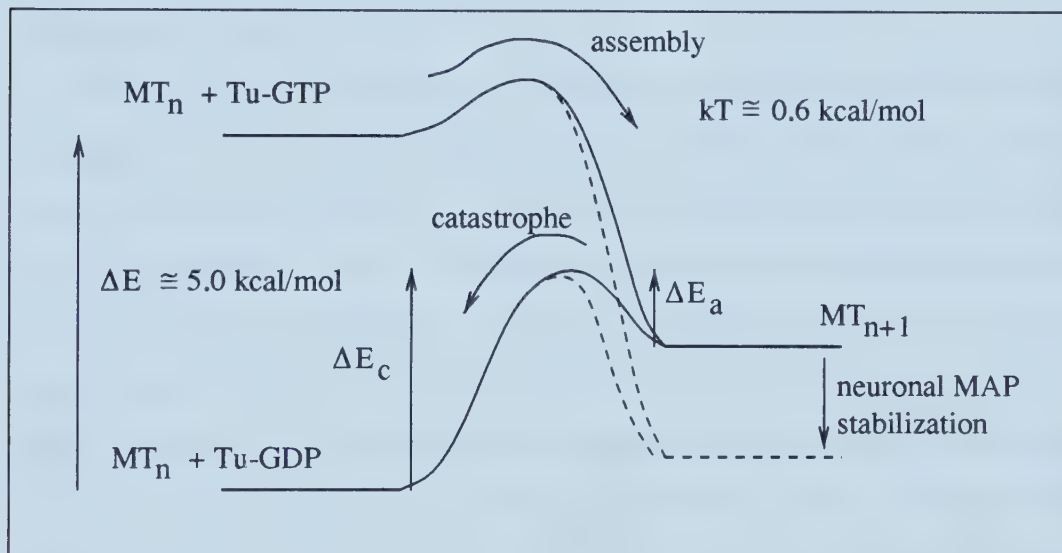


Figure 7.16: Catastrophe event reaction scheme shows the relative free energy change in the various structures. The effect of adding neuronal MAPs is also indicated however, it is only the energy of MT_{n+1} that can currently be calculated.

formational change that accompanies assembly stores potential energy within individual subunits and between the subunits of the lattice as a strain. Whenever thermal fluctuations and molecular vibrations are able to overcome the weak barrier to disassembly, it is the elastic coupling that is able to distribute the collapse energy, ΔE_c , and result in a full collapse. Neuronal MAPs function by stabilizing the MT structure and thereby increasing the activation energy, ΔE_a , for catastrophic collapse. The free energy of the MT can be calculated from its structure but the other structure's energies are not known as atomic structural data is not available. Nevertheless, a simple model of chemical kinetics with an electrostatic basis for molecular free energies predicts that a longer MT should

have a larger catastrophe probability than shorter MTs. In this scheme, the loss of a single tubulin subunit from the end of a MT seems unlikely and in the event of its occurrence, it may be attributed to tubulin leaving the end when hydrolysis and the loss of the phosphate group were not completed. In any case, it seems safe to view the catastrophe event as an exothermic event that releases the stored lattice energy of the MT.

This reaction scheme also makes two testable predictions on the catastrophe phenomenon. The collapse frequency should increase as the length of the MT increases since a transition of any of the tubulin subunits may result in catastrophe. Consequently, the half-life for catastrophe should be proportional to $1/n$ where n is number of subunits. The second prediction made by this scheme is simply electric fields may stabilize or destabilize the MT since the application of a field is equivalent to tilting Figure 7.16 such that the reactants (free tubulin) or product (MT polymer) has a higher or lower free energy. If this were measured, it would explain the interaction between action potentials and neural MT stability.

7.5 Conclusions

As discussed in this thesis, MTs are a dynamic polymer that once fully understood will provide a deeper understanding of many cell functions. Now that a picture of tubulin is available with atomic resolution, we can expect both experimental and theoretical study of the polymer to proceed at an accelerated rate. This is largely because hypotheses may be tested by targeting specific active sites for ligand binding whether GTP, MAPs, motor proteins or man-made ligands such as taxol, colchicine or other drugs. The research of this thesis has been completed over this exciting period and embraces the new structural data in the most recent work while the earlier published work relies more on estimates of

the tubulin structure and its properties. From the basic subunit structure of the MT, I have studied the ordering properties of MT lattices, studied how the MT interacts with action potentials and furthermore investigated the possibility of electronic conduction by these organic polymers. Finally, the MT structure has been studied to compare with the previous work, to comment on models of motor protein movement and to consider how isotype changes affect the electrostatic potential surrounding the MT.

The ordering of MT lattices was studied in MTs with A and B type lattices. It was also considered for different numbers of protofilaments. The transition temperature was determined in order to place a lower limit on the dipole strength of the tubulin dimer for which electrostatic interactions would prove to be important. Plainly, the minimum value of tubulin's dipole for the lattice to remain ordered at physiological temperature was estimated. Since the tubulin structure was imaged, the dipole has been calculated and is indeed larger than this limit, though it remains to be seen how the dipole changes upon the conformational change concomitant with GTP hydrolysis. In addition, the effect of a constant electrostatic field was considered in preparation for the study of the interaction between an action potential and tubulin's dipole. It was found that an electric field oriented along the MT axis could aid the ordering of the MT lattice. Furthermore, the inclusion of MAPs will increase the polarization of the MT lattice at any given temperature since the MAPs act to maintain the tubulin monomers in a fixed conformation.

The interaction between the dipole units of the neuronal MTs and action potentials was next studied. The idea was to improve on earlier models of interactions between the tubulin dimers. I accounted for thermal fluctuations of the lattice by completing a Monte Carlo simulation of lattice dynamics. The simulation accounted for the true cylindrical nature of the MT unlike previ-

ous modelling efforts which considered a planar sheet of tubulin although they admitted periodic boundary conditions. Finally, the dissipation and diffusion of energy following a conformational change was considered. Unlike the earlier modelling which claimed signal propagation, I was able to show that their signal propagation was simply the result of a zero temperature model that admitted an unphysical flip-flop between any two neighbouring dipoles that held an unfavourable configuration. I devised a simple algorithm to solve this sampling problem and found that defects in the MT lattice could propagate provided that some mechanism exists to direct the defect. The lifetime of these defects or signals was proportional to their size and required that the physical temperature was close to the transition temperature. I found that the action potential, which is itself directional, is able to direct the movement of signals along the MT lattice. Furthermore, the studies showing that MTs extend right up to the pre-synaptic membrane imply that such a signal could be important to the mechanism of neurotransmitter release.

Electric conduction along MTs was studied using a Hubbard model. The discovery here was that the lattice structure plays an important role in the conduction properties and that this is a peculiarity of the triangular nature of the lattice. The ability of the lattice to conduct was dependent upon the hopping parameters along the three lattice directions and in addition on the boundary conditions, specifically whether the aggregation of tubulin dimers was wrapped up to form a tube, as in the usual case of a MT, or whether the assemblage of tubulin was in the form of planar sheet. In this respect, it was interesting that the dimeric nature of tubulin did not seem to be particularly important. Calculations showed that individual protofilaments were not capable of electronic conduction except by optical excitation. The threshold to conduction was typically significantly larger than the energy available from GTP so that chemical activation of

charge transfer does not seem possible along the individual protofilaments, although this threshold does decrease with increasing polymer length. The energy threshold to activated conduction was only weakly dependent upon the electron density except where the polymer was half-filled; in which case the threshold was increased by a value approximately equal to the Coulomb parameter.

Once the protofilaments were bound together, the nature of the connections between the protofilaments is important. For a flat tubulin sheet, the conduction was zero except when all of the hopping parameters were non-zero. This was in stark contrast to the MT lattice, whose wrapped configuration allowed turned the polymer into a semi-conductor when the hopping parameter along the protofilament axis and either one or both of the other hopping parameters were non-zero. Even when the hopping parameters along the $\bar{3}$ -start and 8-start helices are both zero, the wrapped lattice has a lower optical threshold to conduction than the flat tubulin lattice. Variation of these optical spectra was explored at finite temperatures but the conclusion was simply that we are in a low temperature state since kT is significantly smaller than the other parameters at physiological temperature. The triangular nature of the lattice is important to the observed conduction effects but the specific width of 13 protofilaments does not seem important in this context. This transition is important to MT function if the centriole is to act as a cellular light sensor as proposed by Albrecht-Bühler [15].

Finally, the new structure of tubulin was examined. From this structure, it was possible to comment on how varied MT ligands act. The ligands may be important to assembly, such as GTP; important to MT stability such as MAPs; and important to cellular transport, such as motor proteins. In many cases, we have been able to see these ligands or post-translational modifications cause their desired effects. The so called ‘multi-tubulin hypothesis’ seems to be explained by considering these electrostatic potentials. Small changes in the

tubulin structure may render the MTs less susceptible to naturally occurring agents which would otherwise bind them and impair their function. The need for a dimer rather than a monomer subunit is still difficult to explain owing to their highly similar structure. However, a dimer does allow more efficient polymerization when one considers that it limits the number of ways that one molecule of tubulin may collide with another and result in successful binding. The hypothesis of electrostatic binding between protofilaments seems to be well founded. The nature of binding between the MT and motor proteins also seems to be electrostatic and can be used to explain the stepping of these motors along the MT surface.

The overall picture created by an examination of the tubulin structure and the success of predictions made with an eye to its electrostatics confirm that a fundamental understanding of this biological structure and its construction lies within the physics of its architecture. I hope that these investigations serve as a point of departure for future inquiry and discussion.

Bibliography

- [1] R. Becker and A. Marino, *Electromagnetism and life*, Suny Press, Albany, 1982.
- [2] I. Iliev and A. Ivanov, Effects of colchicine on the surface electrical properties and sodium channel current in neuroblastoma cells, *J. Bioelectricity* **8**, 133–145 (1989).
- [3] C. E. Dykstra, Electrostatic Interaction Potentials in Molecular Force Fields, *Chem. Rev.* **93**, 2339–2353 (1993).
- [4] E. Nogales, S. Wolf, and K. Downing, Structure of the alpha-beta tubulin dimer by electron crystallography, *Nature (London)* **391**, 199–203 (1998).
- [5] M. Dudek and J. Ponder, Accurate Modeling of the Intramolecular Electrostatic Energy of Proteins, *J. Comput. Chem.* **16**, 791–816 (1995).
- [6] D. Pearlman, D. Case, J. Caldwell, W. Ross, T. C. III, S. DeBolt, D. Ferguson, G. Seibel, and P. Kollman, AMBER, a package of computer programs for applying molecular mechanics, normal mode analysis, molecular dynamics and free energy calculations to simulate the structural and energetic properties of molecules, *Comp. Phys. Commun.* **91**, 1–41 (1995).
- [7] B. Brooks, R. Bruccoleri, B. Olafson, D. States, S. Swaminathan, and M. Karplus, CHARMM: a program for macromolecular energy, minimization, and dynamics calculations, *J. Comput. Chem.* **4**, 187–217 (1983).

- [8] D. Barlow and J. Thornton, The distribution of charged groups in proteins, *Biopolymers* **25**, 1717–1733 (1986).
- [9] D. Sackett, Structure and Function in the Tubulin Dimer and the role of the acidic Carboxyl Terminus, *Subcellular Biochemistry – Proteins: Structure, function and engineering* **24**, 255–302 (1995).
- [10] G. Woehlke, A. Ruby, C. Hart, B. Ly, N. Hom-Booher, and R. Vale, Microtubule Interaction Site of the Kinesin Motor, *Cell* **90**, 207–216 (1997).
- [11] R. Burns and C. Surridge, *Microtubules*, chapter Tubulin: Conservation and structure, pages 3–31, John Wiley and Sons, New York, 1994.
- [12] D. Sackett, B. Bhattacharyya, and J. Wolff, Local Unfolding and the Stepwise loss of the functional properties of tubulin, *Biochemistry* **33**, 12868–12878 (1994).
- [13] D. Odde, L. Cassimeris, and H. Buettner, Kinetics of microtubule catastrophe assessed by probabilistic analysis, *Biophys. J.* **69**, 796–802 (1995).
- [14] A. Desai and T. Mitchison, Microtubule polymerization dynamics, *Annu. Rev. Cell Dev. Biol.* **13**, 83–117 (1997).
- [15] G. Albrecht-Buehler, Altered drug resistance of microtubules in cells exposed to infrared light pulses: Are Microtubules the “Nerves” of Cells?, *Cell Motil. Cytoskel.* **40**, 183–192 (1998).

University of Alberta Library



0 1620 1096 7121

B45358